Developing Materials for Rare-Earth–Element Chelation: Synthesis, Solution Thermodynamics, and Applications

William Ryan Archer

Dissertation submitted to the faculty of the Virginia Polytechnic Institute and State University in partial fulfillment of the requirements for the degree of

Doctor of Philosophy
in
Chemistry

Michael D. Schulz, Chair
Paul A. Deck
Alan R. Esker
James M. Tanko

April 28, 2022
Blacksburg, VA, USA

Keywords: Rare-earth element, Isothermal Titration Calorimetry, Polymer Synthesis

Developing Materials for Rare-Earth–Element Chelation: Synthesis, Solution Thermodynamics, and Applications

William Ryan Archer

ABSTRACT

Rare Earth Elements (REEs: La–Lu, Y, and Sc) are critical components for technological innovations, therefore more effective methods for the domestic extraction and purification of REEs are in ever-increasing demand. Metal-chelating polymers have great potential in these applications due to their relatively low cost and high affinity for target elements. However, while much research has focused on specific ligands attached to polymers, little is known about the effect of polymer architecture itself on metal chelation.

This dissertation reports recent progress in the design, synthesis, and application of polymers for the chelation of various REEs. In addition to synthesizing a series of metal-chelating polymers, we elucidated the thermodynamics of binding using isothermal titration calorimetry (ITC) to gain insight into the specific relationship between polymer structure and metal binding. ITC enables the direct measurement of the binding affinity (K_a), enthalpy changes (ΔH), and stoichiometry of the interactions between macromolecules and metal ions in solution. The thermodynamics of metal chelation underpins many technologies for REE extraction. Consequently, elucidating these parameters enables the rational design of future materials.

Developing Materials for Rare-Earth–Element Chelation: Synthesis, Solution Thermodynamics, and Applications

William Ryan Archer

GENERAL AUDIENCE ABSTRACT

Rare-Earth Elements (REEs) are critical metals used in many modern technologies, therefore more effective methods for the recovery and purification of REEs are in ever-increasing demand. Metal-chelating polymers—materials that can bind metals—have great potential in these applications due to their relatively low cost and high affinity for target elements. However, while much research has focused on the specific metal-binding group attached to the polymer, little is known about the effect of polymer architecture itself on metal chelation.

This dissertation reports recent progress in the design, synthesis, and application of materials that bind to various REEs. In addition to synthesizing a series of metal-binding polymers, we measured the heat absorbed or produced during metal-binding interactions. These experiments produced fundamental insights into the interactions between the polymers, metals ions, and water molecules in solution. Overall, this work produces a depiction of the polymer–metal binding process, which enables insight into each polymer's properties as a metal-binding material. Future researchers can use these guidelines to develop the next generation of materials for the extraction of these critical metals.

Acknowledgements

Throughout my entire graduate career, I was often told that people will only read the "Acknowledgments" section of my dissertation. And I think I am okay with that. So, with that in mind, I have tried to make this the most interesting piece in my entire dissertation.

First, I need to acknowledge my advisor, Prof. Michael Schulz. Joining the Schulz group was hands-down the best decision I ever made in graduate school. Many of my colleagues at the time told me I was crazy to join the lab of a first-year assistant professor—and they may have been right. However, it was the perfect fit for me. I have never met any one person more patient, and selfless than Dr. Schulz. Although we should probably thank Angie (his wife) for that instead. Dr. Schulz never told me "No" on a project idea, and this really sparked my creativity as a scientist. Dr. Schulz firmly believes that happy students are productive students, so I'm glad that he never complained when I would leave town for 5 days at a time to go a horse show at least once a month during the summer.

The Schulz Lab is called "The Fun Lab" in the department for a reason. The large amount of laugher that comes from HHS 2018–2024 is exactly why we had to install sound-proofing material on the walls of our lab. Dr. Brady Hall, Ophelia Wadsworth, Tiffany Thompson, and I were the inaugural members of the Schulz lab in 2017. It was pleasure to work with each of them. Our first summer together as a lab (in addition to working on research) was spent rehearsing for the "Dance Your Ph.D." contest (thanks Brady…). This was quite the bonding experience, and I'll never forget it. While the final product from our dancing days is on YouTube, I'm not about to share that link here…

Over time, the Schulz Group quickly grew over the years with the additions of Rachel Bianculli, Hanan Almuzaini, Jon Mase, Nuren Ifekhar, Meagan Mazza, Connor Gallagher, Zhen

Shi, and Gillian Su. My lab mates tolerated a lot of my shenanigans. For example, the entire month of December when Earl Len Meyer (our lab elf-on-a shelf) would move around the lab and "help" everyone with their reactions. I especially loved traveling to conferences with this crew, although this became challenging due to COVID-19. Don't forget that our group is way overdue for a mini golf rematch from our trip to the ACS meeting in Orlando in March 2019.

I have had the pleasure of directly mentoring several undergraduate students in the Schulz lab during my graduate career. They affectionally called themselves "Ryan Archer's Regiment of Researchers"— and we have the matching beanies to prove it! Most rewarding is the fact that I managed to publish with almost all of them! Sasha Chnyrenkova, Sherrie Heinz-Kunert, Samantha Winn, Marianne Sawyer, Agustin Fiorito, Piper MacNicol, and Grace Dinges have all contributed to each of my projects in various ways. I appreciate each of them for dealing with my short attention span and lack of patience when experiments didn't exactly work that way we planned.

My committee members (Profs. Deck, Tanko, and Matson) deserve special thanks. Each of them provided such helpful insight into my work. I always enjoyed talking with each of them. I was lucky enough to have a couple "honorary committee members" during graduate school. Profs. Richard Gandour and Alan Esker were extremely influential in my research and growth as a scientist, particularly with the ΔC_P work. I was a GTA for 8 semesters, and my all-time favorite GTA assignment was working with Prof. Gandour teaching Organic Chemistry I lecture for 2 semesters. I also need to thank Prof. Alan Esker for stepping in to serve on my committee for my defense.

The Department of Chemistry at VT is home to a lot of great young scientists, many who have become close friends of mine. Ben Stovall was the first person I met during graduate

orientation, and we quickly become close friends. Over the years Sam Scannelli, Sarah Blosch, Brittany Bonnett, Dan Carnie, Cole Gannett, Jacob Chappell (and many many others) have become good friends that I always enjoyed talking too.

I cannot possibly forget to thank those in the department that "keep things running". Sharelle Carbough, Kezia Johnson, Joli Huynh, Amy Kokkinakos, and Corrin Lundquist all became fantastic resources, and I always enjoyed chatting with them. If I ever went missing from the lab in the afternoons for an extended period, you should have checked their offices, because I was probably there talking. Many in the department quickly became keenly aware of this, particularly Prof. Alan Esker who always managed to find me at the Davidson stockroom talking to Sharelle or Kezia.

The folks in the Chemistry and Physics Department at Western Carolina University deserve a special shout-out. Prof. Bill Kwochka took me into his lab as an undergraduate researcher and managed to convert me from a forensic chemist to a synthetic chemist. Other professors at WCU (Prof. Jamie Wallen, Prof. Channa De Silva, and Prof. Alecia Jennings) all continued to be fantastic resources, even while I was at Virginia Tech.

Finally, my parents deserve a lot of credit. During those first few months of graduate school, I lived in small cabin in Cripple Creek, VA (a 1-hour commute, one-way, from Blacksburg) because every apartment we looked at in Blacksburg "was not good enough for me" according to my parents. As I mentioned earlier, I often "vacationed" at horse shows several days each month throughout the year. My parents did a lot of behind the scenes work back at home: Prepared my show horse (Skip) and made sure the horse trailer was packed so I could just drive in from Blacksburg and leave to go to the show. Without the constant support of my parents (and my entire family), my success in graduate school may have not been possible.

Attributions

This dissertation consists of chapters that were written with the help of several co-workers, colleagues, and collaborates. They are acknowledged below along with their affiliations:

Dr. Brady A. Hall (Virginia Tech, Department of Chemistry)

Ms. Tiffany N. Thompson, B.S., M.S. (Virginia Tech, Department of Chemistry and Macromolecules Innovation Institute)

Ms. Ophelia Wadsworth (Virginia Tech, Department of Chemistry)

Mr. Agustin Fiorito (Virginia Tech, Department of Chemistry)

Ms. Sherrie L. Heinz-Kunert (Virginia Tech, Department of Chemistry)

Ms. Piper L. MacNicol (Virginia Tech, Department of Chemistry)

Ms. Samantha A. Winn, B.S. (Virginia Tech, Department of Chemistry)

Mr. Nuren Iftekhar, B.S. (Virginia Tech, Department of Chemistry)

Mr. Connor M.B. Gallagher, B.S. (Virginia Tech, Department of Chemistry)

Prof. Valerie Welborn (Virginia Tech, Department of Chemistry)

Chapter 1

William Archer, Brady Hall, Tiffany Thompson, and Ophelia Wadsworth wrote and edited the manuscript. Michael Schulz is the advisor and committee chair and provided guidance and help with writing and editing.

Chapter 2

William Archer wrote the manuscript. Michael Schulz is the advisor and committee chair and provided guidance and help with writing and editing.

Chapter 3

William Archer wrote the manuscript, synthesized the materials, and conducted ITC experiments. Agustin Fiorito, Sherrie Heinz-Kunert, Piper MacNicol, and Samantha Winn assisted in synthesis. Michael Schulz is the advisor and committee chair and provided guidance and help with writing and editing.

Chapter 4

William Archer wrote the manuscript, synthesized materials, and conducted experiments. Nuren Iftekhar, Agustin Fiorito, and Samantha Winn collected IR data, and conducted flow experiments. Michael Schulz is the advisor and committee chair and provided guidance and help with writing and editing.

Chapter 5

William Archer wrote the manuscript, synthesized materials, and conducted ITC experiments. Tiffany Thompson conducted DSC analysis, and ITC experiments. Michael Schulz is the advisor and committee chair and provided guidance and help with writing and editing.

Chapter 6

William Archer wrote the manuscript, synthesized the materials, and conducted the ITC experiments. Connor Gallagher conducted ITC experiments. Valerie Welborn performed atomist simulations. Michael Schulz is the advisor and committee chair and provided guidance and help with writing and editing.

Chapter 7

William Archer wrote the manuscript, synthesized materials, and conducted ITC experiments. Michael Schulz is the advisor and committee chair and provided guidance and help with writing and editing.

Chapter 8

William Archer wrote the manuscript. Michael Schulz is the advisor and committee chair and provided guidance and help with writing and editing.

Table of Contents

Abstract ii

General Audience Abstract iii

Acknowledgements iv

Attributions vii

Table of Contents x

Chapter 1. Overview 1

1.1 Introduction 1

1.2 References 4

Chapter 2. Isothermal Titration Calorimetry:
Practical Approaches and Current Applications in Soft Matter 5

2.1 Abstract 5

2.2 Introduction 6

2.3 Strategies for Designing and ITC Experiment 8

2.4 Applications of ITC in Soft Matter 15

2.5 Current Limitations for ITC Experiments 34

2.6 Outlook and Conclusion 35

2.7 References 38

Chapter 3. Synthesis and Rare-Earth Element Chelation Properties of
Linear Polyethyleneimine methylenephosphonate 44

3.1 Abstract 44

3.2 Introduction 45

3.3 Results and Discussion 47

3.4 Conclusions 56
3.5 References 58
3.6 Supporting Information 63

Chapter 4. Synthesis of Phosphonated Polymer Resins for the Extraction of Rare-Earth Elements 87
4.1 Abstract 87
4.2 Introduction 88
4.3 Materials and Methods 90
4.4 Results and Discussion 92
4.5 Conclusion 101
4.6 References 103
4.7 Supporting Information 107

Chapter 5. Effect of Copolymer Structure on Rare-Earth-Element Chelation Thermodynamics 122
5.1 Abstract 122
5.2 Introduction 123
5.3 Results and Discussion 124
5.4 Conclusion 131
5.5 References 132
5.6 Supporting Information 135

Chapter 6. Exploring the Role of Polymer Hydrophobicity in Polymer–Metal Binding Thermodynamics 144
6.1 Abstract 144
6.2 Introduction 145
6.3 Results and Discussion 147
6.4 Conclusions 155
6.5 References 156
6.6 Supporting Information 159

Chapter 7: Polymer Tacticity Effects in Metal–Polymer Chelation Thermodynamics 182
7.1 Abstract 182
7.2 Introduction 182
7.3 Results and Discussion 184
7.4 Conclusions 188
7.5 References 189
7.6 Supporting Information 193

Chapter 8. Summary and Future Outlook 206

Appendix A. Error analysis in the extrapolation of thermodynamic data in isothermal titration calorimetry experiments 212

Appendix B. Journal Copyright Permissions 220

Chapter 1. Overview

A portion of this chapter was submitted and accepted for publication in *Polymer International*.[1] Reprinted with permission from Wiley: Archer, W.R; Hall, B.A.; Thompson, T.N.; Wadsworth, O.J. and Schulz, M.D. Polymer sequestrants for biological and environmental applications. *Polym. Int.* **2019**, *68*, 1220–1237. Copyright 2019.

1.1 Introduction

Rare-earth elements (REEs: La–Lu, Y, and Sc) are integral to many technologies such as wind turbines (Nd, Dy), electric vehicle motors (Nd, Dy), and lighting phosphors (Eu, Tb, Y).[2-5] Consequently, REE demand is projected to reach a compound annual growth rate of 10.4% between 2019 and 2025.[6] As world demand for these metals outpaces supply, new and sustainable sources are needed, as well as more efficient methods of extraction and purification. Polymers have several advantages in these applications, including relatively low cost and high affinity for target compounds. Recent advances in polymer chemistry have enabled the design and synthesis of complex polymer architectures that have high affinity for heavy metal ions.[7-12] The research presented in this dissertation illustrates how polymer structure can be used to control the thermodynamics of REE binding.

Chapter 2 introduces the application of isothermal titration calorimetry (ITC) to measure the thermodynamics of interactions in soft matter systems (e.g., polymers, micelles, and guest–host complexation). ITC experiments enable the elucidation of the full thermodynamic profile (ΔH, ΔG, ΔS, K_a, and the binding stoichiometry) of these interactions in solution. The thermodynamics of a given polymer–metal interaction will determine the suitability of that

polymer for extraction or separation applications. Consequently, investigating these governing thermodynamics will ultimately enable the rational design of selective, high-capacity, and recyclable materials.

Chapter 3 describes the synthesis and rare-earth element chelation properties of linear poly(ethyleneimine methylenephosphonate), a material previously synthesized only with a branched architecture. We studied its rare-earth-element chelation properties using ITC as a function of polymer molecular weight (7–680 kDa), and degree of phosphonation (0–85 %). Finally, we characterized the metal-ion-induced aggregation behavior as a function of metal-ion concentration of these polymers using dynamic light scattering.

Chapter 4 reports the synthesis of a phosphonate-containing polymer resin that is functionalized throughout the bulk. We evaluated the REE absorption properties of this material as a function of pH and metal-ion identity. We observed enhanced REE uptake with decreasing ionic radii, as seen in the distribution coefficients for each ion. ITC of a water-soluble polymer analogue revealed similar binding affinities (K_a) across the REE series for each ion, indicating the importance of the network structure to REE separation.

Chapter 5 examines the synthesis and rare-earth element chelation properties of poly(acrylic acid-*co*-methyl acrylate) copolymers. We synthesized copolymers containing varied ratios of acrylic acid and methyl acrylate repeat units, and measured REE binding thermodynamics for each copolymer composition. We found entropically driven binding thermodynamics that appear to be independent of mole fraction of acrylic acid units.

Chapter 6 explores the role of polymer hydrophobicity in REE chelation thermodynamics. We synthesized a series of poly(amino acid acrylamide)s with systematically varied hydrophobicity around a consistent chelating group (carboxylate). We measured the ΔH of Eu^{3+}

as a function of temperature across the polymer series using ITC to give the change in heat capacity (ΔC_P). Atomistic simulations of the polymer–metal–water interactions revealed greater Eu^{3+} and polymer desolvation when binding to more hydrophobic polymers.

Chapter 7 reports the synthesis of a series of metal-chelating polymers with systematic variations in the polymer tacticity (20% – 99% *meso* diads) and the REE binding thermodynamics for these materials. We found that binding thermodynamics became more favorable as the *meso* diad content decreased. ΔH and ΔS decreased with decreasing percent *meso* diad. This study revealed the importance of tacticity in REE binding, a parameter often ignored in this field.

Chapter 8 provides the overall conclusions of this dissertation, and discusses future work related to this research area. Together, this body of work produces a depiction of polymer–metal binding that will serve as the foundation for new metal-chelating materials. Such materials will enable the development of efficient metal extraction and separation technologies.

1.2 References

1. Archer, W. R.; Hall, B. A.; Thompson, T. N.; Wadsworth, O. J.; Schulz, M. D. Polymer sequestrants for biological and environmental applications. *Polym. Int.* **2019,** 68 (7), 1220–1237.
2. Fromer, N. A.; Diallo, M. S. Nanotechnology and clean energy: sustainable utilization and supply of critical materials. *J. Nanopart. Res.* **2013,** 15 (11), 1-15.
3. Smith Stegen, K. Heavy rare earths, permanent magnets, and renewable energies: An imminent crisis. *Energy Policy* **2015,** 79, 1-8.
4. Gutfleisch, O.; Willard, M. A.; Brück, E.; Chen, C. H.; Sankar, S. G.; Liu, J. P. Magnetic Materials and Devices for the 21st Century: Stronger, Lighter, and More Energy Efficient. *Adv. Mater.* **2011,** 23 (7), 821-842.
5. Nelson, J. J. M.; Schelter, E. J. Sustainable Inorganic Chemistry: Metal Separations for Recycling. *Inorg. Chem.* **2019,** 58 (2), 979-990.
6. Research, G. V. Rare Earth Elements Market Size, Share, and Trends Analysis Report by Product (Cerium, Dysprosium, Erbium), by Application (Magnets, Catalyst), by Region, and by Segment forecasts, 2019-2020. **2019**, 208.
7. Diallo, M.; Christie, S.; Swaminathan, P.; Johnson, J.; Goddard, W. Dendrimer Enhanced Ultrafiltration. 1. Recovery of Cu(II) from aqueous solutions using PAMAM dendrimers with ethylene diamne core and terminal NH2 groups. *Environ. Sci. Technol.* **2005,** 29, 1366-1377.
8. Diallo, M.; Kotte, M. R.; Cho, M. Mining Critical Metals and Elements from Seawater: Opprotunities and Challenges. *Environ. Sci. Technol.* **2015,** 49, 9390-9399.
9. Hirotsu, T.; Katoh, S.; Sugasaka, K. Adsorption of Uranium on Cross-Linked Amidoxime Polymer from Seawater. *Ind. Eng. Chem. Res.* **1987,** 26, 1970-1977.
10. Barakat, M. A.; Schmidt, E. Polymer-Enhanced Ultrafiltration Process for Heavy Metals removal from industrical wastewater. *Desalination* **2010,** 256, 90-93.
11. Mangalum, A.; Boadi, F.; Masand, S. A.; Lalancette, R.; Pietrangelo, A. A Pb2+-binding polychelatogen derived from thionated lactide. *RSC Adv.* **2016,** 6, 74250-74253.
12. Bell, C.; Smith, S.; Wittaker, M.; Wittaker, A.; Gahn, L.; Monteiro, M. Surface-Functionalized Polymer Nanoparticles for SelectiveSequestering of Heavy Metals. *Adv. Mater.* **2006,** 18, 582-586.

Chapter 2. Isothermal Titration Calorimetry: Practical Approaches and Current Applications in Soft Matter

*William R. Archer[1] and Michael D. Schulz[1]**

1: Department of Chemistry and Macromolecules Innovation Institute

Virginia Tech, Blacksburg, VA USA 24061

This chapter was submitted and accepted for publication in *Soft Matter*.[1] Reprinted with permission from Royal Society of Chemistry: Archer, W.R.; and Schulz, M.D. Isothermal Titration Calorimetry: Practical Approaches and Current Applications in Soft Matter. *Soft Matter* **2020**, *16*, 8760–8774.

2.1 Abstract

Isothermal Titration Calorimetry (ITC) elucidates the thermodynamic profile (ΔH, ΔS, ΔG, K_a, and stoichiometry) of binding and dissociation reactions in solution. While ITC has primarily been used to investigate the thermodynamics of interactions between biological macromolecules and small molecules, it has become increasingly common for measuring binding interactions between synthetic polymers and small molecules, ions, or nanoparticles. This tutorial review describes applications of ITC in studying synthetic macromolecules and provides experimental guidelines for performing ITC experiments. We also highlight specific examples of applying ITC to soft matter, then discuss the limitations and the future of ITC in this field.

2.2 Introduction

Molecular interactions impact the structure and function of soft matter. The favorability of these interactions controls the operation of self-healing materials, surfactants, and polymeric sequestrants.[2-4] Thermodynamics (ΔH, ΔG, and ΔS) govern each interaction; thus elucidating the binding affinity (K_a), ΔH, ΔG, ΔS, and the binding stoichiometry (N) reveals key information about the favorability and mechanism of these interactions.[5-7] For decades, isothermal titration calorimetry (ITC) has been the gold standard for measuring the thermodynamics of molecular interactions in biological systems, but this technique has been used in synthetic systems with considerably less frequency.[8-10] Nevertheless, its potential is becoming increasingly apparent, and ITC has been used to study a number of polymer–ligand interactions.

In 1956, Keily and Hume derived a series of equations to describe how heats of reaction may be estimated by the slope of thermometric titration curves.[11] Five years later, Bricker and coworkers described a method for conducting thermometric titrations in which they measured the temperature difference between a reaction vessel and a blank solution to directly quantify the heats of reactions ($\Delta H_{reaction}$).[12] Their apparatus consisted of motor-driven burettes and polyethylene cups mounted in a block of Styrofoam™. A series of temperature-sensing devices measured temperature changes as the burette solution was added to the polyethylene cups. Ultimately, the $\Delta H_{reaction}$ of many chemicals (e.g., silver nitrate, ammonia, pyridine, etc.) reacting with HCl (*aq*) were measured using the change in the heating coil voltage inside the sample cup, analyte concentration, and slope of the resulting titration curve. Impressively, their experimental design closely resembles modern ITC instruments.

Most isothermal titration calorimeters encompass the same fundamental pieces: **1**) A reference cell filled with the solvent, **2**) a sample cell, and **3**) an injection syringe (**Fig. 2.1a**).[13]

The reference cell is used to normalize the ΔH of the sample cell during the titration experiment. In a typical ITC experiment, a series of small aliquots of the ligand solution is titrated into the sample cell (**Fig. 2.2**). In the case of soft matter ITC experiments, the ligand solution may contain metal ions, nanoparticles, small molecules, or other polymers; the receptor solution may be either a polymer or small molecule. When a reaction in the sample cell occurs, a change in temperature arises depending on whether the binding reaction is endothermic (a decrease in temperature) or exothermic (an increase in temperature). As a result, the isothermal titration calorimeter applies or reduces power (**Fig. 2.1b**) to maintain a constant ΔT between the reference cell and sample cell—this change in power is the instrument signal.

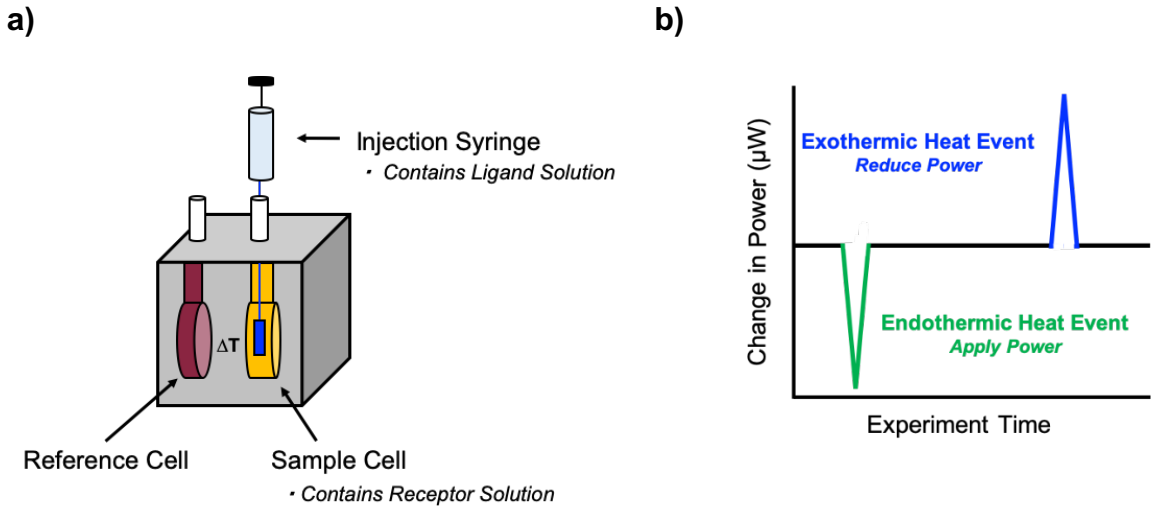


Figure 2.1 a) Schematic diagram of an ITC and **b)** representation of the calorimeter applying or reducing power according to endothermic or exothermic binding events.

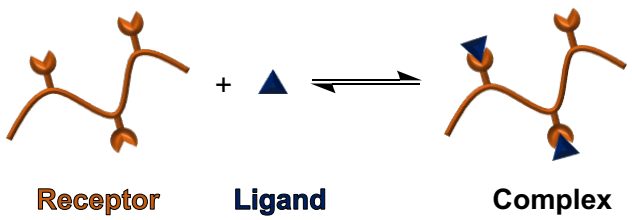


Figure 2.1. Simplified model of complex formation in an ITC experiment.

The collective raw data in an ITC experiment are integrated to produce an *ITC thermogram*; each injection of the syringe solution results in a ΔH for the binding event. Upon integrating the peaks and plotting these integrations against the mole ratio at each injection, a titration curve results (**Fig. 2.3**). The ITC titration curve directly provides ΔH, the binding stoichiometry N, and K_a; ΔG and ΔS are derived from Equations (2.1) and (2.2), below. Together, ΔH, N, and K_a not only describe the favorability and strength of the binding reaction, but also provide insight into the mechanism of binding.[14]

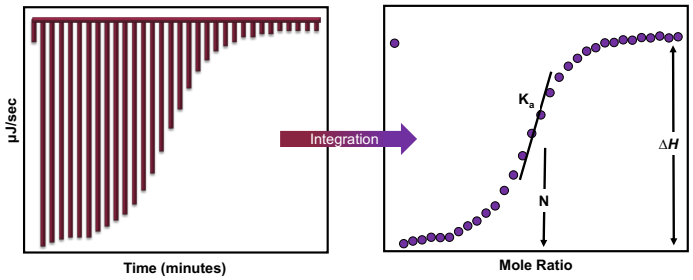


Figure 2.2. Representative ITC thermograph (left) and ITC titration curve (right). ΔH, K_a, and N are obtained directly from the ITC titration curve.

Equations (2.1) and (2.2). Determination of thermodynamic parameters from ITC experiments. K_a and ΔH are obtained directly from the ITC experiment. ΔG and ΔS are calculated according to equations 1 and 2, respectively.

(2.1) $$\Delta G = -RTln(K_a)$$

(2.2) $$\Delta S = \frac{(\Delta H - \Delta G)}{T}$$

2.3 Strategies for Designing an ITC Experiment

The following section offers strategies for designing an ITC experiment. This section is meant to serve as a starting point for running an ITC experiment, but as with any instrument, the experimentalist should consult the instrument's user manual for best practices.

Buffer Selection: As ITC is a solution-calorimetry technique, one must first consider the nature of the solutions when planning ITC experiments with macromolecules as receptors. In many cases, such as with polyelectrolytes, the pH and salt concentration of the solution strongly affect the conformation of the polymer chains due to the various (de)protonation states of the polymer backbone and side chains.[15] As a result, the pH of the solution affects binding to the macromolecular receptor. In many cases, these ITC experiments are performed in buffered, aqueous solutions; however, ITC experiments can be performed in organic solvents. A buffer mismatch, which occurs when the pH and ionic strength of sample solutions are different, results in ΔH of dilution (the heat released or absorbed when the two solutions mix) that are much larger than ΔH of binding.[16] To minimize the ΔH of dilution, the buffer (pH and ionic strength) for the titration syringe and sample cell solutions must be identical. One approach to ensuring identical buffers is to dialyze the receptor in the buffer, then use the dialysate (the solution outside of the dialysis membrane following dialysis) to dissolve the ligand.

Finally, conducting a series of control experiments ensures that there is no significant buffer–ligand or buffer–receptor interactions that would contribute large absolute changes in ΔH. One control experiment is when the solvent (without the ligand present) is titrated into the receptor solution. In a separate control titration, the ligand is titrated into the buffer without the receptor present. The ΔHs from these control experiments are subtracted from the final ITC titration curve during data analysis. The equation to correct for ΔH of dilution observed during the ITC experiment is:

$$\Delta H_{corrected} = \Delta H_{measured} - \Delta H_{dilution\ with\ ligand} - \Delta H_{dilution\ with\ receptor}$$

Equation 2.3. Correction of the observed binding ΔH by subtracting the ΔHs of control experiments.

Experimental Design: A standard incremental ITC experiment consists of 20–30 injections of the syringe solution into the sample cell. The time interval between injections should be long enough to ensure that the titration peaks reach the baseline (achieve equilibrium) after the preceding injection. During the ITC experiment, the changes in ΔH for each injection will initially be quite large because the initial ΔHs are the result of reactions between a large excess of empty binding sites. However, as the receptor in the sample cell becomes saturated with the ligand solution, there are fewer new interactions and the absolute changes in ΔH decrease (**Fig. 2.4**). Alternatively, ITC can also study molecular dissociation (e.g., dimer or micelle to monomers). In this technique, a concentrated solution of dimer or micelle is injected into the buffer in the sample cell. The dimer or micelle dissociates upon entering the cell because the concentration is low. However, as the concentration increases, the dimers or micelles dissociate less as the increase in concentration favors dimer or micelle formation.[17-19]

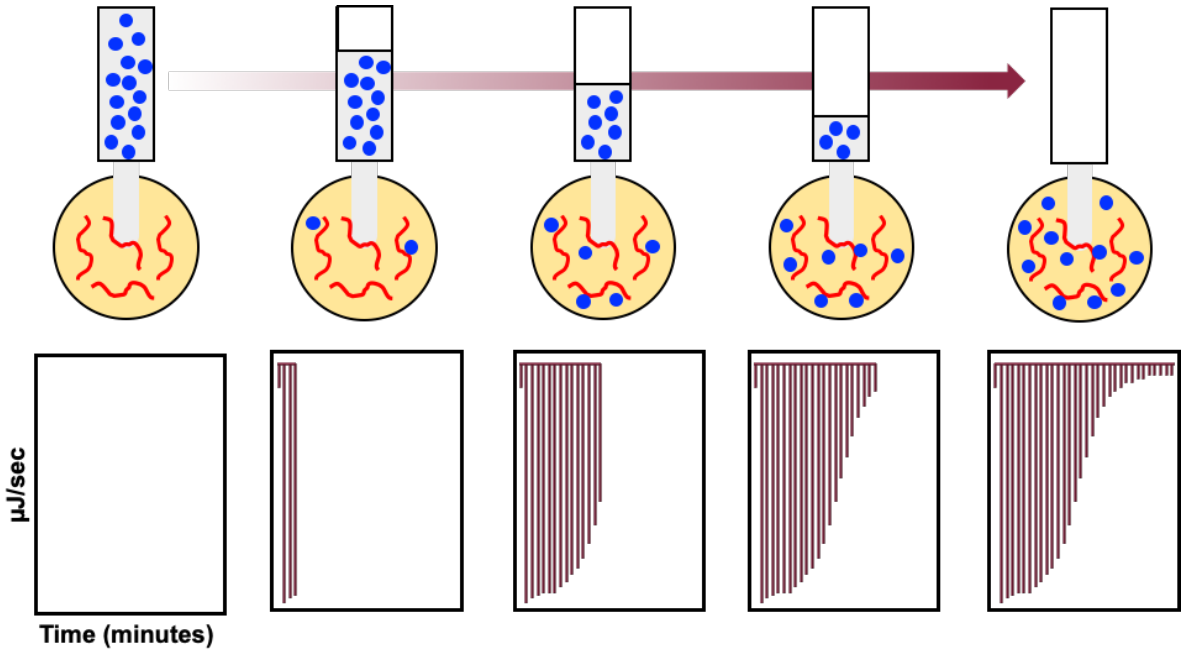


Figure 2.3. Representation of the progression of an ITC experiment adapted from Srivastava and Yadav.[20]

Concentration: The relationship between the titrant and titrand determines the optimal concentration for an ITC experiment. For a one-site model (when one or several identical sites bind to the same analyte with the same enthalpy and binding affinity), the shape of the titration curve changes according to the product of the K_a, *N*, and the sample cell concentration (**Fig. 2.5**).[14] The product of these parameters, called the Wiseman "*c*" parameter, suggests an optimal experimental window where *c* is between 10 and 500, and further suggests that curve fitting is not feasible when $c < 10$.[21] If the expected stoichiometry of the interaction is 1:1, a ratio of 10:1 ([Syringe]:[Cell]) is typically a good starting point. After obtaining preliminary fit parameters from the first ITC titration, experimental design software can be used to improve the experimental concentrations. Freyer and Lewis have provided an in-depth discussion on selecting initial concentrations for ITC experiments.[22]

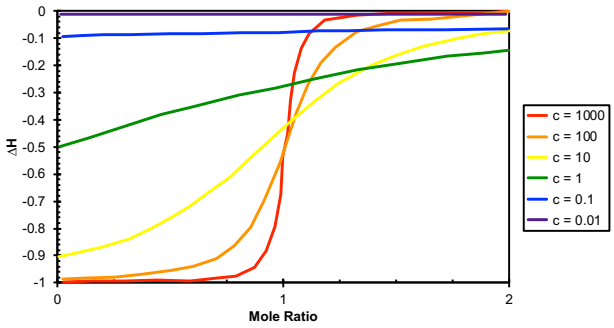


Figure 2.4. Simulated ITC titration curves with various *c* parameters. Each simulated curve has the same ΔH, N, and K_a. Adapted from Ref. 13. Reprinted with permission from the American Chemical Society.

Data Analysis: Most ITC instruments have data analysis programs provided by the instrument manufacturer. Srivastava and Yadav recently provided step-by-step guidance on processing ITC data with the Nanoanalyze Software provided by TA Instruments.[20] Origin® data analysis software also includes a package for routine ITC analysis and curve fitting. The thermodynamic parameters from the ITC titration curve are calculated by applying fit models to the titration curves. The ITC data analysis software applies a non-linear regression——an iterative process in which the model variables are determined by making a series of approximations—to the ITC titration curve to determine the best-fit parameters of the system (ΔH, K_a, and N).[22] The simplest model, the independent sites model, applies to systems where one or several identical sites bind to the same analyte with the same enthalpy and binding affinity (**Fig. 2.6a**).[23] More complex systems, such as those with two or more binding sites in which each binding site has separate enthalpies and binding affinities, may be best modeled using a two-sites or multiple-binding-sites model (**Fig. 2.6b–c**). The simulated ITC titration curves in **Fig. 2.6b–c** show systems with two distinct binding processes. In both cases the binding affinity of the first binding event (K_{a1}) is larger than the binding affinity of the second binding event (K_{a2}). Each binding event, however, also has a unique ΔH. In **Fig. 2.6b**, both binding events are exothermic, whereas in **Fig. 2.6c** the second binding

event is more exothermic than the first. These differences in the observed ΔH of each binding event produce distinct differences in the overall shape of the titration curves.[23]

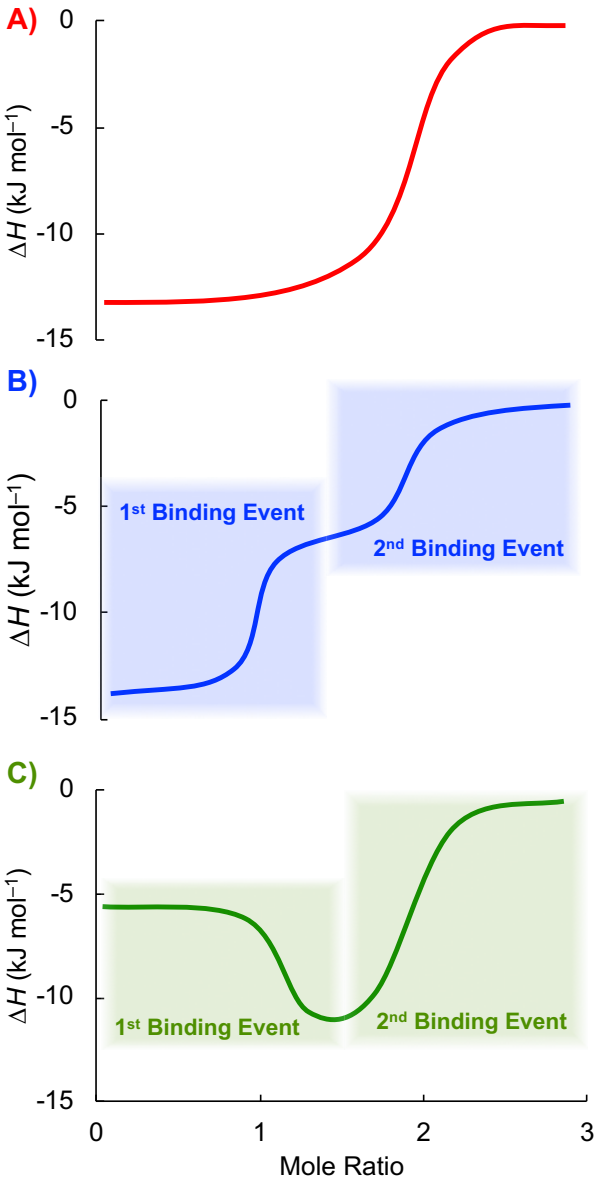


Figure 2.5. Representative ITC titration curves of **a)** a system with multiple binding sites with equal binding affinity, **b)** a system with a high-affinity binding that is more exothermic than a second binding site, and **c)** a high-affinity binding site with a smaller exothermic enthalpy than a second binding site. Adapted from Le et al.[23]

Integration of each peak in the power verses time thermogram yields the ΔH for a given molar ratio of ligand : receptor (**Fig. 2.3**). A nonlinear regression is used to determine the best-fit

of the thermodynamic parameters. First, initial estimates for each parameter (ΔH, K_a, and N) are used to generate a theoretical titration curve.[22] Comparing the theoretical curve to the experimental data generates an error function that indicates how far the theoretical curve deviates from the experimental data. Using this error function, the fit parameters are adjusted to align the theoretical and experimental curves more closely. This process is repeated until the error function is minimized to an acceptable value.[22]

Freyer and Lewis have provided an excellent overview of the mathematical analysis of thermodynamic data.[22] In short, for the independent sites model, **Equation 2.4** is used to calculate the fraction of receptor binding sites, Θ_j, occupied by ligand, L. Here, [L] is the free ligand concentration, and K_j is the binding constant.

(2.4)
$$\Theta_j = \frac{[L]K_j}{1 + [L]K_j}$$

Equation 2.5 describes the equilibrium relationship between the receptor and the ligand, where L_t is the total ligand concentration, P_t is the total receptor concentration, and n_j is the total stoichiometry of the binding reaction.

(2.5)
$$L_t = [L] + P_t \sum_{j=1}^{k} (n_j \Theta_j)$$

Together, **Equations 2.4 and 2.5** describe the equilibrium and mass balance relationship for the receptor–ligand interaction. Each equation is defined for all the potential binding sites on a receptor. For a one-site-independent binding process, substituting **Equation 2.4** into **Equation 2.5** and expanding the polynomial in terms of [L] results in a second-degree polynomial. Thus, to determine a solution for this binding process the roots of this polynomial must be solved.

Substitution of [L] into **Equation 2.4** allows the fraction of binding site j that is occupied to be calculated.[22, 24, 25] **Equation 2.6** gives the total heat produced, Q, in a given binding process, where V_o is the initial volume of the sample cell and ΔH_j is the molar enthalpy change. In the ITC experiment, the solution concentrations (e.g., [L] and [Receptor]) are known, and Q is measured. Nonlinear regression is performed on K, *N*, and ΔH to produce a curve that best fits the experimental data.

(2.6)
$$Q = P_t V_o \left(\sum_{j=1}^{k} n_j \Theta_j \, \Delta H_j \right)$$

2.4 Applications of ITC in Soft Matter

Although ITC has historically been used to study biomacromolecular interactions,[26] the application of ITC to study synthetic polymers and materials has become increasingly common. ITC has been used to measure the binding thermodynamics of polymer–metal complexation, hydrogel formation, polymer aggregation, micelle formation, and guest–host complexation.[19, 27-29]

Polymers Binding to Inorganic Species: Inorganic species, such as heavy-metal ions and SiO_2 particles, are critical to sustainable energy and medicine.[30] Polymers with target-specific chelating groups for inorganic species have gained considerable attention for their high-affinity for target ions and ease of synthesis.[31] ITC enables the determination of the full thermodynamic profile for binding events between polymers and inorganic species, thereby providing insight into the favorability and mechanism of binding.

Recently, we synthesized linear polyethyleneimine functionalized with methylene phosphonic acid groups (PEI-MP) (**Fig. 2.7a**) and used ITC to measure the binding thermodynamics of these materials for rare-earth elements (REEs).[32] We examined various

molecular weights of PEI-MP (7–680 kDa) and REEs (Y(III), Sm(III), Eu(III), Tb(III), and Dy(III)). ITC revealed entropically driven binding for PEI-MP with REEs, which is indicative of the release of solvated water molecules surrounding the metal ion and polymer side chains (**Fig. 2.7b**). The average ΔG for this polymer-REE series was -30 ± 4 kJ mol^{-1}. ITC data for N suggested that the number of REE ions bound per phosphonate repeat unit was also independent of PEI-MP molecular weight. We further used ITC to measure the thermodynamics of REEs binding to a small molecule—diethylenetriamine penta(methylenephosphonic acid) (DETMP)—that mimicked the local structure of PEI-MP and found slightly less favorable binding interactions for REEs with DETMP ($\Delta G = -24 \pm 0.3$ kJ mol^{-1}).[32] Ultimately, ITC facilitated insight into the thermodynamics of REE binding across various polymer molecular weights and REEs.

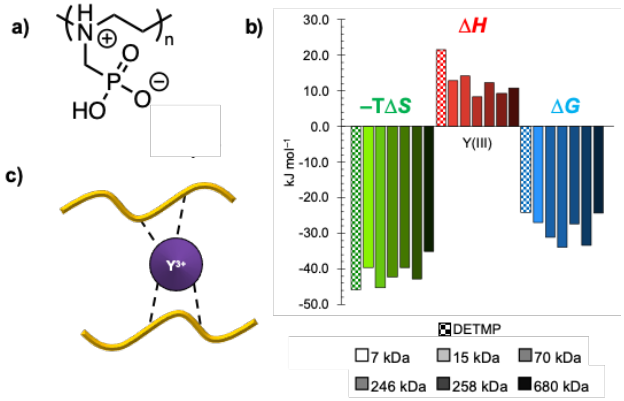


Figure 2.6. a) Structure of PEI-MP, **b)** thermodynamic binding parameters of Y(III) binding to 7, 15, 70, 246, 258, 680 kDa PEI-MP, and DETMP, and **c)** schematic representation of Y(III) binding to PEI-MP. Adapted with permission from the American Chemical Society.[32]

Laccases—copper-containing enzymes—oxidize a range of biological and environmental substrates, producing hydrogen peroxide. Liang et al. synthesized a series of guanosine-containing nanoenzymes that assembled into a metal–organic framework with Cu(II).[33] Here, they employed ITC to measure the thermodynamics and stoichiometry of binding between Cu(II) and guanosine

monophosphate (GMP). The ITC thermogram facilitated insight into the mechanism of Cu(II) binding: Metal-binding was initially endothermic, likely from the release of solvated water molecules (thereby increasing the entropy of the system), followed by exothermic events as the [Cu(II)] increased. The overall ratio of Cu(II):GMP was 3:4, suggesting a higher loading of Cu(II) than typical laccases.[33]

In addition to measuring the binding of metal ions to polymers, ITC can be used to measure the interactions between nanoparticles and polymers/small molecules. Nanoparticles of SiO_2 have enormous relevance as nanocomposite modifiers and other additives. Furthermore, synthesizing SiO_2-polymer hybrids could enable access to materials with enhanced properties; thus, the adsorption behavior of SiO_2 nanoparticles to amphiphilic copolymers has been investigated. Müllen, Klapper, and coworkers measured the thermodynamics of SiO_2 binding to a series of small molecules and amphiphilic copolymers by injecting either a small-molecule macromonomer or copolymer into a silica dispersion.[34] As the binding between SiO_2 and a compound is primarily driven by hydrogen bonding, ITC analysis revealed no binding interaction between SiO_2 and 2-ethylhexyl methacrylate (EHMA). As expected, the binding strength increases for a series of poly(ethylene oxide) methacrylate (PEOMA) macromonomers as the number of ethylene oxide units increases from 5 to 9. As the chain length increases in poly(ethylene oxide), a hydrogen bond acceptor, more binding sites are available to encase the SiO_2 nanoparticles. However, the hydrogen-bonding ability is hindered by the methyl carbon in poly(propylene oxide) methacrylate (PPOMA), thus resulting in a lower ΔH for this macromonomer.[34] In the small molecule series, (PEOMA, 1-(3-Sulfopropyl)-4-vinylpyridinium betaine (4VPSB), and (ethylene glycol) methacrylate phosphate (EGMP)) binding was accompanied by a negative entropy change. However, the three copolymers, PEHMA-*co*-P4VPSB, PEHMA-*co*-PEGMA, and PEHMA-*co*-

PEOMA, exhibited the lowest TΔS terms in the study. In conclusion, comparing the thermodynamics of binding between SiO_2 and the eleven compounds studied, ITC provided insight into the mechanism of binding: TΔS drives binding to hydrophobic regions, while ΔH drives binding to hydrophilic regions.

Hydrogel Interactions: Polymer hydrogels—three-dimensional networks of cross-linked polymers that entrap large amounts of water—find applications in tissue engineering and drug delivery.[35] ITC can analyze the thermodynamics of hydrogel formation, thermal response, and guest–host interactions.

To enhance the mechanical properties of a poly(lysine-*graft*-phenylalanine) hydrogel, Zhang et al. used cucurbit[8]uril (CB[8]) and a dialdehyde as cross-linkers to synthesize a dual-dynamic hydrogel with imine and CB[8] linkages (**Fig. 2.8a**).[36] Using ITC, Zhang et al. quantitively measured the binding affinity of the phenylalanine moiety to CB[8]. The ITC titration curve revealed two binding sites (**Fig. 2.8b**) with binding constants of 1.8×10^7 M^{-1} and 9.2×10^5 M^{-1}. The two-binding-site model suggested that CB[8] bound two phenylalanine moieties, confirming the role of CB[8] as a cross-linking agent in the hydrogel formation.

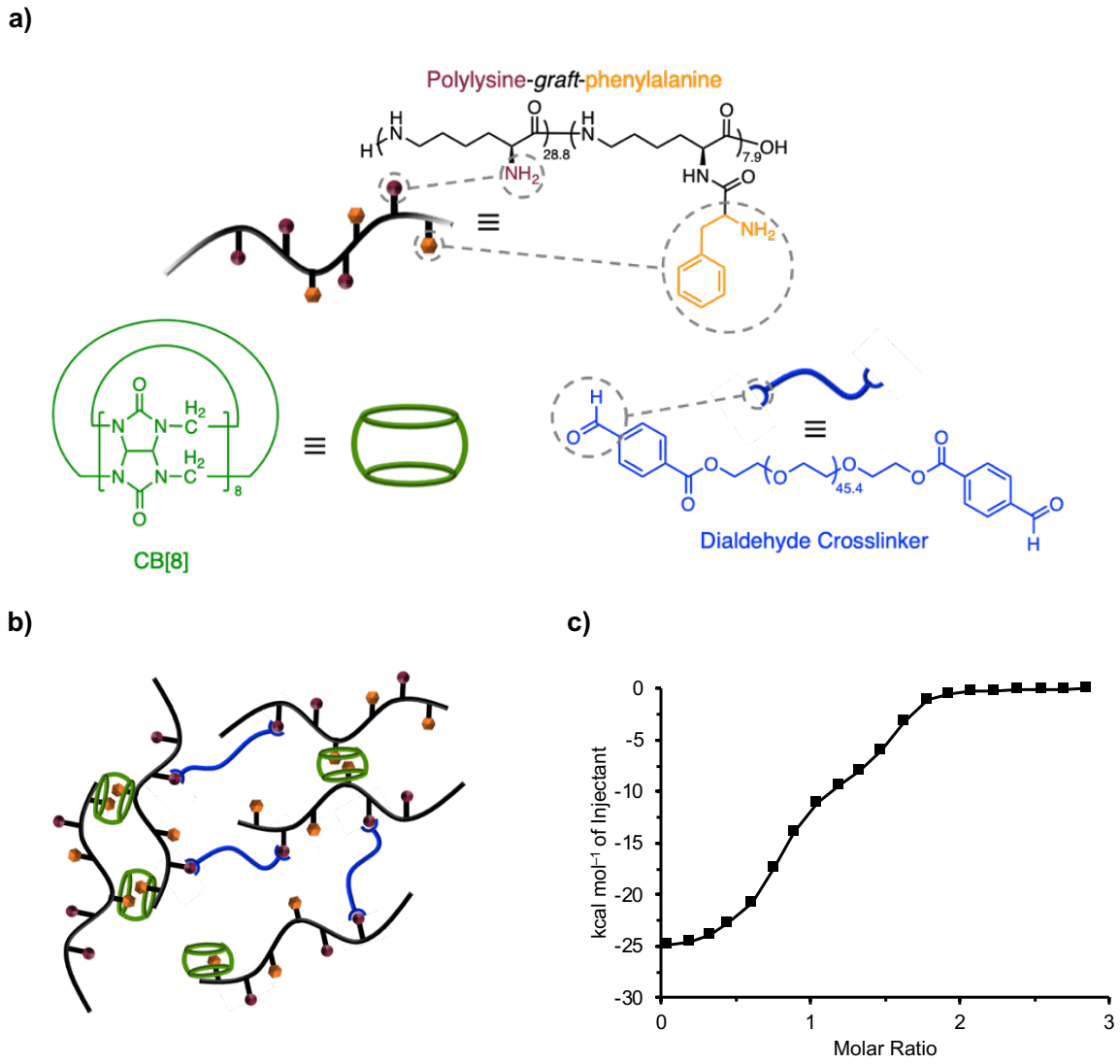


Figure 2.8. a) Chemical structures of polylysine-*graft*-phenylalanine, difunctional cross-linker, and CB[8], **b)** representation of network formation between polylysine-*graft*-phenylalanine, difunctional cross-linker, and CB[8], and **c)** ITC titration curve. Reproduced from Ref. 35 with permission from the Royal Society of Chemistry.

An extension of the typical ITC experiment is to conduct the titrations at various temperatures, such as when examining materials with a thermal responsive behavior. In a study conducted by Giussi et al., ITC was used to characterize the thermodynamics of binding between two molecular weights of poly(allylamine hydrochloride) (PAH) (15 and 50 kDa) and a poly(N-isopropylacrylamide-*co*-methacrylic acid) microgel.[37] In these experiments, the ITC sample cell

was loaded with the microgel in a 5 mM KCl buffer; the titration syringe was loaded with a solution of PAH. Experiments were conducted below and above the lower critical solution temperature of the microgel (20 ˚C and 40 ˚C, respectively) to examine the effect of phase separation on the encapsulation of PAH in the microgel. A two-site model best fit the system: The first binding event is attributed to the incorporation of PAH in the microgel, and the second binding event to interactions between PAH and the microgel surface. The ITC titration curve (**Fig. 2.9a**) revealed the first binding as endothermic, associated with the dehydration and breaking of hydrogen bonds, primarily from the methacrylate portion of the microgel. The second binding was exothermic, which was hypothesized to result from electrostatic interactions between the positively charged PAH and negatively charged microgel. Here, ITC results correlated with dynamic light scattering (DLS) and zeta potential measurements. This correlation indicated that (1) PAH becomes incorporated into the microgel (**Fig. 2.9b**) and (2) electrostatic interactions with the microgel surface occurred also (**Fig. 2.9c**).[37]

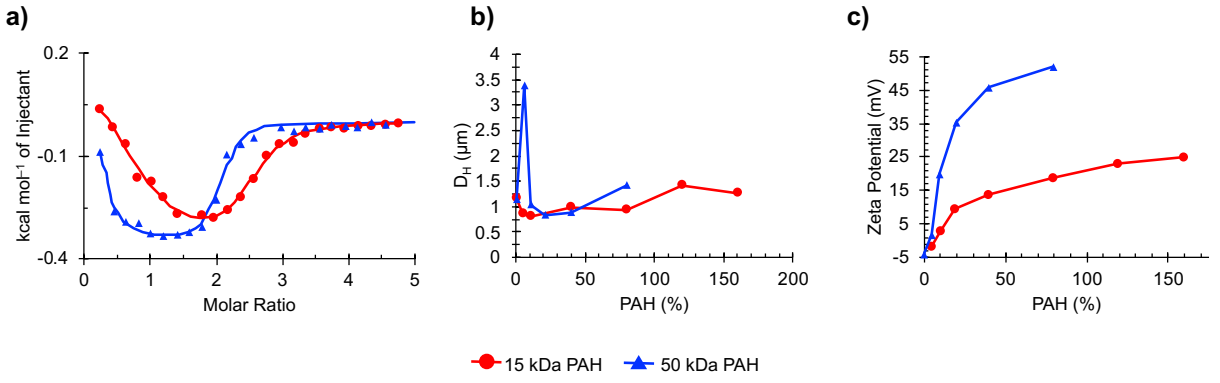


Figure 2.9. a) ITC titration curve **b)** changes in hydrodynamic diameter (D_H), and **c)** zeta potential changes of 15- and 50-kDa PAH interacting with a microgel. Reproduced from Ref. 36 with permission from the Royal Society of Chemistry.

Polymer Self-Association:

Polyelectrolytes, polymers bearing charged groups on the repeat unit, are often used in water treatment, surfactants, and gel formation.[38] Furthermore, the ionic aggregation of these

charged materials—the polyelectrolyte effect—is well-studied.[39] ITC can measure the thermodynamic forces that drive the assembly of these aggregates in solution.[40, 41]

Raju et al. used ITC to measure the association thermodynamics of a series of hydrophobically modified poly((2-acrylamido)-2-methylpropanesulfonic acid)s (HM-PAMPS).[19] These modifications included: 1) HM = grafted dodecyl groups, 2) HM = two octadecyl end-groups, and 3) HM = end-capped with cholesterol (**Fig. 2.10a**). The titration curve of the dodecyl grafted PAMPS (**Fig. 2.10b**) revealed a sigmoidal character, with an aggregation concentration of approximately 7.8 mmol L^{-1} and a $\Delta H_{\text{demicellization}}$ of –70 J mol^{-1}.[19] At low concentrations of cholesterol-PAMPS, ITC revealed a non-sigmoidal thermogram (**Fig. 2.10c**); however, higher concentrations resulted in a complex thermogram (**Fig. 2.10d**). These thermograms indicate a network of interpolymeric micelles, which make extracting meaningful thermodynamic parameters challenging.

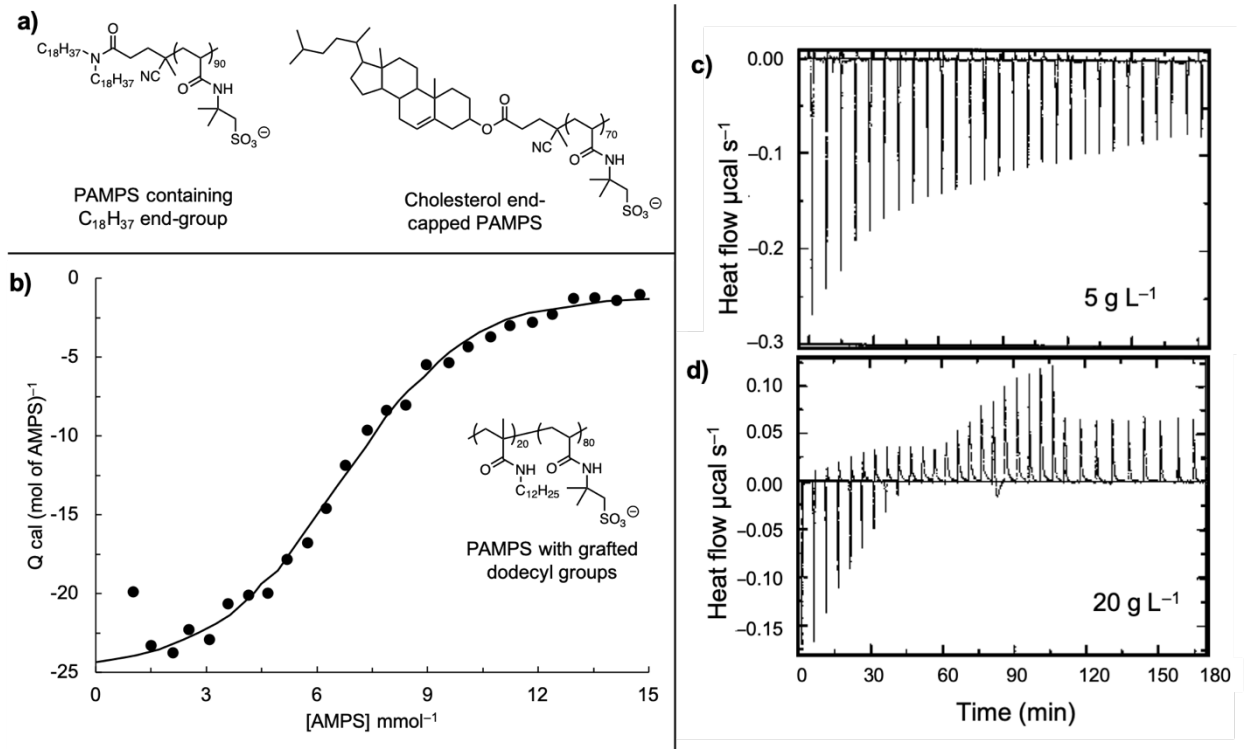


Figure 2.10. a) PAMPS containing two octadecyl end-groups, and PAMPS end-capped with cholesterol. **b)** ITC titration curve of PAMPS with grafted dodecyl groups, and **c)** ITC thermogram of cholesterol end-capped PAMPS at 5 g L^{-1} and 20 g L^{-1}.[19] Reprinted with permission from American Chemical Society.

Polymers with complementary binding sites can also interact. These interpolymer interactions play critical roles in layer-by-layer coatings, biosensors, and pharmaceutical applications.[42] Khutoryanskiy and coworkers demonstrated how ITC can deliver essential insight into polymer–polymer interactions such as those between ionic and non-ionic polymers. Eight non-ionic polymers (Dextran, 2-hydroxyethyl cellulose, poly(vinyl alcohol), poly(ethylene oxide), poly(vinyl pyrrolidone), polyacrylamide, methylcellulose, and poly(methyl vinyl ether)) were titrated into solutions of poly(acrylic acid) or poly(methacrylic acid) in a pH 2.0 solution. At pH 2.0, poly(acrylic acid) (PAA) and poly(methacrylic acid) (PMA) are mostly protonated, thereby reducing the ionic repulsion between the polymers, while increasing the potential for hydrogen bonding with the non-ionic polymers.[42] As expected, PAA and PMA showed no detectable complexation with dextran, a highly hydrophilic polymer.[42] They reported that a majority of the

binding interactions between PAA/PMA with the non-ionic polymers are endothermic, except for polyacrylamide, which displayed exothermic transitions. The authors suggested that while hydrogen bonding was the predominant interaction between PAA/PMA and polyacrylamide, these polymer–polymer interactions were not stabilized *via* hydrophobic effects resulting in exothermic ΔHs. The largest K_a occurred between PAA and poly(methyl vinyl ether), while the smallest K_a was measured between PAA and poly(vinyl alcohol).[42]

In addition to measuring the association thermodynamics of polymers, ITC can probe how the polymer backbone affects the hydrophobicity of polyelectrolytes by comparing the polymer association thermodynamics to small-molecule analogous. Sinn et al. examined the binding interactions of two polyelectrolytes: Poly(sodium acrylate) (NaPAA) and poly(sodium styrenesulfonate) (NaPSS) with water over a broad range of concentrations (**Fig. 2.11**).[43] The researchers conducted dilution experiments in which various molecular weights (degrees of polymerization between 22 and 1040) of NaPAA and NaPSS at varying concentrations were titrated into water. The ΔHs of dilution of NaPAA samples with varying molecular weights were within 2 J mol^{-1} indicating that the ΔHs of dilution depend weakly on changes in molecular weight. Furthermore, over the molecular weight range studied, the ΔG_{mix} for NaPAA was negative in the whole composition range. In a similar experiment, the ΔHs of dilution for NaPSS were compared by using the low molecular weight equivalent, Na_2SO_4 (**Fig. 2.11**). At low [Na_2SO_4], the ΔH is exothermic; as [Na_2SO_4] increases, ΔH becomes endothermic. The $\Delta H_{dilution}$ of NaPSS was more exothermic than the $\Delta H_{dilution}$ of Na_2SO_4. This observation is attributed to the structure of water screening the hydrophobic NaPSS backbone, thereby suggesting a favorable effect of the SO_4^{2-} on the long-range structure of water.[43]

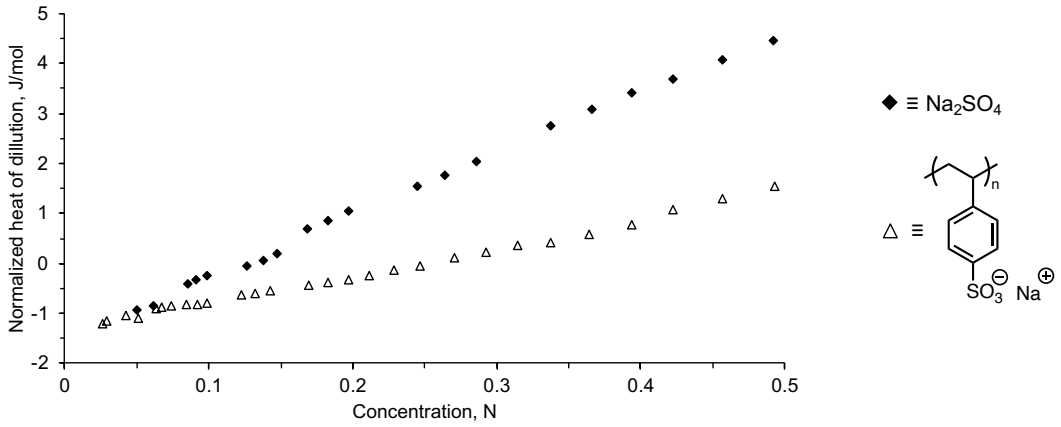


Figure 2.11. Experimental Δ*H*s of dilution for NaPSS and Na_2SO_4.[43] Reprinted with permission from American Chemical Society.

Lounis et al. further investigated how ionic strength and charge density affect the interactions of linear poly(L-lysine) and 5 acrylamide and 2-acrylamido-2-methyl-1-propanesulfonate copolymers. The ionic strength of the polymer solutions was varied by changing the [NaCl] (0.0–1.5 M NaCl) in a 12 mM Tris, 10 mM HCl pH 7.4 buffer, while varying charge density by altering the amount of 2-acrylamido-2-methyl-1-propanesulfonate in the copolymer (15–100 %).[44] The authors note entropy-driven processes for the reactions between oppositely charged polyelectrolytes, presumably resulting from the release of counterions. This hypothesis was supported by larger |–TΔ*S*| terms as the charge density increased. However, Δ*S* became lower as ionic strength increased.[44] Furthermore, ITC revealed that the *N* of poly(L-lysine) binding to the copolymer increases with increasing charge density. However, *N* is largely unaffected by differences in solution ionic strength.

The binding affinities of individual interactions also contribute to self-assembling a supramolecular polymer. Many times, the binding affinity can be measured by NMR; however, the strength of these individual interactions can depend on the solvent. Thus, measuring the K_a of high affinity systems can be challenging by NMR. For example, a bis-urea small molecule, 2,4-

bis(2-ethylhexylureido)toluene (EHUT) (**Fig. 2.12a**), forms hydrogen bonds, resulting in the self-assembly of a reversible supramolecular polymer. Arnaud and Bouteiller measured ΔH of dilution by taking a concentrated solution of EHUT dissolved in various organic solvents and titrating it into the same solvent. The K_a of the EHUT supramolecular polymer had been measured in chloroform using NMR and IR spectroscopies.[45] NMR could not be used to measure this K_a in toluene because it is much higher than that in chloroform, even in dilute solution. However, because ITC is sensitive to slight changes in ΔH, K_a could be successfully measured in toluene.[46] The ΔH for EHUT oligomerization was –37 kJ mol^{-1} in $CHCl_3$ and –48 kJ mol^{-1} in toluene; K_a in toluene is nearly 40 times greater than that in $CHCl_3$.[46] **Fig. 2.12b** further exemplifies how sample concentration affects the shape of the ITC titration curve, resulting from the change in the *c* parameter discussed previously ($c = K_a \times$ [Receptor] $\times N$).

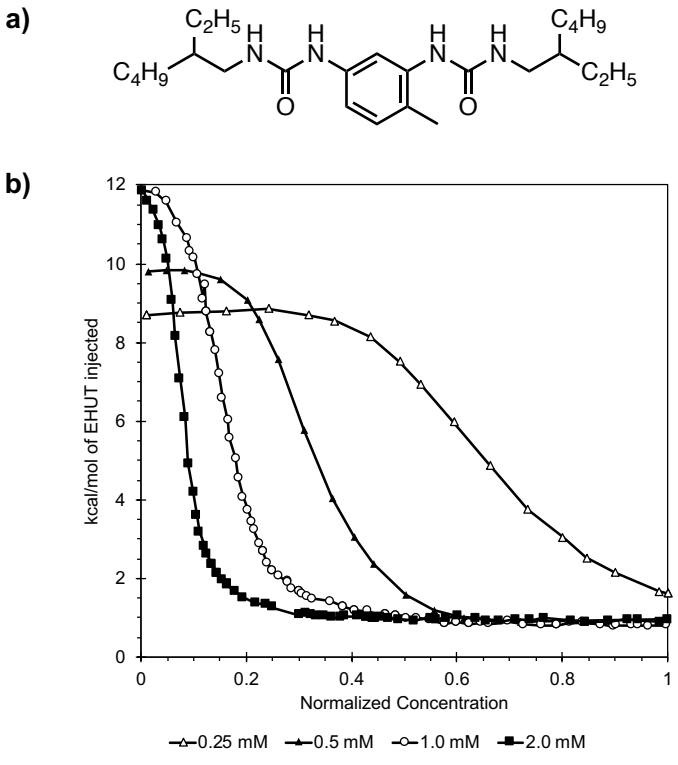


Figure 2.12. **a)** Chemical structure of EHUT and **b)** ITC titration curves of 2-, 1-, 0.5-, and 0.25-mM EHUT solutions in toluene.[46] Reprinted with permission from American Chemical Society.

ITC can also probe association thermodynamics of polymer–surfactant interactions between sodium dodecyl sulfate (SDS) and poly(*N*-vinylpyrrolidone) (PVP), a system previously studied with electromagnetic field (EMF) measurements and surfactant selective electrodes to construct a binding isotherm. In this approach, the EMF from the SDS selective electrode was plotted as a function of SDS concertation with and without PVP present. From this binding isotherm, one can find the concentration at which the onset of binding occurs (T1), and the concentration at which PVP is fully saturated by SDS (T2).[47] Thus, the EMF measurements enabled the construction of a binding isotherm that demonstrated the extent of binding between SDS and PVP. In subsequent work with ITC, a concentrated solution of SDS was titrated into a solution of PVP of the same concentration. Bloor and coworkers measured ΔH associated with interactions between SDS and PVP.[48] The resulting ITC curve (as a function of [SDS]) was overlaid with the EMF plot from the previously reported SDS-PVP data. Interestingly, the concentration that produced the onset of binding (T1) in the EMF plot, matched the pronounced maximum ΔH obtained from the ITC measurement (**Fig. 2.13**). Furthermore, the concentration at which PVP becomes saturated with SDS (T2) matched the minimum ΔH obtained in the ITC experiment.

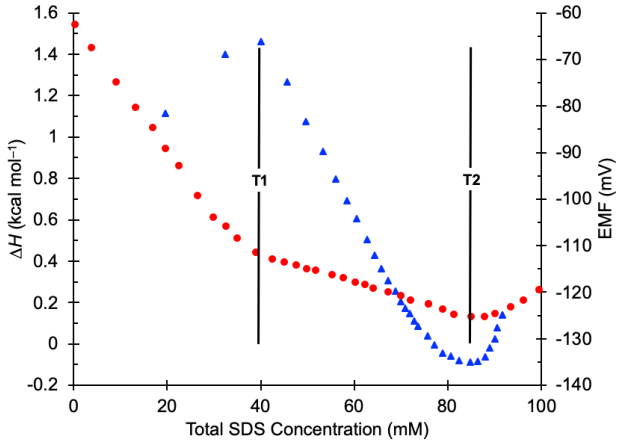


Figure 2.13. ITC titration curve of SDS and PVP interaction (blue) overlaid with EMF measurement (red). Recreated from D.M. Bloor and coworkers.[48] Reprinted with permission from American Chemical Society.

Micellization: Micelles are aggregates of surfactant molecules dispersed in a liquid. In aqueous solution, micelles typically form hydrophilic regions extending outward toward the surrounding aqueous solvent, while hydrophobic regions make up the micelle interior.[49] Amphiphilic polymers—materials that contain both hydrophobic and hydrophilic components—self-assemble spontaneously into micelles when dissolved in a solvent that is selective to either the hydrophilic or hydrophobic regions.[50] In addition to the thermodynamics of micellization, the critical aggregation concentration (CAC)—the concentration of surfactant molecules above which micelles form—can be determined with ITC. One early example, by Eatough and Rehfeld in 1971, reports the CAC and thermodynamics of micellization of SDS in water.[51]

Carbohydrate-based surfactants are of great interest as they are stable, easily synthesized, and useful for biocompatible drug delivery systems. Polarz and coworkers synthesized a library of glycoside surfactants with a carbohydrate head-group and an alkyl-chain tail. Using ITC, the authors studied the effects of structural variations on the CAC by varying the length of the alkyl chain (from 6–12 carbons) and the identity of the carbohydrate head group (galactose, glucose, maltose, mannose, and xylose).[52] The $\Delta G_{\text{aggregation}}$ trended almost linearly with the length of the

alkyl chain; surfactants with longer alkyl chains exhibited lower $\Delta G_{aggregation}$s and CACs. Surfactants with the same chain length and different head group showed small differences in $\Delta H_{aggregation}$.[52]

One method to probe the thermodynamics of micellization by ITC is to measure $\Delta H_{demicellization}$ and dilution by injecting a concentrated surfactant solution into the sample cell containing only water. Using this method, Amado et al. measured $\Delta H_{demicellization}$ of a poly(glycerol monomethacrylate)–poly(propyleneoxide)–poly(glycerol monomethacrylate)– triblock copolymer (**Fig. 2.14**) solution.[53] Although the thermogram was not an asymmetric sigmoidal curve, they calculated the $\Delta H_{demicellization}$ by obtaining the difference between the extrapolated upper-curve and the initial values from the first few injections. The CAC, estimated by the concentration at the half-height point of the thermograph, was found to be 1.9×10^{-5} M for one sample (**Fig. 2.14**). In addition to ITC, the authors determined the CAC of the triblock polymer using surface tension (1.1×10^{-5} M) and fluorescence (8.1×10^{-6} M).[53] The CAC's determined by three techniques (ITC, surface tension, and fluorescence) agreed reasonably well, with the differences in K_a ascribed to the sensitivity of each technique.

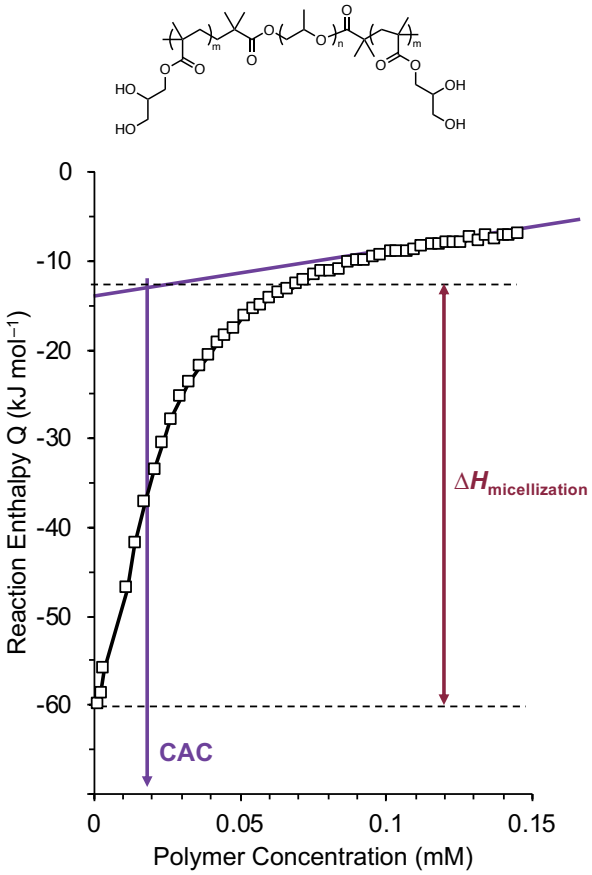


Figure 2.14. Amphiphilic triblock copolymer prepared by Amado et al. and ITC titration curve showing the determination of the cmc and $\Delta H_{micellization}$. [53] Reprinted with permission from American Chemical Society.

Surfactants containing hydrophobic aliphatic side chains coupled to short peptide segments can self-assemble into non-covalent supramolecular assemblies. In biological applications, the nanostructure of the peptide (e.g., spheres, tubes, vesicles, etc.) can affect how the peptide interacts with biological membranes. Zhang et al. used ITC to study how the sequence length of gemini peptide surfactants affect binding to phospholipid membranes.[54] Anionic unsaturated phospholipid 1,2-dioleoyl-*sn*-glycero-3-phospho-(10-*rac*-glycerol) (DOPG, sodium salt) and zwitterionic unsaturated phospholipid 1,2-dioleoyl-*sn*-glycero-3-phosphocholine (DOPC) were used to make vesicles—pure DOPG, pure DOPC, and DOPG/DOPC—that were titrated into the peptide surfactant solutions. The ΔHs of binding of the longer peptides were exothermic; for the shortest

peptide lengths, Δ*H* of binding was endothermic. ITC further revealed that the mid-length peptide exhibited the highest K_a, which correlated with the bacterial activity reported previously.[54]

In a similar study, Wang et al. synthesized a glutamic acid–lysine–glutamic acid gemini surfactant and studied its aggregation at pH 3.0 and 11.0.[55] Altering the pH of the surfactant solution changes the (de)protonation state; the protonation state influences the formation of hydrogen bonds, which alters peptide assembly. ITC analysis revealed two transition points during the titration (**Fig. 2.15a–b**). The first transition was ascribed to the formation of micelles, while the second transition denoted a shift between small aggregates to either fibers or twisted ribbons (as confirmed by circular dichroism spectroscopy). During the first transition at pH 3.0, the $\Delta H_{micellization}$ was –2.4 kJ mol^{-1}, while at pH 11.0 $\Delta H_{micellization}$ was 4.3 kJ mol^{-1}.[55] At pH 3.0 ionic interactions dominate micellization; however, at pH 11.0 non-ionic interactions provide the driving force.[55]

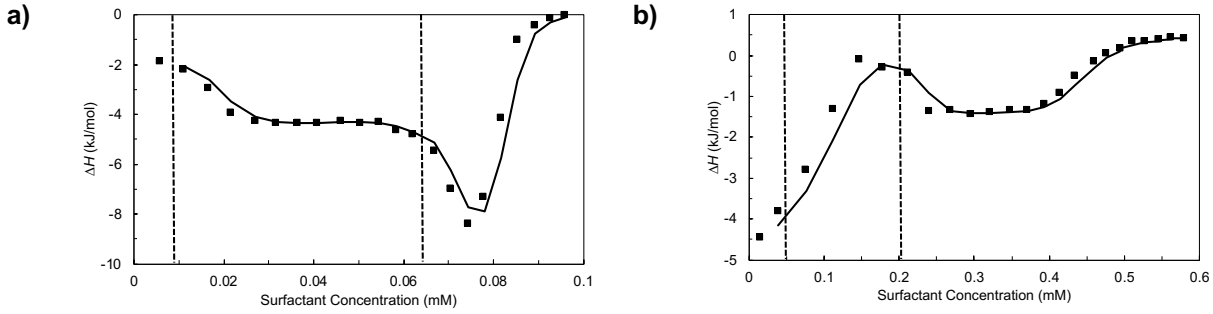


Figure 2.15. Observed Δ*H* as a function of [surfactant] at pH **a)** 3.0 and **b)** 11.0. Dashed lines represent transition points. Reproduced from Ref. 54 with permission from the Royal Society of Chemistry.

While interactions between surfactants and proteins are driven by ionic, dipole, hydrophobic, and van der Waals forces, deconvoluting the exact contribution of each of these forces in protein–ligand binding is challenging.[56] However, by using amino acid homopolymers, Petrauskas and coworkers used ITC to measure the thermodynamics of binding between a series

of cationic and anionic poly(amino acids) and various small molecule surfactants (**Fig. 2.16a**).[56] Using ITC, the authors first reported on the effect of solution ionic strength (0–1 M NaCl). For a 0 M NaCl poly(amino acid) solution, *N* obtained from ITC was 1:1, i.e., one surfactant molecule was bound per amino acid side-chain (**Fig. 2.16b–c**). As the solution ionic strength increased, *N* decreased, resulting from the reduced electrostatic interactions between the polymer side-chain and the surfactant.[56] Furthermore, by conducting variable temperature ITC experiments (13–61 ˚C), the constant-pressure heat capacities (ΔC_p) were determined by plotting the experimental temperature against ΔH (from ITC) and applying a linear fit. The authors report negative ΔC_p values presumably resulting from the interactions between the amino acid hydrophobic tail and the surfactant.[56] However, increasing the alkyl chain length of the surfactant resulted in a more favorable ΔH.

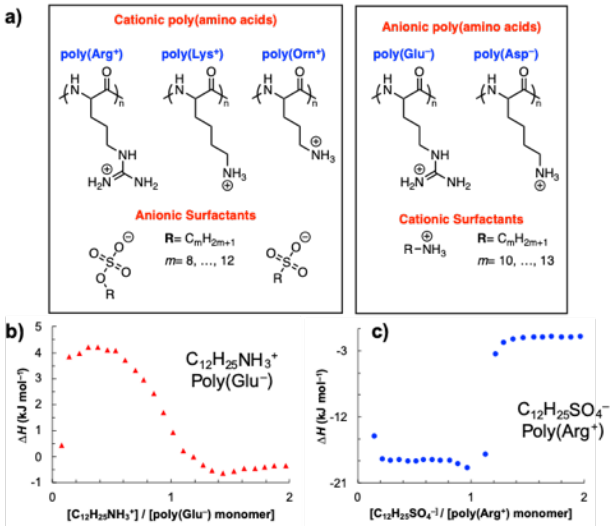


Figure 2.16. a) Poly(amino acids) and surfactants, ITC titration curve of **b)** $C_{12}H_{25}NH_3^+$ and poly(Glu^-) and **c)** $C_{12}H_{25}SO_4^-$ and poly(Arg^+).[56] Reprinted with permission from American Chemical Society.

Guest–Host Complexation: Guest–host complexes are compositions of two or more molecules held together by non-covalent interactions (e.g., ionic or hydrogen bonds). Guest–host systems find applications in biomaterials and controlled-release drug delivery.[57] In the context of guest–

host complexation, ITC can provide not only the thermodynamic profile of the complex formation, but also *N* of the complex.[58, 59]

One common host in guest–host chemistry is ß-cyclodextrin (ß-CD) due to its hydrophobic interior and hydrophilic exterior. Nguyen et al. synthesized ß-CD trimers and studied the guest–host interaction of the ß-CD trimer with adamantyl substituents on a polyacrylate backbone (**Fig. 2.17**).[60] They varied both the length of (1) the tether between the polyacrylate backbone and the adamantyl substituent and (2) the distance between the tri-functional core and the three ß-CDs. With ITC, they studied 12 possible combinations of ß-CD–polyacrylate binding to learn the effects of structural changes on K_a. For the shortest tether lengths, values of *N* ([ß-CD]/[adamantyl substituent]) were < 1, and K_a values were the smallest. They proposed that steric interactions between the ß-CD and polymer backbone caused these inefficiencies.[60] To test this hypothesis they lengthened the tether between the polyacrylate backbone and the adamantyl group to reduce the steric effects from the polymer backbone, thereby increasing ß-CD binding. However, contrary to this hypothesis, *N* for the longer tether was less than that observed for the shorter tether, perhaps due to an increase in the intra-strand aggregation that competed with ß-CD binding. [60]

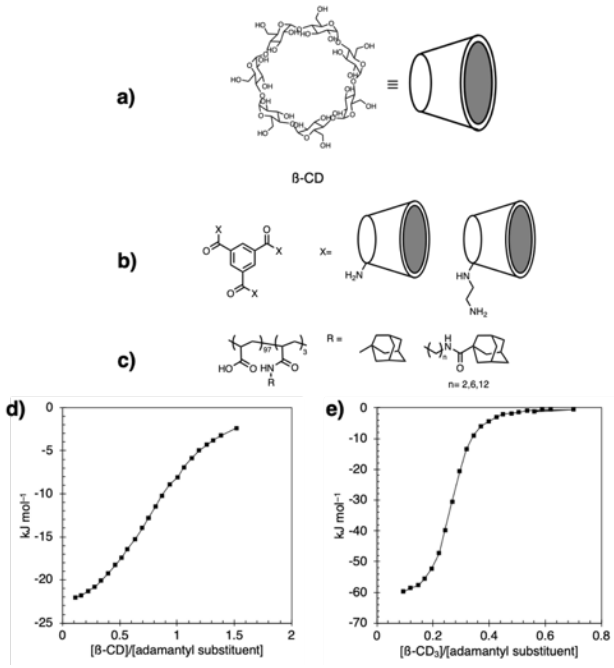


Figure 2.17. Structure of **a)** ß-CD, **b)** the tri-functional core, **c)** polyacrylate, and **d and e)** ITC titrations curves of ß-CD binding to adamantyl tethers. Reproduced from Ref. 59 with permission from the Royal Society of Chemistry.

Many times, ITC is used in conjunction with other analytical techniques to investigate specific binding interactions. In one such example, Chi et al. investigated the ion-dipole interactions between a redox-responsive polypseudorotaxane containing pillar[5]arene and a paraquat-containing homopolymer (**Fig. 2.18**) using both ITC and NMR.[61] The authors report a 1:1 complex and a K_a of $4.2 \pm 0.3 \times 10^4$ M^{-1}, indicating that pillar[5]arene binds to the paraquat derivative with a relatively strong affinity. When studied by ^{1}H NMR, a solution of 1:1 pillar[5]arene/paraquat derivative in D_2O showed upfield chemical shifts, relative to the spectra of the individual components, between 0.26–0.72 ppm for the protons on the paraquat derivative.[61]

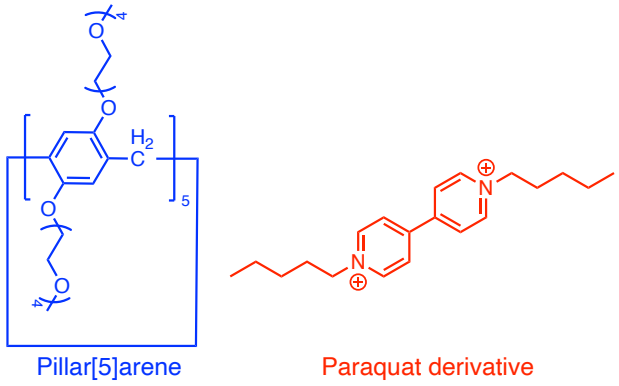


Figure 2.18. Pillar[5]arene and paraquat derivative investigated by X. Chi et al.[61] Reprinted with permission from American Chemical Society.

Another example of guest–host complexation includes ITC titrations for screening a series of guests and hosts with the goal of finding the guest–host complex with the highest K_a. Supramolecular polymers with a degree of polymerization of 100 cannot be achieved unless $K_a > 10^4$ M^{-1}.[29] Price and Gibson used ITC to measure the K_a between a biscryptand and dimethyl paraquat in which multiple binding events could occur. While the binding isotherm revealed high K_as ($K_{a1} = 4.50 \times 10^5$ M^{-1} and $K_{a2} = 1.78 \times 10^4$ M^{-1}), this system was anticooperative, meaning $K_{a1} > K_{a2}$.[29] Here, K_{a1} and K_{a2} correspond to the binding affinities of the first and second binding event, respectively. They hypothesized that the anticooperative behavior resulted from the close proximity of two host cavities and the rigidity of the linker. These structural issues resulted in electrostatic interactions that prevented the strong complexation of the second paraquat. By lengthening the tether between host sites, cooperative complexation, when $K_{a1} < K_{a2}$, was achieved ($K_{a1} = 2.49 \times 10^5$ M^{-1} and $K_{a2} = 6.23 \times 10^5$ M^{-1}).[29]

2.5 Current Limitations for ITC Experiments

While ITC is a powerful technique to measure the thermodynamic parameters associated with various binding reactions, this method has limitations. For example, ITC can require solution

volumes and concentrations that are impractical in some cases due to either the high cost or limited quantities of the analytes. To address this issue, ITC manufacturers such as TA Instruments and Malvern Panalytical offer a lower volume model with smaller sample loading sizes (about 350 μL). However, it is important to note that while lower sample volumes do reduce the sample requirements, smaller volumes also result in a smaller heat signal, Q. Another limitation is the relatively long experiment time, making high-throughput screening challenging. A single ITC experiment can take 1.5–2 hours, depending on how many injections are required. However, fully automated ITC instruments with autosamplers are becoming available.

Very small ($K_a < 10^3\ M^{-1}$) or very large ($K_a > 10^8\ M^{-1}$) K_as present a particularly interesting challenge. The measurement of high affinity systems require concentrations so low that detecting ΔH can be challenging.[62] Turnbull and Daranas showed that it is possible to extract thermodynamic parameters from low-affinity systems (even when $c = 0.01$) as long as most of the titration curve is used for curve fitting, N is known, the concentrations of the sample cell and syringe solutions are accurately known, and the signal-to-noise ratio of the data is adequate.[14]

Finally, remember that heat is a universal signal. Every chemical process that occurs in the sample cell will contribute to heat, thus one must perform control titrations (see ***Buffer Selection***) to evaluate for heat that is not a result of the desired binding reaction. Even with these controls, it is often challenging to deconvolute the effects of multiple contributors to the overall heat.

2.6 Outlook and Conclusion

While ITC provides the *global* thermodynamic parameters of the system, including ΔHs associated with changes in conformation, protonation state, and molecule–solvent interactions, other techniques can facilitate insight into the mechanism by which these changes occur. An

emerging area is the integration of ITC data with information from complementary experimental techniques such as light scattering, NMR, UV-vis, surface plasmon resonance, and differential scanning calorimetry (DSC). For example, dynamic light scattering (DLS) is used to measure the size distribution profile of small particles or polymers (1–1000 nm) in solution. We previously used DLS in conjunction with ITC to characterize the aggregation of PEI-MP as a function of metal concentration. We prepared a series of DLS samples that correspond to the [polymer]:[metal ion] at various points along the ITC titration curve.[32] DLS analysis revealed that as [metal ion] increases, PEI-MP initially forms large aggregates. However, after the [polymer]:[metal ion] is past the inflection point on the ITC titration curve, the aggregate size starts to decrease.[32]

In addition to DLS, DSC can be combined with ITC to produce a more comprehensive description of the binding reaction taking place. DSC enables access to thermodynamic information governing conformational changes.[63] With synthetic polymers, DSC is commonly used to measure the temperature at which thermally induced transitions (e.g., T_g, T_m, and T_c) occur.[64] However, DSC analysis can also be performed with solutions of macromolecules. In this experimental set-up, the excess heat capacity (C_p^{ex}) as a function of the temperature of the macromolecule solution is compared to that of a buffer solution. Integration of the C_p^{ex} versus T curve provides the transition ΔH of the conformation change.[65] In many cases, these data can be fitted to models to obtain ΔG, ΔS, and ΔC_p. ΔC_p is particularly significant in that it can enable insight into the contributions of hydrophobic interactions to the free energy of binding reactions, thereby elucidating changes in solvent-accessible surface areas.[66, 67] Previous studies have used DSC to measure the temperature and pH response of poly(dimethylaminoethyl methacrylate) grafted clay in solution, but the full protentional of this combined ITC-DSC approach has yet to be explored.[68]

NMR and UV-vis are two examples of molecular spectroscopy that can be used in conjunction with ITC to study binding interactions. In the method of continuous variation, also known as a Job plot, the mole fractions of two analytes are varied, and some physical observable, *P*, (e.g., change in chemical shift (NMR) or absorbance signal (UV-vis)) is plotted against the change in the mole ratio (**Fig. 2.19**).[69] The result is a parabolic curve from which *N* and K_a can potentially be determined.[70] For example, ITC has been used in conjunction with ^{1}H NMR Job analysis to confirm the binding between C_{60} fullerenes and the buckycatcher.[71] While Job analysis correlated well with ITC experiments in the C_{60} fullerene–buckycatcher system, Job plots are often poor indicators of stoichiometry in supramolecular complexes with low or moderate association constants.[72, 73] However, Job analysis to study inorganic complexes, in which $K_a >> [\text{Receptor}]^{-1}$, still prove effective.[62] Despite its popularity, Job plots have key limitations that should be accounted for when designing experiments.[74]

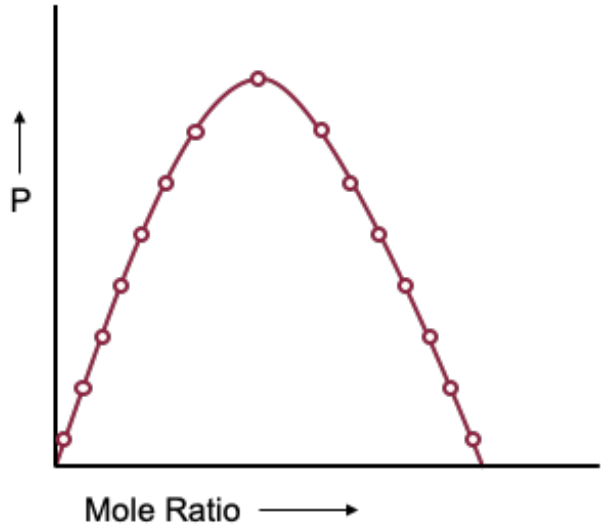


Figure 2.19. Representative Job plot. The change in some physical parameter, *P*, is plotted against the mole ratio.

As a further extension of ITC, Dumas and coworkers reported a procedure, kinITC, for determining kinetic parameters (k_{on} and k_{off}) from ITC experiments. The kinITC method extracts kinetic information from ITC titration curves based on the *shape* of each injection peak.[75] In this method, full-curve-fitting of the raw thermal power signal is used, in conjunction with the injection and mixing times, to extract rate constants. The original kinITC model proposed by Dumas et al. has been simplified to include the measurement of an equilibrium time curve that is obtained from the "effective end time" of each injection.[76] To the best of our knowledge, no publications report using kinITC to study the kinetics of binding of ligands to synthetic polymers.

In conclusion, ITC has enabled insight into polymer–metal binding, hydrogel formation, guest–host complexation, (de)micellization, and other soft matter associations. These examples demonstrate the power of ITC to study the thermodynamics of soft matter in solution and to serve as a springboard for future experiments. With further synthetic advances, burgeoning ITC applications to study soft matter will continue for years to come.

Conflicts of Interest

There are no conflicts of interest to declare.

Acknowledgements

WRA and MDS wish to acknowledge Prof. Richard Gandour and Prof. Harry Gibson for their helpful discussions during the preparation of this tutorial review.

2.7 References

1. Archer, W. R.; Schulz, M. D. Isothermal titration calorimetry: practical approaches and current applications in soft matter. *Soft Matter* **2020,** 16 (38), 8760–8774.

2. Lu, Q.; Wang, J.; Faghihnejad, A.; Zeng, H.; Liu, Y. Understanding the molecular interactions of lipopolysaccharides during E. coli initial adhesion with a surface forces apparatus. *Soft Matter* **2011,** 7 (19), 9366–9379.
3. Stefaniu, C.; Wölk, C.; Brezesinski, G.; Schneck, E. Relationship between structure and molecular interactions in monolayers of specially designed aminolipids. *Nanoscale Adv.* **2019,** 1 (9), 3529–3536.
4. Wool, R. P. Self-healing materials: a review. *Soft Matter* **2008,** 4 (3), 400–418.
5. Yang, Y.; Urban, M. W., CHAPTER 5 Thermodynamics of Self-Healing in Polymeric Materials. In *Healable Polymer Systems*, The Royal Society of Chemistry: 2013; pp 126–148.
6. Paula, S.; Sues, W.; Tuchtenhagen, J.; Blume, A. Thermodynamics of Micelle Formation as a Function of Temperature: A High Sensitivity Titration Calorimetry Study. *J. Phys. Chem.* **1995,** 99 (30), 11742–11751.
7. Yu, S.; Schuchardt, M.; Tölle, M.; van der Giet, M.; Zidek, W.; Dzubiella, J.; Ballauff, M. Interaction of human serum albumin with uremic toxins: a thermodynamic study. *RSC Adv.* **2017,** 7 (45), 27913–27922.
8. Leavitt, S.; Freire, E. Direct measurement of protein binding energetics by isothermal titration calorimetry. *Curr. Opin. Struc. Biol.* **2001,** 11 (5), 560–566.
9. Ramesh, V.; Conn, G. L., Application of Isothermal Titration Calorimetry (ITC) to Biomolecular Interactions. In *Biomolecular and Bioanalytical Techniques*, Wiley, Ed. 2020; pp 279–305.
10. Schoen, A.; Freire, E. Thermodynamics of intersubunit interactions in cholera toxin upon binding to the oligosaccharide portion of its cell surface receptor, ganglioside GM1. *Biochemistry* **1989,** 28 (12), 5019–5024.
11. Keily, H. J.; Hume, D. N. Thermometric Titration Curves. *Anal. Chem.* **1956,** 28 (8), 1294–1297.
12. Tyson, B. C.; McCurdy, W. H.; Bricker, C. E. Differential Thermometric Titrations and the Determination of Heats of Reaction. *Anal. Chem.* **1961,** 33 (12), 1640–1645.
13. Freire, E.; Mayorga, O. L.; Straume, M. Isothermal Titration Calorimetry. *Anal. Chem.* **1990,** 62 (18), 950A–959A.
14. Turnbull, W. B.; Daranas, A. H. On the Value of c: Can Low Affinity Systems Be Studied by Isothermal Titration Calorimetry? *J. Am. Chem. Soc.* **2003,** 125 (48), 14859–14866.
15. Ram-On, M.; Cohen, Y.; Talmon, Y. Effect of Polyelectrolyte Stiffness and Solution pH on the Nanostructure of Complexes Formed by Cationic Amphiphiles and Negatively Charged Polyelectrolytes. *J. Phys. Chem. B* **2016,** 120 (26), 5907–5915.
16. Bian, X.; Lockless, S. W. Preparation To Minimize Buffer Mismatch in Isothermal Titration Calorimetry Experiments. *Anal. Chem.* **2016,** 88 (10), 5549–5553.
17. Matsuyama, B. Y.; Krasteva, P. V.; Navarro, M. V. A. S., Isothermal Titration Calorimetry to Determine Apparent Dissociation Constants (Kd) and Stoichiometry of Interaction (n) of C-di-GMP Binding Proteins. In *c-di-GMP Signaling: Methods and Protocols*, Sauer, K., Ed. Springer New York: New York, NY, 2017; pp 403–416.
18. Egawa, T.; Tsuneshige, A.; Suematsu, M.; Yonetani, T. Method for Determination of Association and Dissociation Rate Constants of Reversible Bimolecular Reactions by Isothermal Titration Calorimeters. *Anal. Chem.* **2007,** 79 (7), 2972–2978.

19. Raju, B. B.; Winnik, F. M.; Morishima, Y. A Look at the Thermodynamics of the Association of Amphiphilic Polyelectrolytes in Aqueous Solutions: Strengths and Limitations of Isothermal Titration Calorimetry. *Langmuir* **2001,** 17 (14), 4416–4421.
20. Srivastava, V. K.; Yadav, R., Chapter 9 - Isothermal titration calorimetry. In *Data Processing Handbook for Complex Biological Data Sources*, Misra, G., Ed. Academic Press: 2019; pp 125–137.
21. Wiseman, T.; Williston, S.; Brandts, J. F.; Lin, L.-N. Rapid measurement of binding constants and heats of binding using a new titration calorimeter. *Anal. Biochem.* **1989,** 179 (1), 131–137.
22. Freyer, M. W.; Lewis, E. A., Isothermal Titration Calorimetry: Experimental Design, Data Analysis, and Probing Macromolecule/Ligand Binding and Kinetic Interactions. In *Method. Cell Biol.* , Academic Press: 2008; Vol. 84, pp 79–113.
23. Le, V. H.; Buscaglia, R.; Chaires, J. B.; Lewis, E. A. Modeling complex equilibria in isothermal titration calorimetry experiments: Thermodynamic parameters estimation for a three-binding-site model. *Anal. Biochem.* **2013,** 434 (2), 233–241.
24. Lewis, E. A.; Murphy, K. P., Isothermal Titration Calorimetry. In *Protein-Ligand Interactions: Methods and Applications*, Ulrich Nienhaus, G., Ed. Humana Press: Totowa, NJ, 2005; pp 1-15.
25. Eatough, D. J. L., E.A., and Hansen, L.D. , Determination of ΔH and Keq values. In *Analytical Solution Calorimetry*, Grime, K., Ed. John Wiley & Sons: New Your, NY, 1985; pp 137–161.
26. Kabiri, M.; Unsworth, L. D. Application of Isothermal Titration Calorimetry for Characterizing Thermodynamic Parameters of Biomolecular Interactions: Peptide Self-Assembly and Protein Adsorption Case Studies. *Biomacromolecules* **2014,** 15 (10), 3463–3473.
27. Termühlen, F.; Kuckling, D.; Schönhoff, M. Isothermal Titration Calorimetry to Probe the Coil-to-Globule Transition of Thermoresponsive Polymers. *J. Phys. Chem. B* **2017,** 121 (36), 8611–8618.
28. Černochová, Z.; Bogomolova, A.; Borisova, O. V.; Filippov, S. K.; Černoch, P.; Billon, L.; Borisov, O. V.; Štěpánek, P. Thermodynamics of the multi-stage self-assembly of pH-sensitive gradient copolymers in aqueous solutions. *Soft Matter* **2016,** 12 (32), 6788–6798.
29. Price, T. L.; Gibson, H. W. Supramolecular Pseudorotaxane Polymers from Biscryptands and Bisparaquats. *J. Am. Chem. Soc.* **2018,** 140 (12), 4455–4465.
30. Zou, Y.; Wang, X.; Khan, A.; Wang, P.; Liu, Y.; Alsaedi, A.; Hayat, T.; Wang, X. Environmental Remediation and Application of Nanoscale Zero-Valent Iron and Its Composites for the Removal of Heavy Metal Ions: A Review. *Environ. Sci. Technol.* **2016,** 50 (14), 7290–7304.
31. Archer, W. R.; Hall, B. A.; Thompson, T. N.; Wadsworth, O. J.; Schulz, M. D. Polymer sequestrants for biological and environmental applications. *Polym. Int.* **2019,** 68 (7), 1220–1237.
32. Archer, W. R.; Fiorito, A.; Heinz-Kunert, S. L.; MacNicol, P. L.; Winn, S. A.; Schulz, M. D. Synthesis and Rare-Earth-Element Chelation Properties of Linear Poly(ethylenimine methylenephosphonate). *Macromolecules* **2020,** 53 (6), 2061–2068.
33. Liang, H.; Lin, F.; Zhang, Z.; Liu, B.; Jiang, S.; Yuan, Q.; Liu, J. Multicopper Laccase Mimicking Nanozymes with Nucleotides as Ligands. *ACS Appl. Mater. Inter.* **2017,** 9 (2), 1352–1360.

34. Chiad, K.; Stelzig, S.; Gropeanu, R.; Weil, T.; Klapper, M.; Mullen, K. Isothermal Titration Calorimetry: A Powerful Technique to Quantify the Interactions in Polymer Hybrid Systems. *Macromolecules* **2009,** 42, 7545–7552.
35. Ahmed, E. M. Hydrogel: Preparation, characterization, and applications: A review. *J. Adv. Res.* **2015,** 6 (2), 105–121.
36. Zhang, J.; Hou, S.; Chen, Y.; Zhou, J.; Chen, H.; Tan, Y. Dual-cross-linked dynamic hydrogels with cucurbit[8]uril and imine linkages. *Soft Matter* **2019,** 15 (47), 9797–9804.
37. Giussi, J. M.; Martínez Moro, M.; Iborra, A.; Cortez, M. L.; Di Silvio, D.; Llarena Conde, I.; Longo, G. S.; Azzaroni, O.; Moya, S. A study of the complex interaction between poly allylamine hydrochloride and negatively charged poly(N-isopropylacrylamide-co-methacrylic acid) microgels. *Soft Matter* **2020,** 16 (4), 881–890.
38. Mortimer, D. A. Synthetic polyelectrolytes—A review. *Polym. Int.* **1991,** 25 (1), 29–41.
39. Lages, S.; Goerigk, G.; Huber, K. SAXS and ASAXS on Dilute Sodium Polyacrylate Chains Decorated with Lead Ions. *Macromolecules* **2013,** 46 (9), 3570–3580.
40. Canterbury, T. R.; Arachchige, S. M.; Brewer, K. J.; Moore, R. B. Probing Co-Assembly of Supramolecular Photocatalysts and Polyelectrolytes Using Isothermal Titration Calorimetry. *J. Phys. Chem. B* **2017,** 121 (25), 6238–6244.
41. Schlenoff, J. B.; Yang, M.; Digby, Z. A.; Wang, Q. Ion Content of Polyelectrolyte Complex Coacervates and the Donnan Equilibrium. *Macromolecules* **2019,** 52 (23), 9149–9159.
42. Bizley, S. C.; Williams, A. C.; Khutoryanskiy, V. V. Thermodynamic and kinetic properties of interpolymer complexes assessed by isothermal titration calorimetry and surface plasmon resonance. *Soft Matter* **2014,** 10 (41), 8254–8260.
43. Sinn, C. G.; Dimova, R.; Antonietti, M. Isothermal Titration Calorimetry of the Polyelectrolyte/Water Interaction and Binding of Ca2+: Effects Determining the Quality of Polymeric Scale Inhibitors. *Macromolecules* **2004,** 37, 3444–3450.
44. Lounis, F. M.; Chamieh, J.; Leclercq, L.; Gonzalez, P.; Geneste, A.; Prelot, B.; Cottet, H. Interactions between Oppositely Charged Polyelectrolytes by Isothermal Titration Calorimetry: Effect of Ionic Strength and Charge Density. *J. Phys. Chem. B* **2017,** 121 (12), 2684–2694.
45. Simic, V.; Bouteiller, L.; Jalabert, M. Highly Cooperative Formation of Bis-Urea Based Supramolecular Polymers. *J. Am. Chem. Soc.* **2003,** 125 (43), 13148–13154.
46. Arnaud, A.; Bouteiller, L. Isothermal Titration Calorimetry of Supramolecular Polymers. *Langmuir* **2004,** 20 (16), 6858–6863.
47. Wan-Badhi, W. A.; Wan-Yunus, W. M. Z.; Bloor, D. M.; Hall, D. G.; Wyn-Jones, E. Equilibrium and kinetic studies associated with the interaction between sodium dodecyl sulfate and polyvinylpyrrolidone in aqueous solution. *Faraday Trans.* **1993,** 89 (15), 2737–2742.
48. Bloor, D. M.; Holzwarth, J. F.; Wyn-Jones, E. Polymer/Surfactant Interactions. The Use of Isothermal Titration Calorimetry and emf Measurements in the Sodium Dodecyl Sulfate/Poly(N-vinylpyrrolidone) System. *Langmuir* **1995,** 11 (6), 2312–2313.
49. Trent, A.; Marullo, R.; Lin, B.; Black, M.; Tirrell, M. Structural properties of soluble peptide amphiphile micelles. *Soft Matter* **2011,** 7 (20), 9572–9582.
50. Zhulina, E. B.; Borisov, O. V. Theory of Block Polymer Micelles: Recent Advances and Current Challenges. *Macromolecules* **2012,** 45 (11), 4429–4440.
51. Eatough, D. J.; Rehfeld, S. J. A Calorimetric Investigation of Micelle Formation in Aqueous Sodium Dodecylsulfate Solution. *Thermochim. Acta* **1971,** 2, 443–456.

52. Voggel, M.; Meinusch, R. M.; Siewert, V.; Kunkel, M.; Wittmann, V.; Polarz, S. Sweet surfactants: packing parameter-invariant amphiphiles as emulsifiers and capping agents for morphology control of inorganic particles. *Soft Matter* **2018,** 14 (35), 7214–7227.
53. Amado, E.; Augsten, C.; Mäder, K.; Blume, A.; Kressler, J. Amphiphilic Water Soluble Triblock Copolymers Based on Poly(2,3-dihydroxypropyl methacrylate) and Poly(propylene oxide): Synthesis by Atom Transfer Radical Polymerization and Micellization in Aqueous Solutions. *Macromolecules* **2006,** 39 (26), 9486–9496.
54. Zhang, N.; Qi, R.; Li, H.; Guan, B.; Liu, Y.; Han, Y.; Wang, Y. Interaction of phospholipid vesicles with gemini surfactants of different lysine spacer lengths. *Soft Matter* **2019,** 15 (46), 9458–9467.
55. Wang, M.; Han, Y.; Qiao, F.; Wang, Y. Aggregation behavior of a gemini surfactant with a tripeptide spacer. *Soft Matter* **2015,** 11 (8), 1517–1524.
56. Skvarnavičius, G.; Dvareckas, D.; Matulis, D.; Petrauskas, V. Thermodynamics of Interactions Between Charged Surfactants and Ionic Poly(amino acids) by Isothermal Titration Calorimetry. *ACS Omega* **2019,** 4 (17), 17527–17535.
57. Rodell, C. B.; Mealy, J. E.; Burdick, J. A. Supramolecular Guest–Host Interactions for the Preparation of Biomedical Materials. *Bioconjugate Chem.* **2015,** 26 (12), 2279–2289.
58. Hof, F. Host–guest chemistry that directly targets lysine methylation: synthetic host molecules as alternatives to bio-reagents. *Chem. Commun.* **2016,** 52 (66), 10093–10108.
59. Lee, M.; Schoonover, D. V.; Gies, A. P.; Hercules, D. M.; Gibson, H. W. Synthesis of Complementary Host- and Guest-Functionalized Polymeric Building Blocks and Their Self-Assembling Behavior. *Macromolecules* **2009,** 42 (17), 6483–6494.
60. Nguyen, H.-T.; Pham, D.-T.; Lincoln, S. F.; Wang, J.; Guo, X.; Easton, C. J.; Prud'homme, R. K. Host–guest chemistry of linked β-cyclodextrin trimers and adamantyl substituted poly(acrylate)s in aqueous solution. *Polym. Chem.* **2013,** 4 (3), 820–829.
61. Chi, X.; Yu, G.; Ji, X.; Li, Y.; Tang, G.; Huang, F. Redox-Responsive Amphiphilic Macromolecular [2]Pseudorotaxane Constructed from a Water-Soluble Pillar[5]arene and a Paraquat-Containing Homopolymer. *ACS Macro Lett.* **2015,** 4 (9), 996–999.
62. Sigurskjold, B. W. Exact Analysis of Competition Ligand Binding by Displacement Isothermal Titration Calorimetry. *Anal. Biochem.* **2000,** 277 (2), 260–266.
63. Jelesarov, I.; Bosshard, H. R. Isothermal titration calorimetry and differential scanning calorimetry as complementary tools to investigate the energetics of biomolecular recognition. *J. Mol. Recognit.* **1999,** 12 (1), 3–18.
64. Liu, W.; Yang, H.; Hsiao, B. S.; Stein, R. S.; Liu, S.; Huang, B., Real-Time Crystallization and Melting Study of Ethylene-Based Copolymers by SAXS, WAXD, and DSC Techniques. In *Scattering from Polymers*, American Chemical Society: 1999; Vol. 739, pp 187–200.
65. Plum, G. E.; Breslauer, K. J. Calorimetry of proteins and nucleic acids. *Curr. Opin. Struc. Biol.* **1995,** 5 (5), 682–690.
66. Ren, J.; Jenkins, T. C.; Chaires, J. B. Energetics of DNA Intercalation Reactions. *Biochemistry* **2000,** 39 (29), 8439–8447.
67. Spolar, R. S.; Record, M. T. Coupling of Local Folding to Site-Specific Binding of Proteins to DNA. *Science* **1994,** 263, 777–784.
68. Niskanen, J.; Karesoja, M.; Rossi, T.; Tenhu, H. Temperature and pH responsive hybrid nanoclay grafted with PDMAEMA. *Polym. Chem.* **2011,** 2 (9), 2027–2036.

69. Shimojo, K.; Goto, M. Solvent Extraction and Stripping of Silver Ions in Room-Temperature Ionic Liquids Containing Calixarenes. *Anal. Chem.* **2004,** 76 (17), 5039–5044.
70. Renny, J. S.; Tomasevich, L. L.; Tallmadge, E. H.; Collum, D. B. Method of Continuous Variations: Applications of Job Plots to the Study of Molecular Associations in Organometallic Chemistry. *Angew. Chem. Int. Edit.* **2013,** 52 (46), 11998–12013.
71. Le, V. H.; Yanney, M.; McGuire, M.; Sygula, A.; Lewis, E. A. Thermodynamics of Host–Guest Interactions between Fullerenes and a Buckycatcher. *J. Phys. Chem. B* **2014,** 118 (41), 11956–11964.
72. Ulatowski, F.; Dąbrowa, K.; Bałakier, T.; Jurczak, J. Recognizing the Limited Applicability of Job Plots in Studying Host–Guest Interactions in Supramolecular Chemistry. *J. Org. Chem.* **2016,** 81 (5), 1746–1756.
73. Brynn Hibbert, D.; Thordarson, P. The death of the Job plot, transparency, open science and online tools, uncertainty estimation methods and other developments in supramolecular chemistry data analysis. *Chem. Commun.* **2016,** 52 (87), 12792–12805.
74. Thordarson, P. Determining association constants from titration experiments in supramolecular chemistry. *Chem. Soc. Rev.* **2011,** 40 (3), 1305–1323.
75. Burnouf, D.; Ennifar, E.; Guedich, S.; Puffer, B.; Hoffmann, G.; Bec, G.; Disdier, F.; Baltzinger, M.; Dumas, P. kinITC: A New Method for Obtaining Joint Thermodynamic and Kinetic Data by Isothermal Titration Calorimetry. *J. Am. Chem. Soc.* **2012,** 134 (1), 559–565.
76. Dumas, P.; Ennifar, E.; Da Veiga, C.; Bec, G.; Palau, W.; Di Primo, C.; Piñeiro, A.; Sabin, J.; Muñoz, E.; Rial, J., Chapter Seven - Extending ITC to Kinetics with kinITC. In *Methods in Enzymology*, Feig, A. L., Ed. Academic Press: 2016; Vol. 567, pp 157–180.

Chapter 3. Synthesis and Rare-Earth Element Chelation Properties of Linear Polyethyleneimine methylenephosphonate

*William R. Archer[1], Agustin Fiorito[1], Sherrie Heinz-Kunert[1], Piper L. MacNicol[1], Samantha A. Winn[1], and Michael D. Schulz[1] **

(AF, SHK, PLM, and SAW contributed equally to this work)

1: Department of Chemistry, Macromolecules Innovation Institute (MII), Virginia Tech, Blacksburg, VA 24061, United States

This chapter was submitted and accepted for publication in *Macromolecules*.[1] Reprinted with permission from American Chemical Society: Archer, W.R; Fiorito, A.; Heinz-Kunert, S.L.; MacNicol, P.L; Winn, S.A.; and Schulz, M.D. Synthesis and Rare-Earth-Element Chelation Properties of Linear Poly(ethylenimine methylenephosphonate). *Macromolecules* **2020**, *53*, 2061–2068. Copyright 2020.

3.1 Abstract

Rare-earth elements (REEs) are indispensable for modern technology, consequently effective materials for REE extraction and separation are in demand. Polymeric chelators—polymers with metal binding functional groups—are often used in these applications due to their low cost and high selectivity for target ions, with phosphonate-containing polymers often proving particularly effective. We synthesized *linear* polyethyleneimine methylenephosphonate, a material previously made only with a branched architecture, and studied its rare-earth-element chelation properties as a function of molecular weight (7 kDa–680 kDa) and degree of phosphonation (0%–85%) using isothermal titration calorimetry (ITC). ITC enabled the determination of the full

thermodynamic profile (ΔG, ΔH, ΔS, K_a, and stoichiometry) for each polymer–REE interaction in aqueous solution. We observed entropically driven metal–polymer binding with five REEs, independent of polymer molecular weight and degree of functionalization. Finally, we characterized the metal-ion-induced aggregation behavior of these polymers using dynamic light scattering.

3.2 Introduction

Rare-earth elements (REEs: La–Lu, Y, and Sc), are critical components in electronics, clean-energy technologies, catalysts, and other applications.[1-4] However, conventional sources of REEs are increasingly insufficient to keep pace with world demand and often have adverse effects on the environment.[5-7] For example, common solvent extraction processes for separating REEs require high volumes of organic extractants and strong acids, leading to negative environmental impacts.[8] Consequently, effective technologies for the extraction and purification of REEs, particularly from waste streams or other unconventional sources, are of great interest.[9-13]

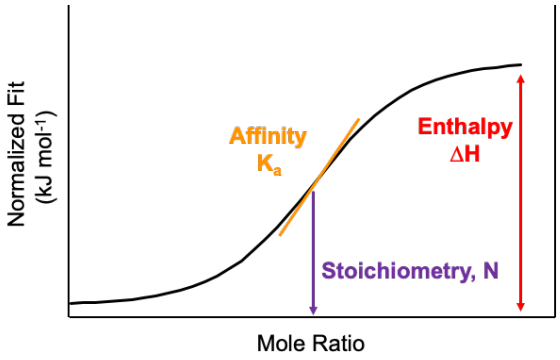
Metal-chelating polymers have great potential in REE-extraction applications due to their low cost and high affinity for target elements. As a result, metal-chelating polymers are used in several current REE extraction and separation technologies such as ion-exchange resins, polymer-enhanced ultrafiltration, and macromolecular sorbants.[14-16] In addition, metal-chelating polymers can be tuned to have a high affinity for target elements by incorporating ligands that specifically chelate a desired metal.[17-22] REEs are hard Lewis acids, thus these metals preferentially coordinate with hard Lewis-basic ligands such as those with oxygen-donor atoms (e.g., amides, malonamides, and phosphine oxides).[23, 24] In particular, phosphonate-containing polymers are often effective at binding REEs.[25-28] For example, branched poly(ethyleneimine methylenephosphonate) (PEI-MP)

has shown promise in several metal-chelation applications, including lanthanide/actinide separation, actinide exposure treatment, and internal radionuclide therapy.[29-36]

Due to the promising metal-binding properties of PEI-MP, we chose to systematically study its REE-chelation. PEI-MP is derived from poly(ethyleneimine) (PEI), commercially sold under the name Lupasol®, which is synthesized by acid-catalyzed cationic ring-opening of aziridine. This polymerization allows for little control over the polymer structure and results in a highly branched polymer with a high dispersity.[37, 38] PEI can then be converted to PEI-MP by the Moedritzer-Irani reaction.[39] Until now, only *branched* PEI-MP has been reported in the literature, and the diversity of chelation sites in the complex branched PEI-MP structure has prevented precise studies of the polymer-metal interactions. To overcome this challenge, we synthesized a series of *linear* PEI-MPs, which have more consistent metal-binding sites due to their simpler topology. Linear PEI has been synthesized by cationic ring-opening polymerization of an oxazoline, followed by hydrolysis to convert the linear polyoxazoline to linear PEI, and linear PEI with a range of molecular weights is now commercially available. [40, 41]

Isothermal titration calorimetry (ITC) is the gold standard for studying binding interactions in solution.[42] ITC is a valuable tool for quantitatively measuring the formation and dissociation of molecular complexes and has been used extensively in biology; however it has largely been underutilized as a tool in polymer chemistry.[43-49] In a molecular binding reaction, heat is either absorbed (endothermic) or released (exothermic). In the context of metal chelation, ITC can measure the change in temperature when aliquots of a metal ion solution are titrated into a (macromolecular) ligand solution adiabatically. This experiment enables the determination of the entire thermodynamic profile (ΔH, ΔS, ΔG, K_a, and the binding stoichiometry N) of the interaction.[50-52] ΔH and K_a are obtained directly from the titration curve (**Fig. 3.1**.); ΔG and ΔS are

calculated according to Equations **(3.1)** and **(3.2)**, respectively. Using ITC, we investigated the thermodynamics of binding between linear PEI-MP and a series of REEs in solution to study the relationship between polymer structure and metal binding with these materials.



$$\Delta G = -RTln(K_a) \qquad \textbf{(3.1)}$$

$$\Delta S = \frac{(\Delta H - \Delta G)}{T} \qquad \textbf{(3.2)}$$

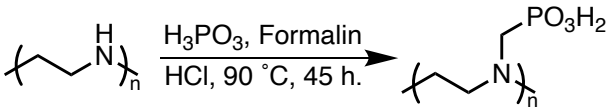
Figure 3.1. Determination of ΔH, N, and K_a from the ITC titration curve and equations used to calculate ΔG and ΔS.

3.3 Results and Discussion

To produce linear PEI-MP, aminomethyl phosphonic acid groups were installed onto linear PEI by the Moedritzer-Irani reaction, which involves the condensation of formaldehyde with an amine, followed nucleophilic addition of the phosphorous acid (**Scheme 3.1**).[39] Briefly, PEI was combined with H_3PO_3 and HCl (*aq*) in a round bottom flask. Formalin was added dropwise to the reaction mixture, which was subsequently refluxed for 40 hours. The resulting polymer was purified by dialysis against DI water. NMR and IR spectroscopy confirmed the incorporation of the phosphonate functional groups into the polymer material and experimental P/N ratios from elemental analysis were used to determine the degree of functionalization. We observed a

broadened ^{31}P NMR signal, which is characteristic of polymers due to the diversity of chemical environments along the polymer chain (see *Supporting Information* for full experimental details). Samples of linear PEI of six molecular weights (2.5, 5.7, 25, 86, 100, and 250 kDa) were 75–85% functionalized with phosphonic acids groups. This relatively consistent degree of functionalization enabled any changes in the binding thermodynamics to be ascribed to the polymer molecular weight rather than degree of functionalization. To evaluate the effect of polymer functionalization on REE binding, a single molecular weight of PEI (86 kDa) was 16, 52, 63, and 85% functionalized with phosphonic acid groups to produce a series of polymers with identical degrees of polymerization, but varied degrees of functionalization.

Scheme 3.1. Synthesis of linear PEI-MP



Using ITC, we measured the thermodynamics of polymer–REE binding in a pH 5 buffered aqueous solution. pH 5 was chosen because insoluble lanthanide hydroxides form above pH 6, thus the thermodynamic parameters presented here are condition-dependent.[53] Pyridine was chosen for the buffer because the pKa of pyridine (~5.2) is close to the desired pH.[54] To ensure consistent ionic strength, the PEI-MP solution was dialyzed against the buffer solution and the final concentration of PEI-MP was determined by UV-vis spectroscopy. Directly measuring the PEI-MP concentration by UV-vis spectroscopy enabled us to correct for slight variations in the polymer concentration following dialysis, which would affect the resulting stoichiometry data. Metal ion solutions were prepared using the dialysis flow-through to ensure the solutions had consistent ionic strengths and to avoid heat evolution associated with buffer mismatch, which occurs when the pH and ionic strength of the titrant and sample solutions are

different.[55] Small heats of dilution determined from control titrations (metal-ion into buffer (*without PEI-MP present*), and buffer into PEI-MP (*without metal-ion present*)) were subtracted before curve fitting, which allowed us to exclude any metal-buffer interactions in the resulting thermodynamic parameters. To provide a benchmark for the error in the ITC measurements, we replicated a subset of the ITC experiments and found the standard deviation of the ΔH, and the binding stoichiometry *N* for the 5 metal ions to be 0.1–0.9 and 0.1–1.4, respectively (**Table 3.S5**).

To confirm the role of the phosphonic acid groups in metal binding, we measured the metal-polymer interaction thermodynamics using unfunctionalized PEI. For this experiment, unfunctionalized PEI was dialyzed in the same pH 5 buffer. ITC analysis revealed no evidence of metal binding (*Supporting information*). We attribute this observation to the fact that at pH 5, most of the nitrogen atoms along the PEI backbone are protonated, which inhibits their ability to chelate.

We evaluated five REEs (Y(III), Sm(III), Eu(III), Tb(III), and Dy(III)) (**Fig. 3.2**) with each polymer molecular weight. These REEs were chosen for this initial investigation due to their importance to clean energy and their limited supply.[56] Each REE–polymer interaction was endothermic, which is characteristic of entropy-driven binding (**Fig. 3.3** and *Supporting Information*). This entropy-driven thermodynamic profile is characteristic of binding interactions that result in the release of complexed water molecules and the reduction of long-range solvent ordering during binding.[57] Across almost two orders of magnitude of polymer molecular weight, the change in the Gibbs free energy stayed largely consistent across the series of metal ions indicating that this system that is robust against perturbations in polymer molecular weight. The consistency across the REE series can be attributed to the similar chemistries of the REE metals. Each of these metal ions has the same oxidation state and coordination chemistry, with only slight differences in the ionic radii.[58]

Additionally, binding stoichiometry (e.g., phosphonate repeat units per metal ion bound) for this series of polymers also appears to be independent of polymer molecular weight (**Fig. 3.4**): Polymers with a lower degree of polymerization required as many phosphonate repeat units to bind an REE ion as polymers with higher degrees of polymerization. These data suggest that each polymer is equally efficient at metal chelation, i.e., potential binding sites remain accessible even as molecular weight increases. Since the coordination numbers for the lanthanide metals typically range between 8–9,[59] these stoichiometry data indicate that PEI-MP forms coordination complexes with multiple phosphonate units either on the same or neighboring polymer chains with the remaining metal coordination sites filled with solvent molecules.

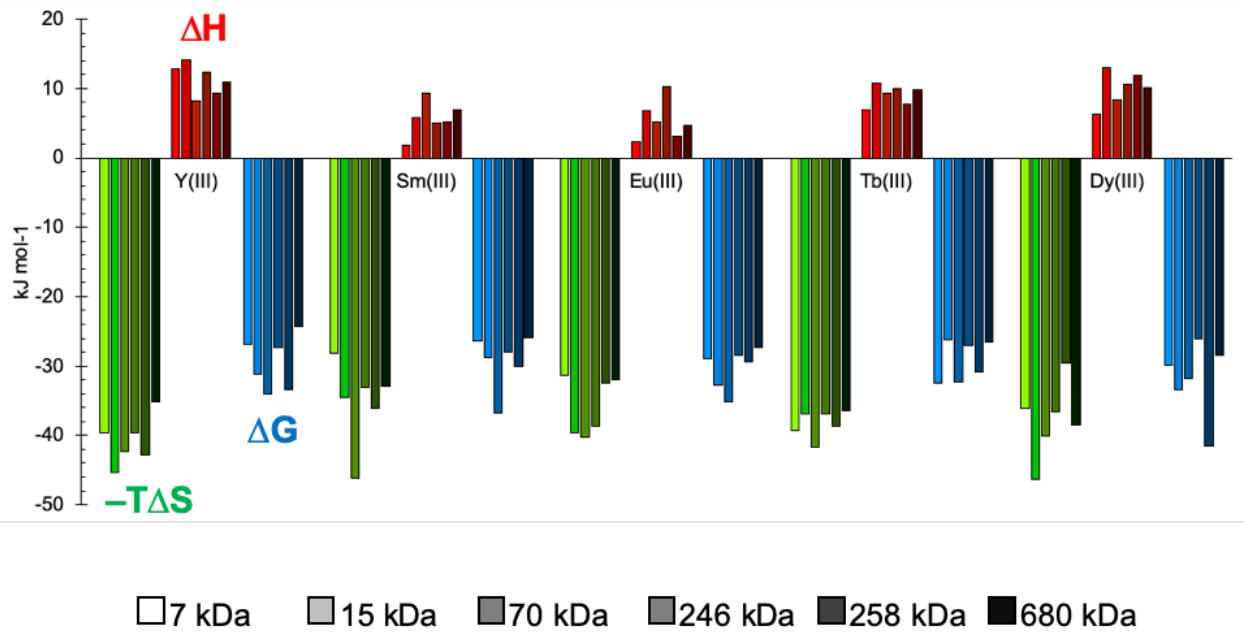


Figure 3.2. Thermodynamic binding parameters of REEs binding to 7, 15, 70, 246, 258, and 680 kDa PEI-MP. The Gibbs free energy (ΔG) of binding stays roughly consistent across the series of metal ions and polymer molecular weights.

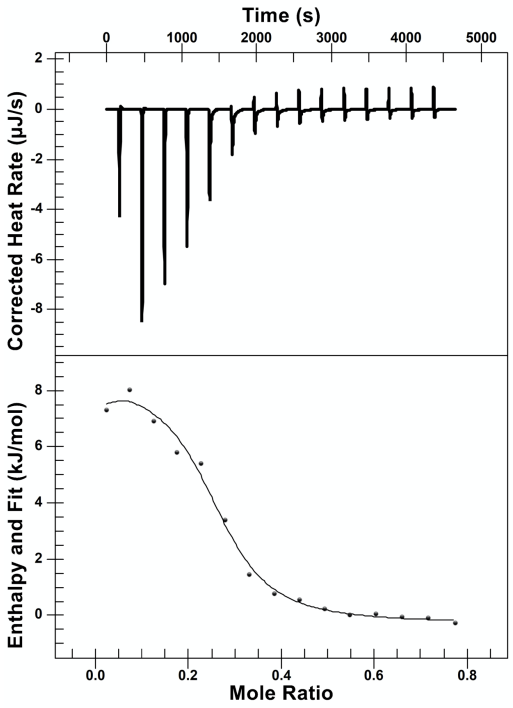


Figure 3.3. Representative ITC thermograph and integrated titration curve resulting from the binding of 246 kDa PEI-MP and Sm(III)

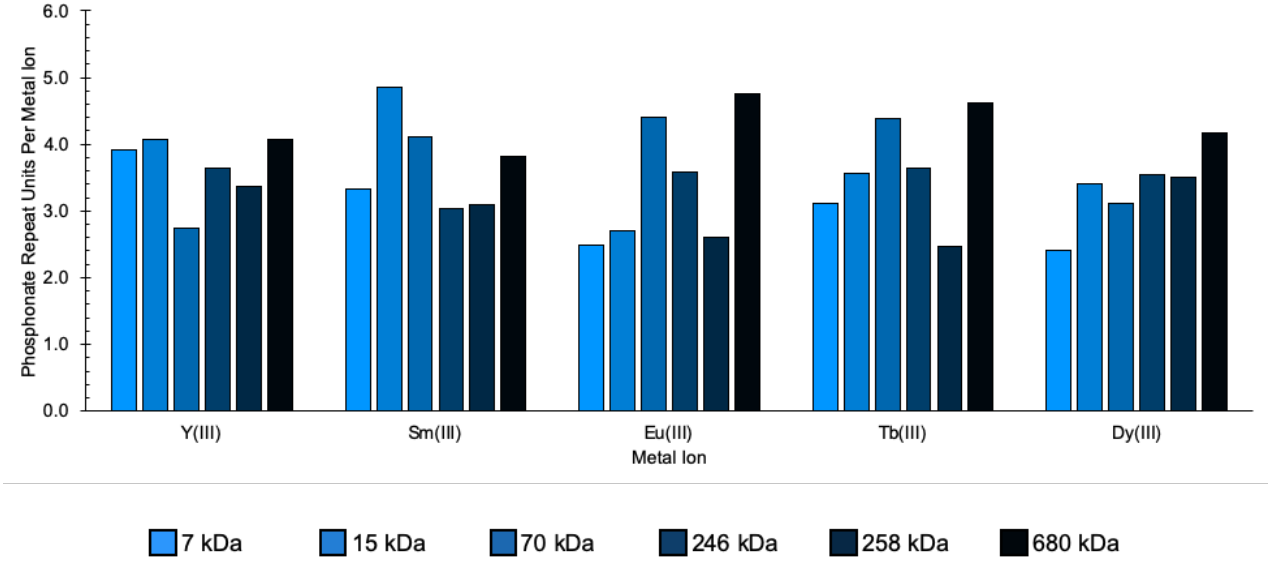


Figure 3.4. Stoichiometry of REE binding for molecular weight series (7, 15, 70, 246, 258, and 680 kDa). These polymers required between 2 and 5 phosphonate repeat units to bind each REE ion.

Because polymer molecular weight did not significantly affect the Gibbs free energy of binding, we investigated whether this trend would hold into the small-molecule regime. Specifically, we evaluated diethylenetriamine penta(methylene phosphonic acid) (DETMP), a small molecule that is structurally analogous to *linear* PEI-MP (**Fig. 3.5**). On average, REE binding to DETMP was $\Delta G = -24 \pm 0.3$ kJ mol^{-1} for these 5 REEs, with approximately one REE metal ion bound to each DETMP molecule (**Fig. 3.6**). These data indicate that REE binding to DETMP is less favorable than binding to PEI-MP ($\Delta G = -30 \pm 4$ kJ mol^{-1}), which is particularly interesting as PEI-MP also required slightly fewer phosphonates on average to bind each REE ion.

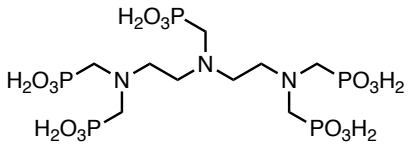


Figure 3.5. Structure of DETMP

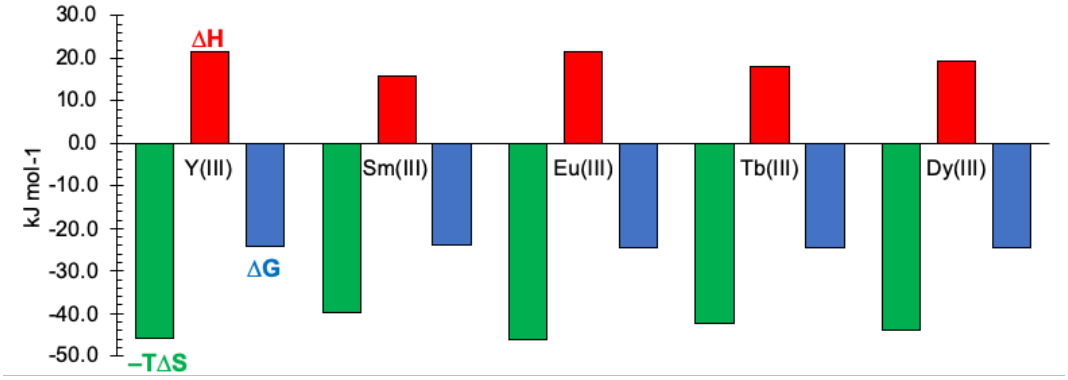


Figure 3.6. Thermodynamic parameters of DETPM binding to REEs

We also investigated how polymer functionalization affects REE-binding thermodynamics. We synthesized a series of PEI-MPs with varying degrees of

functionalization (16, 59, 66, and 85%), but the same degree of polymerization (degree of polymerization ~2,000 repeat units). This varied functionalization was achieved by altering the reaction time and stoichiometry. As before, we observed consistent Gibbs free energy values across the functionalization series (**Fig 3.7**). The thermodynamics of binding is almost identical for each material regardless of the degree of functionalization, however the binding stoichiometry is slightly smaller for the least functionalized materials (**Fig 3.8**).

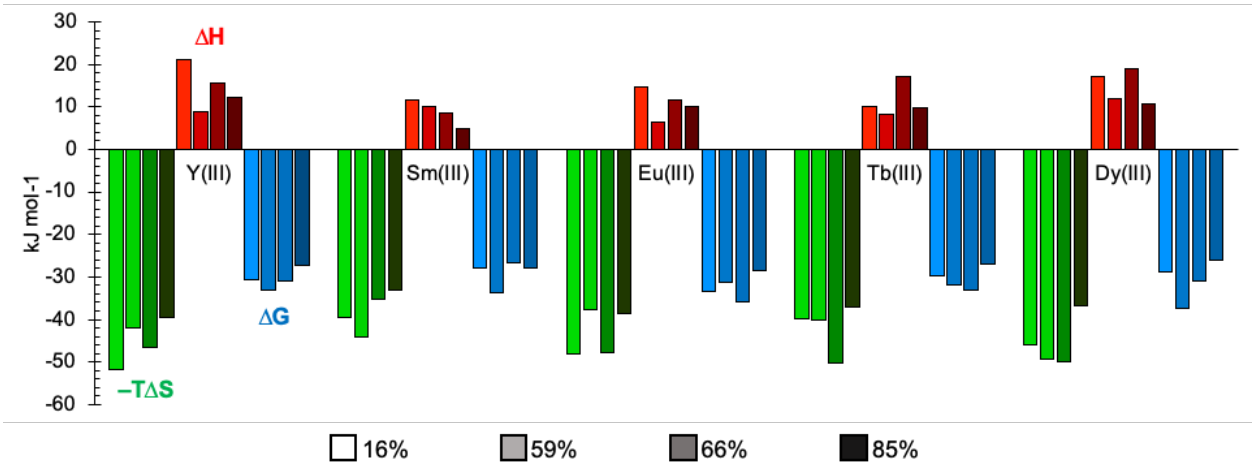


Figure 3.7. Thermodynamic binding parameters of REEs binding to PEI-MP for various degrees of functionalization. The Gibbs free energy (ΔG) of binding stays consistent across the series of metal ions and polymer functionalizations.

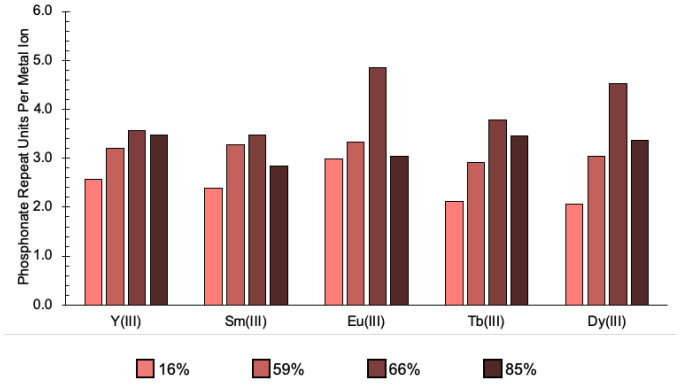


Figure 3.8. Stoichiometry of binding for the functionalization series (16, 59, 66, and 85%).

Under our experimental conditions (pH 5), PEI-MP is zwitterionic (**Fig. 3.9**). Each phosphonic acid group contains two acidic protons: pKa 1.1–2.3 and pKa is 5.3–7.2.[60, 61] Thus, in solution at pH 5, the predominant zwitterionic form of a PEI-MP repeat unit contains a protonated amine and singly deprotonated phosphonic acid. Polyzwitterions—polymers containing both anionic and cationic groups along the polymer chain—have been used previously to bind to trace metals in solution due to their charged nature and solubility in aqueous systems.[62-65] Extensive literature describes aggregation behavior of polyelectrolytes during metal binding, a possibility with linear PEI-MP.[66-68] To investigate aggregation associated with metal–polymer binding events, we used dynamic light scattering (DLS) to examine the change in particle size distribution during the addition of metal ions. In the absence of REEs, we found that a small percentage (~2%) of linear PEI-MP molecules forms aggregates of approximately 255 nm in solution regardless of molecular weight or degree of functionalization, presumably due to the inter- and intramolecular phosphonate–ammonium hydrogen bonds at pH 5 (**Figure 3.9**).

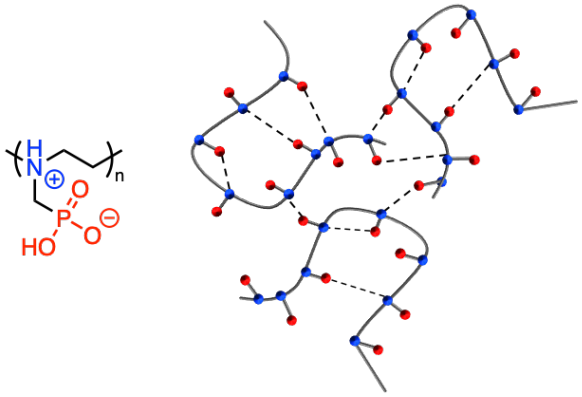


Figure 3.9. Inter- and intramolecular hydrogen bonding between protonated nitrogen and monophosphate within PEI-MP.

Using the ITC titration curve as a guide, we prepared a series of polymer–metal solutions at concentrations that corresponded to specific injections on the ITC titration curve using the same buffered solutions as in the ITC experiment (**Fig. 3.10**). When there is no metal ion present, the polymer exists primarily as unimolecular polymer chains or aggregates of a few chains in solution that are approximately 1–15 nm in size. As soon as metal ions are introduced into the polymer solution, extensive aggregation occurs. We hypothesize that this aggregation is due the formation of interchain coordination complexes with the phosphonic acid groups and REE ions. At the inflection point, the polymer–metal complexes form large aggregates (~825 nm) and then the aggregate size shrinks appreciably as the metal ion concentration continues to increase. We hypothesize that as the metal ion concentration increases, the degree of ionic crosslinking also

increases, collapsing the polymer structure and reducing the aggregate size analogous to reduced swelling with increasing crosslinking density in network polymers.[69]

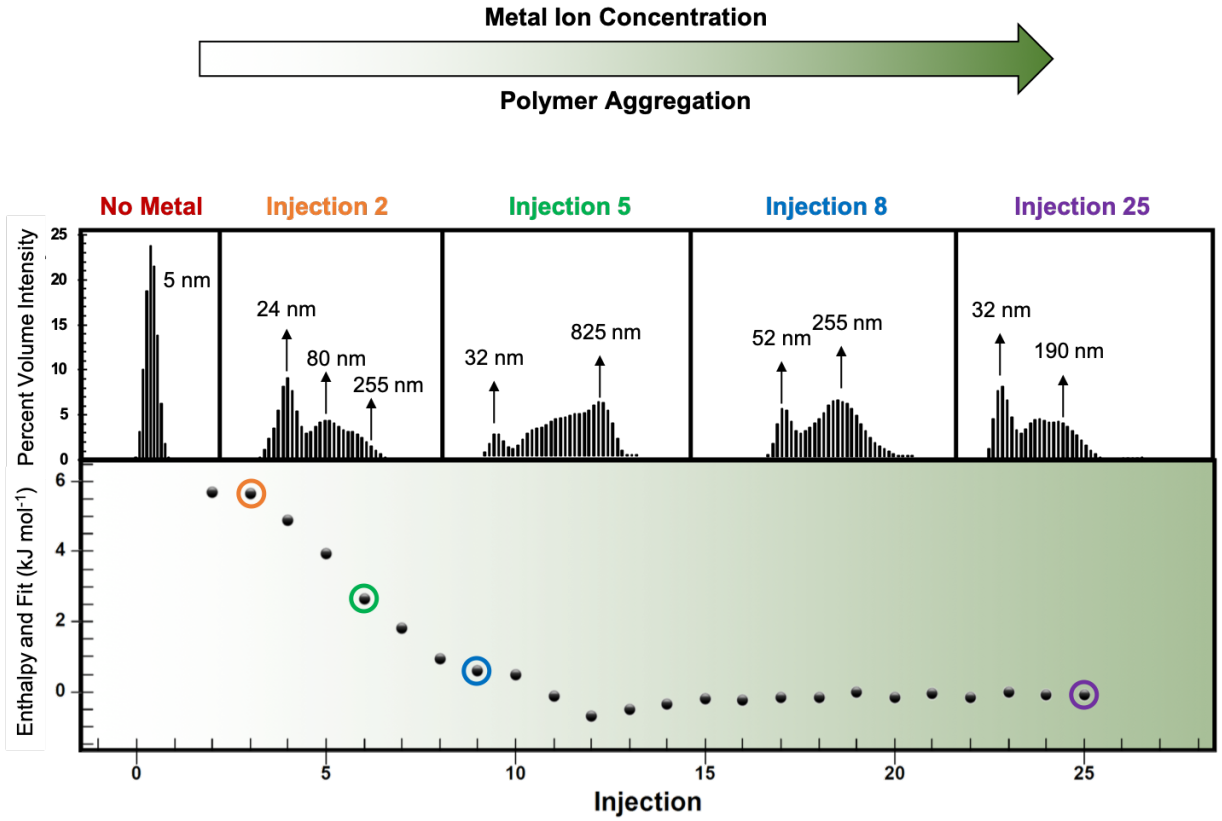


Figure 3.10. ITC thermograph with DLS particle size distribution (volume intensity) overlaid over the corresponding ITC injection. As metal-ion concentration increases, the size of the polymer aggregate increases.

3.4 Conclusions

In this work, we synthesized *linear* poly(ethyleneimine methylenephosophonate) and examined how the degree of polymerization and polymer functionalization affect polymer–REE binding thermodynamics and solution aggregation behavior. Using ITC, we observed consistent

binding thermodynamics across a series of six polymer molecular weights and five REEs. On average, the ΔG for the series of PEI-MP molecular weights and REEs was -30 ± 4 kJ mol^{-1}. DLS experiments revealed that *linear* PEI-MP in solution consists of primarily unimolecular polymer chains and a small amount of zwitterionic aggregates. As metal ions are added into the polymer solution, the polymer forms ionic aggregates.

Our ITC stoichiometry data suggest that PEI-MP serves as an effective and efficient multi-dentate ligand when binding to REEs. Comparing the thermodynamic and stoichiometry data obtained from our small molecule ITC studies with our linear PEI-MP ITC data indicate that the polymer structure does not impede or disrupt metal binding. By studying the thermodynamics and aggregation behavior of these polymer–metal interactions we have gained insight into the impact of polymer molecular weight and functionalization on metal binding with these polymers. This robust polymer system exhibited exergonic binding thermodynamics that are largely consistent across the series of molecular weights and percent polymer functionalization. The results presented here will guide the development of future metal-chelating polymers for corralling and purifying REEs.

Abbreviations

ITC: Isothermal Titration Calorimetry; REEs: Rare-Earth Elements; PEI-MP: poly(ethyleneimine methylene phosphonate)

3.5 References

1. Archer, W. R.; Fiorito, A.; Heinz-Kunert, S. L.; MacNicol, P. L.; Winn, S. A.; Schulz, M. D. Synthesis and Rare-Earth-Element Chelation Properties of Linear Poly(ethylenimine methylenephosphonate). *Macromolecules* **2020,** 53 (6), 2061–2068.
2. Nash, K. L.; Lumetta, G. J.; Clark, S. B.; Friese, J., Significance of the Nuclear Fuel Cycle in the 21st Century. In *Separations for the Nuclear Fuel Cycle in the 21st Century*, American Chemical Society: 2006; Vol. 933, pp 3-20.
3. Diallo, M. S.; Fromer, N. A.; Jhon, M. S. Nanotechnology for sustainable development: retrospective and outlook. *J. Nanopart. Res.* **2013,** 15 (11), 2044.
4. Elshkaki, A.; Graedel, T. E. Dysprosium, the balance problem, and wind power technology. *Appl. Energ.* **2014,** 136, 548-559.
5. Smith Stegen, K. Heavy rare earths, permanent magnets, and renewable energies: An imminent crisis. *Energ. Policy* **2015,** 79, 1-8.
6. Hatch, G. P. Dynamics in the Global Market for Rare Earths. *Elements* **2012,** 8, 341-346.
7. Sholl, D.; Lively, R. P. Seven chemical separations to change the world. *Nature* **2016,** 532 (435–437).
8. Massari, S.; Ruberti, M. Rare earth elements as critical raw materials: Focus on international markets and future strategies. *Resour. Policy* **2013,** 38 (1), 36–43.
9. Vahidi, E.; Zhao, F., Life Cycle Analysis for Solvent Extraction of Rare Earth Elements from Aqueous Solutions. In *REWAS 2016: Towards Materials Resource Sustainability*, Kirchain, R. E., Blanpain, B., Meskers, C., Olivetti, E., Apelian, D., Howarter, J., Kvithyld, A., Mishra, B., Neelameggham, N. R., Spangenberger, J., Eds. Springer International Publishing: Cham, 2016; pp 113-120.
10. Fu, F.; Wang, Q. Removal of heavy metal ions from wastewaters: A review. *J. Environ. Manage.* **2011,** 92, 407–418.
11. Archer, W. R.; Hall, B. A.; Thompson, T. N.; Wadsworth, O. J.; Schulz, M. D. Polymer sequestrants for biological and environmental applications. *Polym. Int.* **2019,** 68 (7), 1220-1237.
12. Nelson, J. J. M.; Schelter, E. J. Sustainable Inorganic Chemistry: Metal Separations for Recycling. *Inorg. Chem.* **2019,** 58 (2), 979-990.
13. Gergoric, M.; Barrier, A.; Retegan, T. Recovery of Rare-Earth Elements from Neodymium Magnet Waste Using Glycolic, Maleic, and Ascorbic Acids Followed by Solvent Extraction. *J. of Sustain. Met.* **2019,** 5 (1), 85-96.
14. Huang, K.; Jia, Y.; Wang, S.; Yang, J.; Zhong, H. A novel method for synthesis of styryl phosphonate monoester and its application in La(III) extraction. *J. Rare Earth.* [Online Early Access]. DOI: 10.1016/j.jre.2019.09.003. Published Online: Sept 20, 2019. https://www.sciencedirect.com/science/article/pii/S1002072119302479 (accessed Nov 21, 2019)
15. Barakat, M. A.; Schmidt, E. Polymer-Enhanced Ultrafiltration Process for Heavy Metals removal from industrical wastewater. *Desalination* **2010,** 256, 90–93.
16. Diallo, M.; Kotte, M. R.; Cho, M. Mining Critical Metals and Elements from Seawater: Opprotunities and Challenges. *Environ. Sci. Technol.* **2015,** 49, 9390–9399.
17. Battsengel, A.; Batnasan, A.; Narankhuu, A.; Haga, K.; Watanabe, Y.; Shibayama, A. Recovery of light and heavy rare earth elements from apatite ore using sulphuric acid leaching, solvent extraction and precipitation. *Hydrometallurgy* **2018,** 179, 100-109.

18. Diallo, M.; Christie, S.; Swaminathan, P.; Johnson, J.; Goddard, W. Dendrimer Enhanced Ultrafiltration. 1. Recovery of Cu(II) from aqueous solutions using PAMAM dendrimers with ethylene diamne core and terminal NH2 groups. *Environ. Sci. Technol.* **2005,** 29, 1366–1377.
19. Geckeler, K. E.; Volchek, K. Removal of Hazardous Substances from Water Using Ultrafiltration in Conjunction with Soluble Polymers. *Environ. Sci. Technol.* **1996,** 30 (3), 725-734.
20. Galhoum, A. A.; Elshehy, E. A.; Tolan, D. A.; El-Nahas, A. M.; Taketsugu, T.; Nishikiori, K.; Akashi, T.; Morshedy, A. S.; Guibal, E. Synthesis of polyaminophosphonic acid-functionalized poly(glycidyl methacrylate) for the efficient sorption of La(III) and Y(III). *Chem. Eng. J.* **2019,** 375, 121932.
21. Knight, A. S.; Zhou, E. Y.; Pelton, J. G.; Francis, M. B. Selective Chromium(VI) Ligands Identified Using Combinatorial Peptoid Libraries. *J. Am. Chem. Soc.* **2013,** 135 (46), 17488-17493.
22. Thanneeru, S.; Milazzo, N.; Lopes, A.; Wei, Z.; Angeles-Boza, A. M.; He, J. Synthetic Polymers To Promote Cooperative Cu Activity for O2 Activation: Poly vs Mono. *J. Am. Chem. Soc.* **2019,** 141 (10), 4252-4256.
23. Zhou, X.; Wang, L.; Wei, Z.; Weng, G.; He, J. An Adaptable Tough Elastomer with Moisture-Triggered Switchable Mechanical and Fluorescent Properties. *Advanced Functional Materials* **2019,** 29 (34), 1903543.
24. Hu, Y.; Florek, J.; Larivière, D.; Fontaine, F.-G.; Kleitz, F. Recent Advances in the Separation of Rare Earth Elements Using Mesoporous Hybrid Materials. *Chem. Rec.* **2018,** 18 (7-8), 1261-1276.
25. Mary, F.; Arrachart, G.; Leydier, A.; Pellet-Rostaing, S. Synthesis of organophosphorus ligands with a central oxygen atom and their applications in solvent extraction. *Tetrahedron* **2019,** 75 (30), 3968-3976.
26. Mitchell, L. A.; Holliday, B. J. Polymeric Materials for the Separation of f-Elements Utilizing Carbamoylmethylphosphine Oxide Chelating Ligands. *ACS Macro Letters* **2016,** 5 (10), 1100-1103.
27. Gomes Rodrigues, D.; Monge, S.; Pellet-Rostaing, S.; Dacheux, N.; Bouyer, D.; Faur, C. A new carbamoylmethylphosphonic acid-based polymer for the selective sorption of rare earth elements. *Chem. Eng. J.* **2019,** 371, 857-867.
28. Illy, N.; Couture, G.; Auvergne, R.; Caillol, S.; David, G.; Boutevin, B. New prospects for the synthesis of N-alkyl phosphonate/phosphonic acid-bearing oligo-chitosan. *RSC Advances* **2014,** 4 (46), 24042-24052.
29. Zhu, X.; Alexandratos, S. D. Development of a new ion-exchange/coordinating phosphate ligand for the sorption of U(VI) and trivalent ions from phosphoric acid solutions. *Chem. Eng. Sci.* **2015,** 127, 126-132.
30. Lahrouch, P.; Sofronov, O.; Creff, G.; Rossberg, A.; Hennig, C.; Den Auwer, C.; Di Giorgio, C. Polyethyleneimine methylphosphonate: towards the design of a new class of macromolecular actinide chelating agents in the case of human exposition. *Dalton Trans.* **2017,** 46, 13869-13877.
31. Popwell, S. J. S., M.D.; Wagener, K.B.; Batich, C.D.; Miler, R.J.; Lagmay, J.; and Bolch, W.E. . Synthesis of Polymeric Phosphonates for Selective Delivery of Radionuclides to Osteosarcoma. *Cancer Biother Radio* **2014,** 29 (7), 273-282.

32. Lahrouch, F.; Siberchicot, B.; Fèvre, J.; Leost, L.; Aupiais, J.; Solari, P. L.; Den Auwer, C.; Di Giorgio, C. Carboxylate- and Phosphonate-Modified Polyethylenimine: Toward the Design of Actinide Decorporation Agents. *Inorg. Chem.* **2020,** 59 (1), 128-137.
33. Abderrahim, O.; Didi, M. A.; Moreau, B.; Villemin, D. A New Sorbent for Selective Separation of Metal: Polyethylenimine Methylenephosphonic Acid. *Solvent Extraction and Ion Exchange* **2006,** 24 (6), 943-955.
34. Jansen, D. R.; Zeevaart, J. R.; Kolar, Z. I.; Djanashvili, K.; Peters, J. A.; Krijger, G. C. 31P NMR study of the valence stability of tin in its 1-hydroxyethylene-diphosphonate (HEDP) and N,N′,N′-trimethylenephosphonate-polyethyleneimine (PEI-MP) complexes. *Polyhedron* **2008,** 27 (6), 1779-1786.
35. Villemin, D.; Monteil, C.; Bar, N.; Didi, M. A. Phosphonated Polyethyleneimines (PEIP) as Multi-Use Polymers. *Phosphorus, Sulfur, and Silicon and the Related Elements* **2015,** 190 (5-6), 879-890.
36. Abderrahim, O.; Didi, M. A.; Villemin, D. Polyethyleneimine Methylenephosphonic Acid for the Solid-Phase Sorption of Lead(II). *Analytical Letters* **2009,** 42 (9), 1233-1244.
37. Abderrahim, O.; Didi, M. A.; Villemin, D. A new sorbent for uranium extraction: Polyethyleniminephenylphosphonamidic acid. *Journal of Radioanalytical and Nuclear Chemistry* **2009,** 279 (1), 237-244.
38. Bahulekar, R.; Ayyangar, N. R.; Ponrathnam, S. Polyethyleneimine in immobilization of biocatalysts. *Enzyme Microb. Tech.* **1991,** 13 (11), 858-868.
39. Kobayashi, S. Ethylenimine polymers. *Prog. Poly. Sci.* **1990,** 15 (5), 751-823.
40. Moedritzer, K.; Irani, R. R. The Direct Synthesis of α-Aminomethylphosphonic Acids. Mannich-Type Reactions with Orthophosphorous Acid. *J. Org. Chem.* **1966,** 31 (5), 1603-1607.
41. Wiesbrock, F.; Hoogenboom, R.; Leenen, M. A. M.; Meier, M. A. R.; Schubert, U. S. Investigation of the Living Cationic Ring-Opening Polymerization of 2-Methyl-, 2-Ethyl-, 2-Nonyl-, and 2-Phenyl-2-oxazoline in a Single-Mode Microwave Reactor. *Macromolecules* **2005,** 38 (12), 5025-5034.
42. Antonietti, L.; Aymonier, C.; Schlotterbeck, U.; Garamus, V. M.; Maksimova, T.; Richtering, W.; Mecking, S. Core−Shell-Structured Highly Branched Poly(ethylenimine amide)s: Synthesis and Structure. *Macromolecules* **2005,** 38 (14), 5914-5920.
43. Ghai, R.; Falconer, R.; Collins, B. Applications of isothermal titration calorimetry in pure and applied research—survey of the literature from 2010. *J. Mol. Recognit.* **2012,** 25, 32–52.
44. Turnbull, W. B.; Daranas, A. H. On the Value of c: Can Low Affinity Systems Be Studied by Isothermal Titration Calorimetry? *J. Am. Chem. Soc.* **2003,** 125 (48), 14859-14866.
45. Henzler, K.; Haupt, B.; Lauterbach, K.; Wittemann, A.; Borisov, O.; Ballauff, M. Adsorption of β-Lactoglobulin on Spherical Polyelectrolyte Brushes: Direct Proof of Counterion Release by Isothermal Titration Calorimetry. *J. Am. Chem. Soc.* **2010,** 132 (9), 3159-3163.
46. Arnaud, A.; Bouteiller, L. Isothermal Titration Calorimetry of Supramolecular Polymers. *Langmuir* **2004,** 20 (16), 6858-6863.
47. Moers, C.; Nuhn, L.; Wissel, M.; Stangenberg, R.; Mondeshki, M.; Berger-Nicoletti, E.; Thomas, A.; Schaeffel, D.; Koynov, K.; Klapper, M.; Zentel, R.; Frey, H. Supramolecular

Linear-g-Hyperbranched Graft Polymers: Topology and Binding Strength of Hyperbranched Side Chains. *Macromolecules* **2013,** 46 (24), 9544-9553.
48. Kelly, C. V.; Liroff, M. G.; Triplett, L. D.; Leroueil, P. R.; Mullen, D. G.; Wallace, J. M.; Meshinchi, S.; Baker, J. R.; Orr, B. G.; Banaszak Holl, M. M. Stoichiometry and Structure of Poly(amidoamine) Dendrimer−Lipid Complexes. *ACS Nano* **2009,** 3 (7), 1886-1896.
49. Lounis, F. M.; Chamieh, J.; Leclercq, L.; Gonzalez, P.; Geneste, A.; Prelot, B.; Cottet, H. Interactions between Oppositely Charged Polyelectrolytes by Isothermal Titration Calorimetry: Effect of Ionic Strength and Charge Density. *J. Phys. Chem. B* **2017,** 121 (12), 2684-2694.
50. Sinn, C. G.; Dimova, R.; Antonietti, M. Isothermal Titration Calorimetry of the Polyelectrolyte/Water Interaction and Binding of Ca2+: Effects Determining the Quality of Polymeric Scale Inhibitors. *Macromolecules* **2004,** 37, 3444–3450.
51. Chiad, K.; Stelzig, S.; Gropeanu, R.; Weil, T.; Klapper, M.; Mullen, K. Isothermal Titration Calorimetry: A Powerful Technique to Quantify the Interactions in Polymer Hybrid Systems. *Macromolecules* **2009,** 42, 7545–7552.
52. Kabiri, M.; Unsworth, L. D. Application of Isothermal Titration Calorimetry for Characterizing Thermodynamic Parameters of Biomolecular Interactions: Peptide Self-Assembly and Protein Adsorption Case Studies. *Biomacromolecules* **2014,** 15 (10), 3463-3473.
53. Feng, X.; Leduc, M.; Pelton, R. Polyelectrolyte complex characterization with isothermal titration calorimetry and colloid titration. *Colloid Surface A* **2008,** 317 (1), 535-542.
54. Cawthray, J. F.; Creagh, A. L.; Haynes, C. A.; Orvig, C. Ion Exchange in Hydroxyapatite with Lanthanides. *Inorg. Chem.* **2015,** 54 (4), 1440-1445.
55. *CRC handbook of chemistry and physics*. 100th ed.; CRC Press: 2019.
56. Bian, X.; Lockless, S. W. Preparation To Minimize Buffer Mismatch in Isothermal Titration Calorimetry Experiments. *Anal. Chem.* **2016,** 88 (10), 5549-5553.
57. Report on Rare Earth Elements from Coal and Coal Byproducts. Energy, D. O., Ed. 2017.
58. Steed, J. W.; Atwood, J. L., *Supramolecular Chemsitry*. John Wiley & Sons: 2013.
59. Ellis, R. J.; Brigham, D. M.; Delmau, L.; Ivanov, A. S.; Williams, N. J.; Vo, M. N.; Reinhart, B.; Moyer, B. A.; Bryantsev, V. S. "Straining" to Separate the Rare Earths: How the Lanthanide Contraction Impacts Chelation by Diglycolamide Ligands. *Inorg. Chem.* **2017,** 56 (3), 1152-1160.
60. Martinez-Gomez, N. C.; Vu, H. N.; Skovran, E. Lanthanide Chemistry: From Coordination in Chemical Complexes Shaping Our Technology to Coordination in Enzymes Shaping Bacterial Metabolism. *Inorg. Chem.* **2016,** 55 (20), 10083-10089.
61. Franz, R. G. Comparisons of pKa and log P values of some carboxylic and phosphonic acids: Synthesis and measurement. *AAPS PharmSci* **2001,** 3 (2), 1.
62. Sevrain, C. M.; Berchel, M.; Couthon, H.; Jaffrès, P.-A. Phosphonic acid: preparation and applications. *Beilstein J. Org. Chem.* **2017,** 13, 2186-2213.
63. Saleh, T. A.; Rachman, I. B.; Ali, S. A. Tailoring hydrophobic branch in polyzwitterionic resin for simultaneous capturing of Hg(II) and methylene blue with response surface optimization. *Sci. Rep.* **2017,** 7 (1), 4573.
64. Lowe, A. B.; McCormick, C. L. Synthesis and Solution Properties of Zwitterionic Polymers. *Chem. Rev.* **2002,** 102 (11), 4177-4190.

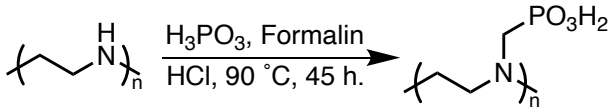
65. Weller, D.; Medina-Oliva, A.; Claus, H.; Gietzen, S.; Mohr, K.; Reuter, A.; Schäffel, D.; Schöttler, S.; Koynov, K.; Bros, M.; Grabbe, S.; Fischer, K.; Schmidt, M. Solution Properties and Potential Biological Applications of Zwitterionic Poly(ε-N-methacryloyl-l-lysine). *Macromolecules* **2013,** 46 (21), 8519-8527.
66. Ezhova, A.; Huber, K. Contraction and Coagulation of Spherical Polyelectrolyte Brushes in the Presence of Ag+, Mg2+, and Ca2+ Cations. *Macromolecules* **2016,** 49 (19), 7460-7468.
67. Lages, S.; Goerigk, G.; Huber, K. SAXS and ASAXS on Dilute Sodium Polyacrylate Chains Decorated with Lead Ions. *Macromolecules* **2013,** 46 (9), 3570-3580.
68. Morishima, K.; Ishiwari, F.; Matsumura, S.; Fukushima, T.; Shibayama, M. Mesoscopic Structural Aspects of Ca2+-Triggered Polymer Chain Folding of a Tetraphenylethene-Appended Poly(acrylic acid) in Relation to Its Aggregation-Induced Emission Behavior. *Macromolecules* **2017,** 50 (15), 5940-5945.
69. Ezhova, A.; Huber, K. Specific Interactions of Ag+ Ions with Anionic Polyacrylate Chains in Dilute Solution. *Macromolecules* **2014,** 47 (22), 8002-8011.
70. Flory, P. J.; Rehner, J. Statistical Mechanics of Cross-Linked Polymer Networks II. Swelling. *J. Chem. Phys.* **1943,** 11 (11), 521-526.

3.6 Supporting Information

Materials Synthesis and Characterization

Linear polyethyleneimine was purchased from PolySciences. $YCl_3 \cdot 6H_2O$, $SmCl_3 \cdot 6H_2O$, $DyCl_3 \cdot 6H_2O$, $EuCl_3 \cdot 6H_2O$, and $TbCl_3 \cdot 6H_2O$ (trace metals grade), pyridine, and H_3PO_3 were purchased from Sigma Aldrich. Formalin (37 wt% solution, ACS grade), and diethylenetriaminepentaskis(methylphosphonic acid) were purchased from Oakwood chemical. Concentrated HCl (*aq*) was purchased from Fisher Scientific. Dialysis bags (pre-treated regenerated cellulose tubing, 1 kDa molecular weight cut-off) were purchased from Spectrum Labs. All chemicals were used as-is.

Polymer Functionalization



Scheme 3.S1. Synthesis of linear poly(ethyleneimine methylphosphonate) (PEI-MP)

Poly(ethylene imine) was functionalized as depicted in Scheme **3**.**S1**. In general, H_3PO_3 (21.0 mmol, 5.0 eq.) and linear poly(ethyleneimine) (4.2 mmol, 1.0 eq.) were added to 2 mL of concentrated HCl (*aq.*) and 1.5 mL of DI water in a 25 mL round bottom flask with a magnetic stir bar and heated to 90 ˚C. Formalin (18.5 mmol, 4.0 eq.) was added dropwise over the course of one hour and the mixture was refluxed at 90˚C for 4 hours. After 4 hours, additional formalin (18.5 mmol, 4.0 eq.) was added dropwise over one hour and continued to reflux for 40 hours. The reaction mixture was cooled to RT, placed in a dialysis bag, and dialyzed against DI water to remove excess reagents. The polymer product was collected after evaporation of the water

following dialysis. The degree of polymer functionalization was determined using the P/N ratio obtained from elemental analysis (**Table 3.S1 and 3.S2**).

Isothermal Titration Calorimetry

The ITC instrument used was an Affinity-ITC (TA Instruments, New Castle, DE), which operated at constant temperature of 298 K. To carry out a binding experiment, a sample solution was prepared by dissolving PEI-MP in a pH 5.0, 100 mM pyridine buffer. To ensure consistent ionic strength, the PEI-MP solution was dialyzed against the buffer solution and the final concentration of PEI-MP was determined by UV-Vis spectroscopy. Metal ion solutions were prepared using the dialysis flow-through.

Before the ITC experiment, each solution was degassed for 15 minutes. The PEI-MP solution was placed in the sample cell (350 μL) and the reference cell was filled with water (300 μL). Both cells were mounted in an adiabatic chamber, whose temperature was kept constant during the measurement (295 K). A long-needle syringe with a twisted paddle fastened to its end, was filled with the metal ion solution. The syringe was placed inside the sample cell, and the entire syringe assembly was rotated continuously (185 RPM) to provide proper mixing of the content of the sample cell within a few seconds after an injection. After reaching thermal equilibrium, the injection of the metal ion solution was automatically conducted stepwise until the PEI-MP was saturated with the metal ion. Due to the possible dilution of the first measurement, the first injection was ignored in the analysis of data, which is standard practice for ITC experiments. The first 1.0 μL injection was followed by a series of injections of 2.0 μL each. The chosen time interval between two consecutive injections was 300 seconds to ensure that the thermodynamic equilibrium was reached before the next injection.

For the ITC analysis of diethylenetriaminepentaskis(methylphosphonic acid) (DETMP), DETMP was dissolved in pH 5.0, 100 mM pyridine buffer. Metal ion solutions were made using an identical buffer. Dilution enthalpies from the control experiment were subtract before curve fitting.

Nonlinear least-squares curve fitting was conducted using TA Instruments Nano Analyze using TA Instruments Independent model. Heats of dilution from control titrations (metal-ion into buffer (*without PEI-MP present*), and buffer into PEI-MP (*without metal-ion present*)) were subtracted before curve fitting.

Dynamic Light Scattering

Dynamic light scattering and zeta potential measurements were conducted using a Malvern Instruments (Worchestershire, UK) Zetasizer Nano-ZS. Samples were filtered using .22 μm filters before analysis. Following a 2-minute equilibration, samples were recorded for 120 seconds and three accumulated runs were averaged to obtain the particle size distribution. The particle size distributions are reported as percent volume intensity.

Table 3.S1. Theoretical and experimental combustion analysis results for molecular weight PEI-MP series. P/N ratio was used to calculate % functionalization.

	Theoretical Composition (%)	**Experimental Composition (%) MW of PEI Used**					
		2.5 kDa	**5.7 kDa**	**25 kDa**	**87 kDa**	**100 kDa**	**250 kDa**
% C	26.3	26.5	26.3	26.8	24.0	26.4	26.0
% H	5.9	7.3	6.8	7.2	6.7	7.2	7.2
% N	10.2	9.8	9.9	10.1	8.9	10.0	9.7
% P	22.6	17.4	16.5	18.6	16.9	16.1	16.9
P/N	2.1	1.7	1.6	1.8	1.8	1.6	1.7
C/N	2.6	2.7	2.6	2.6	2.7	2.6	2.7
% Functionalization	100	80.9	76.2	85.7	85.7	76.2	80.9

Table 3.S2. Theoretical and experimental combustion analysis results for functionalization PEI-MP series. P/N ratio was used to calculate % functionalization.

	Theoretical Composition (%)	**Experimental Composition (%) MW of PEI Used**			
		87 kDa	**87 kDa**	**87 kDa**	**87 kDa**
% C	26.3	47.4	28.2	27.9	24.0
% H	5.9	10.7	7.2	8.2	6.7
% N	10.2	30.7	10.9	10.6	8.9
% P	22.6	10.92	14.3	14.7	16.9
P/N	2.1	0.36	1.3	1.4	1.8
C/N	2.6	1.5	2.6	2.6	2.6
% Functionalization	100	16.1	59.6	66.7	85.7

Figure 3.S1: Representative ^{1}H NMR Spectra of functionalized PEI

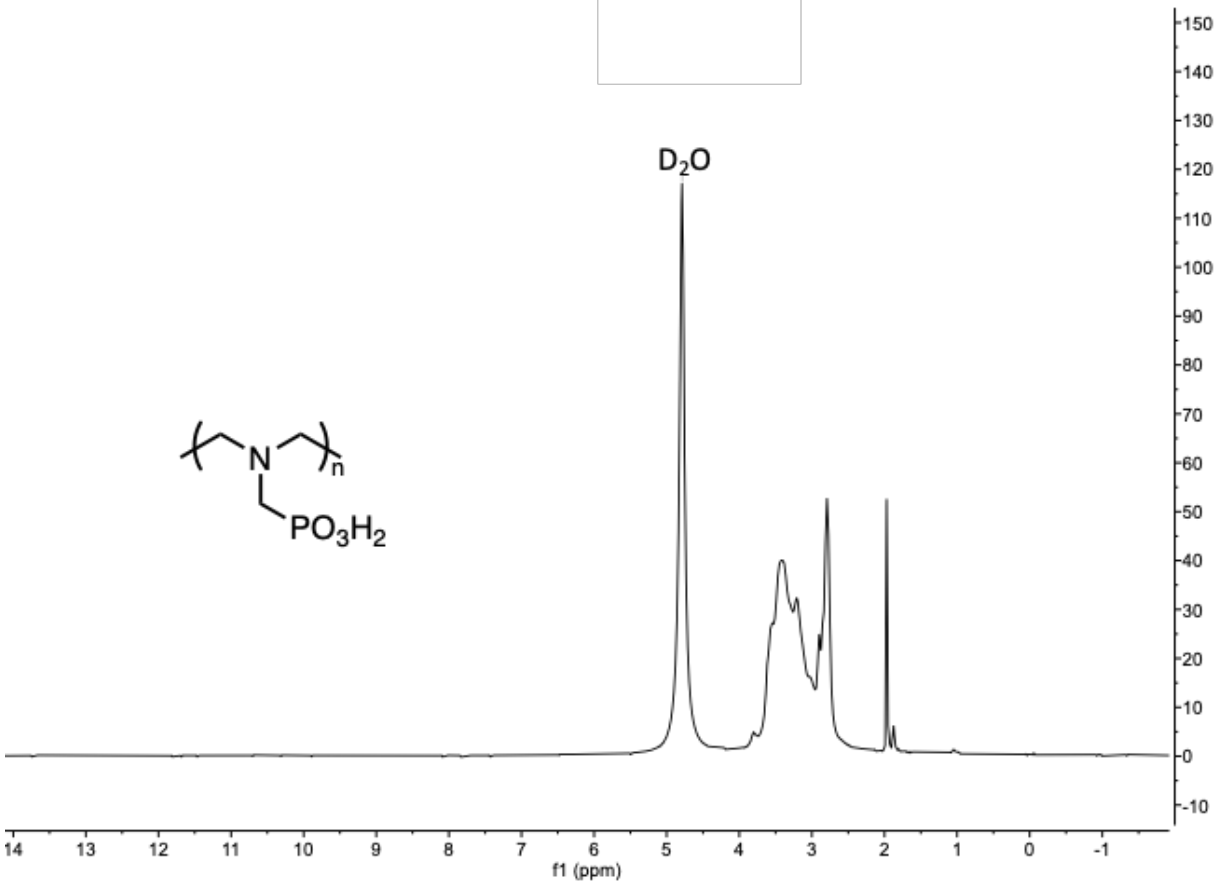


Figure 3.S2: Representative ^{31}P NMR Spectra of functionalized PEI.

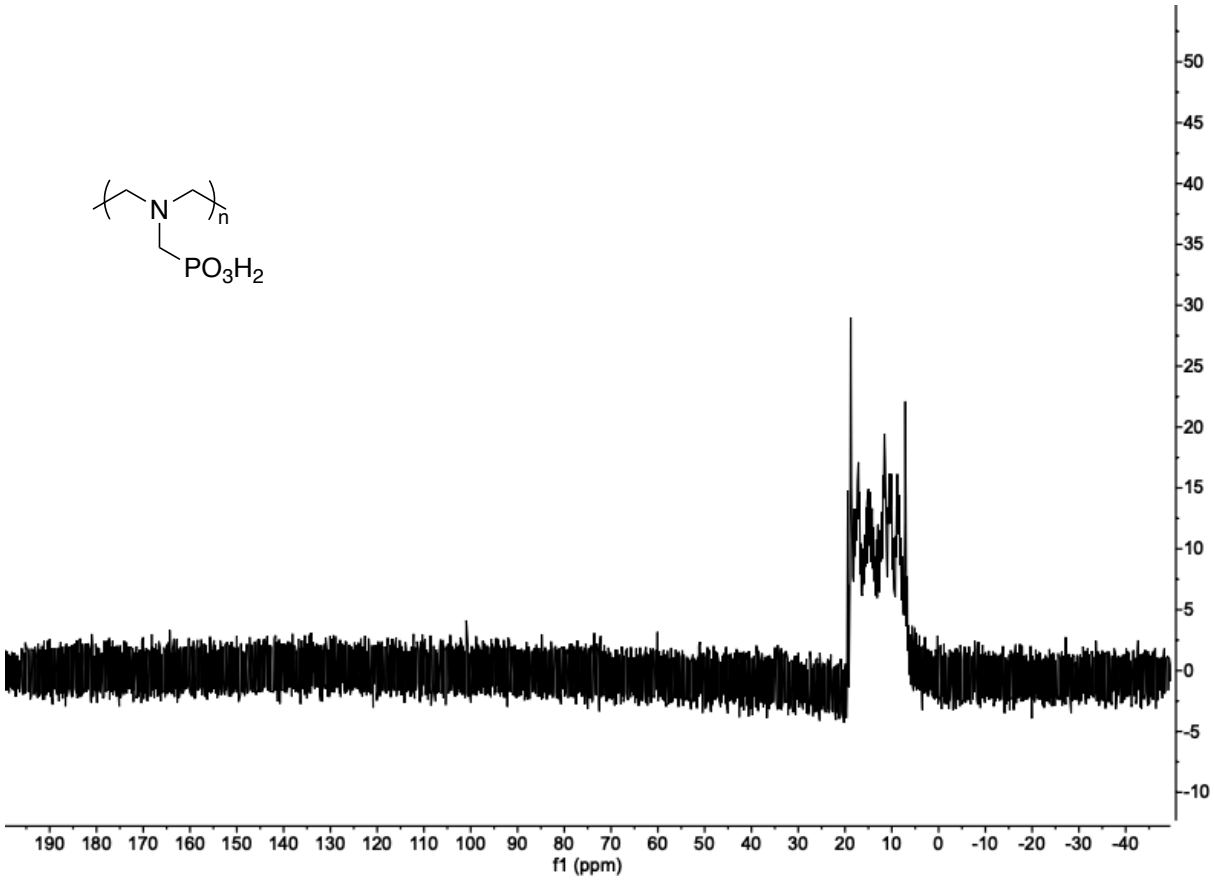


Figure 3.S3: Representative IR Spectra of functionalized PEI.

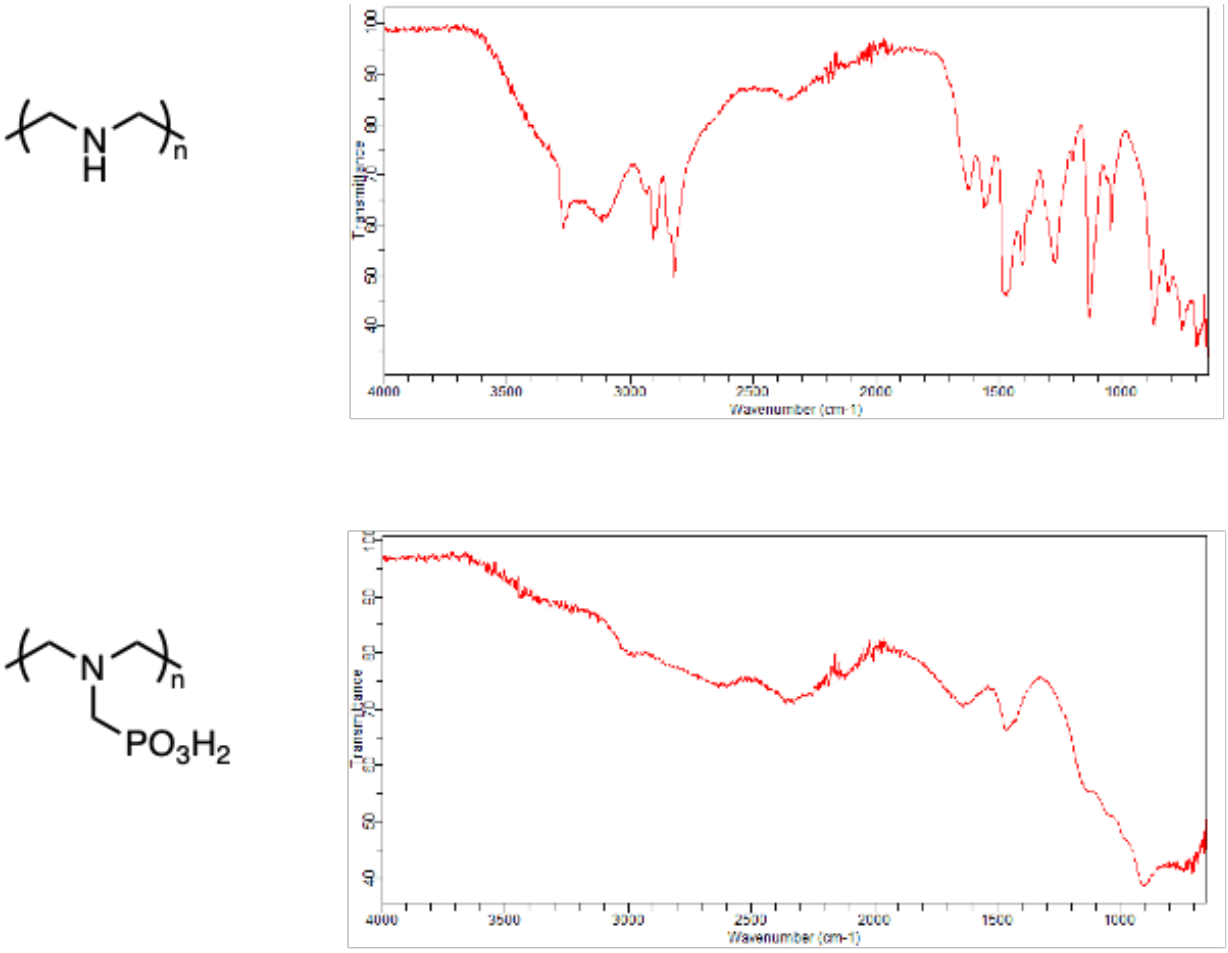


Table 3.S3: Metal and polymer concentrations used for molecular weight effect ITC studies. The concentration of PEI-MP is reported with respect to the concentration of functionalized repeat unit.

Sample	Concentration (mM)					
Molecular Weight of PEI (kDa)	**PEI-MP**	**Y(III)**	**Sm(III)**	**Eu(III)**	**Dy(III)**	**Tb(III)**
7	1.47	4.9	6.1	4.9	4.7	4.9
15	1.35	3.5	2.2	2.1	2.6	1.9
70	1.41	2.6	2.2	2.5	1.3	2.6
246	1.27	7.4	8.1	7.3	7.6	8.6
258	1.34	3.4	3.6	3.3	3.5	3.5
680	1.40	4.8	4.8	4.8	4.6	4.4

Table 3.S4: Metal and polymer concentrations used for functionalization effect ITC studies. The concentration of PEI-MP is reported with respect to the concentration of functionalized repeat unit.

Sample	Concentration (mM)					
Percent Functionalization of PEI	**PEI-MP**	**Y(III)**	**Sm(III)**	**Dy(III)**	**Eu(III)**	**Tb(III)**
85.7	1.6	7.4	8.1	7.3	7.6	8.6
66.7	1.3	5.9	6.8	6.9	5.0	6.2
59.6	1.4	6.9	6.6	2.9	4.5	4.5
16.1	0.56	3.4	2.2	2.6	2.1	1.9

Figure 3.S4. Representative ITC thermograph showing Sm(III) titration into 680 kDa PEI-MP, polymer into buffer blank, and metal ion into buffer blank titrations.

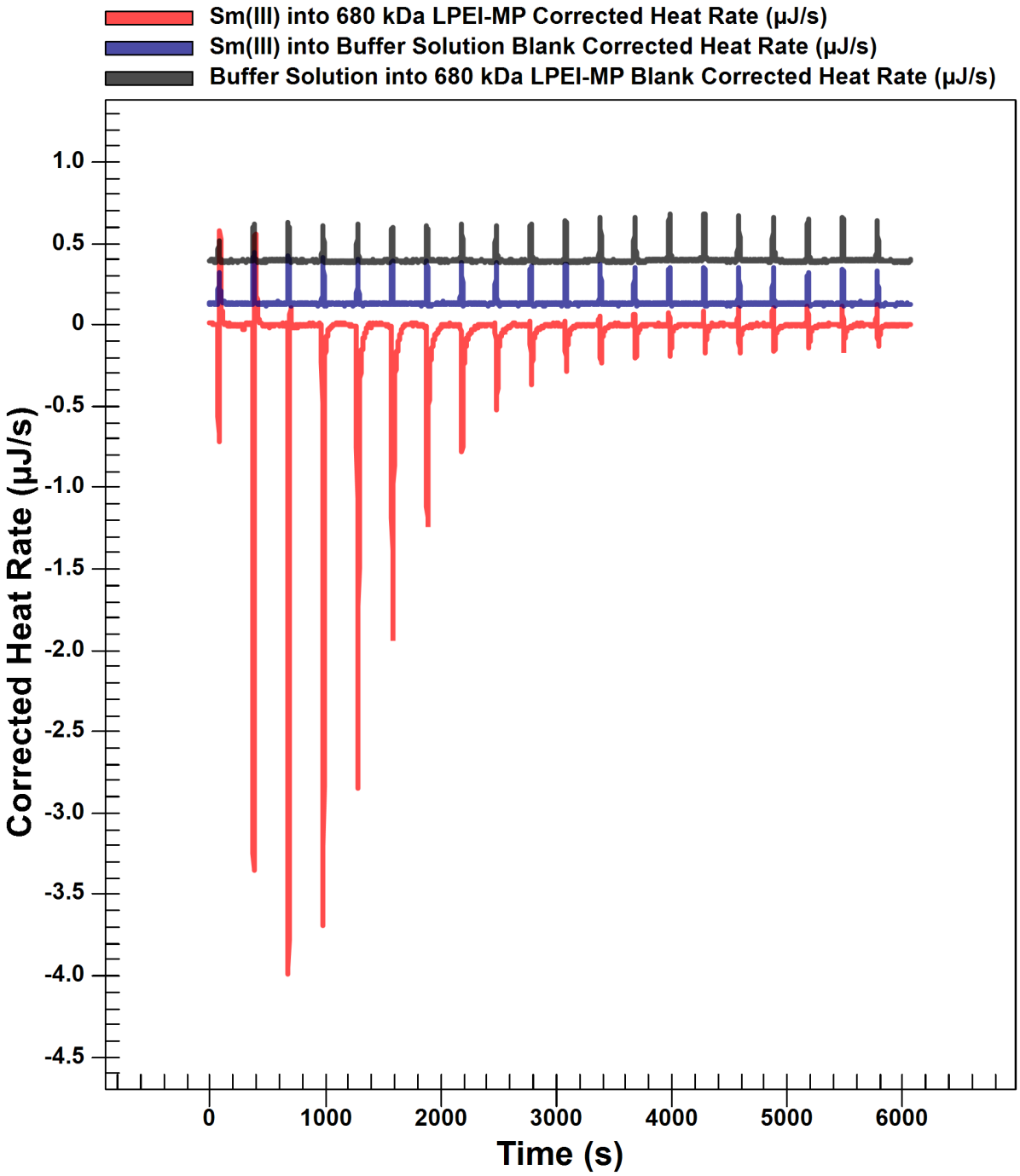


Figure 3.S5: ITC Thermograph of Eu(III) titration into unfunctionalized PEI

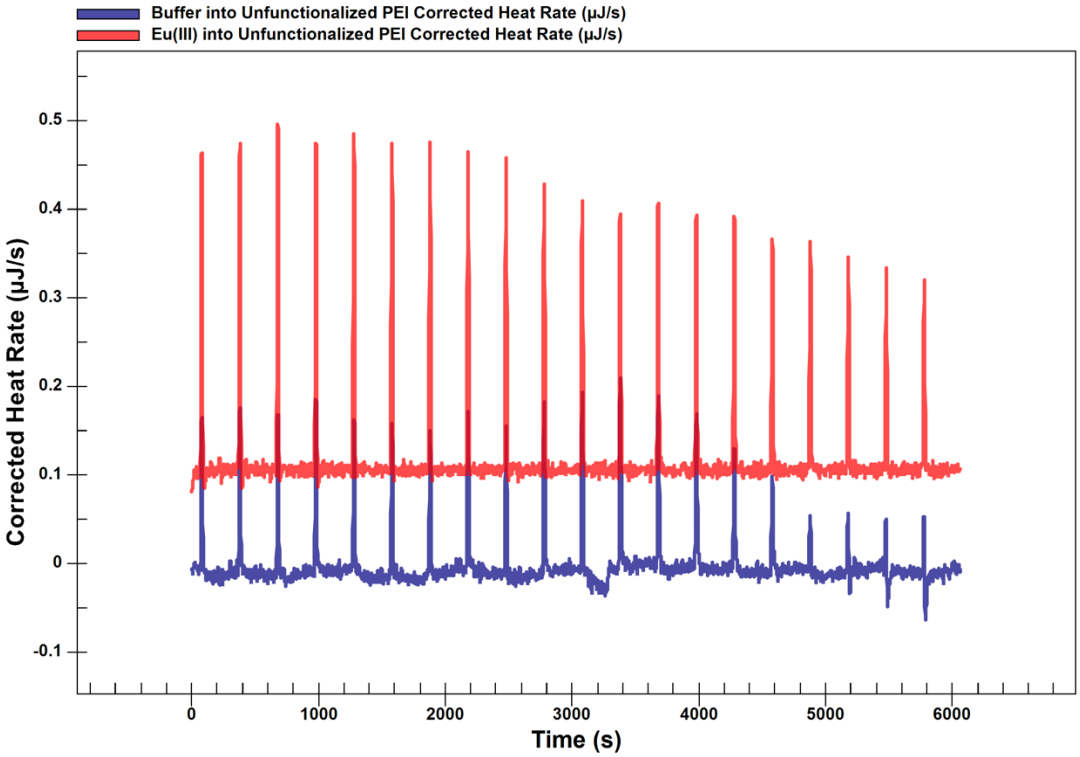


Figure 3.S6. ITC thermographs of 7 kDa PEI-MP (80.9% functionalized) and **a**) Y(III), **b**) Sm(III), **c**) Eu(III), **d**) Tb(III), and **e)** Dy(III).

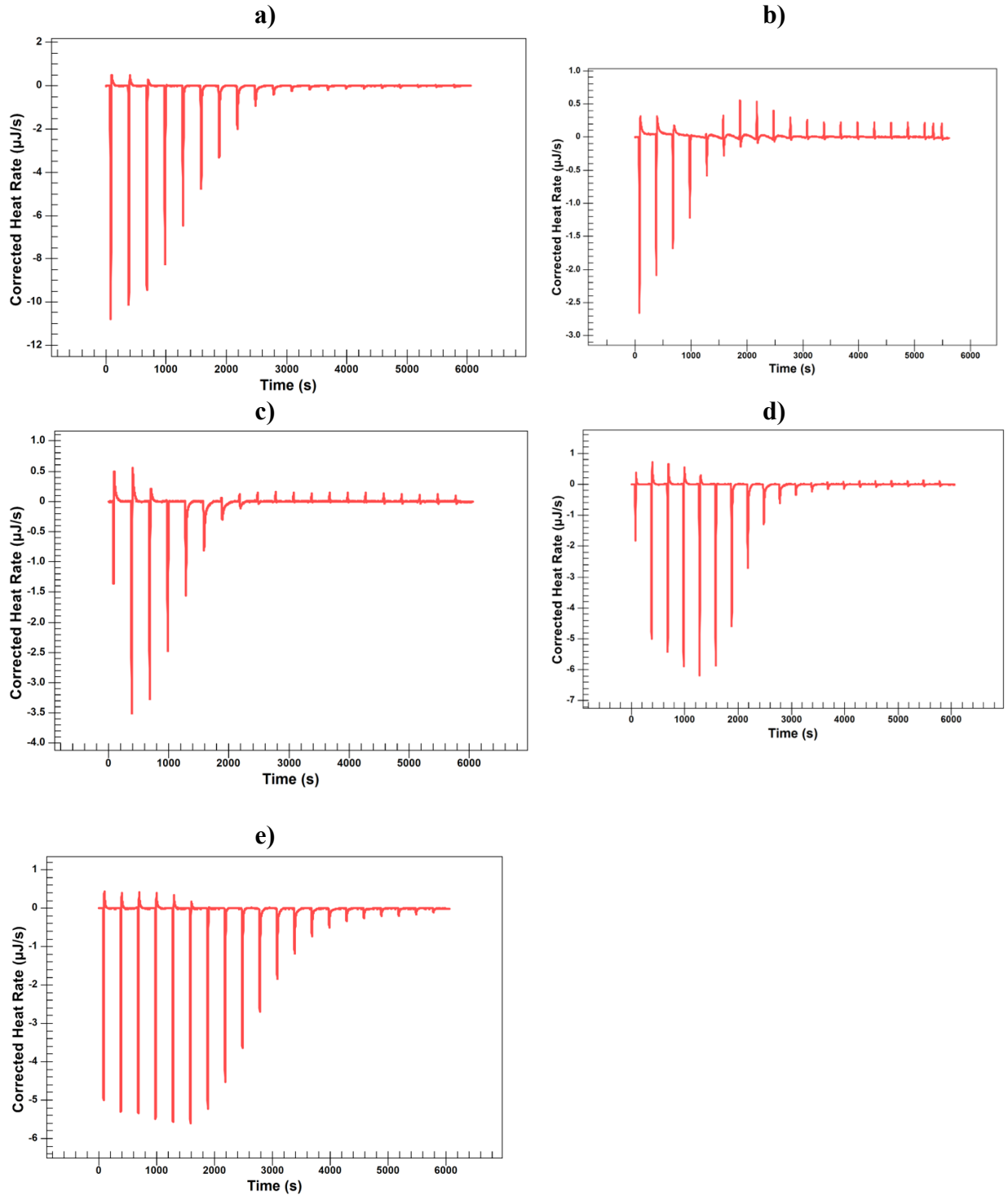


Figure 3.S7. ITC thermographs of 15 kDa PEI-MP (76.2% functionalized) and **a**) Y(III), **b**) Sm(III), **c**) Eu(III), **d**) Tb(III), and, **e)** Dy(III).

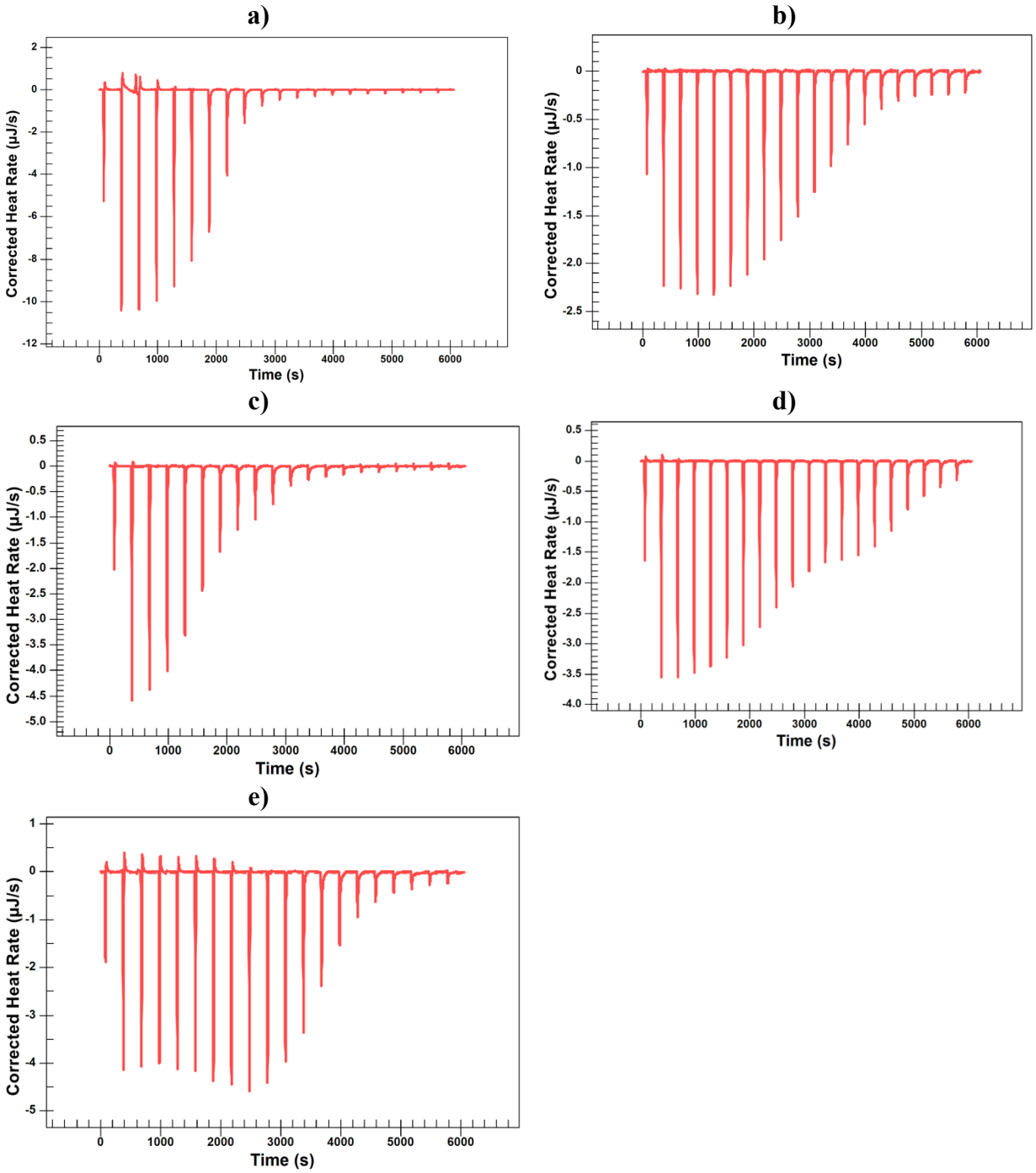


Figure 3.S8. ITC thermographs of 70 kDa PEI-MP (85.7% functionalized) and **a**) Y(III), **b**) Sm(III), **c**) Eu(III), **d**) Tb(III), and **e)** Dy(III).

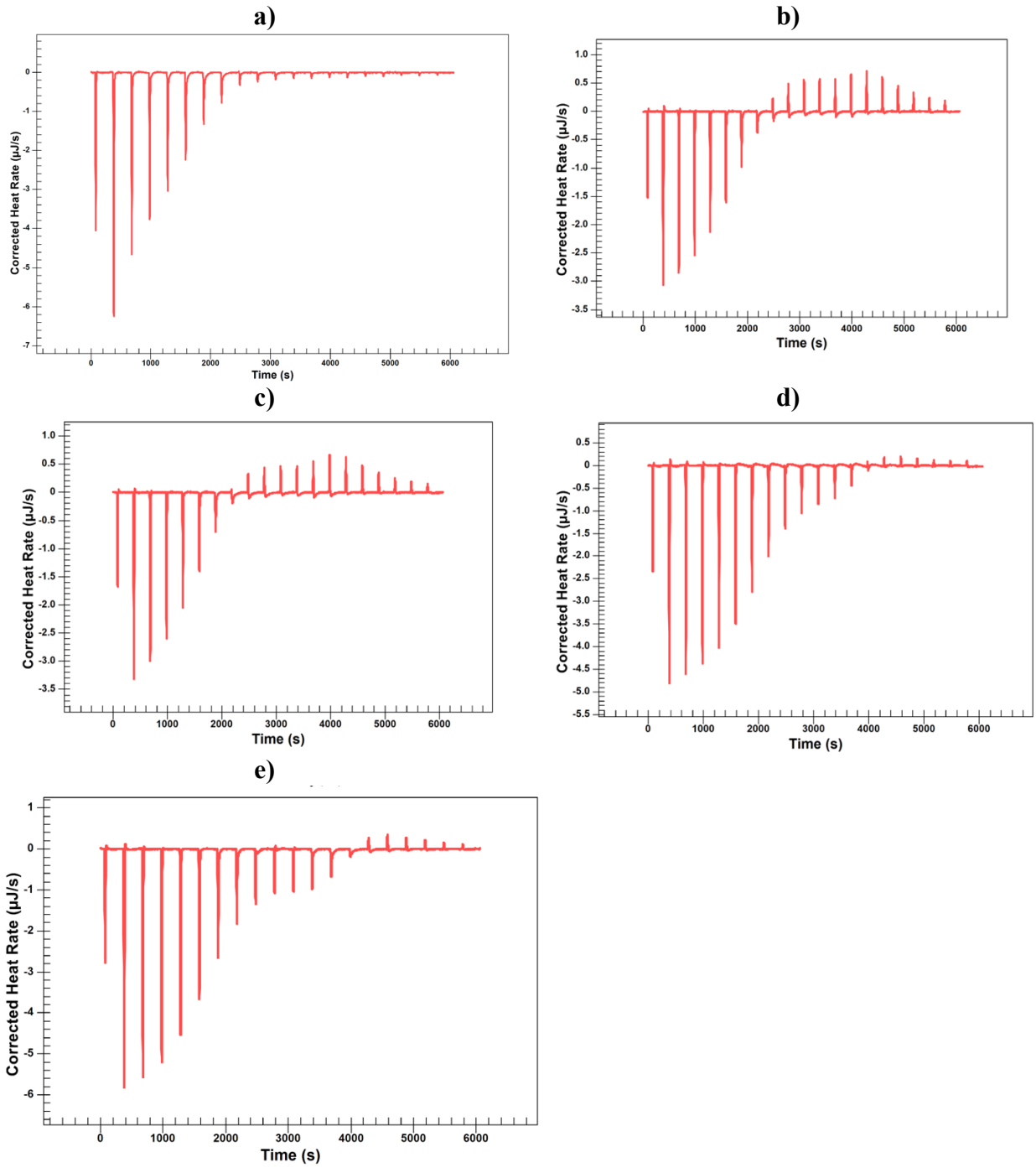


Figure 3.S9. ITC thermographs of 246 kDa PEI-MP (85.7% functionalized) and **a**) Y(III), **b**) Sm(III), **c**) Eu(III), **d**) Tb(III), and **e)** Dy(III).

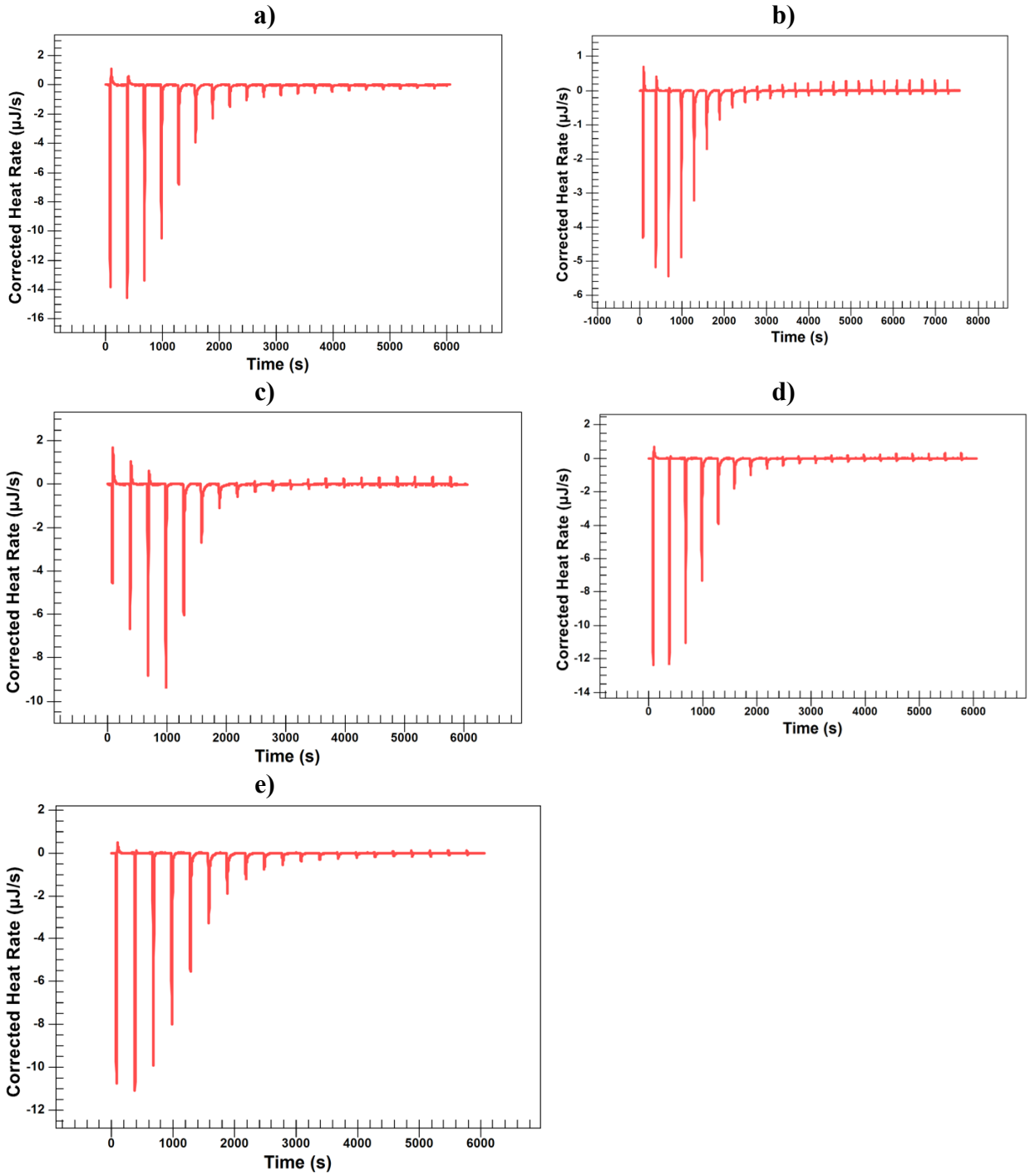


Figure 3.S10. ITC thermographs of 258 kDa PEI-MP (76.2% functionalized) and **a**) Y(III), **b**) Sm(III), **c**) Eu(III), **d**) Tb(III), and **e)** Dy(III).

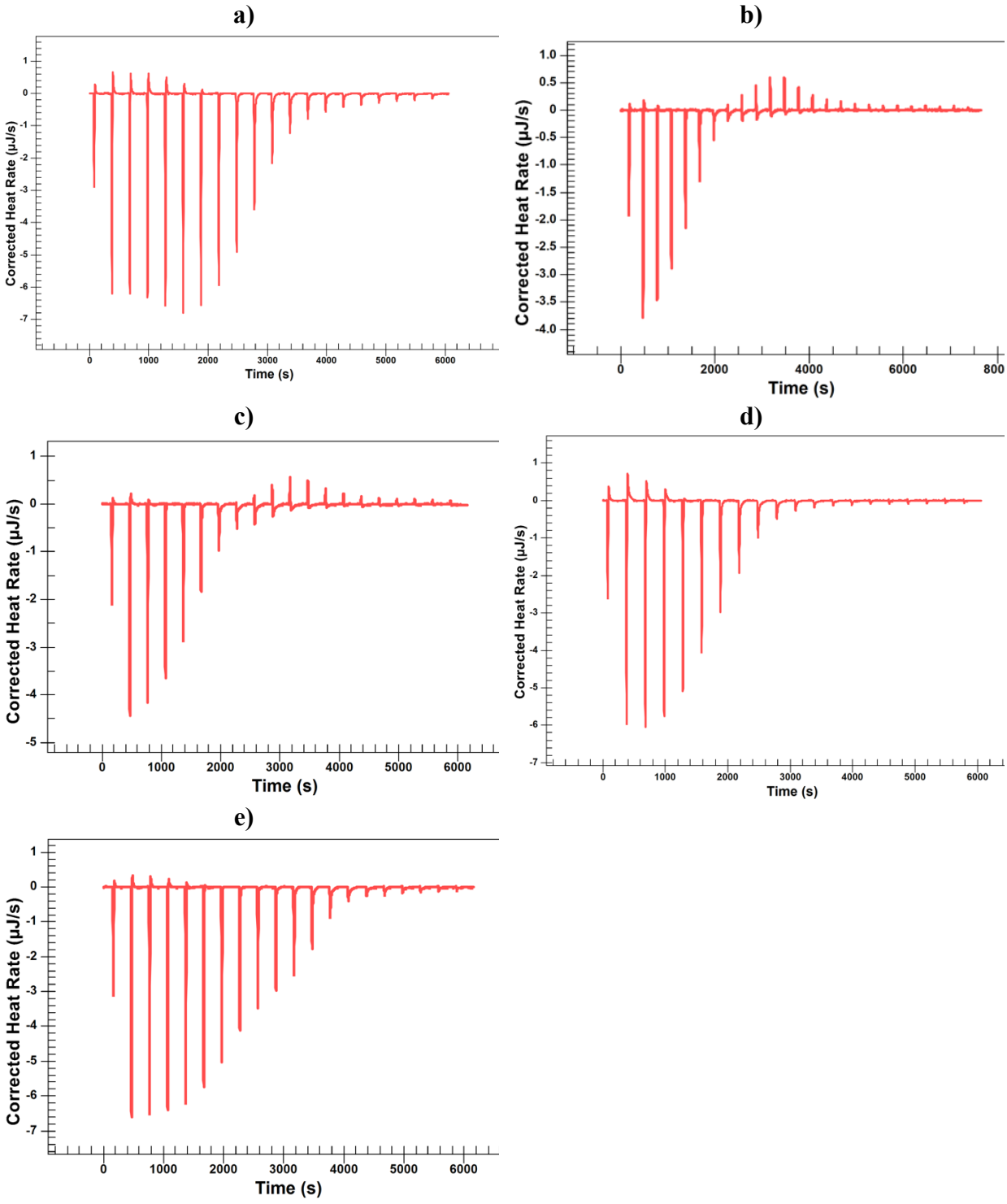


Figure 3.S11. ITC thermographs of 680 kDa PEI-MP (80.9% functionalized) and **a**) Y(III), **b**) Sm(III), **c**) Eu(III), **d**) Tb(III), and **e)** Dy(III).

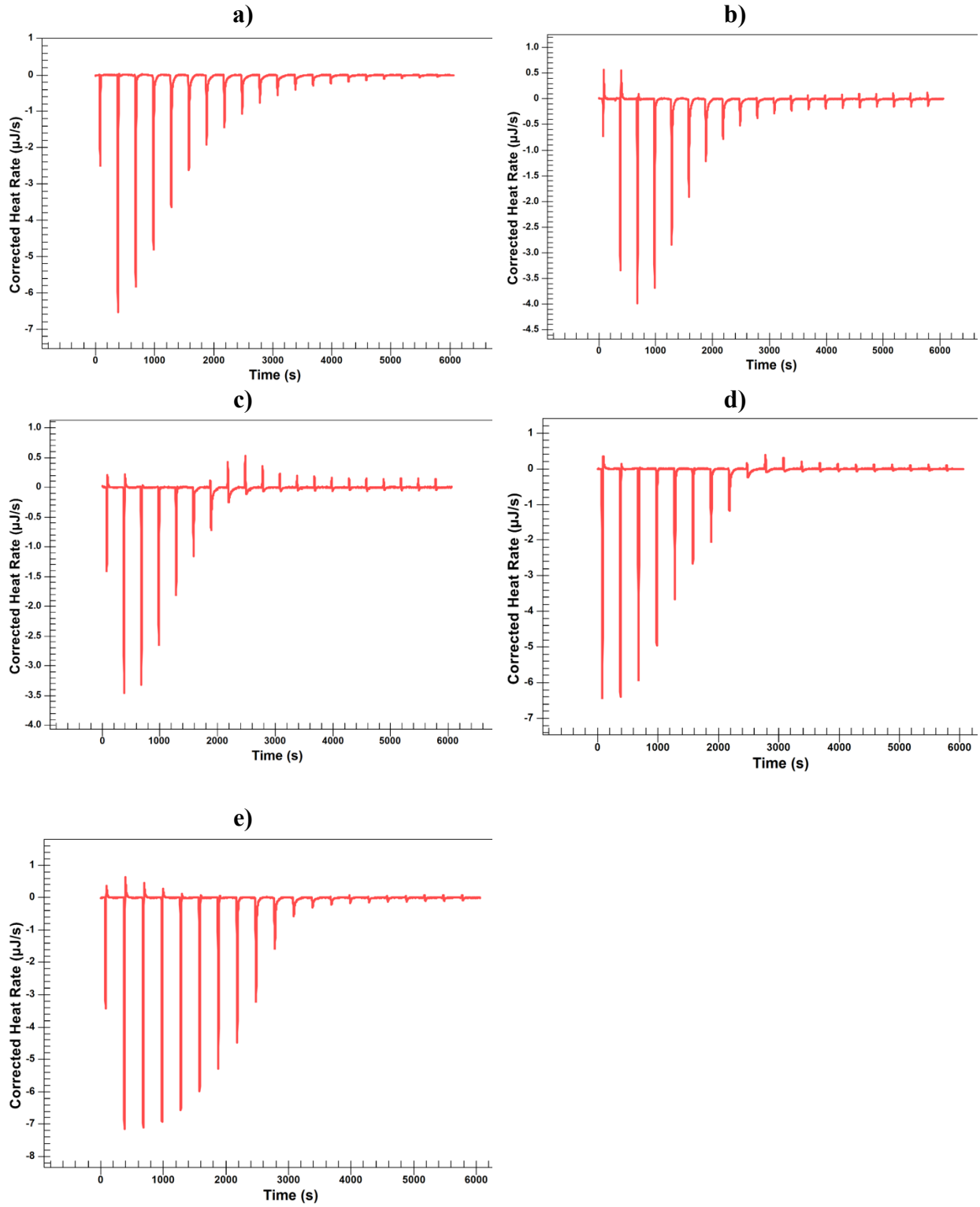


Figure 3.S12. ITC thermographs of 85% functionalized 87 kDa PEI-MP and **a**) Y(III), **b**) Sm(III), **c**) Eu(III), **d**) Tb(III), and **e)** Dy(III).

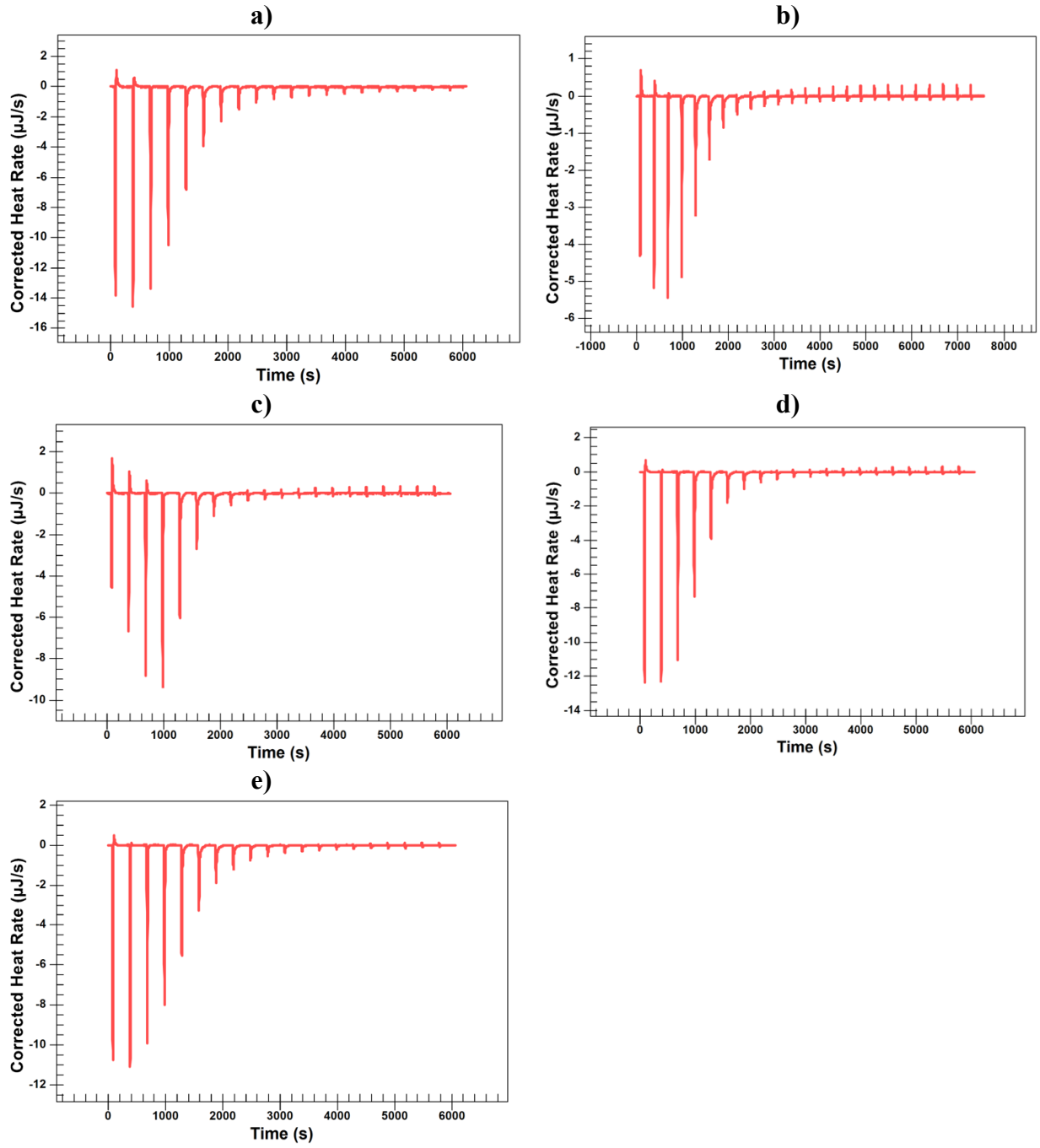
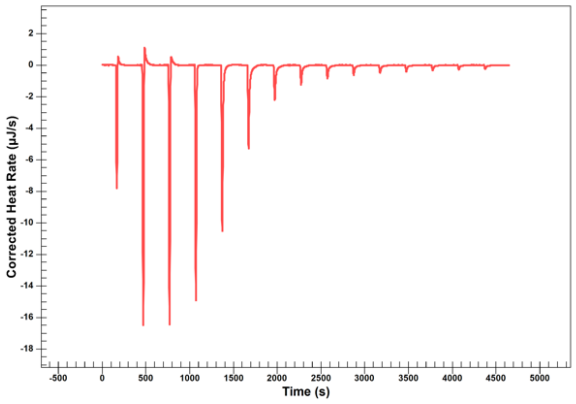
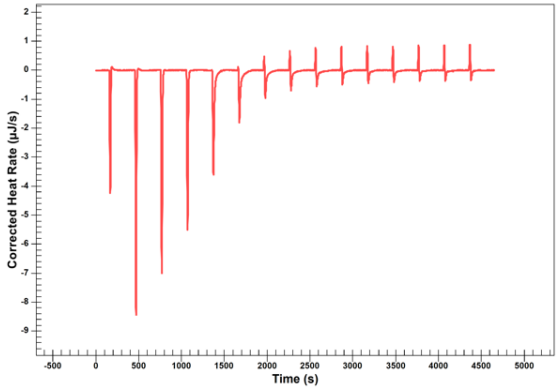


Figure 3.S13. ITC thermographs of 66% functionalized 87 kDa PEI-MP and **a**) Y(III), **b**) Sm(III), **c**) Eu(III), **d**) Tb(III), and **e)** Dy(III).

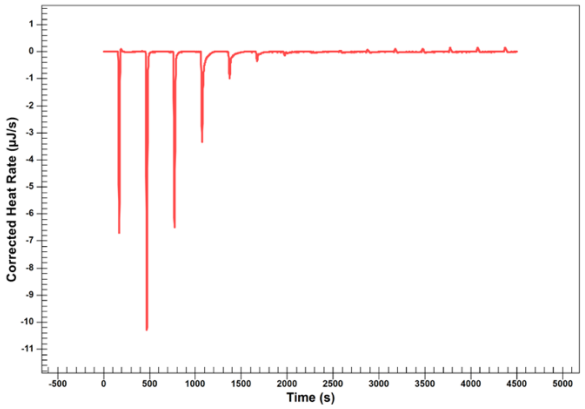
a)


Corrected Heat Rate (µJ/s)
Time (s)

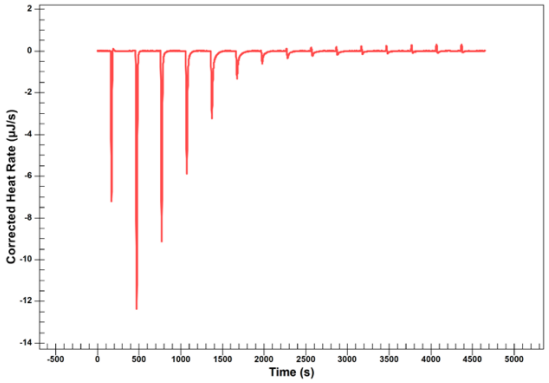
b)


Corrected Heat Rate (µJ/s)
Time (s)

c)


Corrected Heat Rate (µJ/s)
Time (s)

d)


Corrected Heat Rate (µJ/s)
Time (s)

e)

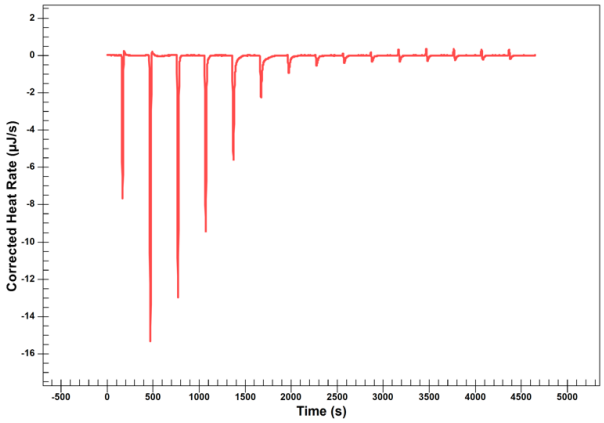

Corrected Heat Rate (µJ/s)
Time (s)

Figure 3.S14. ITC thermographs of 59% functionalized 87 kDa PEI-MP and **a**) Y(III), **b**) Sm(III), **c**) Eu(III), **d**) Tb(III), and **e)** Dy(III).

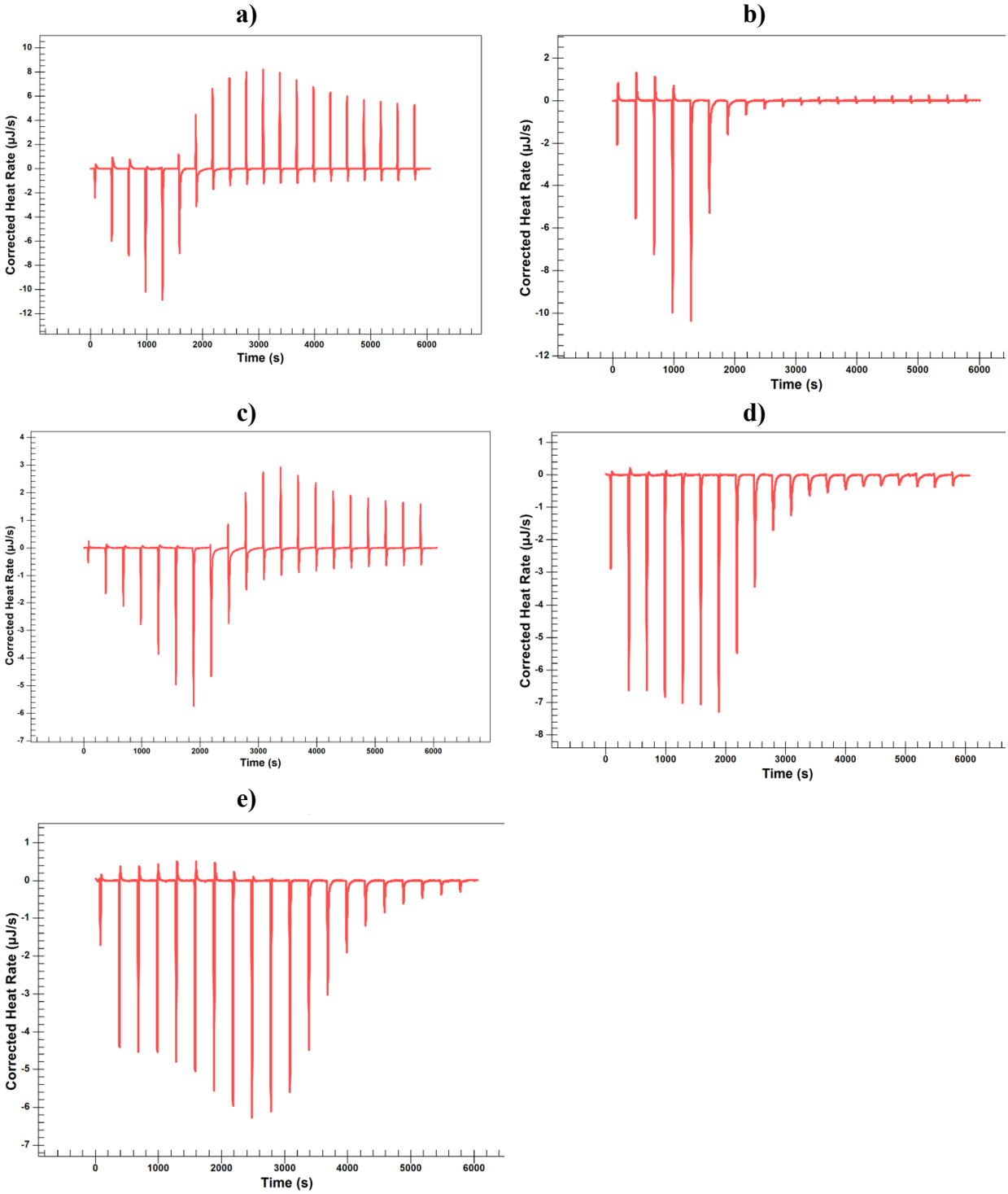


Figure 3.S15. ITC thermographs of 16% functionalized 87 kDa PEI-MP and **a**) Y(III), **b**) Sm(III), **c**) Eu(III), **d**) Tb(III), and **e)** Dy(III).

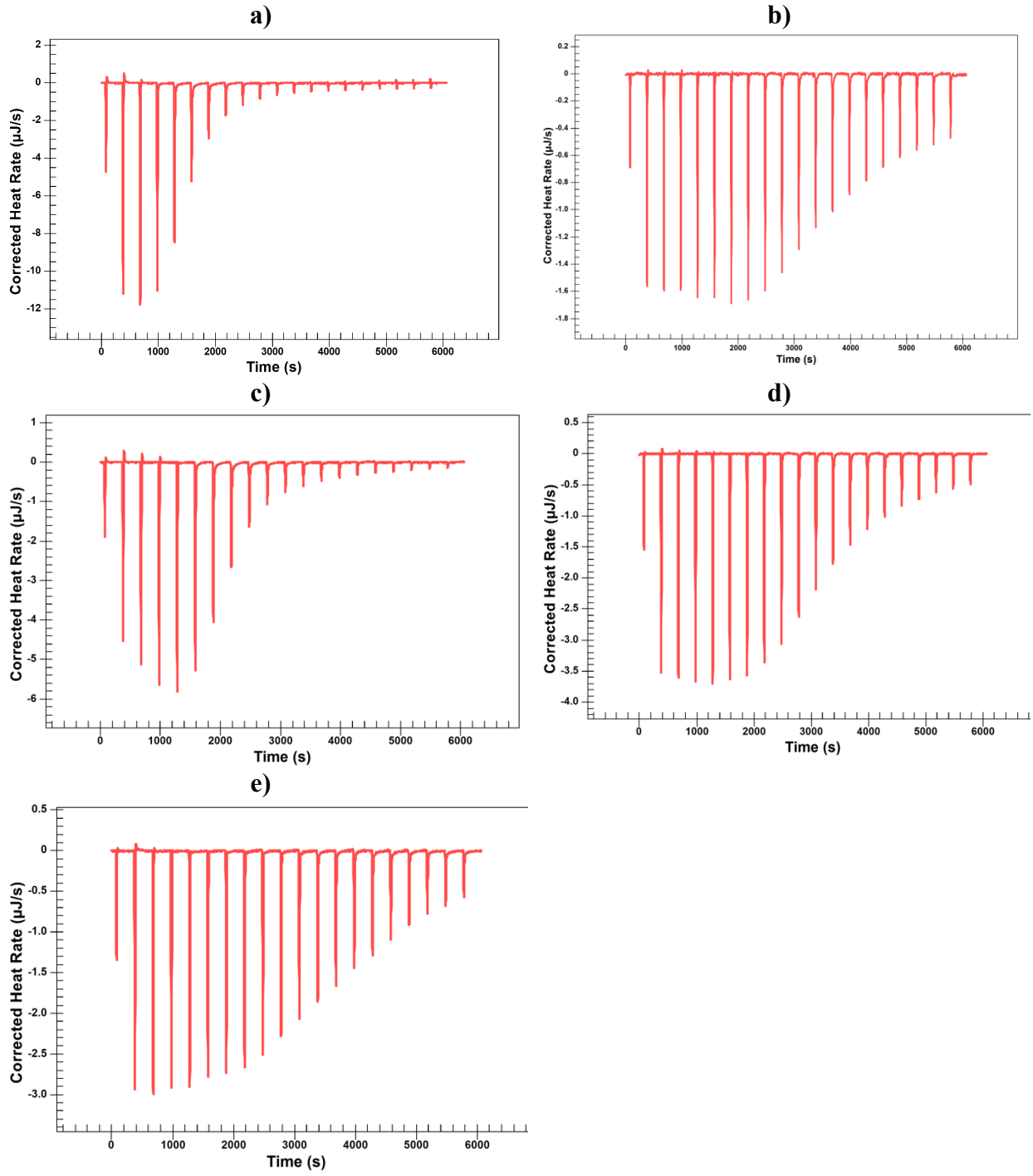


Figure 3.S16: Thermograph and titration curve of REEs binding to DEPMA **a)** Y(III), **b)** Sm(III), **c)** Eu(III), **d)** Tb(III), and **e)** Dy(III).

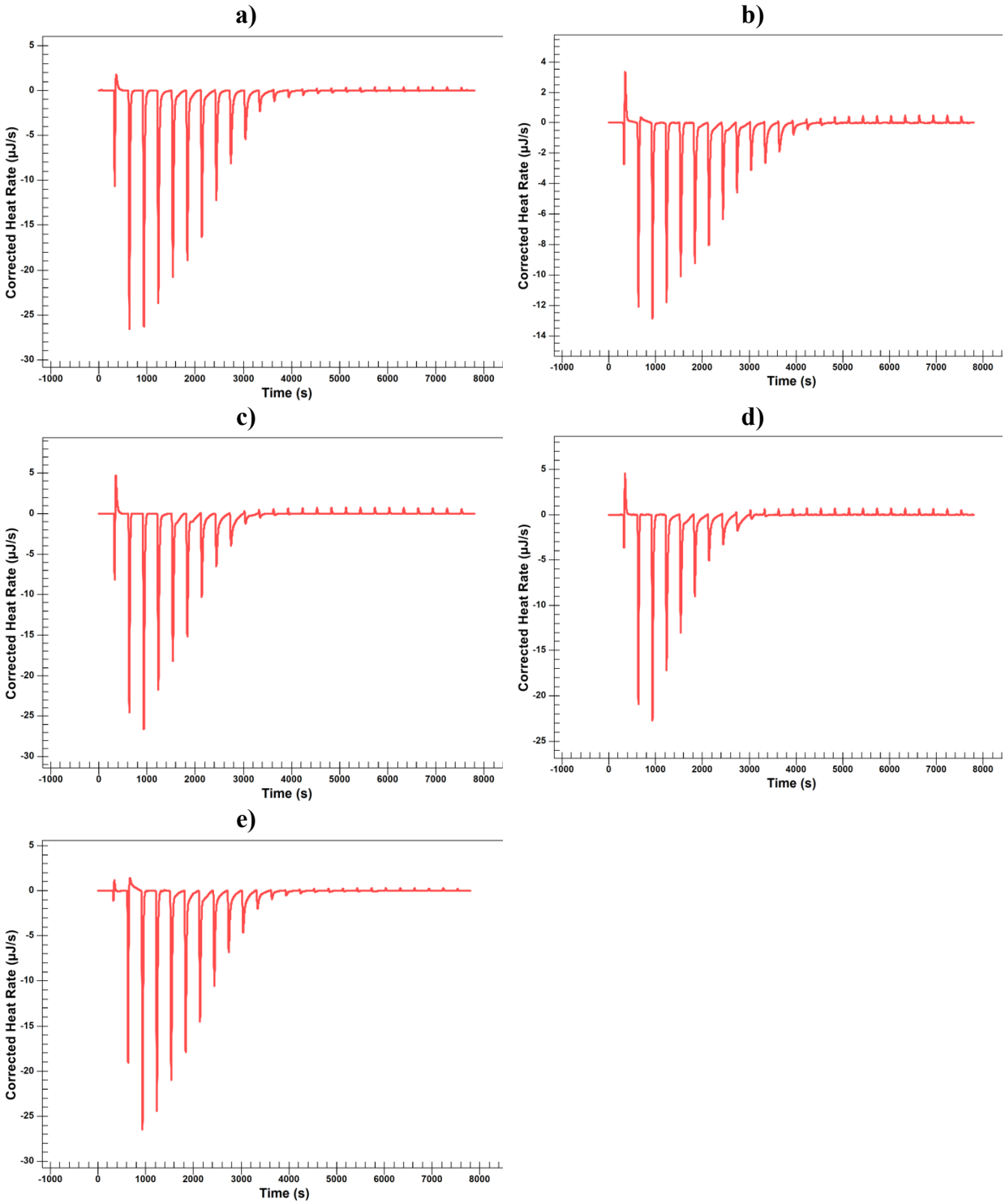


Figure 3.S17. Particle size analysis of functionalized PEI (Molecular Weight Series) **a)** 7 kDa, **b)**15 kDa, **c)** 70 kDa, **d)** 246 kDa, **e)** 258 kDa, and **f)** 680 kDa.

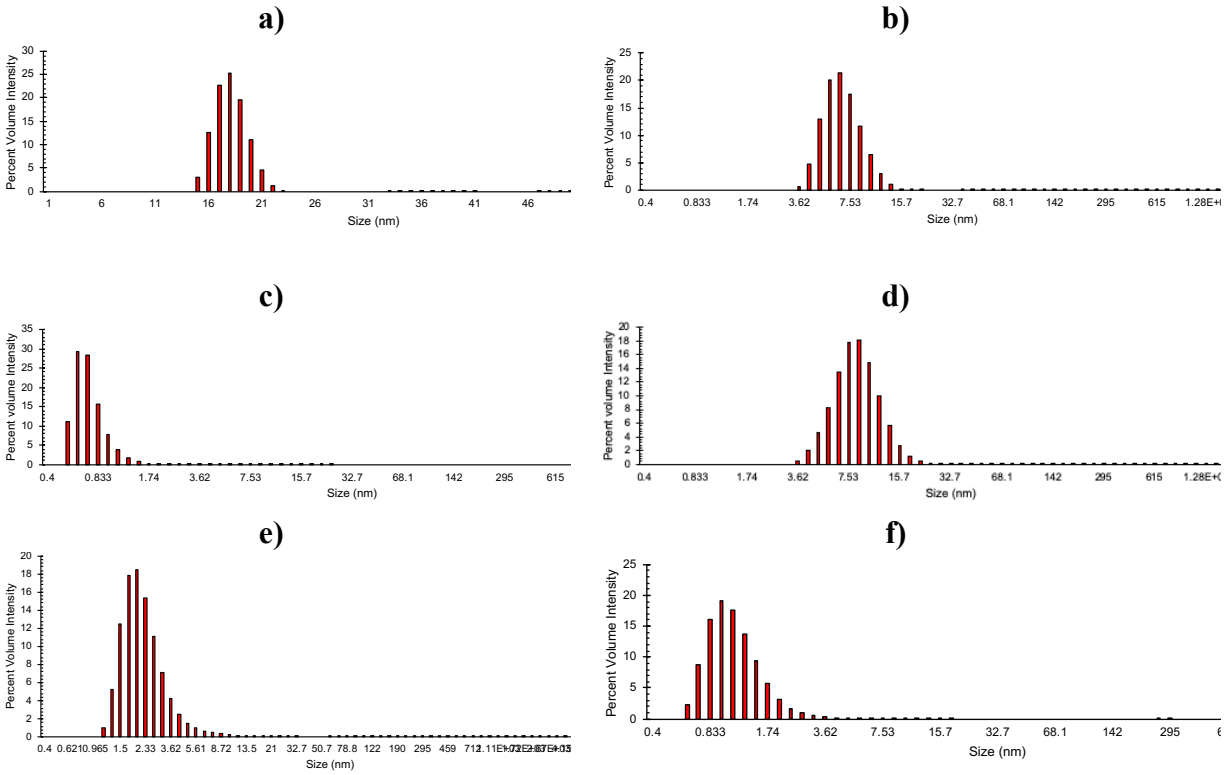


Figure 3.S18. Particle size analysis of functionalized PEI (Functionalization Series) **a)** 16%, **b)** 59%, **c)** 66%, **d)** 85% functionalization.

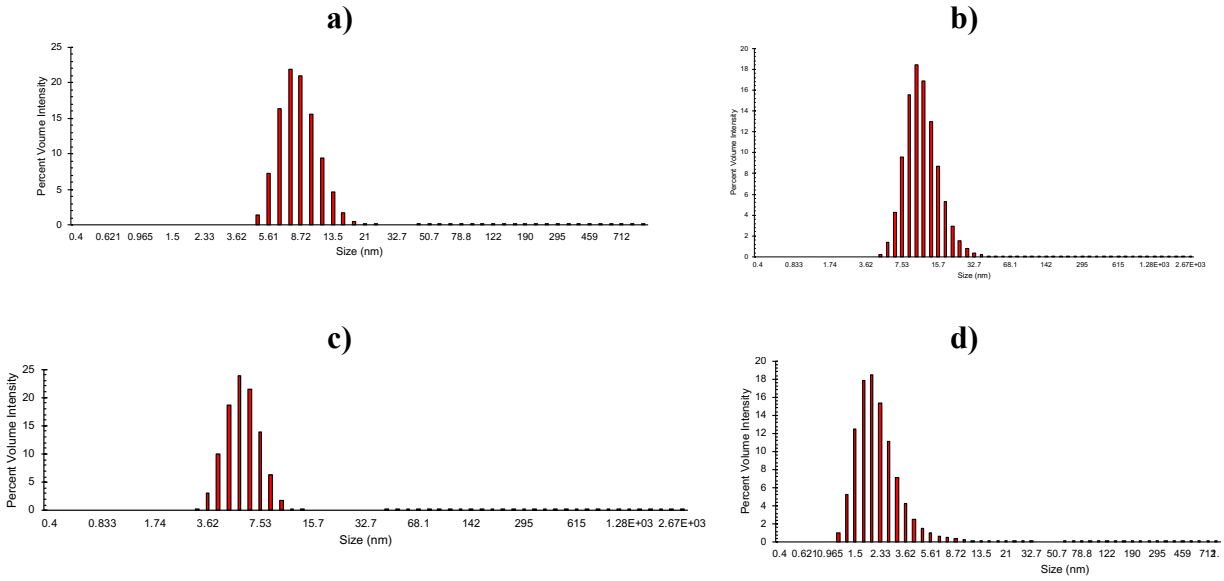
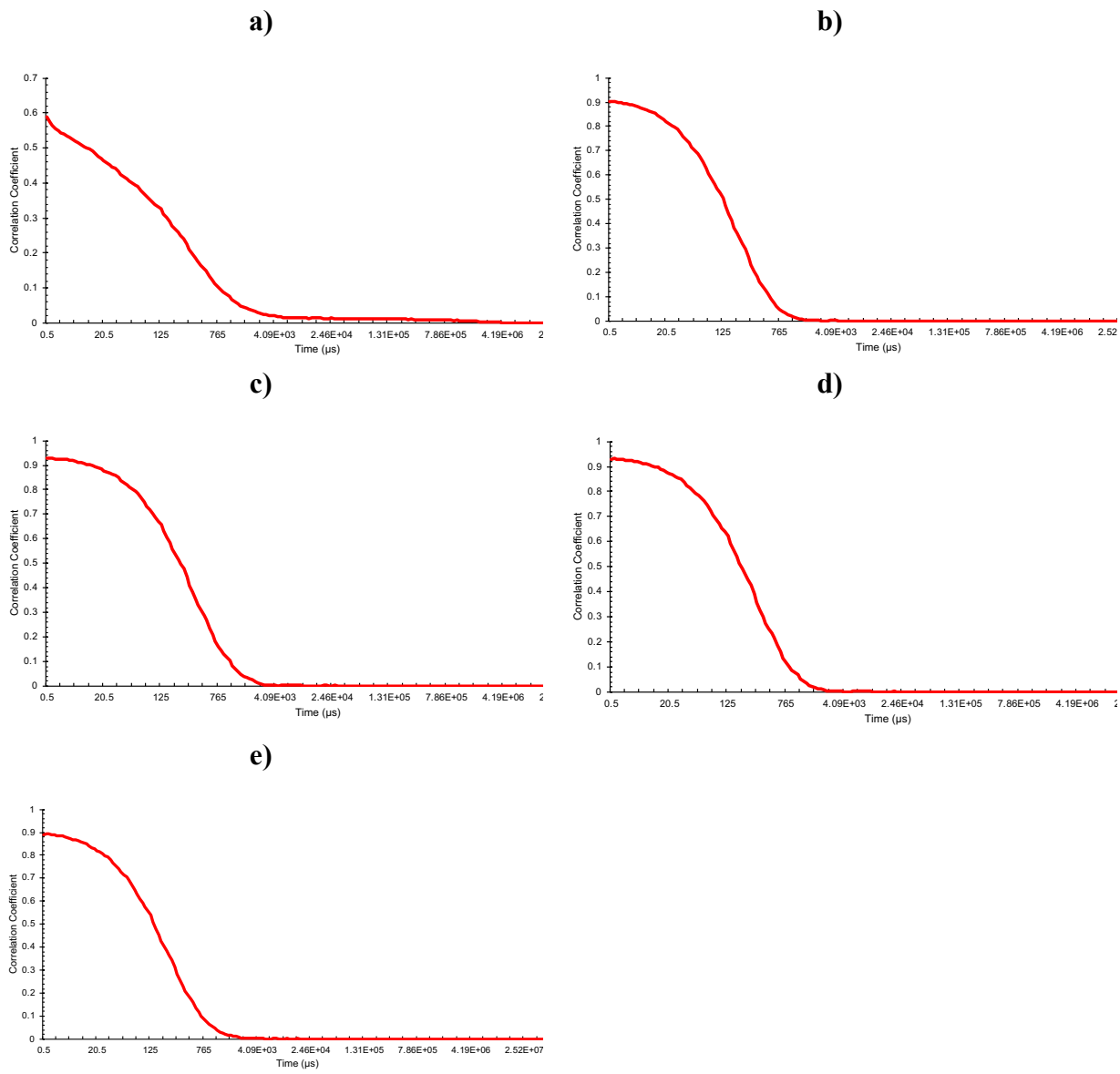


Figure 3.S19. DLS correlation functions for aggregation induced metal-binding (Fig. 3.10). **a)** No metal ion, **b)** Injection 2, **c)** Injection 5, **d)** Injection 8, and **e)** Injection 25.



Chapter 4. Synthesis of Phosphonated Polymer Resins for the Extraction of Rare-Earth Elements

*William R. Archer[1], Nuren Iftekhar[1], Agustin Fiorito[1], Samantha A. Winn[1], and Michael D. Schulz**

1: Department of Chemistry, and Macromolecules Innovation Institute,

Virginia Tech, Blacksburg, VA, 24061 USA

AF, and SW contributed equally to this work.

This chapter was submitted and accepted for publication in *ACS Applied Polymer Materials*.[1]
Reprinted with permission from American Chemical Society: Archer, W.R; Iftekhar, N.; Fiorito, A.; Winn, S.A.; and Schulz, M.D. Synthesis of Phosphonated Polymer Resins for the Extraction of Rare-Earth Elements. *ACS Appl. Polym. Mater.* **2022**, *4*, 2506–2512. Copyright 2022.

4.1 Abstract

Rare-earth elements (REEs: Y, Sc, La–Lu) are critical components in many modern technologies. With REE demand projected to increase over the next 15 years, materials capable of extracting REEs from complex solutions are needed. Solid-phase extractants can be used to capture or concentrate REEs, but this approach requires materials with high capacity for target elements. To address this challenge, we synthesized a phosphonate-containing polymer resin that is functionalized throughout the bulk, and evaluated REE absorption as a function of pH and metal ion identity in both batch and flow experiments. We observed enhanced REE uptake with decreasing ionic radii, as seen in the distribution coefficients for each ion. To gain further insight, we measured REE–polymer binding thermodynamics with isothermal titration calorimetry (ITC) using a water-

soluble polymer analogue, which revealed similar binding affinities (K_a) across the REE series for each ion. The combined microcalorimetry and solid-phase extraction experiments demonstrate the potential of these materials as future REE extractants.

4.2 Introduction

Rare-earth elements (REEs: Y, Sc, La–Lu) enable many modern technologies including catalysts, cell phones, hard drives, magnets, and a host of clean energy technologies, resulting in ever-increasing demand for these metals.[2-6] To meet this demand, unconventional sources of REEs are being investigated; however, these sources often contain low concentrations of REEs.[7, 8] For example, coal mining produces large amounts of REE-rich aqueous drainage, which could be a source of these critical elements.[9, 10] Thus, efficient methods for extracting REEs from dilute conditions would open underutilized REE sources, where REE concentration can be as low as 1–100 ppm.[11-14] Once the REEs are concentrated, individual elements may be separated.[15, 16] One approach to addressing this challenge is solid-phase extraction.

In solid-phase extraction, a solution containing REEs passes over a sorbent material where target elements are selectively adsorbed.[17-19] Several classes of solid-phase extractants have been developed, e.g., chelating resins, ligand-impregnated resins, or composite beads.[20] For example, surface-functionalized silica particles containing metal-chelating ligands can be quite effective for metal extraction applications due to their high surface area.[21, 22] However, in surface-functionalized materials only the surface functionality participates in the extraction. Alternatively, bulk-functionalized materials possess chelating ligands throughout the material, rather than only on the surface. However, many bulk-functionalized materials contain non-chelating moieties (e.g., polystyrene)

that are included to enhance the physical properties of the material.[23] Thus, we hypothesized that a material made predominately of chelating groups would have a higher capacity.

Phosphonate-based ligands have proven particularly effective at binding REEs.[24-26] For example, we previously synthesized linear poly(ethylenimine methylenephosphonate) (PEI-MP) and observed strong REE binding in aqueous solution (**Fig. 4.1A**).[27] This work suggested that a resin with an analogous structure could be an effective material for solid-phase REE extraction. Here we report an easy-to-synthesize REE-chelating resin featuring phosphonate groups throughout the bulk of the material. This material design enables higher REE capacity relative to surface-functionalized solid-phase extractants, and uses covalently attached ligands, which impart greater chemical stability over multiple cycles of acid regeneration and reuse.[28, 29]

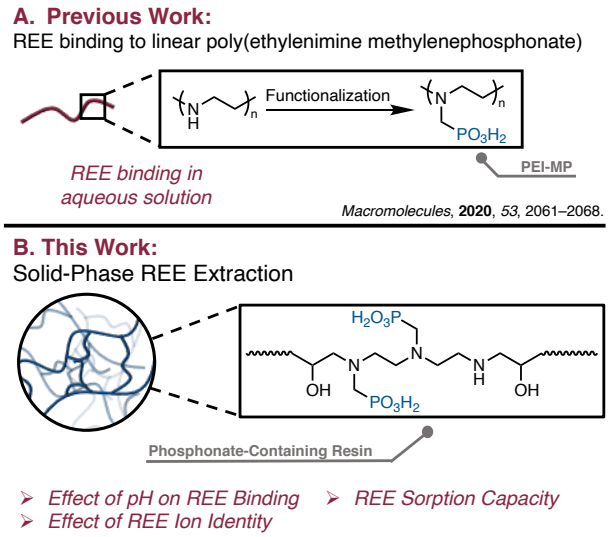


Figure 4.1. A. Previous[27] and **B**. present work with the extraction of REEs from solution by phosphonate-containing materials.

4.3 Materials and Methods

4.3.1 Chemicals and Reagents

Phosphorous acid and lanthanide chloride salts (trace metals grade) were purchased from Sigma Adrich. Diethylene triamine (DETA), formalin (37 % aqueous solution), and epichlorohydrin were purchased from Oakwood Chemical. 12 N HCl (*aq*) and 15.8 N HNO_3 (*aq*) were purchased from Fisher Scientific.

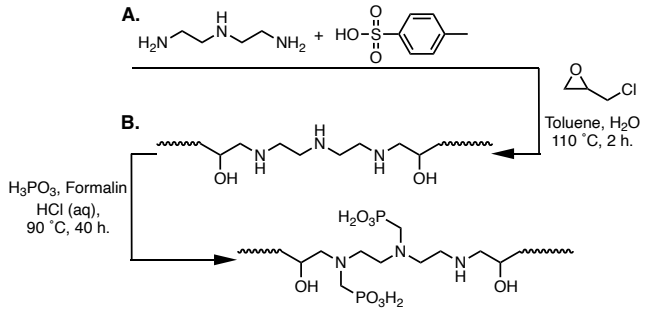
4.3.2 Synthesis of net-Poly(diethylenetriamine)-ν-epichlorohydrin-methylenephosphonate (netPoly(DETA)-ν-ECH-MP)

NetPoly(DETA)-ν-ECH was synthesized according to a modified previously reported procedure (**Scheme 4.1A.**).[30] In general, diethylenetriamine (20.4 mmol, 1.0 equiv.) and *para*-toluenesulfonic acid (0.40 mmol, 0.02 equiv.) were combined in a 500 mL round bottom flask with DI water (90 mL) and toluene (400 mL). After stirring for 15 min, epichlorohydrin (50.9 mmol, 2.5 equiv.) was added dropwise and the reaction mixture stirred while refluxing for 1 h after which time the solution turned yellow. The solution was filtered and the solid was dried in a vacuum oven at 100 ˚C overnight to afford a yellow solid.

To install methyl phosphonate groups onto netPoly(DETA)-ν-ECH (**Scheme 4.1B**.), H_3PO_3 (5.2 mmol, 1.0 equiv.), and netPoly(DETA)-ν-ECH (9.3 mmol, 1.0 equiv.) were combined with 12 M HCl (1 mL) and DI water (10 mL) in a 25 mL round bottom flask with a magnetic stir bar and heated to 90 ˚C. Formalin (18.5 mmol, 5.0 equiv. with respect to the formaldehyde concentration) was added dropwise over the course of 1 h and the mixture was refluxed at 90˚C. After 24 h, additional formalin (18.5 mmol, 4.0 equiv.) was added dropwise over 20 min and continued to reflux for 24 h. The reaction mixture was cooled to room temperature and filtered. The resin

was washed with 100 mL of IPA,100 mL of EtOH, and 100 mL DI water to remove excess reagents. The resulting functionalized resin was dried overnight.

Scheme 4.1. A. Synthesis and netPoly(DETA)-*v*-ECH and **B.** functionalization with methylene phosphonic acid groups.



4.3.3 Resin Flow Experiment

Flow experiments were conducted by packing 100 mg of the phosphonated resin into a 7 cm × 0.9 cm plastic column. An REE solution of specific concentrations (see results and discussion section, below) were passed over the phosphonated resin at a constant rate of 0.5 mL min^{-1}. Samples for inductively coupled plasma mass spectrometry (ICP-MS) were collected after elution from the resin-packed column. To determine the concentration of REEs captured by the resin, the REE concentration measured by ICP-MS analysis of the elution samples was compared with the REE concentration in the initial solution, assuming mass balance. The concentration of REEs absorbed on the resin was calculated according to **Equation 4.1**, where C_0 is the initial concentration of REEs, C_f is the REE concentration in the liquid phase after flowing through the resin, and C_A is the mass of the resin.V_0 and V_f are the volumes of the initial and final REE solutions, respectively.

Equation 4.1: Calculation of the μg REE absorbed per mg of polymer resin.

$$q_t = \frac{(C_0V_0)-(C_fV_f)}{C_A}$$

4.4 Results and Discussion

4.4.1 Synthesis and Characterization of netPoly(DETA)-*ν*-ECH-MP

Our approach to REE extraction is based on a crosslinked polymer network synthesized by reacting diethylenetriamine (DETA) with epichlorohydrin. This material has been previously synthesized on a commercial scale for use as a pharmaceutical agent.[31, 32] The resulting resin was then functionalized with methylene phosphonic acid groups by the Moedritzer-Irani reaction, which involves the condensation of formaldehyde with an amine, followed by nucleophilic addition of the phosphorous acid.[33] The IR spectrum of the polymer resin exhibited characteristic bands at 1349–1498 cm^{-1} (C–N), and 2906–3648 cm^{-1} (–OH) (**Fig. 4.S1**). These bands persisted in the functionalized resin; however, we observed additional absorption bands in the ranges of 852–954 cm^{-1} (P–O), and 1103–1263 cm^{-1} (P=O) for the functionalized resin that were in agreement with previously published IR spectra of similar phosphonate-containing molecules.[34, 35] Furthermore, energy dispersive X-ray spectroscopy (EDS) of the functionalized resin confirmed the presence of P and N on the functionalized resin surface (**Fig. 4.S2** and **4.S3**).

We used scanning electron microscopy (SEM) to characterize the morphology of the net-Poly(DETA)-*ν*-ECH-MP particles. SEM analysis of the unfunctionalized resin revealed particle sizes that were 80 ± 22 μm in diameter (**Fig. 4.2A**). Upon functionalization with methyl phosphonate groups, the average particle size was 64 ± 27 μm (**Fig. 4.2B**). After flowing the metal solution over the polymer resin, the average particle size was approximately 84 ± 6 μm (**Fig. 4.2C**). Overall, the particle sizes remained consistent (within error) throughout these processes. Pore size distributions of netPoly(DETA)-*ν*-ECH-MP were calculated *via* nitrogen adsorption–desorption isotherms using the Brunauer–Emmett–Teller (BET) method.[36] netPoly(DETA)-*ν*-ECH-MP exhibited a distinct hysteresis of N_2 adsorption–desorption at $0.4 < P/P_0 < 0.9$ ascribed to filling and

emptying of the pores (**Fig. 4.3A**).[37, 38] The average pore size diameter was calculated to be 66.5 Å, however the corresponding pore width distribution (**Fig. 4.3B**) revealed smaller pores between 29–34 Å, and larger pores greater than 70 Å.

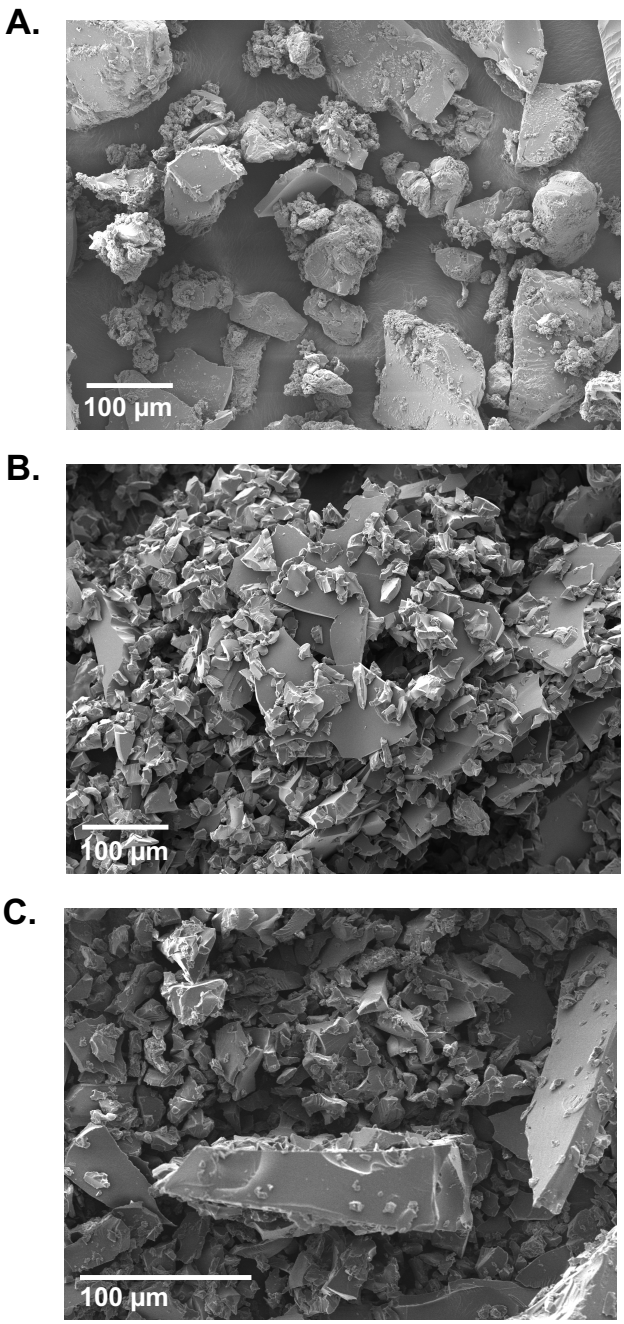


Figure 4.2. SEM images of the **A.** netPoly(DETA)-ν-ECH, **B.** netPoly(DETA)-ν-ECH-MP, and **C.** netPoly(DETA)-ν-ECH-MP after REE capture.

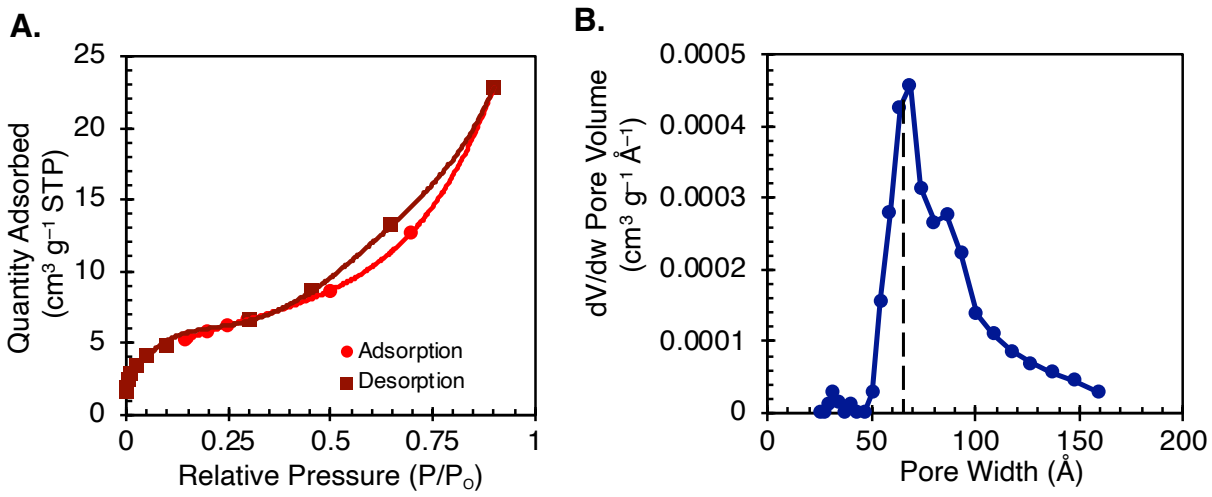


Figure 4.3. A. Nitrogen sorption isotherm at –196 ˚C, and **B.** corresponding pore width distribution. The dotted line at 65 Å is to guide the eye.

4.4.2 Effect of solution pH on REE Removal

We first examined the effect of pH on REE extraction by varying the solution pH (pH 1–6). Insoluble lanthanide hydroxides form above pH 6, precluding testing at higher pH.[39] To mimic the dilute concentrations of many REE sources, we flowed five 5 mL fractions of representative REEs (approximately 19 ppb of each REE, 115 ppb total REE: Pr (III), Nd (III), Gd (III), Ho (III) Er (III), and Lu (III)) over 50 mg of the functionalized resin and collected the resulting fractions. The amount of REE absorbed onto the resin (q_t) was calculated according to **Equation 4.1.** We found that the REE sorption was highest at pH 6 (approximately 0.07 µg REE per mg resin), and lowest at more acidic pHs (< 0.02 µg REE per mg resin) (**Fig. 4.4**). This result suggests that the protonation state of the resin plays an important role in REE binding. Each phosphonic acid group contains two acidic protons: pK_a 1.1–2.3 and pK_a is 5.3–7.2.[40, 41] Thus, when the phosphonic acid is mostly deprotonated (above pH 5), the oxygens are available to ionically interact with the REEs;

however, at pH < 5, the phosphonic acids and the nitrogens in the resin backbone become protonated, significantly reducing their ability to bind REEs.

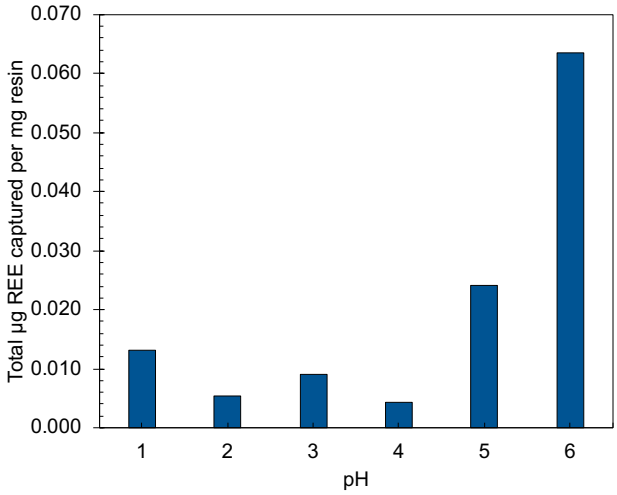


Figure 4.4. The effect of pH on REE sorption of netPoly(DETA)-*v*-ECH-MP

4.4.3 Effect of REE identity on sorption

To examine the effect of REE identity on resin capture, we flowed a solution of REEs (approximately 5 ppm each REE, 13 REEs total, pH 6) over the resin and collected a series of fractions for analysis by ICP-MS. After adding 15 mL (3 × 5 mL) of the REE solution, 3 mL of 0.5 M HNO_3 was passed over the same resin to desorb the bound REEs. To establish an initial baseline for REE capture, we performed a flow experiment using the unfunctionalized resin. When using netPoly(DETA)-*v*-ECH (the unfunctionalized resin), no REE capture was detected by ICP-MP. For the functionalized material, we found that the mol fraction of REEs captured by the resin was highest for the heavy lanthanides (**Fig. 4.5**). Typically, ligand coordination to the lanthanide ions in solution relies heavily on the concentration of both the ligands and REE ion. However, in this system the phosphonate ligands are immobilized by the resin, thus the number of ligands coordinating to the REE cannot change. Therefore, only those REE ions that have an appropriate

radius for the bite angle of the ligand are retained by the resin. Furthermore, previous research indicates that in solution REE–polymer binding is driven by ΔS, resulting from the release of complexed water molecules during binding.[42] Interestingly, ΔH_{Hydr} also decreases with increasing atomic number for the lanthanide series.[43] Thus, we hypothesize that, in addition to variations in ionic radii, the decrease in the number of coordinated water molecules and ΔH_{Hydr} also produces this difference in REE selectivity. We observed the opposite trend when 0.5 M HNO_3 was passed over the resin; the larger REE ions detached from the resin more readily, resulting in a greater desorption for these ions (**Fig. 4.S4**). The distribution coefficient, K_d, which describes the affinity and selectivity for the resin for each REE and was calculated according to **Equation 4.2**, where V, m, C_0, and C_f are the volume of the solution, mass of REE, and the initial and final concentrations, respectively.[16] We found a clear correlation between the REE Shannon ionic radii (coordination number 8) and the percent capture for each REE and the calculated distribution coefficient in our resin flow experiment (**Fig. 4.6**).[44]

Equation 4.2: Calculation of the distribution coefficient for REEs using the initial and final concentrations of each REE.

$$K_d = \frac{V}{m} \times \frac{(C_0 - C_f)}{C_f}$$

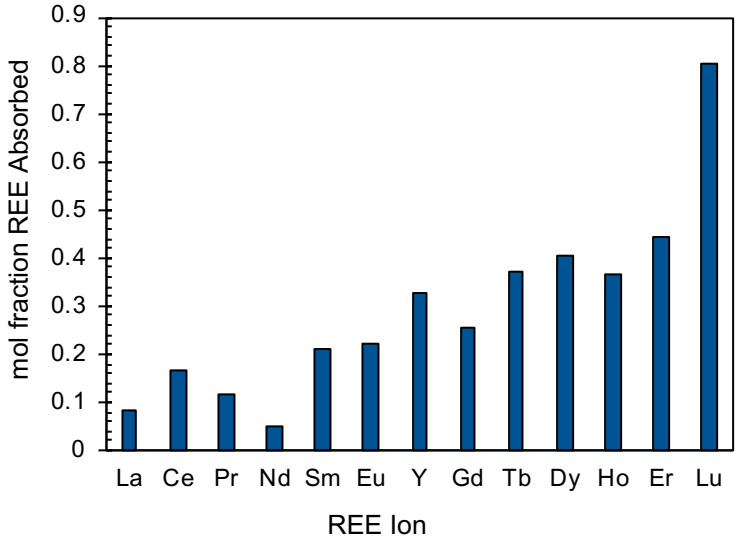


Figure 4.5. Mol fraction of REE captured in the first flow fraction. Ionic radii decreases with increasing atomic number.

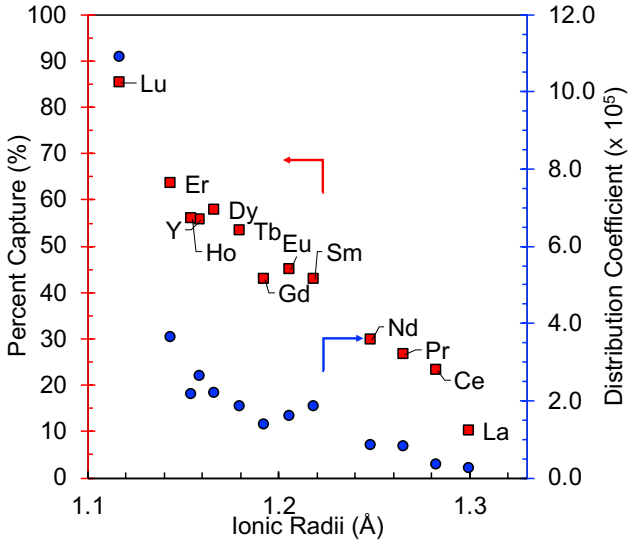


Figure 4.6. Correlation between percent capture, REE Shannon (coordination number = 8) ionic radii, and calculated distribution coefficient.

4.4.4 Resin Capacity

In contrast to materials functionalized only on the surface, this material possesses chelating functional groups throughout the bulk of the material, i.e., this resin is porous and swellable, enabling access to chelation sites throughout the material. Thus, we hypothesized that our resin would exhibit a higher REE sorption capacity compared to previously reported materials. To evaluate the REE sorption capacity of our resin, we performed a bulk sorption experiment where the resin (~100 mg) was placed in an REE stock solution (22 or 45 ppm total REE) and allowed to stir for 72 h. After 72 h, REE sorption was determined by ICP-MS. Based on this experiment, the absorption capacity of the phosphonated resin was 64 mg of REE per g of resin in a 22 ppm REE solution, and 76 mg REE per g of resin in a 45 ppm REE solution. This material performs in line with many of the previously reported REE extraction systems (**Fig. 4.7** and **Table 4.S4**).

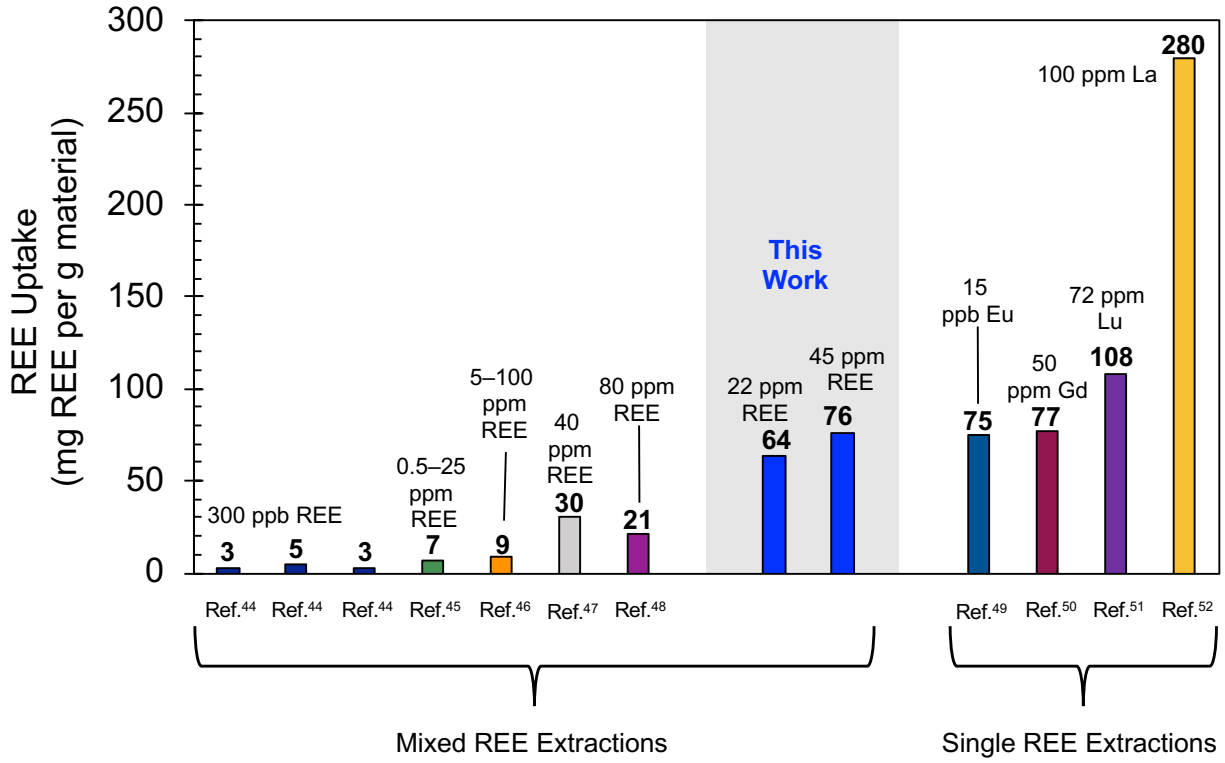


Figure 4.7. Comparison of REE capacities for various polymer resins. Selected examples from references [45-53].

4.4.5 REE Separation Factors

We used batch and flow experiments to calculate separation factors (SFs) for this material as a function of REE identity. SFs were calculated as D_{metal2}/D_{metal1} where $D=[REE]_{TF}/[REE]_{T0}$.[54] Here, SFs near 1 suggest an equal preference for ion absorption, while SFs much greater (or less) than 1 indicate partiality for a particular ion over another. Sorption selectivity among the REEs

was observed in both batch and flow experiments (**Fig. 4.8**). In this case, SFs confirmed that this material preferentially chelates heavier REEs: SFs varied between 0.5–30.

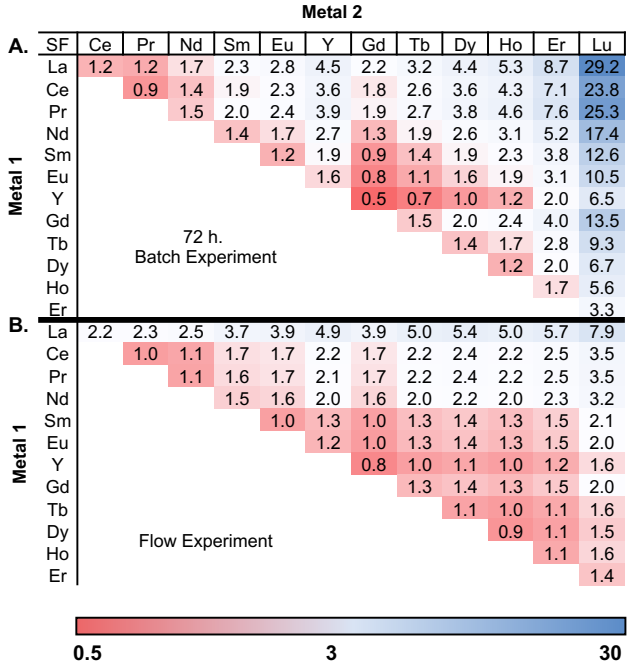


Figure 4.8. Comparison of separation factors (SF) for REE series in **A.** batch and **B**. flow experiments.

4.4.6 Isothermal Titration Calorimetry

To probe the underlying thermodynamics of the REE–resin interaction, we performed a series of ITC experiments, as ITC can directly determine binding thermodynamics (ΔH, ΔG, ΔS, K_a, and stoichiometry) of reactions in solution.[55-57] As a solution technique, however, ITC cannot be used to evaluate the resin directly. Consequently, we measured the K_a of PEI-MP, a soluble analogue of netPoly(DETA)-*v*-ECH-MP. The K_a obtained from ITC was roughly constant across the REE series (**Fig. 4.9**). These data suggest that the selectivity of the resin results from the network architecture rather than the chelation thermodynamics of the specific ligand. We hypothesize

that the differences in selectivity arise from conformational differences in the chelating sites: In the solution calorimetry experiments, the polymer chains have greater conformational freedom than the relatively rigid chelating sites of the solid-phase crosslinked network. A chelating polymer in solution can adopt multiple conformations to accommodate chelation of different ions, while the binding sites in a polymer network are more restricted and therefore have different affinities for different ions. Additionally, smaller ions may better penetrate the polymer network, resulting in higher uptake. Full ITC experimental details and representative ITC thermograms and fit parameters can be found in the supporting information (**Fig. 4.S5** and **Table 4.S3**.)

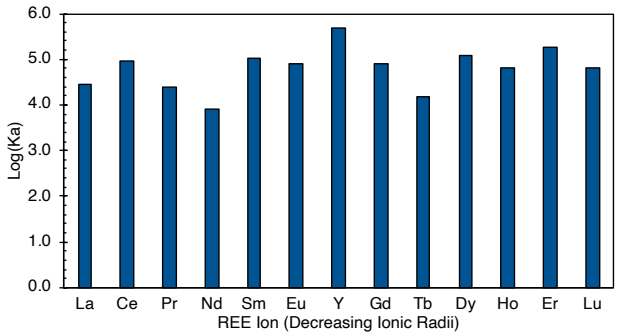


Figure 4.9. Comparison of $K_{a(ITC)}$ of the REE series in order of increasing ionic radii.

4.5 Conclusions

Extracting and separating individual REEs is key to advancing the diverse technologies that require these critical metals, irrespective of the REE source. We have developed a highly functionalized resin and evaluated the ability of this material to extract REEs from a simulated waste stream (i.e., a solution with realistic concentrations of REES for a waste stream). The relatively high capacity of this material demonstrates the advantage of polymer resins incorporating chelating moieties throughout the bulk of the material. Additionally, we used ITC to probe the

REE–polymer interaction thermodynamics, which enabled us to probe the relative contributions of network architecture and ligand identity to the overall binding selectivity. Integrating ITC thermodynamic data with resin performance measurements offers new insight into material–REE interactions, informing future materials design. Ultimately, efficient REE extraction and separation processes will reduce the need for environmentally harmful REE mining by enabling access to currently underutilized REE sources. High-capacity, solid-phase REE sorbents will likely play a key role in this area.

Acknowledgements

The authors acknowledge the assistance of Dr. Jeffrey Parks for the collection of ICP-MS data. This work was performed in part at the Nanoscale Characterization and Fabrication Laboratory, which is supported by the Virginia Tech National Center for Earth and Environmental Nanotechnology Infrastructure (NanoEarth), a member of the National Nanotechnology Coordinated Infrastructure (NNCI), supported by NSF (ECCS 1542100 and ECCS 2025151).

Conflict of Interest Disclosure

The authors declare the following competing financial interest: Virginia Tech has filed for intellectual property protection of this material based on these findings.

4.6 References

1. Archer, W. R.; Iftekhar, N.; Fiorito, A.; Winn, S. A.; Schulz, M. D. Synthesis of Phosphonated Polymer Resins for the Extraction of Rare-Earth Elements. *ACS Appl. Polym. Mater.* **2022,** 4 (4), 2506–2512.
2. Massari, S.; Ruberti, M. Rare earth elements as critical raw materials: Focus on international markets and future strategies. *Resour. Policy* **2013,** 38 (1), 36–43.
3. Bonificio, W. D.; Clarke, D. R. Rare-Earth Separation Using Bacteria. *Environ. Sci. Technol. Lett.* **2016,** 3 (4), 180–184.
4. Wang, Q.; Wilfong, W. C.; Kail, B. W.; Yu, Y.; Gray, M. L. Novel Polyethylenimine–Acrylamide/SiO2 Hybrid Hydrogel Sorbent for Rare-Earth-Element Recycling from Aqueous Sources. *ACS Sustainable Chem. Eng.* **2017,** 5 (11), 10947–10958.
5. Rademaker, J. H.; Kleijn, R.; Yang, Y. Recycling as a Strategy against Rare Earth Element Criticality: A Systemic Evaluation of the Potential Yield of NdFeB Magnet Recycling. *Environ. Sci. Technol.* **2013,** 47 (18), 10129–10136.
6. Alonso, E.; Sherman, A. M.; Wallington, T. J.; Everson, M. P.; Field, F. R.; Roth, R.; Kirchain, R. E. Evaluating Rare Earth Element Availability: A Case with Revolutionary Demand from Clean Technologies. *Environ. Sci. Technol.* **2012,** 46 (6), 3406–3414.
7. Wilfong, W. C.; Kail, B. W.; Bank, T. L.; Howard, B. H.; Gray, M. L. Recovering Rare Earth Elements from Aqueous Solution with Porous Amine–Epoxy Networks. *ACS Appl. Mater. Inter.* **2017,** 9 (21), 18283–18294.
8. Deshmane, V. G.; Islam, S. Z.; Bhave, R. R. Selective Recovery of Rare Earth Elements from a Wide Range of E-Waste and Process Scalability of Membrane Solvent Extraction. *Environ. Sci. Technol.* **2020,** 54 (1), 550–558.
9. Maes, S.; Zhuang, W.-Q.; Rabaey, K.; Alvarez-Cohen, L.; Hennebel, T. Concomitant Leaching and Electrochemical Extraction of Rare Earth Elements from Monazite. *Environ. Sci. Technol.* **2017,** 51 (3), 1654–1661.
10. Taggart, R. K.; Hower, J. C.; Dwyer, G. S.; Hsu-Kim, H. Trends in the Rare Earth Element Content of U.S.-Based Coal Combustion Fly Ashes. *Environ. Sci. Technol.* **2016,** 50 (11), 5919–5926.
11. Westerhoff, P.; Lee, S.; Yang, Y.; Gordon, G. W.; Hristovski, K.; Halden, R. U.; Herckes, P. Characterization, Recovery Opportunities, and Valuation of Metals in Municipal Sludges from U.S. Wastewater Treatment Plants Nationwide. *Environ. Sci. Technol.* **2015,** 49 (16), 9479–9488.
12. Verplanck, P. L.; Furlong, E. T.; Gray, J. L.; Phillips, P. J.; Wolf, R. E.; Esposito, K. Evaluating the Behavior of Gadolinium and Other Rare Earth Elements through Large Metropolitan Sewage Treatment Plants. *Environ. Sci. Technol.* **2010,** 44 (10), 3876–3882.
13. Honaker, R. Q.; Zhang, W.; Werner, J. Acid Leaching of Rare Earth Elements from Coal and Coal Ash: Implications for Using Fluidized Bed Combustion To Assist in the Recovery of Critical Materials. *Energy Fuels* **2019,** 33 (7), 5971–5980.
14. Dong, Z.; Deblonde, G.; Middleton, A.; Hu, D.; Dohnalkova, A.; Kovarik, L.; Qafoku, O.; Shutthanandan, V.; Jin, H.; Hsu-Kim, H.; Theaker, N.; Jiao, Y.; Park, D. Microbe-Encapsulated Silica Gel Biosorbents for Selective Extraction of Scandium from Coal Byproducts. *Environ. Sci. Technol.* **2021,** 55 (9), 6320–6328.

15. Archer, W. R.; Hall, B. A.; Thompson, T. N.; Wadsworth, O. J.; Schulz, M. D. Polymer sequestrants for biological and environmental applications. *Polym. Int.* **2019,** 68 (7), 1220–1237.
16. Hu, Y.; Misal Castro, L. C.; Drouin, E.; Florek, J.; Kählig, H.; Larivière, D.; Kleitz, F.; Fontaine, F.-G. Size-Selective Separation of Rare Earth Elements Using Functionalized Mesoporous Silica Materials. *ACS Appl. Mater. Inter.* **2019,** 11 (26), 23681–23691.
17. Poole, C. F. New trends in solid-phase extraction. *Trends Anal. Chem.* **2003,** 22 (6), 362–373.
18. Li, Y.; Yang, J.-l.; Jiang, Y. Trace Rare Earth Element Detection in Food and Agricultural Products Based on Flow Injection Walnut Shell Packed Microcolumn Preconcentration Coupled with Inductively Coupled Plasma Mass Spectrometry. *J. Agric. Food Chem.* **2012,** 60 (12), 3033–3041.
19. Ansari, S. A.; Mohapatra, P. K. A review on solid phase extraction of actinides and lanthanides with amide based extractants. *J. Chromatogr. A* **2017,** 1499, 1–20.
20. Modolo, G.; Asp, H.; Schreinemachers, C.; Vijgen, H. Recovery of actinides and lanthanides from high-level liquid waste by extraction chromatography using TODGA+TBP impregnated resins. *Radiochimica Acta* **2007,** 95 (7), 391-397.
21. Callura, J. C.; Perkins, K. M.; Noack, C. W.; Washburn, N. R.; Dzombak, D. A.; Karamalidis, A. K. Selective adsorption of rare earth elements onto functionalized silica particles. *Green Chem.* **2018,** 20 (7), 1515-1526.
22. Florek, J.; F.;, C.; Bilodeau, F.; D.;, L.; Kleitz, F. Nanostructured Hybrid Materials for the Selective Recovery and Enrichment of Rare Earth Elements. *Adv. Funct. Mater.* **2014,** 24, 2668–2676.
23. Kołodyn´ska, D. Diphonix Resin® in sorption of heavy metal ions in the presence of the biodegradable complexing agents of a new generation. *Chem. Eng. J.* **2010,** 159, 27-36.
24. Popwell, S. J.; Schulz, M. D.; Wagener, K. B.; Batich, C. D.; Miler, R. J.; Lagmay, J.; and Bolch, W. E. Synthesis of Polymeric Phosphonates for Selective Delivery of Radionuclides to Osteosarcoma. *Cancer Biother Radio* **2014,** 29 (7), 273–282.
25. Gomes Rodrigues, D.; Monge, S.; Pellet-Rostaing, S.; Dacheux, N.; Bouyer, D.; Faur, C. A new carbamoylmethylphosphonic acid-based polymer for the selective sorption of rare earth elements. *Chem. Eng. J.* **2019,** 371, 857–867.
26. Koehne, I.; Lik, A.; Gerstel, M.; Bruhn, C.; Reithmaier, J. P.; Benyoucef, M.; Pietschnig, R. Functionalised phosphonate ester supported lanthanide (Ln = La, Nd, Dy, Er) complexes. *Dalton Trans.* **2020,** 49 (46), 16683–16692.
27. Archer, W. R.; Fiorito, A.; Heinz-Kunert, S. L.; MacNicol, P. L.; Winn, S. A.; Schulz, M. D. Synthesis and Rare-Earth-Element Chelation Properties of Linear Poly(ethylenimine methylenephosphonate). *Macromolecules* **2020,** 53 (6), 2061–2068.
28. Ma, C.; Gao, J.; Wang, D.; Yuan, Y.; Wen, J.; Yan, B.; Zhao, S.; Zhao, X.; Sun, Y.; Wang, X.; Wang, N. Sunlight Polymerization of Poly(amidoxime) Hydrogel Membrane for Enhanced Uranium Extraction from Seawater. *Adv. Sci.* **2019,** 6 (13), 1900085.
29. Piechowicz, M.; Chiarizia, R.; Skanthakumar, S.; Rowan, S. J.; Soderholm, L. Leveraging Actinide Hydrolysis Chemistry for Targeted Th and U Separations using Amidoxime-Functionalized Poly(HIPE)s. *ChemPhysChem* **2020,** 21 (11), 1157-1165.
30. Thomas, R. C.; Hsi, R. S. P.; Harpootlian, H.; Johnson, T. D.; Judy, R. W. Preparation of [14c]colestipol hydrochloride and its disposition in the human, dog and rat. *Atherosclerosis* **1978,** 29 (1), 9–23.

31. Elder, D. P. Pharmaceutical Applications of Ion-Exchange Resins. *J. Chem. Educ.* **2005,** 82 (4), 575.
32. Dhal, P. K.; Huval, C. C.; Holmes-Farley, S. R. Functional Polymers as Human Therapeutic Agents. *Ind. Eng. Chem.* **2005,** 44 (23), 8593–8604.
33. Moedritzer, K.; Irani, R. R. The Direct Synthesis of α-Aminomethylphosphonic Acids. Mannich-Type Reactions with Orthophosphorous Acid. *J. Org. Chem.* **1966,** 31 (5), 1603-1607.
34. Yang, Y.; Pushie, M. J.; Cooper, D. M. L.; Doschak, M. R. Structural Characterization of SmIII(EDTMP). *Mol. Pharmaceutics* **2015,** 12 (11), 4108–4114.
35. Illy, N.; Couture, G.; Auvergne, R.; Caillol, S.; David, G.; Boutevin, B. New prospects for the synthesis of N-alkyl phosphonate/phosphonic acid-bearing oligo-chitosan. *RSC Adv.* **2014,** 4 (46), 24042–24052.
36. Brunauer, S.; Emmett, P. H.; Teller, E. Adsorption of Gases in Multimolecular Layers. *J. Am Chem. Soc.* **1938,** 60 (2), 309–319.
37. Ambroz, F.; Macdonald, T.; Martis, V.; Parkin, I. Evaluation of the BET Theory for the Characterization of Meso and Microporous MOFs. *Small Methods* **2018,** 2, 1800173.
38. Dolai, J.; Ali, H.; Jana, N. R. Molecular Imprinted Poly-Cyclodextrin for Selective Removal of Dibutyl Phthalate. *ACS Appl. Polym. Mater.* **2020,** 2 (2), 691–698.
39. Cawthray, J. F.; Creagh, A. L.; Haynes, C. A.; Orvig, C. Ion Exchange in Hydroxyapatite with Lanthanides. *Inorg. Chem.* **2015,** 54 (4), 1440–1445.
40. Franz, R. G. Comparisons of pKa and log P values of some carboxylic and phosphonic acids: Synthesis and measurement. *AAPS PharmSci* **2001,** 3 (2), 1.
41. Sevrain, C. M.; Berchel, M.; Couthon, H.; Jaffrès, P.-A. Phosphonic acid: preparation and applications. *Beilstein J. Org. Chem.* **2017,** 13, 2186–2213.
42. Steed, J. W.; Atwood, J. L., *Supramolecular Chemsitry*. John Wiley & Sons: 2013.
43. Bertha, S. L.; Choppin, G. R. Hydration thermodynamics of the lanthanide ions. *Inorg Chem.* **1969,** 8 (3), 613–617.
44. Shannon, R. D. Revised effective ionic radii and systematic studies of interatomic distances in halides and chalcogenides. *Acta Crystallographica Section A* **1976,** 32 (5), 751-767.
45. Callura, J. C.; Perkins, K. M.; Baltrus, J. P.; Washburn, N. R.; Dzombak, D. A.; Karamalidis, A. K. Adsorption kinetics, thermodynamics, and isotherm studies for functionalized lanthanide-chelating resins. *J. Colloid Interface Sci.* **2019,** 557, 465–477.
46. Hérès, X.; Blet, V.; Di Natale, P.; Ouaattou, A.; Mazouz, H.; Dhiba, D.; Cuer, F. Selective Extraction of Rare Earth Elements from Phosphoric Acid by Ion Exchange Resins. *Metals* **2018,** 8 (9), 682.
47. Hu, Y.; Drouin, E.; Larivière, D.; Kleitz, F.; Fontaine, F.-G. Highly Efficient and Selective Recovery of Rare Earth Elements Using Mesoporous Silica Functionalized by Preorganized Chelating Ligands. *ACS Appl. Mater. Interfaces* **2017,** 9 (44), 38584–38593.
48. Adel, A. H. A.-R.; Ibrahim, E. E. A.; Fadia, Y. A.; Mohammed, F. H. Studies on the Uptake of Rare Earth Elements on Polyacrylamidoxime Resins from Natural Concentrate Leachate Solutions. *J. Disper. Sci. Technol.* **2010,** 31, 1128–1135.
49. Hovey, J. L.; Dardona, M.; Allen, M. J.; Dittrich, T. M. Sorption of rare-earth elements onto a ligand-associated media for pH-dependent extraction and recovery of critical materials. *Sep. Purif. Technol.* **2021,** 258, 118061.

50. Florek, J.; Mushtaq, A.; Larivière, D.; Cantin, G.; Fontaine, F.-G.; Kleitz, F. Selective recovery of rare earth elements using chelating ligands grafted on mesoporous surfaces. *RSC Adv.* **2015,** 5 (126), 103782–103789.
51. Zheng, X.; Wang, C.; Dai, J.; Shi, W.; Yan, Y. Design of mesoporous silica hybrid materials as sorbents for the selective recovery of rare earth metals. *J. Mater. Chem. A* **2015,** 3 (19), 10327–10335.
52. Roosen, J.; Spooren, J.; Binnemans, K. Adsorption performance of functionalized chitosan–silica hybrid materials toward rare earths. *J. Mater. Chem. A* **2014,** 2 (45), 19415–19426.
53. Zhao, F.; Yang, Z.; Wei, Z.; Spinney, R.; Sillanpää, M.; Tang, J.; Tam, M.; Xiao, R. Polyethylenimine-modified chitosan materials for the recovery of La(III) from leachates of bauxite residue. *Chem. Eng. J.* **2020,** 388, 124307.
54. Li, W.; Wang, X.; Zhang, H.; Meng, S.; Li, D. Solvent extraction of lanthanides and yttrium from nitrate medium with CYANEX 925 in heptane. *J. Chem. Technol. Biotechnol.* **2007,** 82 (4), 376–381.
55. Archer, W. R.; Schulz, M. D. Isothermal titration calorimetry: practical approaches and current applications in soft matter. *Soft Matter* **2020,** 16 (38), 8760–8774.
56. Archer, W. R.; Thompson, T. N.; Schulz, M. D. Effect of Copolymer Structure on Rare-Earth-Element Chelation Thermodynamics. *Macromol. Rapid Commun.* **2021,** 42 (8), 2000614.
57. Archer, W. R.; Gallagher, C. M. B.; Vaissier Welborn, V.; Schulz, M. D. Exploring the role of polymer hydrophobicity in polymer–metal binding thermodynamics. *Phys. Chem. Chem. Phys.* **2022,** 24 (6), 3579–3585.

4.7 Supporting Information

Materials and Characterization

Lanthanide trichloride salts (trace metals grade), and H_3PO_3 were purchased from Sigma Aldrich. Formalin (37 wt% solution, ACS grade), epichlorohydrin, and para-toluenesulfonic acid were purchased from Oakwood chemical. HCl(aq) and HNO_3(aq) was purchased from Fisher Scientific. All chemicals were used as-is. For the water-soluble polymer analog studies, linear PEI-MP was synthesized and used as previously reported.[27]

SEM images were acquired using the JEOL IT500HR Scanning Electron Microscope. Scope was operated at 5kV accelerating voltage and images collected with the Everhart-Thornley secondary electron detector. The samples were coated with 5nm of 80%Pt-20%Pd, to alleviate sample charging, using a Leica ACE600 sputter coater. Particle size distributions were calculated using the analyze particles function within the ImageJ software.

Pore size distributions were conducted using a Micromeritics 3 Flex (Micromeritics Instrument Corp). N_2 adsorption–desorption isotherms were obtained at 77 K. Prior to the experiment, the phosphonated resin was heated to 120 ˚C for 15 h under vacuum to remove any moisture. The pore sizes were calculated using a Brunauer-Emmett-Teller (BET) method.

ICP-MS was collected using a Thermo Electron iCAP-RQ inductively coupled plasma mass spectrometer (ICP-MS) per Standard Method 3125-B (APHA, AWWA, and WEF, 1998).[1] Samples and calibration standards were prepared in a matrix of 2% nitric acid by volume.

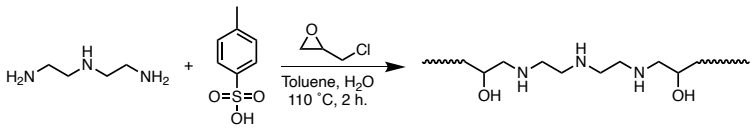
Isothermal titration calorimetry experimental procedure:

The ITC instrument used was an Affinity-ITC (TA Instruments, New Castle, DE), which operated at constant temperature (278–308 K). To carry out a binding experiment, a sample solution was prepared by dissolving the polymer and $EuCl_3$ in a pH 5, 100-mM pyridine buffer.

Before the ITC experiment, each solution was degassed for 15 min. The polymer solution (350 μL) was placed in the sample cell and the reference cell was filled with deionized H_2O (300 μL). Both cells were mounted in an adiabatic chamber at a constant temperature during the measurement. A long-needle syringe with a twisted paddle fastened to its end, was filled with the metal-ion solution. The syringe was placed inside the sample cell, and the entire syringe assembly was rotated continuously (185 RPM) to provide proper mixing of the contents of the sample cell within a few seconds after an injection. After reaching thermal equilibrium, the injection of the metal ion solution was automatically conducted stepwise until the polymer was saturated with metal ion. Due to the possible dilution of the first measurement, the first injection was ignored in the data analysis, which is standard practice for ITC experiments.[2,3] The first 1.0-μL injection was followed by a series of 2.0-μL injections. The chosen time interval between two consecutive injections was 300 sec to ensure that the equilibrium was reached before the next injection.

Nonlinear least-squares curve fitting was conducted with TA Instruments Nano Analyze and TA Instruments Independent model. Heats of dilution from control titrations (metal ion into buffer (no polymer present), and buffer into polymer (without metal ion present)) were subtracted before curve fitting.

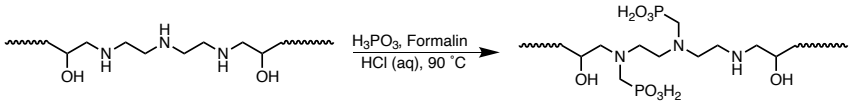
Synthesis of netPoly(DETA)-ν-ECH



Scheme 4.2. Synthesis of netPoly(DETA)-ν-ECH.

The resin was synthesized as depicted in **Scheme 4.S1**. Diethylenetriamine (23.2 mL, 214 mmol) was combined with p-toluenesulfonic acid (0.46 mL, 1.5 mmol, 60 % solution in water) in 90 mL of DI H_2O and 5 mL of toluene. After 5 min, 400 mL of toluene was added to the reaction mixture, and epichlorohydrin (43.0 mL, 532 mmol) was added dropwise. The solution was heated to reflux for 2 h after which it was cooled to room temperature, filtered, and dried in an oven at 100 ˚C overnight.

Synthesis of netPoly(DETA)-ν-ECH MP



Scheme 4.S2. Synthesis of netPoly(DETA)-ν-ECH MP.

The resin was functionalized as depicted in **Scheme 4.S2**. In general, H_3PO_3 (5.2 mmol, 1.0 equiv.) and resin (9.3 mmol, 1.0 equiv.) were added to 2 mL of concentrated HCl (*aq.*) and 1.5 mL of DI H_2O in a 25 mL round bottom flask with a magnetic stir bar and heated to 90 ˚C. Formalin (18.5 mmol, 4.0 equiv.) was added dropwise over the course of 1 h and the mixture was refluxed at 90 ˚C for 4 h. After 4 h, additional formalin (18.5 mmol, 4.0 equiv.) was added dropwise over 1 h and continued to reflux for 40 hrs. The reaction mixture was cooled to rt, filtered, and washed with IPA and H_2O to remove excess reagents.

Table 4.S1. Experimental combustion analysis results for netPoly(DETA)-ν-ECH and net-Poly(DETA)-ν-ECH MP.

	Experimental Composition (%) netPoly(DETA)-ν-ECH	**Experimental Composition (%) netPoly(DETA)-ν-ECH MP**
% C	40.1	31.1
% H	8.2	6.7
% N	12.7	8.3
% P	N/A	10.4
C/N	3.2	3.7
P/N	N/A	1.2

Figure 4.S1: IR spectra of netPoly(DETA)-*ν*-ECH *and* netPoly(DETA)-*ν*-ECH MP.

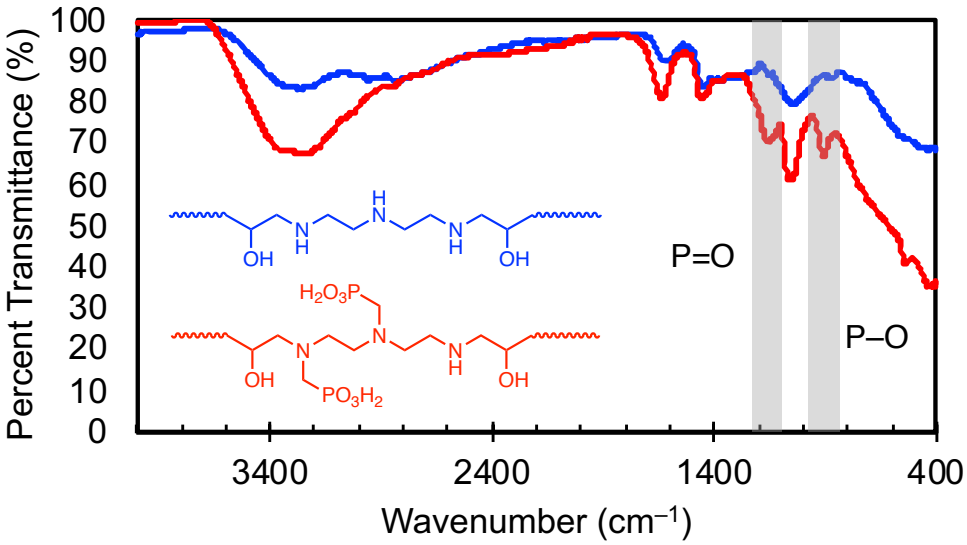


Figure 4.S2: Energy dispersive X-ray spectroscopy (EDS) of netPoly(DETA)-*ν*-ECH.

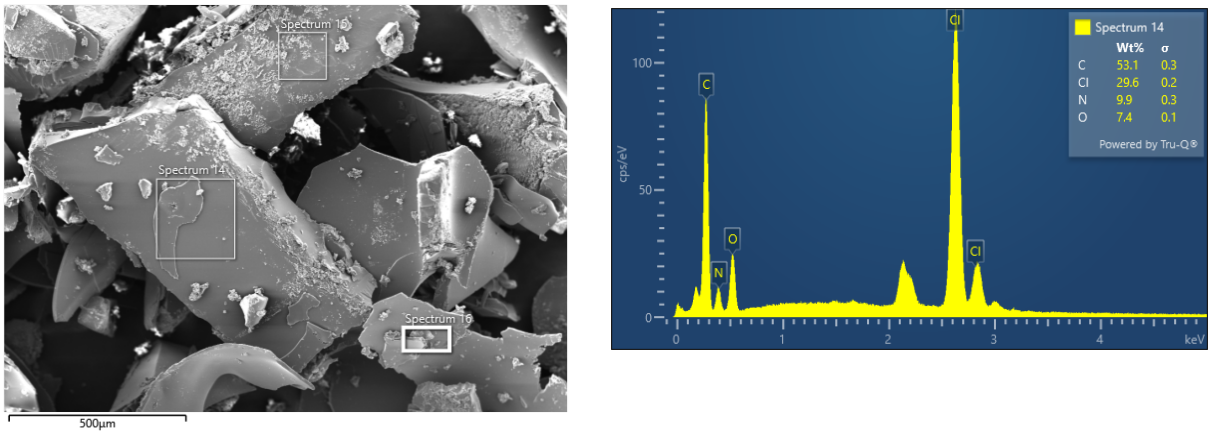


Figure 4.S3: Energy dispersive X-ray spectroscopy (EDS) of netPoly(DETA)-*ν*-ECH MP.

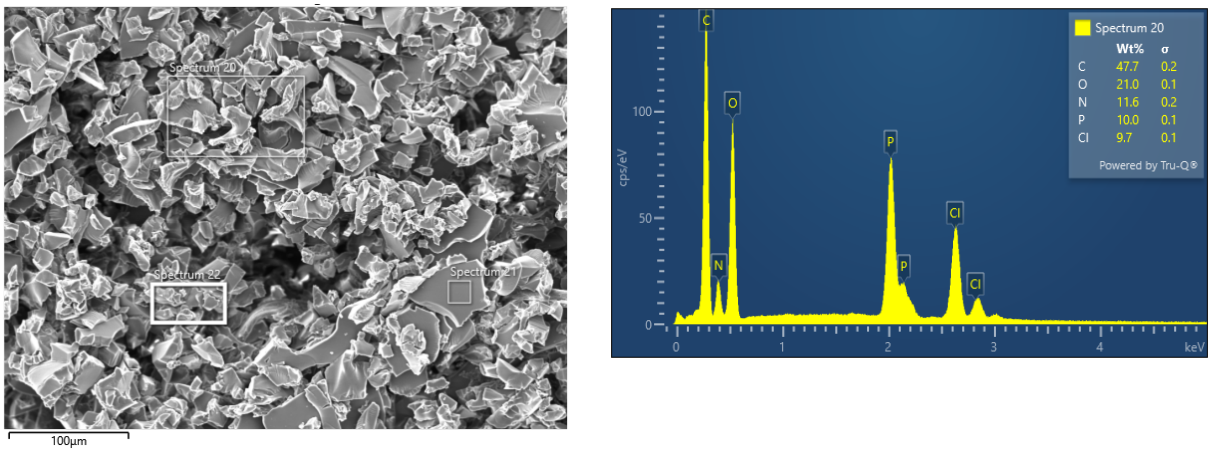


Figure 4.S4: REE desorption after acid wash. After adding 15 mL (3 × 5 mL) of the REE solution, 3 mL of 0.5 M HNO3 was passed over the same resin to desorb the bound REEs.

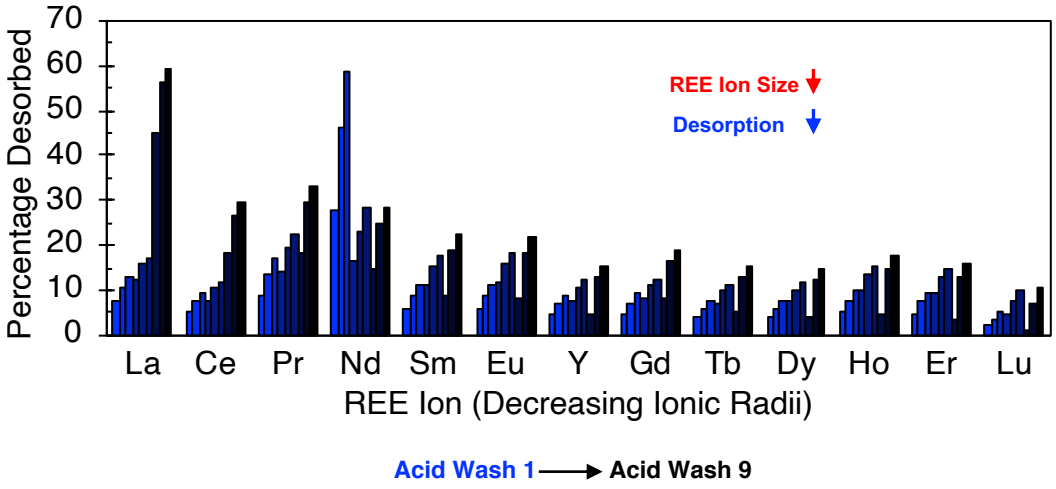
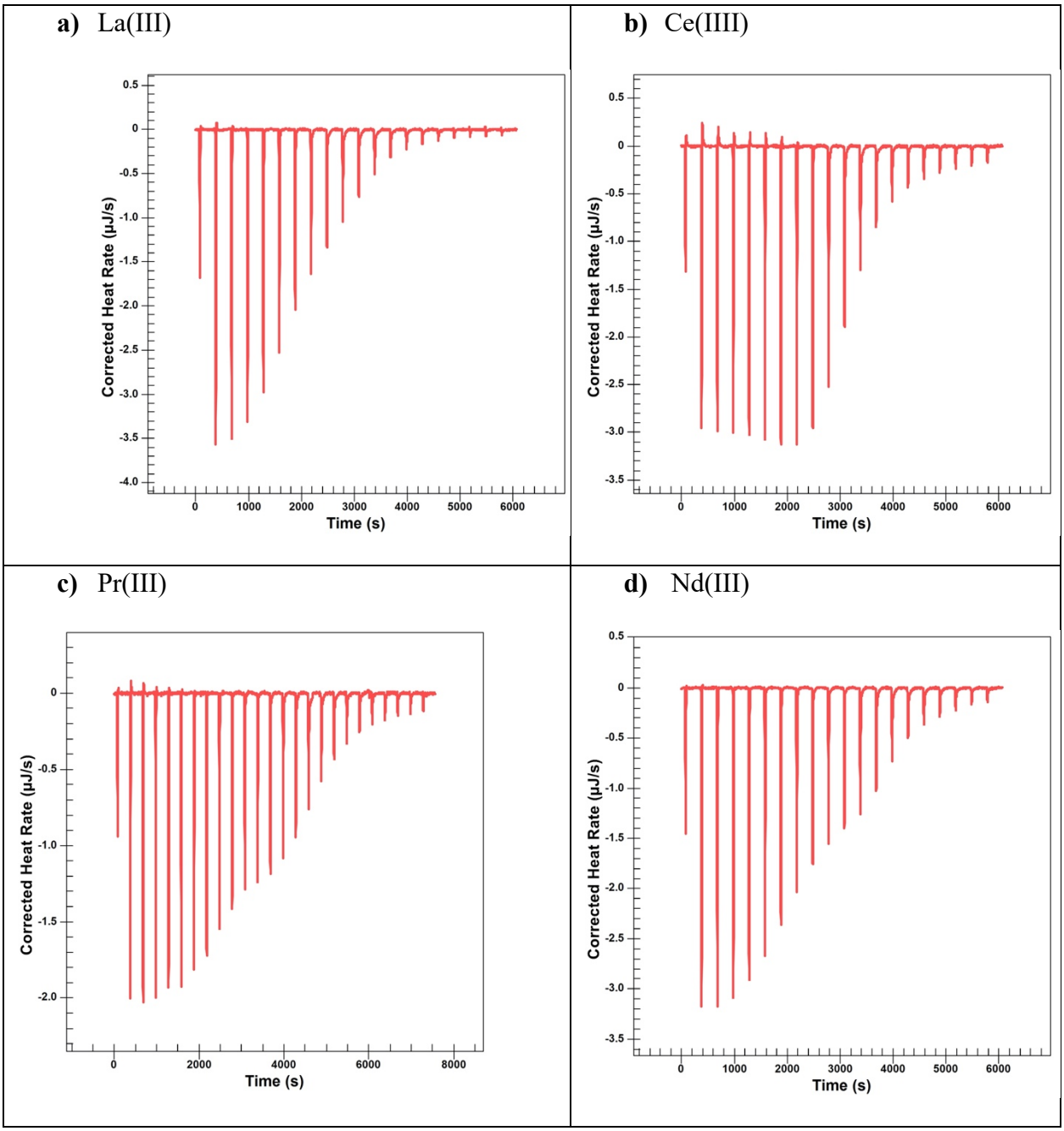
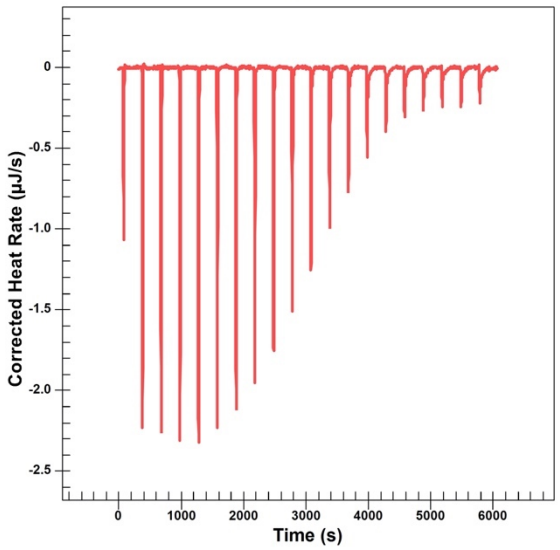


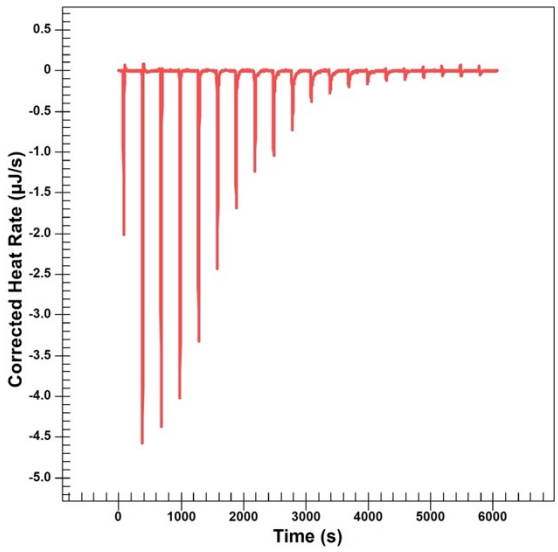
Figure 4.S5: ITC thermograms for REE–PEI-MP titrations.



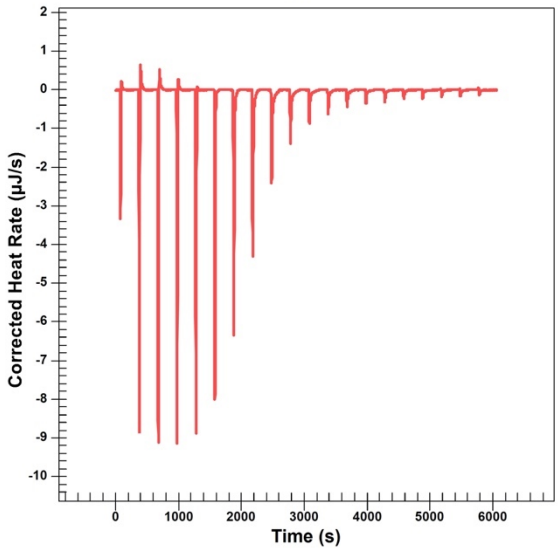
e) Sm(III)



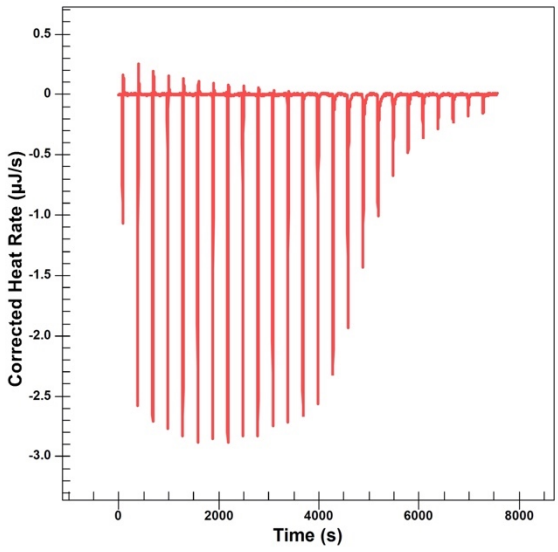
f) Eu(III)



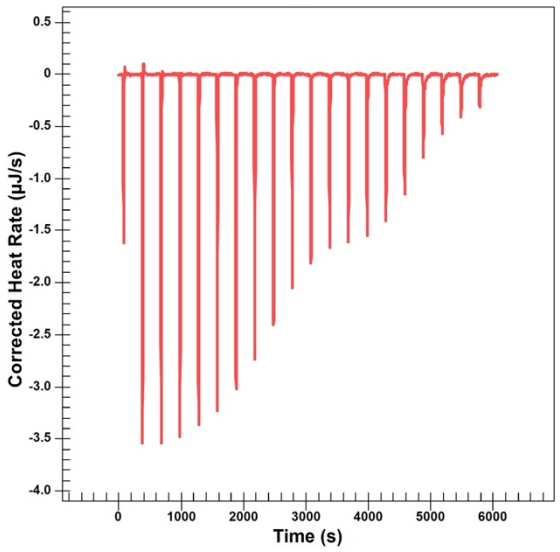
g) Y(III)



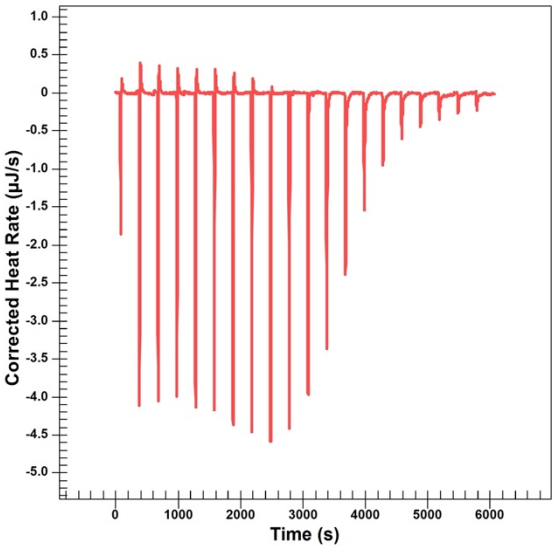
h) Gd(III)



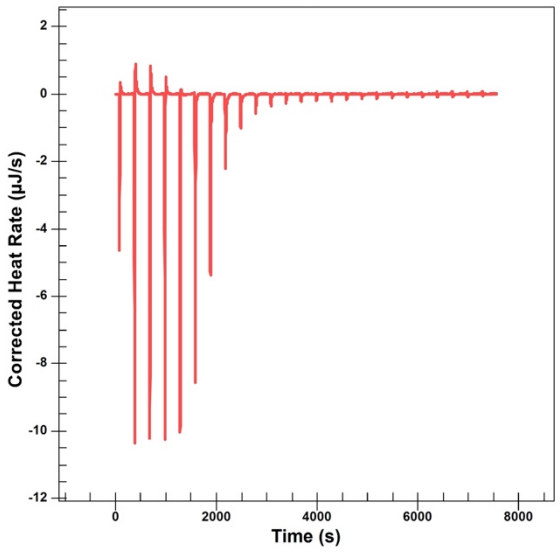
i) Tb(III)



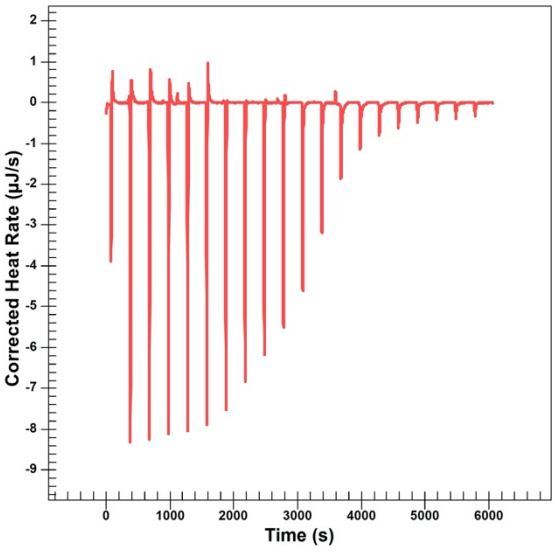
j) Dy(III)



k) Ho(III)



l) Er(III)



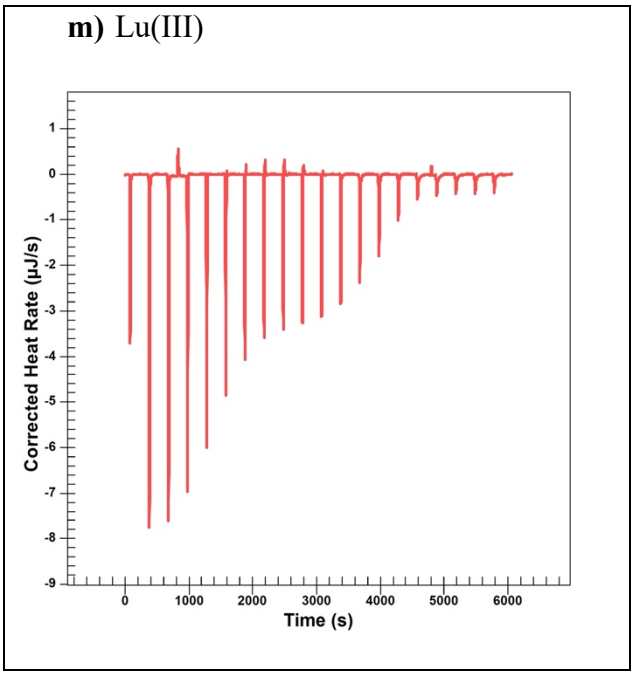
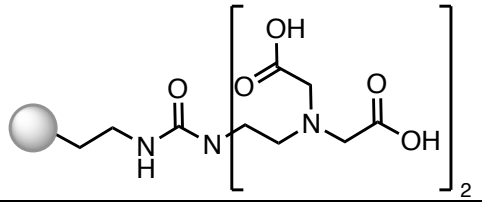
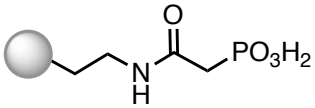
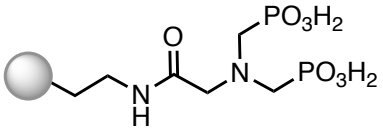
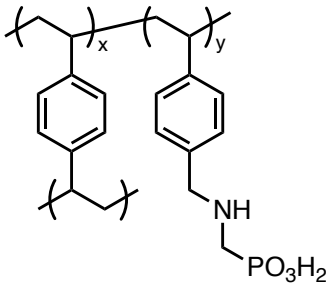
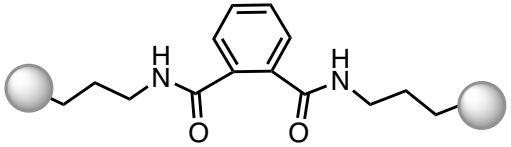
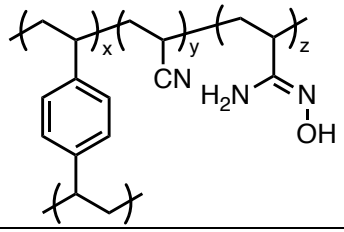
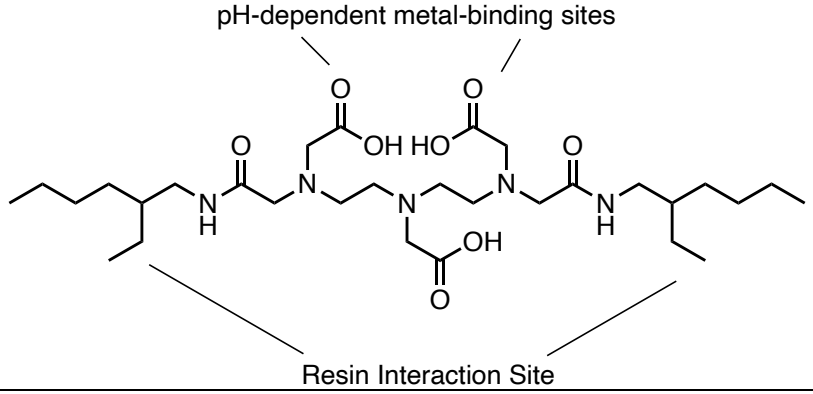
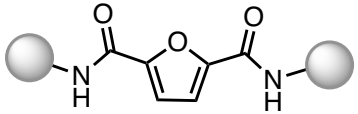
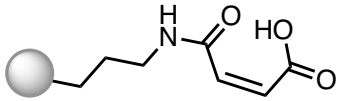


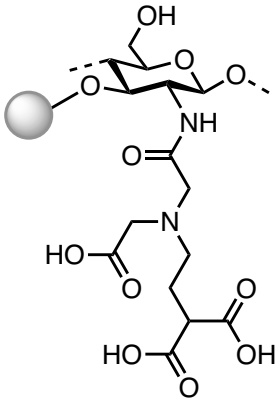
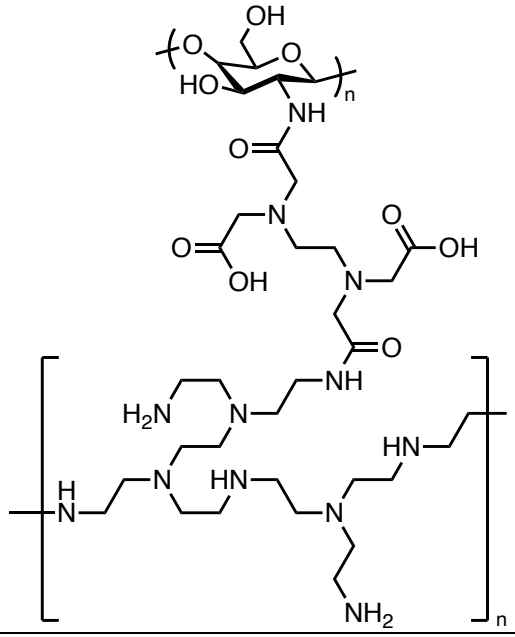
Table 4.S2: Metal and polymer concentrations used for ITC experiments.

Sample	Concentration (mM)	Sample	Concentration(mM)
La(III)	2.1	Gd(III)	3.6
Ce(III)	3.5	Tb(III)	1.9
Pr(III)	3.5	Dy(III)	2.6
Nd(III)	2.5	Ho(III)	5.3
Sm(III)	2.2	Er(IIII)	3.2
Eu(III)	2.1	Lu(III)	5.3
Y(III)	3.6	PEI-MP	1.5

Table 4.S3: Chemical structure, contact time, initial concentration, and REE capacity of comparison materials reported in Fig. 7.

Reference	Chemical Structure	Contact Time	Initial Concentration	Capacity (mg REE per g material)
J. Colloid Interface Sci. **2019,** 557, 465–477.		4 h.	300 ppb REE	3
J. Colloid Interface Sci. **2019,** 557, 465–477.		4 h.	300 ppb REE	5
J. Colloid Interface Sci. **2019,** 557, 465–477.		4 h.	300 ppb REE	3
Metals **2018,** 8, 682.		24 h.	0.5–100 ppm REE	7
ACS Appl. Mater. Interfaces **2017,** 9, 38584–38593.		2 h.	5–100 ppm REE	9

J. Disper. Sci. Technol. **2010,** 31, 1128–1135.		16 h.	40 ppm REE	30
Sep. Purif. Technol. **2021,** 258, 118061.		24 h.	80 ppm REE	21
RSC Adv. **2015,** 5, 103782–103789.		Flow 1 mL min^{-1}	15 ppb Eu	75
J. Mater. Chem. A **2015,** 3, 10327–10335.		4 h.	50 ppm Gd	77

J. Mater. Chem. A **2014,** 2, 19415–19426.		4 h.	72 ppm Lu	108
Chem. Eng. J. **2020,** 388, 124307.		6 h**.**	100 ppm Lu	280

References:

1. APHA; AWWA; WEF, *Standard Methods for Examination of Water and Wastewater*. 20 ed.; 1998.
2. Freyer, M. W.; Lewis, E. A., Isothermal Titration Calorimetry: Experimental Design, Data Analysis, and Probing Macromolecule/Ligand Binding and Kinetic Interactions. In *Method. Cell Biol.* , Academic Press: 2008; Vol. 84, pp 79–113.
3. Mizoue, L. S.; Tellinghuisen, J. The role of backlash in the "first injection anomaly" in isothermal titration calorimetry. *Anal. Biochem.* **2004,** 326 (1), 125–127.

Chapter 5. Effect of Copolymer Structure on Rare-Earth-Element Chelation Thermodynamics

William R. Archer[1], Tiffany N. Thompson[1], and Michael D. Schulz[1]

1: Department of Chemistry and Macromolecules Innovation Institute
Virginia Tech, Blacksburg, VA USA 24061

This chapter was submitted and accepted for publication in *Macromolecular Rapid Communications*.[1] Reprinted with permission from Wiley: Archer, W.R.; Thompson, T.N; and Schulz M.D. Effect of Copolymer Structure on Rare-Earth-Element Chelation Thermodynamics. *Macromol. Rapid Commun*. **2021**, *42*, 2000614. Copyright 2021.

5.1 Abstract

Rare-earth elements (REEs) are crucial to modern technology, leading to a high demand for materials capable of REE extraction and purification. Metal-chelating polymers (e.g., polycarboxylic acids, polyamines, and others) are particularly useful in these applications due to their synthetic accessibility and high selectivity. We synthesized copolymers with varied mole fractions of acrylic acid and methyl acrylate and used isothermal titration calorimetry (ITC) to measure the thermodynamics of REE binding for each material. Across a series of copolymer compositions, we found entropically driven binding thermodynamics (ΔG, ΔH, and ΔS) that appear to be independent of $\chi_{Acrylic\ Acid}$. ITC stoichiometry data for N revealed that each copolymer required between 4–5 repeat units to bind each REE. These data suggest that alterations in the copolymer structure do not affect the overall binding thermodynamics of REEs to these copolymers.

5.2 Introduction

In 2016, the global production of rare-earth elements (REEs: La–Lu, Y, Sc) was estimated to be 125,000 metric tons.[2] As REEs are critical components in modern technologies including batteries, magnets, and phosphors, REE demand is expected to reach a compounded annual growth rate of 10.4% between 2019 and 2025.[3-5] Commercially, REEs are extracted from primary minerals such as bastnaesite and monazite by multi-step operations that generate high volumes of toxic waste.[6] Additionally, REE extraction from secondary sources (e.g., clay and coal seams, recycled magnets, etc.) can be accomplished using ionic solvents or materials.[7-9]

One approach for extracting and purifying REEs is to employ polymeric chelators—polymers containing ligands that can selectivity bind REEs in solution—in conjunction with polymer enhanced ultrafiltration (PEUF).[10, 11] In PEUF, water-soluble, high-molecular-weight polymer chelators bind to the desired metal ion in solution.[12] After binding, the polymer–metal ion complex is rejected by an ultrafiltration membrane. Specifically, poly(acrylic acid) and related copolymers have been used in PEUF applications due to their high water solubility, ease of synthesis, and high affinity for metal ions.[13-15] The carboxylates on poly(acrylic acid) (Lewis bases) ionically interact with REEs (Lewis acids) at pH > 4.0.[16-18] Derivatives and copolymers of poly(acrylic acid) have proven useful in metal-chelating applications; however, few studies have systemically studied the effect of monomer composition of poly(acrylic acid) copolymers on REE binding.

Isothermal titration calorimetry (ITC) enables the direct measurement of the ΔH, binding affinity (K_a), and stoichiometry (N) of binding reactions in solution.[19-22] From these parameters, ΔS, and ΔG of binding are calculated according to **Equations 5.1** and **5.2**. Using ITC, we previously quantified the thermodynamics of REE binding to linear poly(ethylenimine

methylenephosphonate) (PEI-MP).[23] Here, we synthesized poly(acrylic acid–*co*–methyl acrylate) copolymers and examined the effect of copolymer composition on REE-binding thermodynamics using ITC.

Equations 5.1 and 5.2. Calculation of thermodynamic parameters from the ITC titration curve.

(5.1) $$\Delta G = -RT\ln(K_a)$$

(5.2) $$\Delta H = \Delta G - T\Delta S$$

5.3 Results and Discussion

We used reversible addition-fragmentation chain-transfer (RAFT) polymerization to synthesize a series of copolymers with tailored compositions of acrylic acid (AA) and methyl acrylate (MA) units by varying the relative feed ratios between each monomer (**Table 5.1**). In each case, the percent conversion of AA and MA were nearly identical, indicating that the polymerizations resulted in materials with final compositions in close agreement with the initial feed ratios. The reactivity ratios of AA and MA are approximately 1.1 and 0.95, respectively, which further suggests nearly random incorporation of each monomer.[24, 25] Each copolymer exhibited acceptable agreement between the theoretical and experimental molecular weight with narrow molecular weight distributions ($Đ \leq 1.3$), and size-exclusion chromatography (SEC) traces of the final polymers were monomodal and narrow (**Table 5.1 and SI**). To ensure the trithiocarbonate end-groups would not affect our REE-binding thermodynamic measurements, we reduced them *via* reaction with $(TMS)_3SiH$ and ultraviolet light (**Fig. 5.1**).[26] Successful removal of the trithiocarbonate end-group was confirmed both visually by a color change of the polymer solution from yellow to clear, and spectroscopically using ^1H NMR and UV-vis (**SI**).

Table 5.1. Properties of poly(AA–*co*–MA) (co)polymer series.

Entry	Feed Ratio[a]	% Conversion[b]	M_n(Theoretical)[b] (g mol^{-1})	M_n(SEC)[c] (g mol^{-1})	Đ[d]
1	100:0	94.4	7,160	8,830	1.3
2	90:10	89.9	7,130	7,750	1.3
3	80:20	95.3	7,550	9,580	1.1
4	60:40	96.9	7,980	6,350	1.1
5	40:60	88.6	8,710	6,970	1.2
6	10:90	86.6	9,880	5,070	1.1

[a][Acrylic acid]:[Methyl acrylate]. [b]Determined from ^{1}H NMR spectroscopy by comparing the integrations of the monomer acrylate signals before and after the polymerization. [c]Determined from size exclusion chromatography. [d]M_w/M_n.

To further confirm the final polymer compositions following RAFT polymerization, we measured the glass-transition (T_g) temperature of each (co)polymer. The Fox equation (**Equation 5.3**) defines the relationship between the $T_{g,\ copolymer}$ and the weight fraction of each monomer ($\omega_{Acrylic\ Acid}$ and $\omega_{Methyl\ Acrylate}$), where $T_{g,Acrylic\ Acid}$ and $T_{g,Methyl\ Acrylate}$ are the T_g's of the two homopolymers (poly(AA) and poly(MA)), respectively.[27-29] The Fox equation predicts that as the MA content of a copolymer increases, the T_g will decrease. For our copolymer series, we found good agreement between the predicted and experimental T_g's (**SI**), further confirming the final monomer composition of each polymer.

Equation 5.3. The Fox equation for predicting the T_g of copolymers.

(5.3)
$$\frac{1}{T_{g,copolymer}} \approx \frac{\omega_{Acrylic\ Acid}}{T_{g,Acrylic\ Acid}} + \frac{\omega_{Methyl\ Acrylate}}{T_{g,Methyl\ Acryalte}}$$

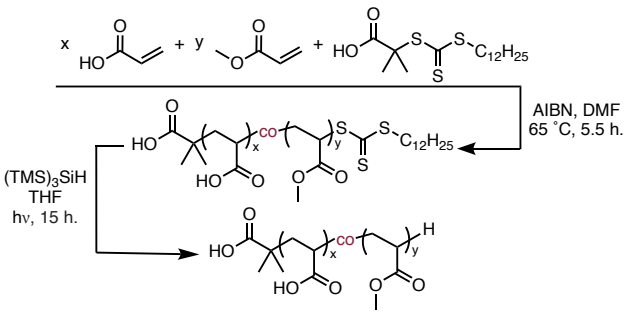


Figure 5.1. Synthesis of poly(acrylic acid–*co*–methyl acrylate) via RAFT polymerization and subsequent removal of the trithiocarbonate end-group.

Using ITC, we measured the thermodynamics of polymer–REE binding in a pH 5 buffered aqueous solution. Small heats of dilution determined from control experiments (REE into buffer (*without polymer present*) and buffer into polymer (*without REE present*)) were subtracted before curve fitting (**Fig. 5.2A–B**). These control experiments confirmed the absence of any significant buffer–polymer and buffer–REE interactions.

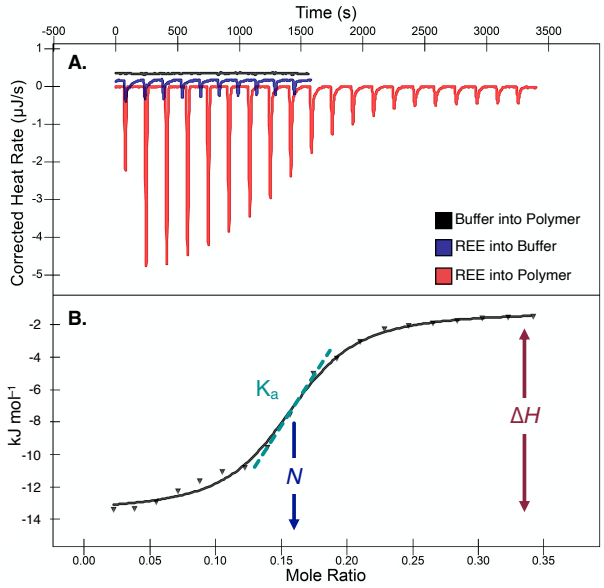


Figure 5.2. A. Representative ITC thermogram (red) overlaid with control titrations (blue and black) and **B.** ITC titration curve annotated with ΔH, K_a, and N.

We first measured the binding thermodynamics of a poly(AA) homopolymer to a series of REEs (La(III), Eu(III), Ho(III), and Lu(III)) (**Fig. 5.3A**). In the ITC thermogram (**Fig. 5.2A**), the downward peaks represent endothermic Δ*H*'s that arise from the injection of the REE solution into the polymer solution. Initially, the Δ*H*'s are large because there are many binding interactions, however as the polymer becomes saturated with the metal ions, there are fewer binding reactions, thus the Δ*H* for each injection becomes smaller. Binding thermodynamics of the poly(AA) homopolymer chelating to the REE series was largely uniform. The average Δ*G* was –27.9 ± 1.3 kJ mol^{-1} (95 % Confidence interval (CI), [–28.6, –27.2]), indicating poly(AA) binds to each REE with approximately the same degree of favorability. The mole ratio at the inflection point in the ITC titration curve represents the binding stoichiometry, *N* (**Fig. 5.2B**). For this REE series, the binding stoichiometry was approximately 5:1, suggesting that on average each REE was bound by approximately five acrylic acid repeat units (95 % CI, [5.4, 5.8]) (**Fig. 5.4A**). This result correlates well with the expected coordination numbers for the lanthanides, which can vary between 5–9 ligands.[30]

Since binding thermodynamics across this series of REEs was nearly uniform when chelating the poly(AA) homopolymer, we chose to use one REE (Eu(III)) for the remaining poly(AA–*co*–MA) series. To examine the effect of $\chi_{Acrylic\ Acid} : \chi_{Methyl\ Acylate}$ on REE binding, ITC experiments were conducted on each of the copolymers in triplicate by titrating a Eu(III) solution into a copolymer solution. Again, the thermodynamics of binding were nearly identical for each copolymer (**Fig. 5.3B**). The average Δ*G* for the copolymer series binding with Eu(III) was –26.7 ± 1.2 kJ mol^{-1} (95 % CI, [–27.3, –26.2]). Furthermore, each binding event was endothermic, with a relatively large |–TΔ*S*| term. This result indicates that REE binding is entropically driven,

likely due to the release of solvent (water) molecules surrounding both the REE ion and polymer chain.[31]

The (de)protonation state of the acrylic acid units is an important consideration in REE binding. The pKa of the carboxylic acid moiety in the AA repeat unit is approximately 4.8, thus at pH 5 (the pH at which these ITC experiments were performed), we would expect approximately 60 % of AA in poly(AA–*co*–MA) to be deprotonated and anionic.[32] In salt (e.g., buffer) solutions, anionic polymers typically adopt a random coil conformation resulting from the screening of repulsive forces, allowing the polymer to assume a more entropically favored conformation.[33, 34] We would expect that as the χ_{AA} decreases, the copolymer conformation would change as the number of ionic repulsions decreases due to fewer neighboring AA moieties. The change in polymer conformation with decreasing χ_{AA} could influence the magnitude of the $-T\Delta S$ term during REE binding; however, this is not the case as the average $-T\Delta S$ was –39.1 ± 1.0 kJ mol^{-1} (95 % CI, [–39.5, –38.6]), with only a marginal decrease in $-T\Delta S$ as χ_{MA} increased. We hypothesize that the ΔS associated with the release of solvent molecules is much greater than the ΔS associated with polymer conformational changes, leading to this observation. While we cannot disregard the importance of the polymer conformational changes during REE binding, the ITC experiments presented here cannot deconvolute the exact entropic contributions of solvation and conformational changes.

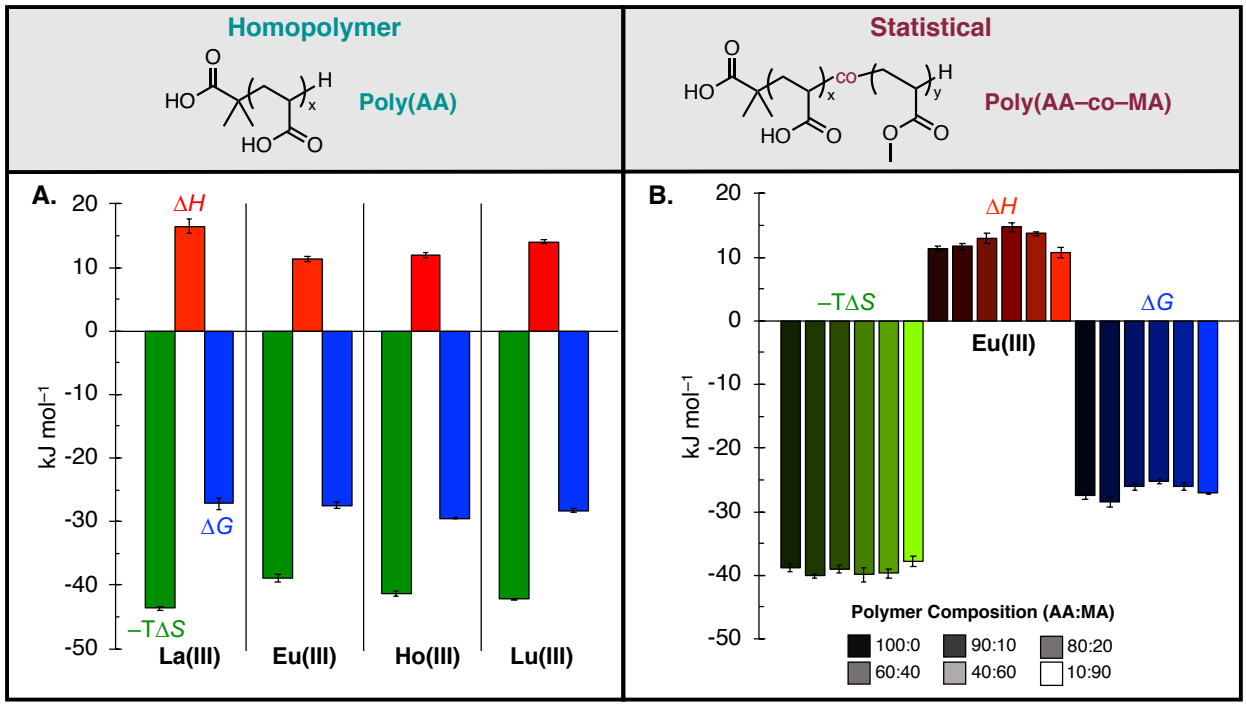


Figure 5.3. Binding thermodynamics of **A**. REEs (La(III), Eu(III), Ho(III), and Lu(III)) binding to poly(AA) homopolymer and **B.** Eu(III) binding to poly(AA–*co*–MA) statistical copolymers ($\chi_{Acrylic\ Acid} : \chi_{Methyl\ Acylate}$= 1.0:0.0, 0.9:0.1, 0.8:0.2, 0.6:0.4, 0.4:0.6, and 0.1:0.9). Values represented as the average of 3 measurements, error bars are the standard deviations of 3 measurements.

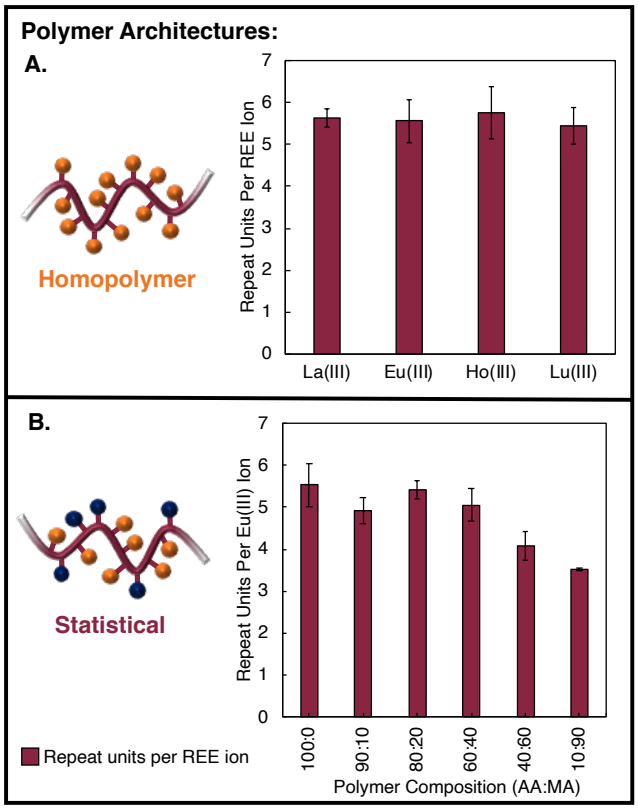


Figure 5.4. Binding stoichiometry of **A**. REEs (La(III), Eu(III), Ho(III), and Lu(III)) binding to poly(AA) homopolymer and **B.** Eu(III) binding to poly(AA–*co*–MA) statistical copolymers (χ_{AA} : χ_{MA}= 1.0:0.0, 0.9:0.1, 0.8:0.2, 0.6:0.4, 0.4:0.6, and 0.1:0.9). Values represented as the average of 3 measurements, error bars are the standard deviations of 3 measurements.

The binding stoichiometry, *N*, of the statistical copolymers binding to Eu(III) revealed a noteworthy trend (**Fig. 5.4B**). For the poly(AA) homopolymer, each Eu(III) was bound, on average, by ~5 AA repeat units. For each of the statistical copolymers, the average binding stoichiometry was 4.8 ± 0.8 polymer repeat units (95 % CI, [4.4, 5.1]). The binding stoichiometry remained largely uniform for copolymers with higher AA content; however, the number of repeat units per Eu(III) slightly decreased as χ_{AA} decreased below 0.6, presumably due to the decreased number of AA units along the polymer chain. The fact that the copolymer with smallest χ_{AA} (0.10 : 0.90) was still able to bind Eu(III) suggests an inefficiency in binding REEs with the AA homopolymer where not every AA repeat unit is available for binding. Further, this result suggests

that incorporating non-chelating monomers (e.g., MA) into the polymer structure may increase REE sorption capacity as a fewer AA units seems to result in a higher binding efficiency, i.e., more REEs are bound per repeat unit.

The ability to release the absorbed metal ions and regenerate the sorbent is critical in PEUF processes. The equilibrium binding affinity obtained in the ITC experiment, K_a, provides information on the strength and reversibility of the binding interaction: Higher binding affinity implies that fewer chelating units are required to fully capture the metal ions in solution.[35] However, higher binding affinity also indicates that stronger polymer-metal complexes will form, making the interaction less reversible. This lack of reversibility may pose a challenge to recovering the captured metal and recycling the chelating materials. K_a was largely uniform across the series of (co)polymers; the average K_a was $5.4 \times 10^4 \pm 2.8 \times 10^4$ M^{-1} (95 % CI, [4.1×10^4, 6.7×10^4]), indicating that each copolymer bound Eu(III) with nearly the same effectiveness.

5.4 Conclusions

In conclusion, we synthesized a series of AA and MA statistical copolymers ($\chi_{AA} : \chi_{MA}$ between 1:0 and 0.1:0.9) and examined the effect of copolymer composition on the thermodynamics of REE binding using ITC. We first examined the binding thermodynamics of poly(AA) to a series of REEs and found that each ion exhibited uniform binding thermodynamics. From this REE series, we chose to closely examine the binding of Eu(III) to poly($AA_{1–0.1}$–*co*–$MA_{0–0.9}$). For our copolymers, we found entropically driven thermodynamics that appear to be independent of copolymer composition (ΔG = –27.1 ± 0.9 kJ mol^{-1}). Interestingly, ITC data for N indicated that incorporating methyl acrylate into the polymer structure slightly reduced the number of repeat units required to bind a REE. This data on the underlying thermodynamics of polymer–

REE binding will inform the design of future materials for REE extraction and recovery. This work further suggests the potential application of ITC in evaluating the selectivity of metal ions to predict the behavior of perspective materials for PEUF.

Acknowledgements

The authors wish to acknowledge the Virginia Tech Department of Chemistry Faculty Start-up funds for financial support. Additionally, WRA and TNT wish to acknowledge the help of Mr. Benjamin Stovall for his assistance with the collection of DSC data of the copolymers.

Keywords

Rare-earth elements (REEs), Isothermal titration calorimetry (ITC), and metal-binding polymers.

5.5 References

1. Archer, W. R.; Thompson, T. N.; Schulz, M. D. Effect of Copolymer Structure on Rare-Earth-Element Chelation Thermodynamics. *Macromol. Rapid Commun.* **2021,** 42 (8), 2000614.
2. Zhou, B.; Li, Z.; Chen, C. Global Potential of Rare Earth Resources and Rare Earth Demand from Clean Technologies. *Minerals* **2017,** 7 (11), 203.
3. Pandey;, B. D.; Abhilash;; Meshram, P., An Overview of the Recent Status of Critical and Strategic Metal Production and Development in India. In *Critical and Rare Earth Elements*, Akcil, A. a. A., Ed. CRC Press: 2019; pp 1–36.
4. Zhang, W.; Noble, A. Mineralogy characterization and recovery of rare earth elements from the roof and floor materials of the Guxu coalfield. *Fuel* **2020,** 270, 117533.
5. Ellis, R. J.; Brigham, D. M.; Delmau, L.; Ivanov, A. S.; Williams, N. J.; Vo, M. N.; Reinhart, B.; Moyer, B. A.; Bryantsev, V. S. "Straining" to Separate the Rare Earths: How the Lanthanide Contraction Impacts Chelation by Diglycolamide Ligands. *Inorg. Chem.* **2017,** 56 (3), 1152-1160.
6. Sui, N.; Huang, K.; Zhang, C.; Wang, N.; Wang, F.; Liu, H. Light, Middle, and Heavy Rare-Earth Group Separation: A New Approach via a Liquid–Liquid–Liquid Three-Phase System. *Ind. Eng. Chem. Res.* **2013,** 52 (17), 5997–6008.
7. Yoon, H.-S.; Kim, C.-J.; Chung, K.-W.; Kim, S.-D.; Lee, J.-Y.; Kumar, J. R. Solvent extraction, separation and recovery of dysprosium (Dy) and neodymium (Nd) from

aqueous solutions: Waste recycling strategies for permanent magnet processing. *Hydrometallurgy* **2016,** 165, 27–43.
8. Zhang, W.; Noble, A.; Yang, X.; Honaker, R. A Comprehensive Review of Rare Earth Elements Recovery from Coal-Related Materials. *Minerals* **2020,** 10 (5).
9. Sarfo, P.; Frasz, T.; Das, A.; Young, C. Hydrometallurgical Recovery and Process Optimization of Rare Earth Fluorides from Recycled Magnets. *Minerals* **2020,** 10 (4).
10. Archer, W. R.; Hall, B. A.; Thompson, T. N.; Wadsworth, O. J.; Schulz, M. D. Polymer s equestrants for biological and environmental applications. *Polym. Int.* **2019,** 68 (7), 1220–1237.
11. Duan, H.; Lin, J.; Gong, Z.; Huang, J.; Yang, S. Removal of high-salinity matrices through polymer-complexation–ultrafiltration for the detection of trace levels of REEs using inductively coupled plasma mass spectrometry. *Talanta* **2015,** 143, 287–293.
12. Huang, Y.; Feng, X. Polymer-enhanced ultrafiltration: Fundamentals, applications and recent developments. *J. Membr. Sci.* **2019,** 586, 53–83.
13. Rivas, B. L.; Palencia, M. Removal-concentration of pollutant metal-ions by water-soluble polymers in conjunction with double emulsion systems: A new hybrid method of membrane-based separation. *Separ. Purif. Technol.* **2011,** 81 (3), 435–443.
14. Rivas, B. L.; Pereira, E. D.; Moreno-Villoslada, I. Water-soluble polymer–metal ion interactions. *Prog. Polym. Sci.* **2003,** 28 (2), 173–208.
15. Rivas, B. L.; Martínez, E.; Pereira, E.; Geckeler , K. E. Synthesis, characterization and polychelatogenic properties of poly[(2-acrylamido-2-methyl-1-propane sulfonic acid)-co-(methacrylic acid)]. *Polym. Int.* **2001,** 50 (4), 456-462.
16. Giroux, S.; Aury, S.; Henry, B.; Rubini, P. Complexation of Lanthanide(III) Ions with Polyhydroxy Carboxylic Acids in Aqueous Solutions. *Eur. J. Inorg. Chem.* **2002,** 2002 (5), 1162–1168.
17. Qi, X.; Wang, Z.; Ma, S.; Wu, L.; Yang, S.; Xu, J. Complexation behavior of poly(acrylic acid) and lanthanide ions. *Polymer* **2014,** 55 (5), 1183–1189.
18. Montavon, G.; Hennig, C.; Janvier, P.; Grambow, B. Comparison of complexed species of Eu in alumina-bound and free polyacrylic acid: A spectroscopic study. *J. Colloid Interface Sci.* **2006,** 300 (2), 482–490.
19. Turnbull, W. B.; Daranas, A. H. On the Value of c: Can Low Affinity Systems Be Studied by Isothermal Titration Calorimetry? *J. Am. Chem. Soc.* **2003,** 125 (48), 14859–14866.
20. Weber, A.; Dettling, M.; Brunner, H.; Tovar, G. E. M. Isothermal Titration Calorimetry of Molecularly Imprinted Polymer Nanospheres. *Macromol. Rapid Commun.* **2002,** 23 (14), 824–828.
21. Archer, W. R.; Schulz, M. D. Isothermal titration calorimetry: practical approaches and current applications in soft matter. *Soft Matter* **2020,** 16 (38), 8760–8774.
22. Illy, N.; Majonis, D.; Herrera, I.; Ornatsky, O.; Winnik, M. A. Metal-Chelating Polymers by Anionic Ring-Opening Polymerization and Their Use in Quantitative Mass Cytometry. *Biomacromolecules* **2012,** 13 (8), 2359–2369.
23. Archer, W. R.; Fiorito, A.; Heinz-Kunert, S. L.; MacNicol, P. L.; Winn, S. A.; Schulz, M. D. Synthesis and Rare-Earth-Element Chelation Properties of Linear Poly(ethylenimine methylenephosphonate). *Macromolecules* **2020,** 53 (6), 2061–2068.
24. Chapiro, A. Influence of solvents on apparent reactivity ratios in the free radical copolymerization of polar monomers. *Eur. Polym. J.* **1989,** 25 (7), 713-–17.

25. Eldridge, R. J.; Treloar, F. E. Reactivity ratios for acrylic acid–methyl acrylate copolymerization in 1,4-dioxane. *J. Polym. Sci. Polym. Chem. Ed.* **1976,** 14 (11), 2831–2834.
26. Bou Zerdan, R.; Geng, Z.; Narupai, B.; Diaz, Y. J.; Bates, M. W.; Laitar, D. S.; Souvagya, B.; Van Dyk, A. K.; Hawker, C. J. Efficient synthesis of branched poly(acrylic acid) derivatives via postpolymerization modification. *J. Polym. Sci.* **2020,** 58 (14), 1989–1997.
27. Fox, T. G. Influence of diluent and of copolymer composition on the glass temperature of a polymer system. *Bull. Am. Phys. Soc.* **1956,** 1, 123.
28. Maurer, J. J.; Eustace, D. J.; Ratcliffe, C. T. Thermal characterization of poly(acrylic acid). *Macromolecules* **1987,** 20 (1), 196–202.
29. Barton, J. M. Relation of glass transition temperature to molecular structure of addition copolymers. *J. Polym. Sci., C Polym. Symp.* **1970,** 30 (1), 573–597.
30. Cotton, S. A., Scandium, Yttrium & the Lanthanides: Inorganic & Coordination Chemistry. In *Encyclopedia of Inorganic and Bioinorganic Chemistry*.
31. Steed, J. W.; Atwood, J. L., *Supramolecular Chemsitry*. John Wiley & Sons: 2013.
32. Michaels, A. S.; Morelos, O. Polyelectrolyte Adsorption by Kaolinite. *Ind. Eng. Chem.* **1955,** 47 (9), 1801–1809.
33. Mortimer, D. A. Synthetic polyelectrolytes—A review. *Polym. Int.* **1991,** 25 (1), 29–41.
34. Rathee, V. S.; Sidky, H.; Sikora, B. J.; Whitmer, J. K. Explicit Ion Effects on the Charge and Conformation of Weak Polyelectrolytes. *Polymers* **2019,** 11 (1), 183.
35. Hong, L.; Simon, J. D. Current Understanding of the Binding Sites, Capacity, Affinity, and Biological Significance of Metals in Melanin. *J. Phys. Chem. B* **2007,** 111 (28), 7938-7947.

5.6 Supporting Information

Materials

$LaCl_3 \cdot 6H_2O$, $HoCl_3 \cdot 6H_2O$, $EuCl_3 \cdot 6H_2O$, and $LuCl_3 \cdot 6H_2O$ (trace metals grade) were purchased from Sigma Aldrich. DMF, $(TMS)_3SiH$, acrylic acid, and methyl acrylate were obtained from Fisher Scientific. AIBN was recrystallized from MeOH before use. All other chemicals were used as-is.

Polymer characterization

^1H NMR, and ^{13}C NMR spectra were acquired on an Agilent MR4 400 MHz spectrometer. Chemical shifts in the ^1H NMR and ^{13}C NMR spectra were referenced to the residual solvent resonance signals.

Size exclusion chromatography (SEC) eluting with DMAc was conducted on a Shimadzu (Kyoto, Japan). The system was equilibrated at 50 °C in prefiltered DMAc containing 0.05 M LiCl with the flow rate set to 1.00 mL/min. Data analysis was performed using Astra version 7.2.2.10 software (Wyatt Technologies). Molecular weights were determined relative to the dn/dc of polystyrene standards (30 and 200 Da). Polymer solutions were prepared at a concentration of ca. 3 mg/mL, and an injection volume of 200 μL was used.

Differential scanning calorimetry experimental procedure

A DSC Q2000 (TA instruments, New Castle, DE) equipped with an autosampler was used to examine the thermal transitions of the polymer series. Sample masses ranging from 5-9 mg were crimped in a Tzero pan with a Tzero hermetic lid and then loaded into the DSC cell alongside a reference pan. A heat-cool-heat regimen was applied where samples were first heated from room temperature to 150 °C at a rate of 10 °C min^{-1}, then cooled to –50 °C at a rate of –10 °C min^{-1}

followed by a second heat to 150 °C at a rate of 10 °C min^{-1}. The midpoint of the slope from the baseline of an endothermic transition was used to determine the T_g.

Isothermal titration calorimetry experimental procedure

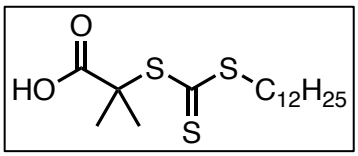
The ITC instrument used was an Affinity-ITC (TA Instruments, New Castle, DE), which operated at constant temperature of 298 K. To carry out a binding experiment, a sample solution was prepared by dissolving the polymer and REE in a pH 5, 100 mM sodium acetate buffer.

Before the ITC experiment, each solution was degassed for 15 minutes. The polymer solution was placed in the sample cell (350 μL) and the reference cell was filled with water (300 μL). Both cells were mounted in an adiabatic chamber, whose temperature was kept constant during the measurement (295 K). A long-needle syringe with a twisted paddle fastened to its end, was filled with the metal ion solution. The syringe was placed inside the sample cell, and the entire syringe assembly was rotated continuously (185 RPM) to provide proper mixing of the content of the sample cell within a few seconds after an injection. After reaching thermal equilibrium, the injection of the metal ion solution was automatically conducted stepwise until the polymer was saturated with the metal ion. Due to the possible dilution of the first measurement, the first injection was ignored in the analysis of data, which is standard practice for ITC experiments. The first 1.0 μL injection was followed by a series of injections of 2.0 μL each. The chosen time interval between two consecutive injections was 300 seconds to ensure that the thermodynamic equilibrium was reached before the next injection.

Nonlinear least-squares curve fitting was conducted using TA Instruments Nano Analyze using TA Instruments Independent model. Heats of dilution from control titrations (metal-ion into

buffer (*without polymer present*), and buffer into polymer (*without metal-ion present*)) were subtracted before curve fitting.

Synthesis of 2-(Dodecylthiocarbonothioylthio)-2-methylpropionic acid (DDMAT)

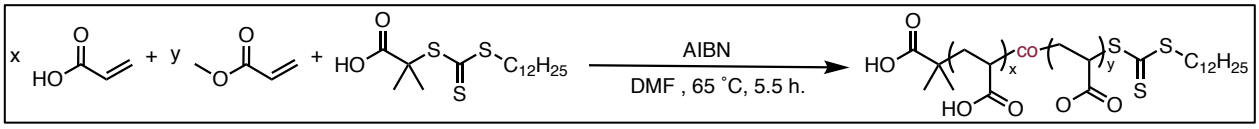


DDMAT was prepared according to the previously reported procedure.[1] Dodecanethiol (5.0 mL, 20.9 mmol, 1.3 eq.) and K_3PO_4 (3.60 g, 16.9 mmol, 1.1 eq.) was combined in a 100 mL round bottomed flak with 70 mL of acetone. After stirring for 20 minutes, CS_2 (3.0 mL, 49.6 mmol, 3.1 eq.) was added dropwise, during which the reaction solution turned yellow. 2-bromo-2-methylpropionic acid (2.64 g, 15.8 mmol, 1.0 eq.) was added to the stirring solution in one portion, and continued to stir overnight at room temperature. 200 mL of 1M HCl (aq) was added to the reaction mixture and then poured into a separatory funnel. The mixture was extracted with DCM (2 x 150 mL). The combined organic layers were dried over $MgSO_4$ and the solvent was removed under reduced pressure. The crude product was recrystallized from hexanes to afford DDMAT as yellow crystals (65 % recovery).

^{1}H NMR (400 MHz, $CDCl_3$, δ): 3.28 (t, 2H), 1.73 (s, 6 H), 1.68 (m, 2H), 1.38 (m, 2 H), 1.28 (s, 16 H), 0.87 (t, 3 H).

^{13}C NMR (100 MHz, $CDCl_3$, δ): 221.3, 178.2, 55.9, 37.5, 32.4, 30.1, 30.0, 29.9, 29.8, 29.6, 29.4, 28.3, 25.7, 23.2, 14.6.

Scheme 5.S1: Synthesis of copolymers *via* RAFT Polymerization



Representative synthesis of 80:20 AA:MA copolymer: Acrylic acid (12.9 mmol, 80 eq.), methyl acrylate (3.43 mmol, 20 eq.), DDMAT (0.160 mmol, 1.0 eq), and AIBN (2.6 mg, 0.1 eq.) were combined in a 20 mL glass vial with 2.5 mL of dry DMF. 1,3,5-trioxane was added as an internal standard. The vial was subsequently sealed with a septum and parafilm, and purged with N_2 for 45 minutes. The vials were then placed in a heating block equilibrated at 65 ˚C. After 5.5 hours, the vials were removed from the heating block and the DMF was removed under reduced pressure. The polymers were dissolved in THF, and precipitated into cold hexanes resulting in a hydroscopic, yellow solid.

Figure 5.S1: Representative ^{1}H NMR of poly(AA–*co*–MA)

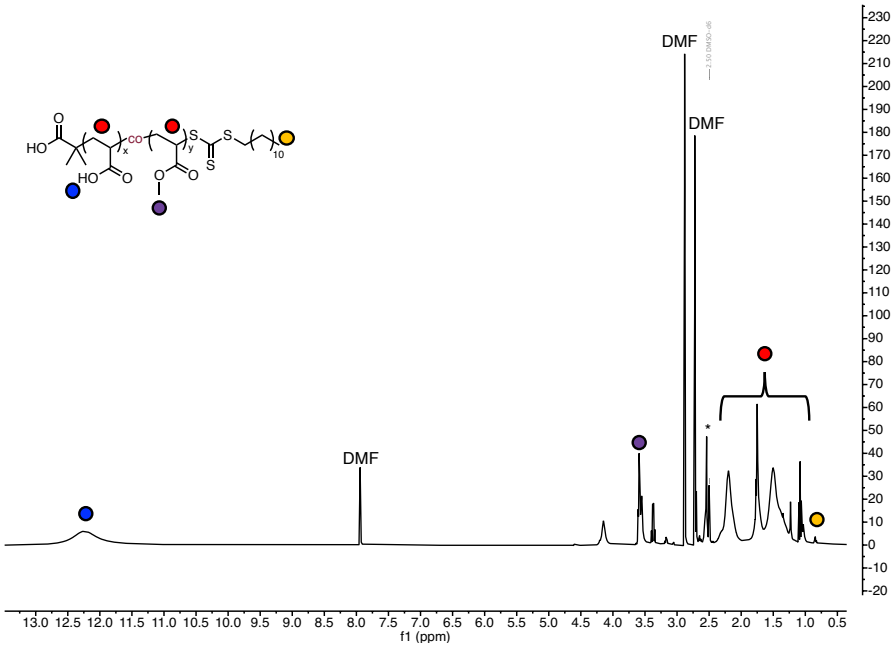


Figure 5.S2: Size exclusion chromatography traces of poly(AA–*co*–MA)

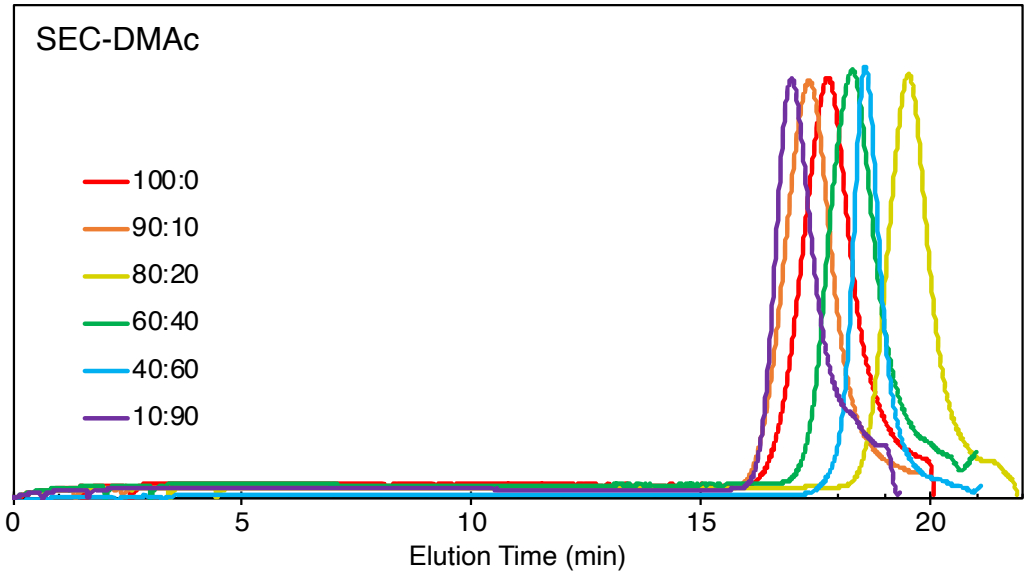


Figure 5.S3: Differential scanning calorimetry thermograms (second heat) of copolymer series

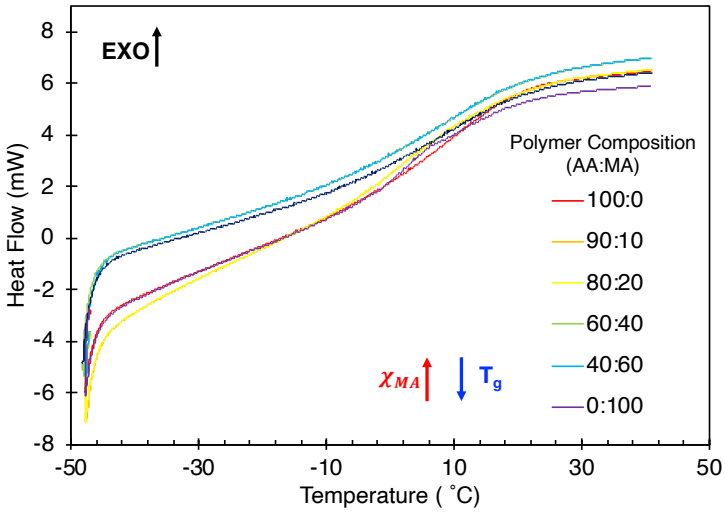
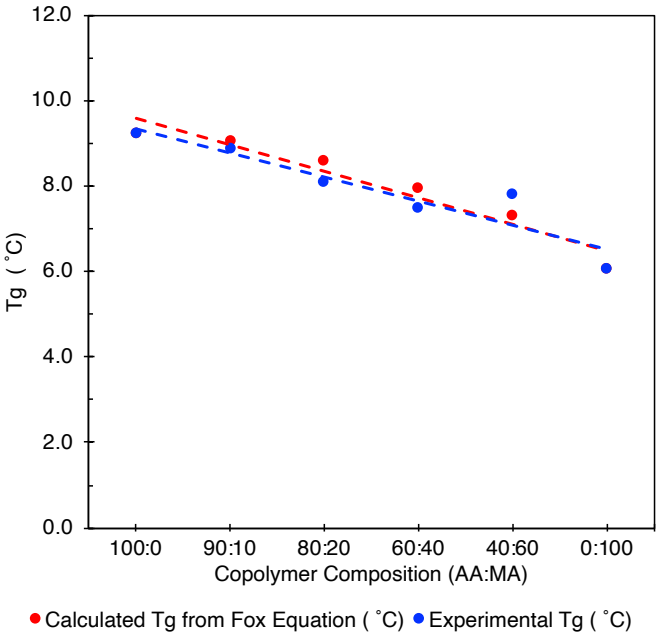
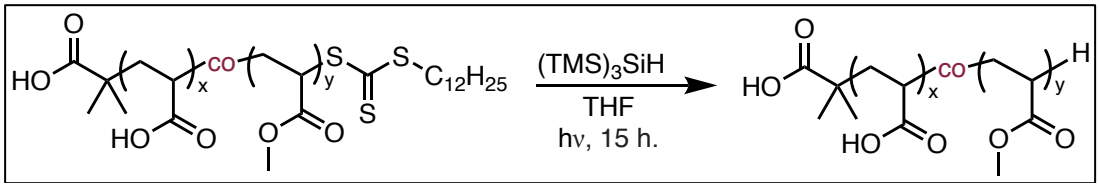


Figure 5.S4: Calculated and experimental T_g's of poly(AA–*co*–MA)



Representative procedure for removal of trithiocarbonate end-group



The trithiocarbonate end-group of the resulting RAFT copolymers was removed according the previously reported literature procedure.[2] The resulting RAFT copolymer was dissolved in 5 mL of THF in a glass vial. $(TMS)_3SiH$ (6 eq. per chain end) was added to the solution and the reaction mixture was sparged with N_2 for 5 minutes. The solution was irradiated with UV-light for 15 hours with stirring. After 15 hours, the solution was precipitated into diethyl ether to provide a white hydroscopic solid.

Figure 5.S5: UV-vis absorption spectra of poly(AA–*co*–MA) before and after end-group removal

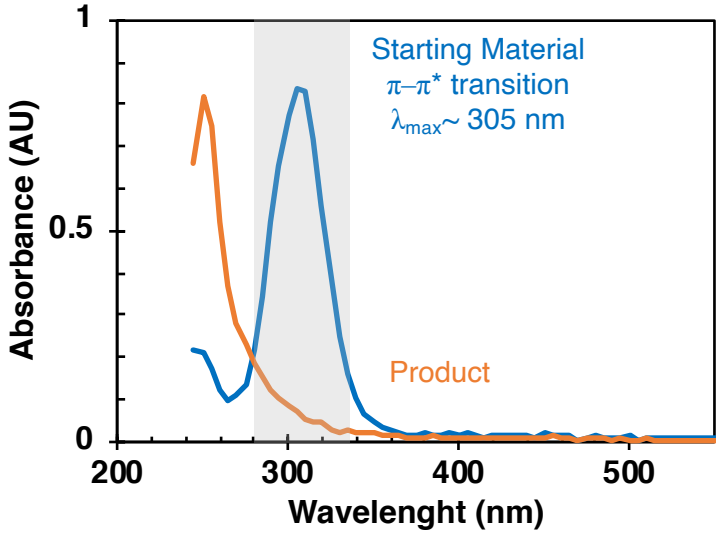


Table 5.S1: Metal and polymer concentrations used for ITC experiments

Sample	Concentration (mM)				
Polymer Composition (AA:MA)	**Poly(AA–*co*–MA)**	**La(III)**	**Eu(III)**	**Ho(III)**	**Lu(III)**
100:0	1.51	2.24	2.24	2.23	2.24
90:10	1.50		2.24		
80:20	1.49		2.24		
60:40	1.49		2.24		
40:60	1.49		2.24		
10:90	1.49		2.24		

Table 5.S2: Average and standard deviations of thermodynamic parameters (n=3).

Polymer Composition (AA:MA)	Δ***H*** (kJ/mol)	–TΔ***S*** (kJ/mol)	Δ***G*** (kJ/mol)	Repeat Units per Eu(III)
100:0	11.4 ± 0.4	–38.8	–27.5	5.5 ± 0.5
90:10	11.7 ± 0.5	–40.1	–28.5	4.9 ± 0.3
80:20	12.9 ± 0.8	–39.1	–26.1	5.4 ± 0.2
60:40	14.7 ± 0.7	–39.9	–25.2	5.0 ± 0.4
40:60	13.7 ± 0.2	–39.7	–26.0	4.1 ± 0.3
10:90	10.8 ± 0.8	–37.8	–27.0	3.5 ± 0.4

References

1. Willersinn, J.; Bogomolova, A.; Cabré, M. B.; Schmidt, B. V. K. J. *Polym. Chem.* **2017**, *8*, 1244–1254.
2. Bou Zerdan, R.; Geng, Z.; Narupai, B.; Diaz, Y. J.; Bates, M. W.; Laitar, D. S.; Souvagya, B.; Van Dyk, A. K.; Hawker, C. J. *J. Polym. Sci.* **2020**, *58*, 1989–1997.

Chapter 6. Exploring the Role of Polymer Hydrophobicity in Polymer–Metal Binding Thermodynamics

William R. Archer[†], *Connor M.B. Gallagher*[†], *V. Vaissier Welborn*[†], *Michael D. Schulz*[†*]

[†] Department of Chemistry, Macromolecules Innovation Institute (MII), Virginia Tech, Blacksburg, VA 24061, United States

This chapter was submitted and accepted for publication in *Physical Chemistry Chemical Physics*.[1] Reprinted with permission from Royal Society of Chemistry: Archer, W.R; Gallagher, C.M.B., Welborn, V.V.; and Schulz, M.D. Exploring the role of polymer hydrophobicity in polymer–metal binding thermodynamics. *Phys. Chem. Chem. Phys.* **2022**, *24*, 3579–3585. Copyright 2022.

6.1 Abstract

Metal-chelating polymers play a key role in rare-earth element (REE) extraction and separation processes. Often, these processes occur in aqueous solution, but the interactions among water, polymer, and REE are largely under-investigated in these applications. To probe these interactions, we synthesized a series of poly(amino acid acrylamide)s with systematically varied hydrophobicity around a consistent chelating group (carboxylate). We then measured the ΔH of Eu^{3+} chelation as a function of temperature across the polymer series using isothermal titration calorimetry (ITC) to give the change in heat capacity (ΔC_P) We observed an order of magnitude variation in ΔC_P (39–471 J mol^{-1} K^{-1}) with changes in the hydrophobicity of the polymer. Atomistic simulations of the polymer–metal–water interactions revealed greater Eu^{3+} and polymer desolvation when binding to the more hydrophobic polymers. These combined experimental and computational results demonstrate that metal binding in aqueous solution can be modulated not

only by directly modifying the chelating groups, but also by altering the molecular environment around the chelating site, thus suggesting a new design principle for developing increasingly effective metal-chelating materials.

6.2 Introduction

Rare-earth elements (REEs: Y, Sc, La–Lu) underpin many modern communications, environmental, and sustainability technologies; however, REE demand rapidly outpaces current supply.[2, 3] Consequently, effective methods for REE extraction and separation are needed. Several such approaches (e.g., polymer-enhanced ultrafiltration) use metal-chelating polymers to selectively bind and extract REEs.[4, 5] Thus, quantifying metal binding thermodynamics in aqueous solution is critical, but the interactions among metal-ion, polymer, and water are complex.[6-8]

To probe these complexities, the thermodynamics (ΔG, ΔH, and ΔS) of the polymer–metal interaction have been studied: Binding is entropy driven, suggesting the critical role of water in REE chelation.[9, 10] However, the intricate interactions among metal, polymer, and water make designing effective metal-chelating materials a challenge.[11, 12] Thus, understanding and ultimately controlling these interactions will enable more efficient and selective REE-extracting materials.[13]

Contrary to most synthetic materials, nature achieves high metal-binding affinity by influencing the molecular environment around the metal and ligand.[14] For example, carbonic anhydrase binds Zn in strong preference to similar metals, achieving this selectivity by optimizing desolvation. In contrast, Lanmodulin achieves a remarkable 10^8-fold selectivity for REEs over other ions via specific conformational changes in the protein structure that occur upon REE binding.[15-17] Each of these examples suggests that selectivity can be enhanced by tuning the

molecular environment around the chelating ligands (e.g., hydrophobicity, sterics, etc.), thereby affecting the structure of the water around both the metal ion and the polymer itself.

Water structure profoundly affects myriad biological processes.[18, 19] Consequently, various approaches have been developed to probe water structure during binding events,[20, 21] and designing materials with increasingly effective chelation properties requires accounting for these solvent–(macro)molecule interactions.[22] Measuring heat capacity changes (ΔC_P) in particular, has emerged as a powerful approach to probing water structure, and this single parameter (C_P) relates to the other three thermodynamic parameters by **Equation 6.1**.[23]

$$C_P = \left(\frac{\delta H}{\delta T}\right)_P = T\left(\frac{\delta S}{\delta T}\right)_P = -T^2\left(\frac{\delta^2 G}{\delta T^2}\right)_P \qquad \textbf{(6.1)}$$

The usefulness of measuring ΔC_P is perhaps best exemplified in the extensive literature on protein folding thermodynamics and the hydrophobic effect.[24-26] For example, changes in hydration heat capacity account for almost all the heat capacity changes associated with protein folding or binding. This change in hydration heat capacity often arises from the burial of nonpolar groups, a process that largely stabilizes protein folding and binding. Generally, desolvation of hydrophobic surfaces produces a negative ΔC_P, whereas desolvation of polar or ionic surfaces produces a positive ΔC_P. Few studies have explored heat capacity changes with synthetic systems, and these largely focus on micelle formation, cyclodextrins, or polyelectrolyte interactions.[27-33] Here, we probed the effect of polymer structure on ΔC_P during REE binding.

6.3 Results and Discussion

Activated ester polymers, such as poly(2,3,5,6-tetrafluorophenyl acrylate) (poly(TFPA)), enable efficient post-polymerization modification, which produces libraries of structurally diverse polymer derivatives without disrupting key parameters such as degree of polymerization, Đ, and tacticity.[34-38] We synthesized linear (poly(TFPA)) *via* reversible addition-fragmentation chain transfer (RAFT) polymerization (M_n = 12.5 kDa, Đ = 1.1) (**Fig. 6.1A** and **6.S1–6.S3**). We then modified this poly(TFPA) with a series of amino acids (glycine, D,L-alanine, D,L-valine, or D,L-leucine) to install chelating carboxylate groups with side-chains of varying hydrophobicity (**Fig. 6.1B**). Following functionalization, the resulting polymers were dialyzed in DI water to remove any trace impurities. ^{1}H and ^{19}F NMR confirmed that each post-polymerization modification was quantitative; we observed complete removal of the aromatic proton corresponding to the TFPA repeat unit and the absence of any ^{19}F signals in the final polymer (**Fig. 6.S4–6.S8**). This polymer series varies only in the R group of the amino acid side-chain; all other structural parameters are consistent, which enables straight-forward comparisons among the different materials.

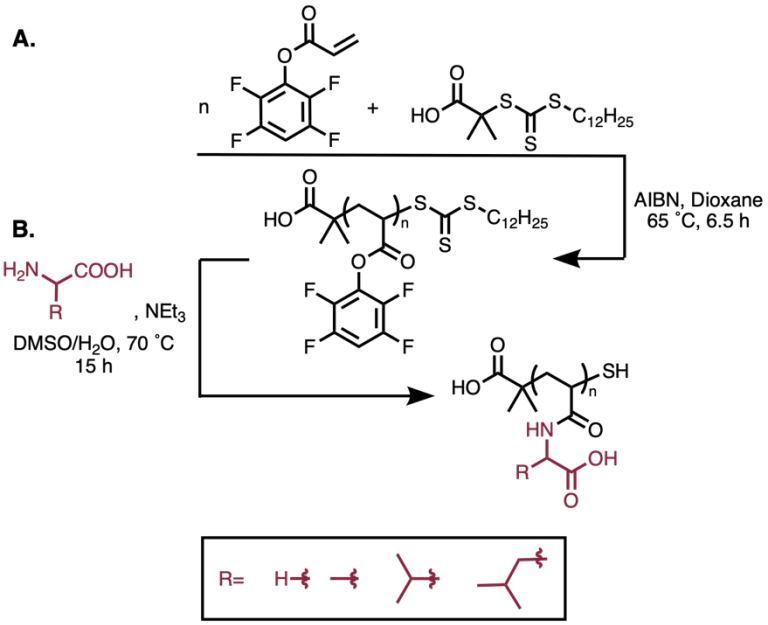


Figure 6.1. A. Synthesis of linear poly(TFPA) *via* RAFT polymerization and **B.** subsequent post-polymerization modification to produce the poly(amino acid acrylamide)s.

We used Eu^{3+} as a representative lanthanide ion to study polymer–metal binding, having previously observed similar binding thermodynamics across a subset of lanthanide ions with poly(acrylic acid).[10] We conducted isothermal titration calorimetry (ITC) experiments by titrating small aliquots of a Eu^{3+} solution into each polymer solution (pH 5 NaOAc–HOAc buffer). Control experiments (metal ion into buffer, and buffer into polymer solution) allowed us to subtract any observed heat change that was not the direct result of polymer–metal binding (**Fig. 6.S9–6.S13**).[39] ITC enables the direct measurement of ΔH and K_a; ΔG and ΔS are subsequently calculated according to **Equation 6.2**.[40] Each binding interaction was driven by a large positive ΔS, which increased with increasingly polymer hydrophobicity (**Fig. 6.2A**). We hypothesized that this large entropy term is driven by the release of solvating water molecules around the metal ion and that more hydrophobic polymers produce greater desolvation.[41, 42] To investigate this hypothesis, we conducted atomistic molecular dynamics simulations using the AMOEBA polarizable force field,[43] which enabled us to probe the metal–polymer–water interactions in conjunction with our

ITC experiments (**Fig. 6.4**, also discussed below). We chose the AMOEBA force field because it accounts for electrostatic anisotropy and electronic polarizability effects,[44-46] which is key to describing the ion–polymer interaction in solution.[47-52] Further, AMOEBA parameters for solvated Eu^{3+} have already been developed and validated.[47, 53] The simulation data showed greater metal desolvation with increasing polymer hydrophobicity, consistent with our interpretation of ITC data, and previous studies. The simulation data showed greater metal desolvation with increasing polymer hydrophobicity, consistent with our interpretation of ITC data, and previous studies.[54-57]

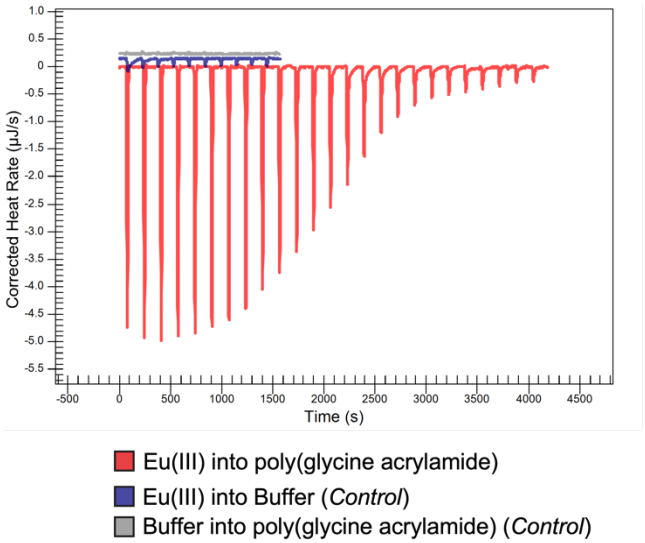


Figure 6.2. Representative ITC thermogram (red) overlaid with control titrations (blue and gray).

$$\Delta G = -RTln(K_a) = \Delta H - T\Delta S \qquad \textbf{(6.2)}$$

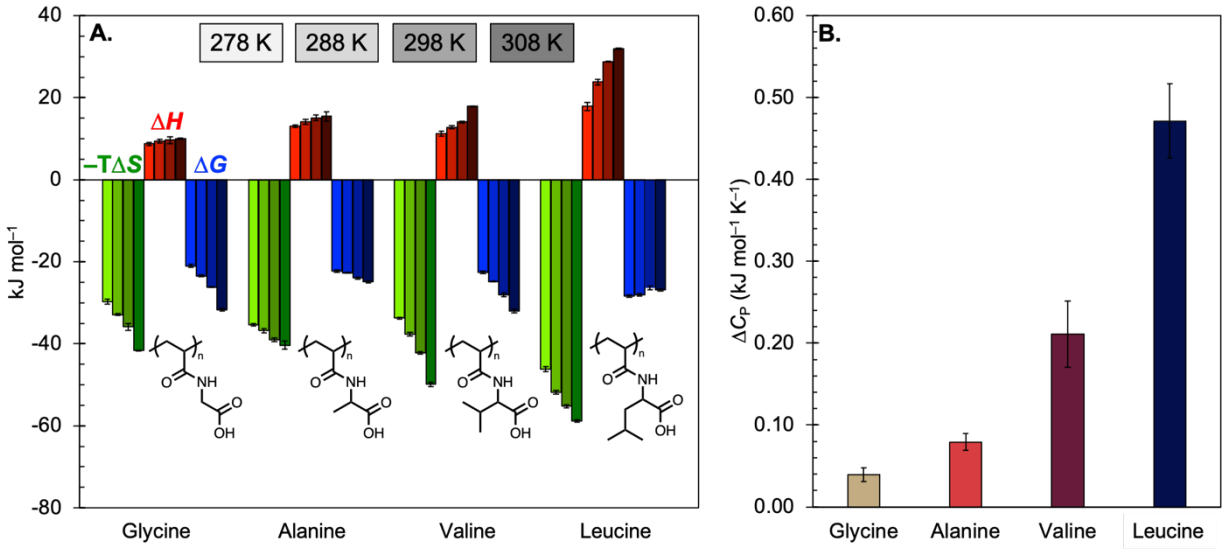


Figure 6.3. A. Thermodynamic parameters of Eu^{3+} binding to poly(amino acid acrylamide) series (278–308 K), and **B.** ΔC_P of poly(amino acid acrylamide) series.

Previous small-molecule studies have reported the thermodynamic parameters for carboxylate–lanthanide complexation, showing that loss of water from hydration shells around the metal affects both ΔH and ΔS of complexation.[55-57] Interestingly, subtle structural differences impact these interactions. For example, propanoate and 2-methylpropanoate complex Eu^{3+}, both driven by a positive ΔS; both also have positive values of ΔH.[57] However, 2-methylpropanoate complexation has larger positive values of ΔS and ΔH than those of propanoate (a difference of one methyl group), but both carboxylates have nearly identical values of ΔG. The increase in ΔS relates to releasing water molecules from the hydration shells.[54]

Water in solvation shells has a different C_P than bulk water. Additionally, the C_P of solvating water varies depending on the specific solute. Water solvating metal ions and polar groups has a lower C_P than bulk water, while water solvating hydrophobic groups has a higher C_P.[23] We hypothesized that ΔC_P would increase with increasing polymer hydrophobicity because the hydrophobic group would induce greater desolvation of the metal-ion. To test this hypothesis,

we conducted ITC measurements at 4 temperatures (278–308 K) to measure the effect of polymer hydrophobicity on ΔC_P (**Fig. 6.3B**, **Table 6.S2**). We found that the ΔC_P for each polymer–REE interaction was positive, and increasing the hydrophobicity of the polymer increased ΔC_P over an order of magnitude across the series (39–471 J mol^{-1} K^{-1}). We hypothesize that the origin of this overall positive ΔC_P results from two main contributors. First, the water surrounding the hydrophobic polymer is more structured (see simulations below), resulting in a higher C_P for the water in this region, as is seen with hydration of hydrophobic groups in general.[23] Second, lanthanide ions are kosmotropes, that is, they increase the organization of solvating water molecules and increase the overall density of hydrogen bonding in solution beyond their own hydration shell.[58] Thus, the water solvating the carboxylate and the metal ion has a lower C_P. No experimental data for ΔS and ΔC_P for hydration of Eu^{3+} exist,[59] but estimates indicate that the ΔC_P for hydration of Eu^{3+} is negative,[59, 60] further supporting our hypothesis. When this lower-heat-capacity water is displaced during chelation, C_P increases.

Simulations data provided further insight. In these polymer solutions, the entropy at the beginning of the titration is not constant: Solvated poly(glycine acrylamide) is a higher entropy solution than solvated poly(leucine acrylamide). This difference in entropy is seen in the polymer--water radial distribution functions (RDFs) (**Fig. 6.4**). The ordered water around the carboxylates and metal ions has a lower C_P than bulk water.[23] When metal ions are added to the polymer solution, water from the first hydration shell of the polymer is displaced (**Fig. 6.4**), and this displaced ordered water consequently becomes higher C_P bulk water. These simulations revealed greater carboxylate and Eu^{3+} desolvation when binding to increasingly hydrophobic polymers. Thus, this displaced water is the main contributor to the ΔC_P we observed.

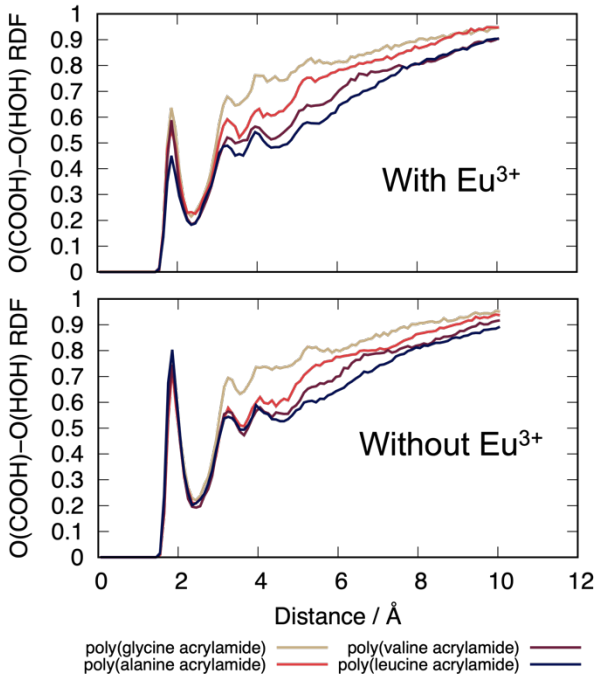


Figure 6.4. Control radial distribution function (RDF) between oxygens of the polymer and those of water. Top: With Eu^{3+}. Bottom: Without Eu^{3+}.

The differences in binding stoichiometry are also noteworthy: Poly(glycine acrylamide) (R=H) required approximately 2.5 repeat units to bind Eu^{3+} at 298 K, whereas poly(leucine acrylamide) ($R=CH_2CH(CH_3)_2$) required approximately 7.2 repeat units per Eu^{3+}. Atomistic simulations suggested that bulkier side chains induce more order in the polymer chains (i.e., they have less conformational flexibility). This increased ratio, however, does not appear to be due to steric crowding around the carboxylate group, but rather to a restriction in the conformation s the polymer (and consequently the chelating carboxylates) can adopt. The structure and ordering in each polymer can be quantified by computing the side-chain Cα–Cα RDF (**Fig. 6.5**). In water, without Eu^{3+}, we observed wider peaks indicative of disorder for all polymers, suggesting that the polymer side chains adopt a multitude of conformations. However, steric bulk restricts these conformations, which manifests as peaks centered on a smaller Cα–Cα distance for polymers with bulkier side chains.

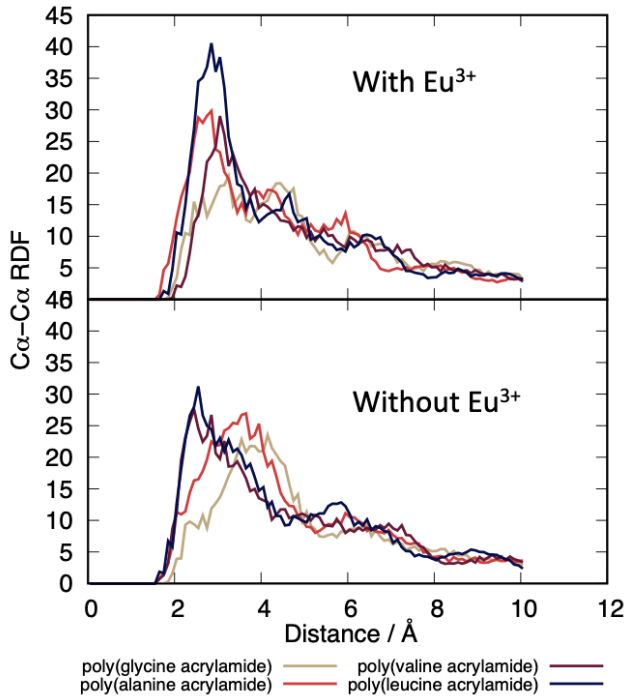


Figure 6.5. RDF as a function of Cα–Cα distance, quantifying disorder in the polymer side chains. We compare side-chain ordering in water with Eu^{3+} (top) to side chain ordering in water without Eu^{3+} (bottom). The presence of Eu^{3+} in the environment produces order in the polymer side chains, an effect that is more pronounced for bulkier side chains (e.g., leucine).

In the presence of Eu^{3+}, the peaks in the Cα–Cα RDF for all but poly(glycine acrylamide) are narrower and shifted towards shorter Cα–Cα distances. These data suggest that Eu^{3+} binding induces side-chain ordering. Analyzing binding modes along the molecular dynamics trajectories, we see that Eu^{3+} binds to side chains with solvent exposed carboxylates (**Fig. 6.S14**). However, in poly(leucine acrylamide), the bulkiness of the side chains reduces the number of ways in which carboxylates can be exposed to the solvent and accompanying Eu^{3+} ions (**Table 6.S3**). This conformational restriction produces a much sharper peak in the poly(leucine acrylamide) RDF than for the other polymer chains. Interestingly, these conformational restrictions also result in increased frequency of multidentate binding.

The RDF of Eu^{3+} with respect to the oxygens of the carboxylates (**Fig. 6.6**) revealed sharp peaks centered at 2.3 Å for all polymers, suggesting small fluctuations in the Eu–O equilibrium distance. However, the probability of finding a carboxylate oxygen 2.3 Å from Eu^{3+} systematically increases across the series: poly(leucine acrylamide) > poly(valine acrylamide) > poly(alanine acrylamide) > poly(glycine acrylamide). These data suggest that more carboxylate oxygens are involved in the binding of each Eu^{3+} ion for polymers with bulkier side-chains.

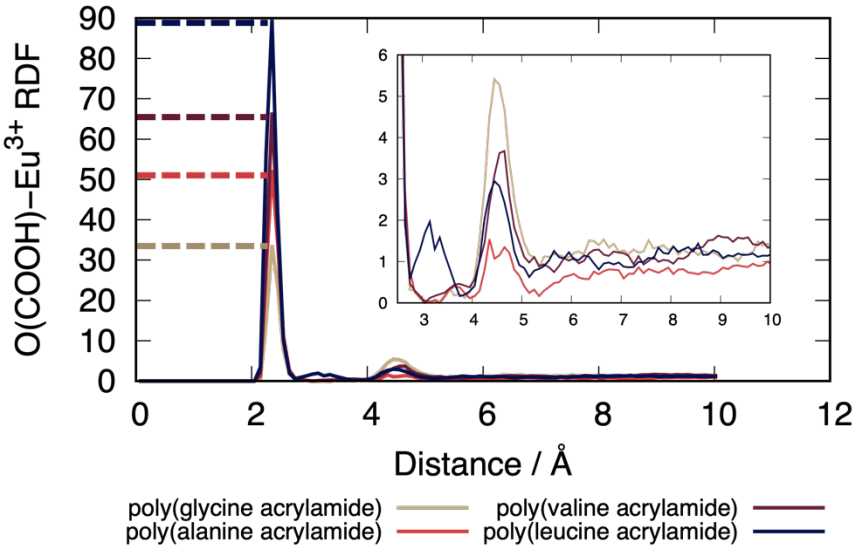


Figure 6.6. RDF as a function of Eu^{3+}–O(Carboxylate) distance.

The temperature dependence of the equilibrium binding affinity (K_a) varied with polymer structure (**Fig. 6.7**). Poly(glycine acrylamide) and poly(valine acrylamide) exhibited a higher K_a with increasing temperature (278–308 K), but poly(leucine acrylamide) exhibited the opposite trend. Interestingly, temperature appears to have no effect on the K_a of Eu^{3+} binding with poly(alanine acrylamide) in this temperature range. To provide further insight into these observations, we conducted variable temperature simulations. The Cα–Cα RDFs revealed

increased side chain disorder as a function of temperature for poly(leucine acrylamide), whereas the remaining polymers showed no distinguishable differences in side chain disorder at different temperatures (**Fig. 6.16**).

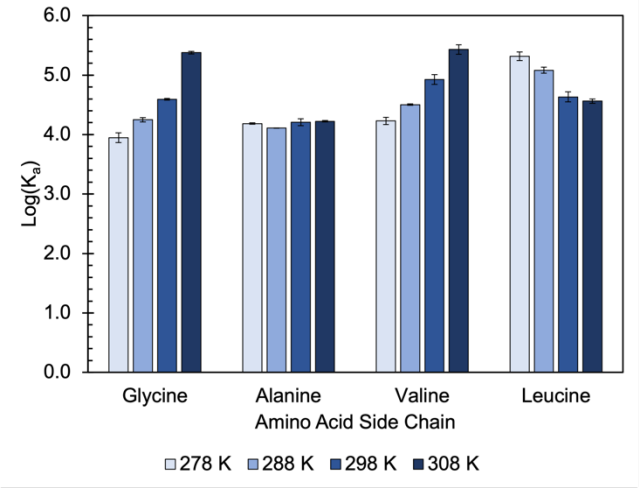


Figure 6.7. The temperature dependence of the equilibrium binding affinity (K_a).

6.4 Conclusions

In conclusion, we used a series of poly(amino acid acrylamide)s to systematically examine the effect of polymer hydrophobicity on Eu^{3+} binding thermodynamics. This work reveals the critical role of polymer structure in REE chelation and highlights the value of combining precise synthesis, thermodynamics measurements, and simulations. Perturbing the structure of water around the chelating sites produced large variations in ΔC_P, which directly affected the temperature dependence of the K_a. This capability introduces a new design parameter for controlling polymer–metal binding, with implications for producing more effective materials for metal extraction and separation.

6.5 References

1. Archer, W. R.; Gallagher, C. M. B.; Vaissier Welborn, V.; Schulz, M. D. *Phys. Chem. Chem. Phys.* **2022**, *24*, 3579–3585.
2. Mattocks, J. A.; Ho, J. V.; Cotruvo, J. A. *J. Am. Chem. Soc.* **2019**, *141*, 2857–2861.
3. Golev, A.; Scott, M.; Erskine, P. D.; Ali, S. H.; Ballantyne, G. R. *Resour. Policy* **2014**, *41*, 52–59.
4. Gomes Rodrigues, D.; Dacheux, N.; Pellet-Rostaing, S.; Faur, C.; Bouyer, D.; Monge, S. *Polym. Chem.* **2015**, *6*, 5264–5272.
5. Archer, W. R.; Hall, B. A.; Thompson, T. N.; Wadsworth, O. J.; Schulz, M. D. *Polym. Int.* **2019**, *68*, 1220–1237.
6. Huang, Y.; Feng, X. *J. Membr. Sci.* **2019**, *586*, 53–83.
7. Musale, D. A.; Kulkarni, S. S. *Rev. Macromol. Chem. Phys. C* **1998**, *38*, 615–636.
8. Rivas, B. L.; Perieira, E.; Maureira, A. *Polym. In.* **2009**, *38*, 1093–1114.
9. Archer, W. R.; Fiorito, A.; Heinz-Kunert, S. L.; MacNicol, P. L.; Winn, S. A.; Schulz, M. D. *Macromolecules* **2020**, *53*, 2061–2068.
10. Archer, W. R.; Thompson, T. N.; Schulz, M. D. *Macromol. Rapid Commun.* **2021**, *42*, 2000614.
11. Geckeler, K. E.; Volchek, K. *Environ. Sci. Technol.* **1996**, *30*, 725-734.
12. Liu, G.; Yu, S.; Yang, H.; Hu, J.; Zhang, Y.; He, B.; Li, L.; Liu, Z. *Environ. Sci. Technol.* **2016**, *50*, 1393–1402.
13. Baldwin, A. G.; Ivanov, A. S.; Williams, N. J.; Ellis, R. J.; Moyer, B. A.; Bryantsev, V. S.; Shafer, J. C. *ACS Cent. Sci.* **2018**, *4*, 739–747.
14. DiTusa, C. A.; Christensen, T.; McCall, K. A.; Fierke, C. A.; Toone, E. J. *Biochemistry* **2001**, *40*, 5338–5344.
15. Cotruvo, J. A.; Featherston, E. R.; Mattocks, J. A.; Ho, J. V.; Laremore, T. N. *J. Am. Chem. Soc.* **2018**, *140*, 15056–15061.
16. Deblonde, G. J. P.; Mattocks, J. A.; Park, D. M.; Reed, D. W.; Cotruvo, J. A.; Jiao, Y. *Inorg. Chem.* **2020**, *59*, 11855–11867.
17. Cook, E. C.; Featherston, E. R.; Showalter, S. A.; Cotruvo, J. A. *Biochemistry* **2019**, *58*, 120–125.
18. Darby, J. F.; Hopkins, A. P.; Shimizu, S.; Roberts, S. M.; Brannigan, J. A.; Turkenburg, J. P.; Thomas, G. H.; Hubbard, R. E.; Fischer, M. *J. Am. Chem. Soc.* **2019**, *141*, 15818–15826.
19. Maassen, S. J.; Huskens, J.; Cornelissen, J. J. L. M. *J. Phys. Chem. B* **2019**, *123*, 9733–9741.
20. Batchelor, J. D.; Olteanu, A.; Tripathy, A.; Pielak, G. J. *J. Am. Chem. Soc.* **2004**, *126*, 1958–1961.
21. Gallagher, K. R.; Sharp, K. A. *J. Am. Chem. Soc.* **2003**, *125*, 9853–9860.
22. Chen, X.; Yang, T.; Kataoka, S.; Cremer, P. S. *J. Am. Chem. Soc.* **2007**, *129*, 12272–12279.
23. Sharp, K. A.; Madan, B. *The Journal of Physical Chemistry B* **1997**, *101*, 4343-4348.
24. Kabiri, M.; Bushnak, I.; McDermot, M. T.; Unsworth, L. D. *Biomacromolecules* **2013**, *14*, 3943–3950.
25. Cooper, A. *Biophys. Chem.* **2005**, *115*, 89–97.
26. Li, Z.; Lazaridis, T. *J. Am. Chem. Soc.* **2003**, *125*, 6636–6637.

27. Dai, C.; Du, M.; Zhao, M.; You, Q.; Guan, B.; Wang, X.; Liu, P. *J. Phys. Chem. B* **2013**, *117*, 9922–9928.
28. Chen, L.-J.; Sheu, Y.-H.; Li, P.-J. *J. Phys. Chem. B* **2004**, *108*, 19096–19098.
29. Paul, B. K.; Ghosh, N.; Mukherjee, S. *J. Phys. Chem. B* **2016**, *120*, 3963–3968.
30. Paul, B. K.; Ghosh, N.; Mondal, R.; Mukherjee, S. *J. Phys. Chem. B* **2016**, *120*, 4091–4101.
31. Heerklotz, H.; Tsamaloukas, A.; Kita-Tokarczyk, K.; Strunz, P.; Gutberlet, T. *J. Am. Chem. Soc.* **2004**, *126*, 16544–16552.
32. Hildebrand, A.; Garidel, P.; Neubert, R.; Blume, A. *Langmuir* **2004**, *20*, 320–328.
33. Zeng, Z.; Patel, J.; Lee, S.-H.; McCallum, M.; Tyagi, A.; Yan, M.; Shea, K. J. *J. Am. Chem. Soc.* **2012**, *134*, 2681–2690.
34. Bachler, P. F., K.; Sparks, C.; Schulz, M.; Wagener, K.; and Sumerlin, B. . *Polym. Chem.* **2016**, *7*, 4155–4159.
35. Das, A.; Theato, P. *Macromolecules* **2015**, *48*, 8695–8707.
36. Das, A.; Theato, P. *Chem. Rev.* **2016**, *116*, 1434–1495.
37. Gibson, M. I.; Fröhlich, E.; Klok, H.-A. *J. Polym. Sci. A Polym. Chem.* **2009**, *47*, 4332–4345.
38. Roy, D.; Nehilla, B. J.; Lai, J. J.; Stayton, P. S. *ACS Macro Lett.* **2013**, *2*, 132-136.
39. Archer, W. R.; Schulz, M. D. *Soft Matter* **2020**, *16*, 8760–8774.
40. Freire, E.; Mayorga, O. L.; Straume, M. *Anal. Chem.* **1990**, *62*, 950A–959A.
41. Bucur, C. B.; Sui, Z.; Schlenoff, J. B. *J. Am. Chem. Soc.* **2006**, *128*, 13690–13691.
42. Terpstra, T.; McNally, J.; Han, T.-H.-L.; Ha-Duong, N.-T.; El-Hage-Chahine, J.-M.; Bou-Abdallah, F. *J. Inorg. Biochem.* **2014**, *136*, 24–32.
43. Shi, Y.; Xia, Z.; Zhang, J.; Best, R.; Wu, C.; Ponder, J. W.; Ren, P. *J. Chem. Theory Comput.* **2013**, *9*, 4046–4063.
44. Ponder, J. W.; Wu, C.; Ren, P.; Pande, V. S.; Chodera, J. D.; Schnieders, M. J.; Haque, I.; Mobley, D. L.; Lambrecht, D. S.; DiStasio, R. A.; Head-Gordon, M.; Clark, G. N. I.; Johnson, M. E.; Head-Gordon, T. *J. Phys. Chem. B* **2010**, *114*, 2549–2564.
45. Zhang, C.; Lu, C.; Jing, Z.; Wu, C.; Piquemal, J.-P.; Ponder, J. W.; Ren, P. *J. Chem. Theor. Comput.* **2018**, *14*, 2084–2108.
46. Laury, M. L.; Wang, L.-P.; Pande, V. S.; Head-Gordon, T.; Ponder, J. W. *J. Phys. Chem. B* **2015**, *119*, 9423–9437.
47. Marjolin, A.; Gourlaouen, C.; Clavaguéra, C.; Ren, P. Y.; Piquemal, J.-P.; Dognon, J.-P. *J. Mol. Model* **2014**, *20*, 2471.
48. Qiao, B.; Skanthakumar, S.; Soderholm, L. *J. Chem. Theory Comput.* **2018**, *14*, 1781–1790.
49. Melcr, J.; Martinez-Seara, H.; Nencini, R.; Kolafa, J.; Jungwirth, P.; Ollila, O. H. S. *J. Phys. Chem. B* **2018**, *122*, 4546–4557.
50. Melcr, J.; Ferreira, T. M.; Jungwirth, P.; Ollila, O. H. S. *J. Chem. Theor. Comput.* **2020**, *16*, 738–748.
51. Gebala, M.; Herschlag, D. *Biophys. J.* **2019**, *117*, 1116–1124.
52. Ma, C. Y.; Pezzotti, S.; Schwaab, G.; Gebala, M.; Herschlag, D.; Havenith, M. *Phys. Chem. Chem. Phys.* **2021**, *23*, 23203–23213.
53. Marjolin, A.; Gourlaouen, C.; Clavaguéra, C.; Ren, P. Y.; Wu, J. C.; Gresh, N.; Dognon, J.-P.; Piquemal, J.-P. *Theor. Chem. Acc.* **2012**, *131*, 1–14.
54. Choppin, G. R. *Pure Appl. Chem.* **1971**, *27*, 23_42.

55. Grenthe, I. *Acta Chem. Scand.* **1964**, *18*, 293–299.
56. Praudiere, P. L.; Staveley, L. A. K. *J. Inorg. Nucl. Chem.* **1964**, *26*, 1713–1719.
57. Choppin, G. R.; Graffeo, A. J. *Inorg. Chem.* **1965**, *4*, 1254–1257.
58. Marcus, Y. *Chem. Rev.* **2009**, *109*, 1346–1370.
59. Johnson, D. A.; Nelson, P. G. *Inorg. Chem.* **2020**, *59*, 10756–10767.
60. Marcus, Y. *Biophys. Chem.* **1994**, *51*, 111–127.

6.6 Supporting Information

Materials:

Trace metals grade $EuCl_3 \times 6H_2O$, AIBN, 1,4-dioxane, and 1,3,5-trioxane were purchased from Sigma Aldrich. 2,3,4,5-Tetrafluorophenol was purchased from Synquest. Acryloyl chloride was purchased from Alfa Aesar. Glycine, DL-alanine, DL-valine, and DL-leucine were purchased from Oakwood Chemical. Dialysis bags (pre-treated regenerated cellulose tubing, 1 kDa molecular weight cut-off) were purchased from Spectrum Labs. AIBN was recrystallized from MeOH prior to use. All other chemicals were used as-is.

Characterization:

NMR: ^{1}H NMR, ^{19}F, and ^{13}C NMR spectra were acquired on an Agilent MR4 400 MHz spectrometer. Chemical shifts in the ^{1}H NMR and ^{13}C NMR spectra were referenced to the residual solvent resonance signals.

Size Exclusion Chromatography:

Size exclusion chromatography (SEC) was performed in tetrahydrofuran (THF) at 1 mL min^{-1} at 30 °C on two MIXED-B Agilent PLgel 10 μm columns connected in series with a Wyatt Optilab Rex refractive index detector and a Wyatt Dawn Heleos 2 light scattering detector. Data analysis was performed using Astra version 7.2.2.10 software (Wyatt Technologies). Molecular weights were calculated relative to the dn/dc of polystyrene standards (30 and 200 kDa).

Isothermal titration calorimetry experimental procedure:

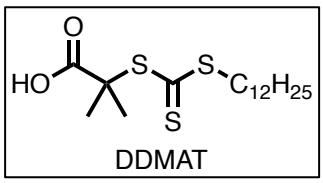
The ITC instrument used was an Affinity-ITC (TA Instruments, New Castle, DE), which operated at constant temperature (278–308 K). To carry out a binding experiment, a sample

solution was prepared by dissolving the polymer and $EuCl_3$ in a pH 5, 100-mM NaOAc–HOAc buffer.

Before the ITC experiment, each solution was degassed for 15 min. The polymer solution (350 µL) was placed in the sample cell and the reference cell was filled with deionized H_2O (300 µL). Both cells were mounted in an adiabatic chamber at a constant temperature during the measurement. A long-needle syringe with a twisted paddle fastened to its end, was filled with the metal-ion solution. The syringe was placed inside the sample cell, and the entire syringe assembly was rotated continuously (185 RPM) to provide proper mixing of the contents of the sample cell within a few seconds after an injection. After reaching thermal equilibrium, the injection of the metal ion solution was automatically conducted stepwise until the polymer was saturated with metal ion. Due to the possible dilution of the first measurement, the first injection was ignored in the data analysis, which is standard practice for ITC experiments.[1, 2] The first 1.0-µL injection was followed by a series of 2.0-µL injections. The chosen time interval between two consecutive injections was 300 sec to ensure that the equilibrium was reached before the next injection.

Nonlinear least-squares curve fitting was conducted with TA Instruments Nano Analyze and TA Instruments Independent model. Heats of dilution from control titrations (metal ion into buffer (*no polymer present*), and buffer into polymer (*without metal ion present*)) were subtracted before curve fitting.

Synthesis of 2-(Dodecylthiocarbonothioylthio)-2-methylpropionic acid (DDMAT):



DDMAT

DDMAT was prepared according to the previously reported procedure.[3] Dodecanethiol (5.0 mL, 20.9 mmol, 1.3 equiv) and K_3PO_4 (3.60 g, 16.9 mmol, 1.1 equiv) was combined in a 100 mL round bottomed flak with 70 mL of acetone. After stirring for 20 minutes, CS_2 (3.0 mL, 49.6 mmol, 3.1 equiv) was added dropwise, during which the reaction solution turned yellow. 2-bromo-2-methylpropionic acid (2.64 g, 15.8 mmol, 1.0 equiv) was added to the stirring solution in one portion; stirring continued overnight at room temperature. To the reaction mixture, 1M HCl (aq, 200 mL) was added; the solution was then poured into a separatory funnel. The mixture was extracted with DCM (2 × 150 mL). The combined organic layers were dried over $MgSO_4$; the solvent was removed under reduced pressure. The crude product was recrystallized from hexanes to afford DDMAT as yellow crystals (65 % recovery).

^{1}H NMR (400 MHz, $CDCl_3$, δ): 3.28 (t, 2H), 1.73 (s, 6H), 1.68 (m, 2H), 1.38 (m, 2H), 1.28 (s, 16H), 0.87 (t, 3H) ppm.

^{13}C NMR (100 MHz, $CDCl_3$, δ): 221.3, 178.2, 55.9, 37.5, 32.4, 30.1, 30.0, 29.9, 29.8, 29.6, 29.4, 28.3, 25.7, 23.2, 14.6 ppm.

Synthesis of 2,3,5,6-tetrafluorophenyl acrylate (TFPA):

Scheme 6.S1. Synthesis of 2,3,5,6-tetrafluorophenyl acrylate.



TFPA was prepared according to the previously reported procedure.[4] In general, 2,3,5,6-tetrafluorophenol (134.6 mmol, 1.0 equiv) was dissolved in approximately 50 mL of DCM under nitrogen at 0 ˚C. Triethylamine (208 mmol, 1.5 equiv) was added to the reaction flask and stirred for 20 min. Acryloyl chloride (148.5 mmol, 1.1 equiv) was added dropwise over 45 min. The reaction continued to stir overnight. The reaction mixture was filtered into a separatory funnel, extracted with 3 M HCl (3 × 25 mL), and brine (3 × 25 mL). The organic layer was dried over $MgSO_4$ and concentrated *in vaccuo*. The resulting oil was purified by vacuum distillation at 78 ˚C to provide a clear liquid in 73 % yield.

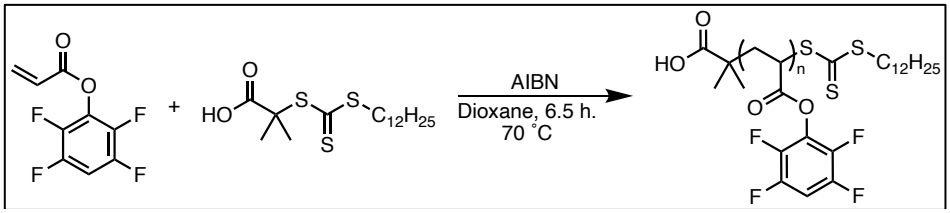
^{1}H NMR (400 MHz, $CDCl_3$, δ): 7.0 (tt, 1H), 6.8 (dd, 1H), 6.4 (dd, 1H), 6.2 (dd, 1H) ppm.

^{13}C NMR (100 MHz, $CDCl_3$, δ): 161.6, 147.3, 144.8, 139.5, 135.1, 125.5, 103.1 ppm.

^{19}F NMR (375 MHz, $CDCl_3$, δ): –139.1, –153.0 ppm.

Synthesis of poly(2,3,5,6-tetrafluorophenyl acrylate) *via* RAFT polymerization:

Scheme 6.S2. Synthesis of poly(TFPA).



TFPA (22.9 mmol, 100.0 equiv), DDMAT (0.23 mmol, 1.0 equiv), and AIBN (3.6 mg, 0.1 equiv) were combined in a 20 mL glass vial with 1,4-dioxane (3.5 mL). 1,3,5-trioxane was added as an internal standard. The vial was subsequently sealed with a septum and parafilm, and purged with N_2 for 30 min. The vial was then placed in a heating block equilibrated at 70 ˚C. After 6.5 h, the vial was removed from the heating block and exposed to air. ^{1}H NMR of the crude reaction solution confirmed that the monomer conversion was 94%. The solution was precipitated into cold MeOH resulting in an off-white solid. The solid was re-dissolved in THF and reprecipitated into MeOH; this process was repeated twice more. SEC (PS standards, THF): M_n = 12.5 kDa, M_w = 14.8 kDa, Đ = 1.18.

Figure 6.S1: ^{1}H NMR of poly(TFPA)

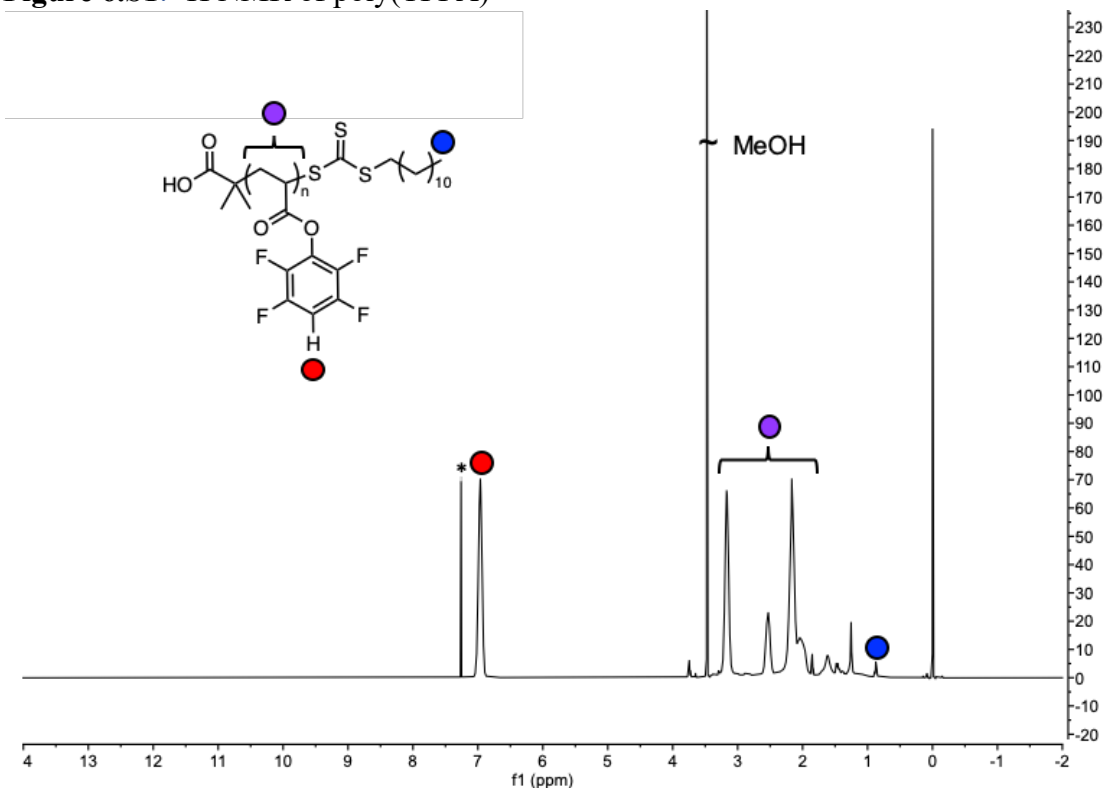


Figure 6.S2: ^{19}F NMR of poly(TFPA)

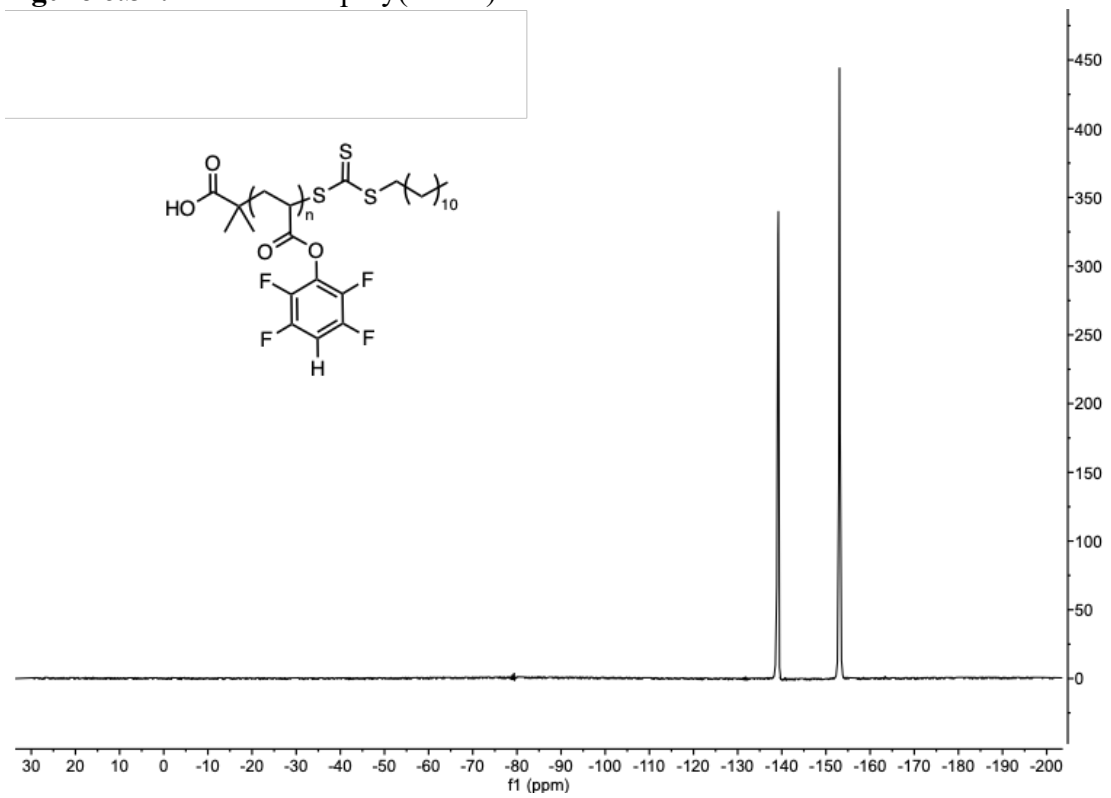
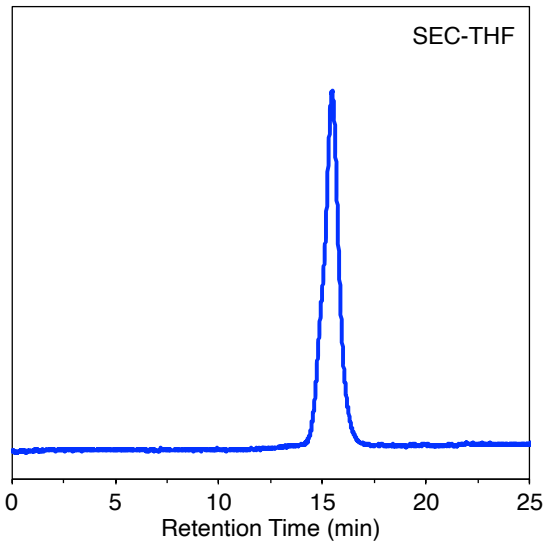


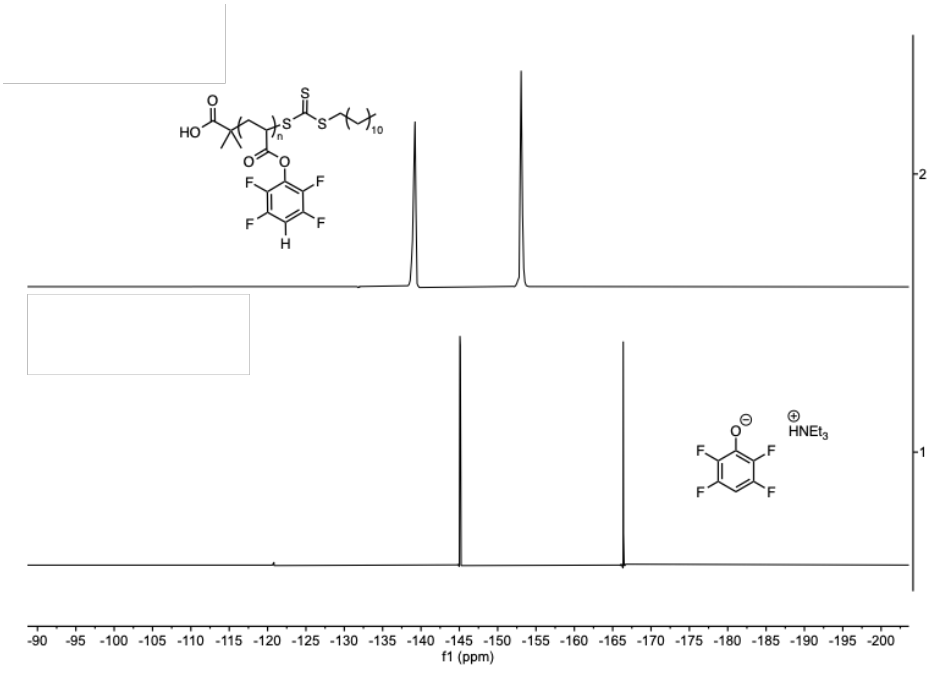
Figure 6.S3: SEC trace of poly(TFPA)



Representative post-polymerization modification procedure to synthesize poly(glycine acrylamide):

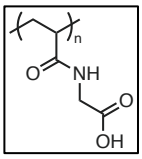
Poly(TFPA) (499.5 mg, 2.3 mmol, 1.0 equiv with respect to the mass of the repeat unit) was dissolved in DMSO (4 mL). Glycine (216.2 mg, 2.9 mmol, 1.3 equiv) was dissolved separately in a vial with triethylamine (0.5 mL, 1.6 equiv) and DI H_2O (5 mL). The resulting solution was added to the dissolved polymer solution in one portion and heated at 70 ˚C. After a few min, complete dissolution of the reaction solution occurred. The reaction mixture continued to stir for 10 h at 70 ˚C, after which the reaction mixture was cooled to rt and the solvent was removed under reduced pressure. ^{19}F NMR of the crude reaction mixture showed only signals for 2,3,5,6-tetrafluorophenoxide (**Fig. 6.S4**). The reaction mixture was redissolved in of DI H_2O (5 mL), placed in a dialysis bag, and exhaustively dialyzed in DI H_2O for 3 d.

Figure 6.S4: Representative ^{19}F NMR of reaction solution following post-polymerization modification



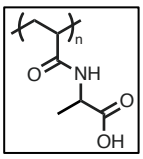
Characterization of poly(amino acid acrylamides) following post-polymerization modification:

Poly(glycine acrylamide): Brown crystalline solid purified from dialysis from DI H_2O. (84 mg



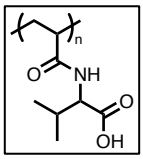
= 32 % isolated yield); ^{1}H NMR (400 MHz, D_2O, δ): 3.9 (br, 2H), 2.3 (br, 1H), 1.6 (br, 2H) ppm.

Poly(DL-alanine acrylamide): Brown solid purified from dialysis from DI H_2O (47.5 mg = 17



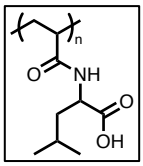
% isolated yield); ^{1}H NMR (400 MHz, D_2O, δ): 4.2 (br, 1H), 2.2 (br, 1H), 1.5 (br, 2H), 1.3 (br, 3H) ppm.

Poly(DL-valine acrylamide): White solid purified from dialysis from DI H_2O (138 mg = 40 %



isolated yield); ^{1}H NMR (400 MHz, DMSO-d6, δ): ppm: 3.9 (br, 1H), 2.0 (br, 3H), 0.8 (br, 6H) ppm.

Poly(DL-leucine acrylamide): Brown solid purified from dialysis from DI H_2O (75 mg = 19 %



isolated yield); ^{1}H NMR (400 MHz, DMSO-d6, δ): ppm: 4.1 (br,1H), 2.2 (br, 1H), 1.6 (br, 2H), 1.4 (br, 3H), 0.8 (br, 6H) ppm.

Figure 6.S5: ^{1}H NMR of poly(glycine acrylamide)

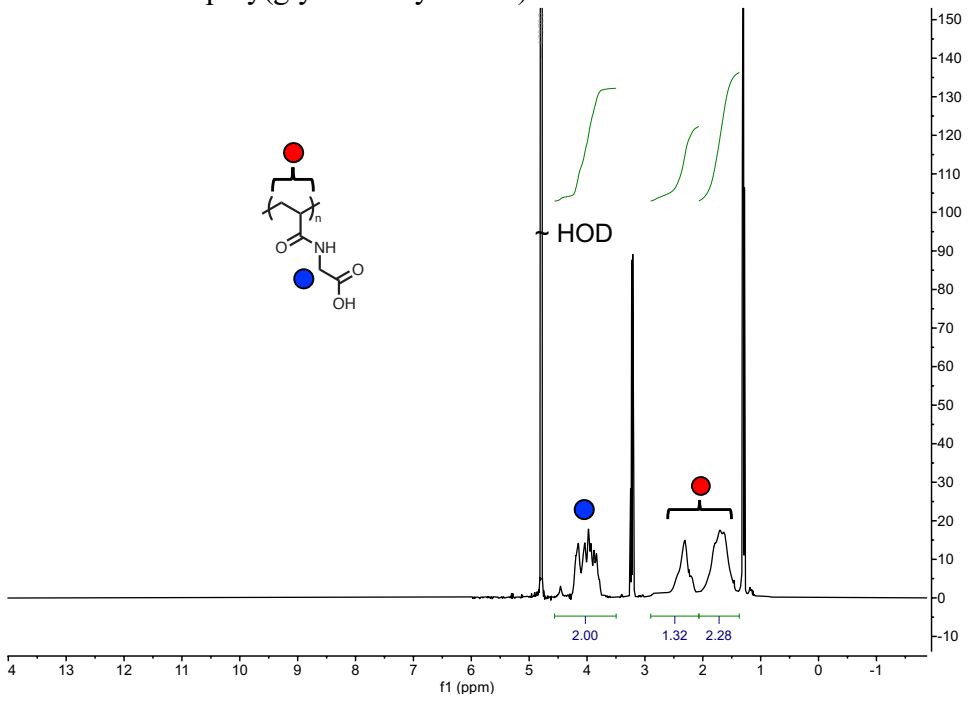


Figure 6.S6: ^{1}H NMR of poly(DL-alanine acrylamide)

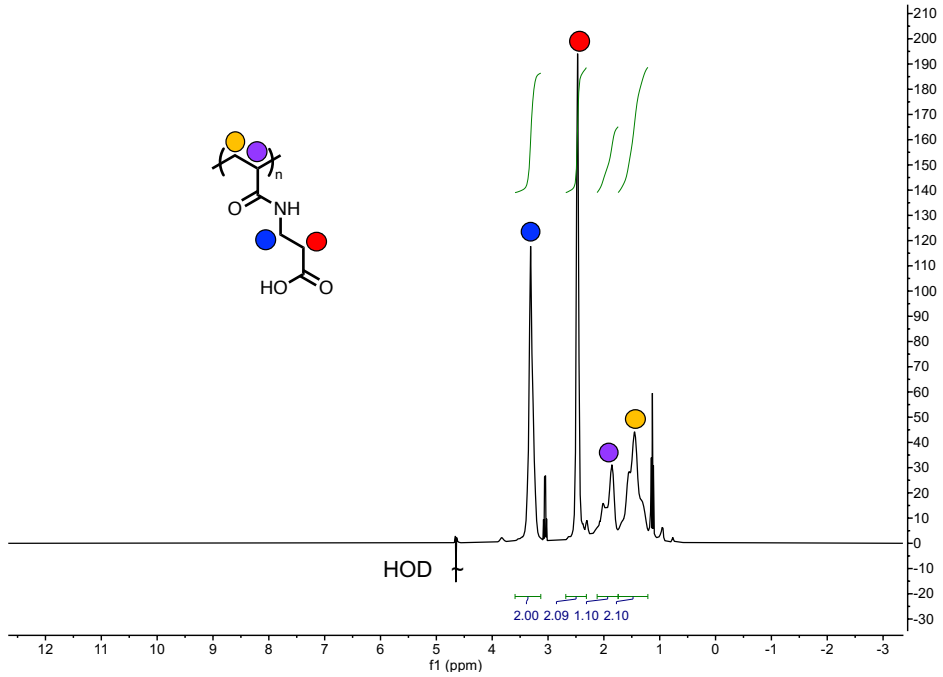


Figure 6.S7: ^{1}H NMR of poly(DL-valine acrylamide)

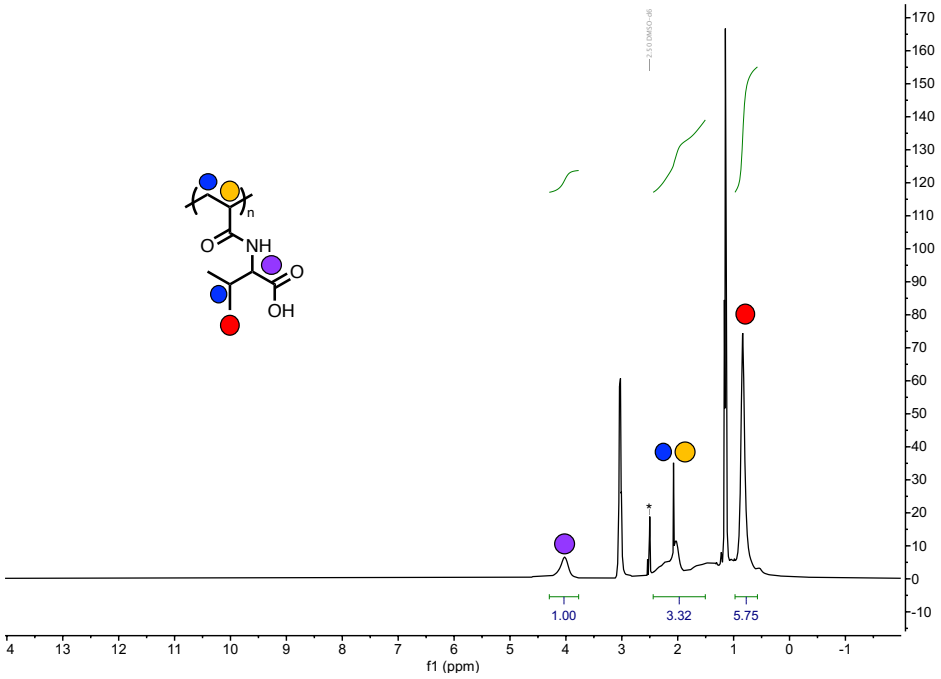


Figure 6.S8: ^{1}H NMR of poly(DL-leucine acrylamide)

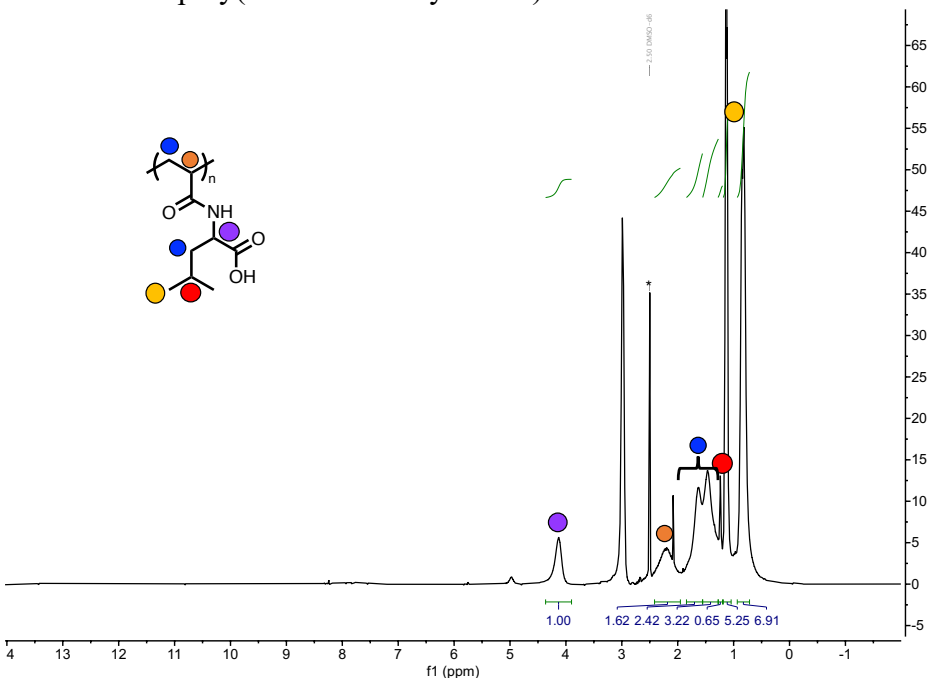


Table 6.S1: Metal and polymer concentrations used for ITC experiments

Sample	**Concentration (mM)**	
Polymer Side Chain	**Poly(amino acid acrylamide)**	**Eu(III)**
Glycine	1.5	3.4
DL-Alanine	2.0	3.5
DL-Valine	1.5	3.5
DL-Leucine	2.0	2.3

Table 6.S2: Thermodynamic properties of Eu(III) binding to amino acid acrylamide polymers in pH 5 acetate buffer. N, K_a, and ΔH are fitting parameters measured by ITC. ΔG and $-T\Delta S$ are calculated according to **Equations 6.2.** N, K_a, ΔH, ΔG, and $-T\Delta S$ are the reported as the average and standard deviations of duplicate measurements. ΔC_p is the linear dependence ΔH on temperature as shown in **Equation 6.1**. Error in ΔC_p was determined from the variance in the slope of the linear line of best fit.

Side Chain	**T (K)**	***N*** **(Repeat units per metal ion)**	**K_a (10^4 M^{-1})**	**ΔG (kJ mol^{-1})**	**ΔH (kJ mol^{-1})**	**$-T\Delta S$ (kJ mol^{-1})**	**ΔS (J mol^{-1} K^{-1})**	**ΔC_p (kJ mol^{-1} K^{-1})**
Glycine 	278	3.2 ± 0.1	0.88 ± 0.02	–21.0 ± 0.4	8.7 ± 0.4	–29.7 ± 0.6	108.0 ± 0.7	0.04 ± 0.01
	288	2.4 ± 0.2	1.8 ± 0.1	–23.4 ± 0.2	9.5 ± 0.5	–32.9 ± 0.2	114.2 ± 0.8	
	298	2.5 ± 0.1	3.9 ± 0.1	–26.2 ± 0.1	9.6 ± 0.8	–35.9 ± 0.8	118.8 ± 1.4	
	308	2.6 ± 0.1	24.8 ± 2.6	–31.7 ± 0.3	9.9 ± 0.2	–41.7 ± 0.1	135.6 ± 0.1	
DL-Alanine 	278	5.6 ± 0.7	1.5 ± 0.2	–22.3 ± 0.3	13.1 ± 0.3	–35.4 ± 0.3	127.7 ± 1.2	0.08 ± 0.01
	288	4.5 ± 0.1	1.3 ± 0.04	–22.7 ± 0.1	14.1 ± 0.6	–36.8 ± 0.5	126.8 ± 1.7	
	298	4.1 ± 0.2	1.6 ± 0.2	–24.0 ± 0.2	15.0 ± 0.7	–39.1 ± 0.5	131.3 ± 2.1	
	308	4.7 ± 0.2	1.7 ± 0.2	–24.9 ± 0.3	15.4 ± 1.1	–40.4 ± 0.9	131.5 ± 4.5	
DL-Valine 	278	4.8 ± 0.1	1.7 ± 0.2	–22.5 ± 0.3	11.3 ± 0.6	–33.8 ± 0.3	121.4 ± 0.9	0.21 ± 0.04
	288	3.8 ± 0.1	3.2 ± 0.1	–24.8 ± 0.1	12.8 ± 0.4	–37.6 ± 0.5	130.8 ± 1.6	
	298	3.5 ± 0.1	8.4 ± 1.5	–28.1 ± 0.5	14.1 ± 0.2	–42.2 ± 0.3	141.5 ± 0.2	
	308	4.0 ± 0.1	26.9 ± 4.9	–32.0 ± 0.5	17.8 ± 0.1	–49.9 ± 0.6	161.9 ± 1.8	
DL-Leucine 	278	7.5 ± 0.5	20.8 ± 2.8	–28.3 ± 0.3	17.8 ± 0.9	–46.2 ± 0.7	166.1 ± 2.4	0.47 ± 0.05
	288	7.7 ± 0.4	12.1 ± 1.4	–28.0 ± 0.3	23.8 ± 0.7	–51.8 ± 0.5	186.4 ± 1.7	
	298	7.2 ± 0.3	4.3 ± 0.8	–26.4 ± 0.5	28.8 ± 0.1	–55.2 ± 0.4	198.7 ± 1.6	
	308	7.1 ± 0.6	3.7 ± 0.3	–26.9 ± 0.2	31.9 ± 0.2	–58.8 ± 0.3	211.6 ± 1.3	

Figure 6.S9: Representative ITC titration curve showing independent model fit, raw area data, and standard deviations around curve fitting.

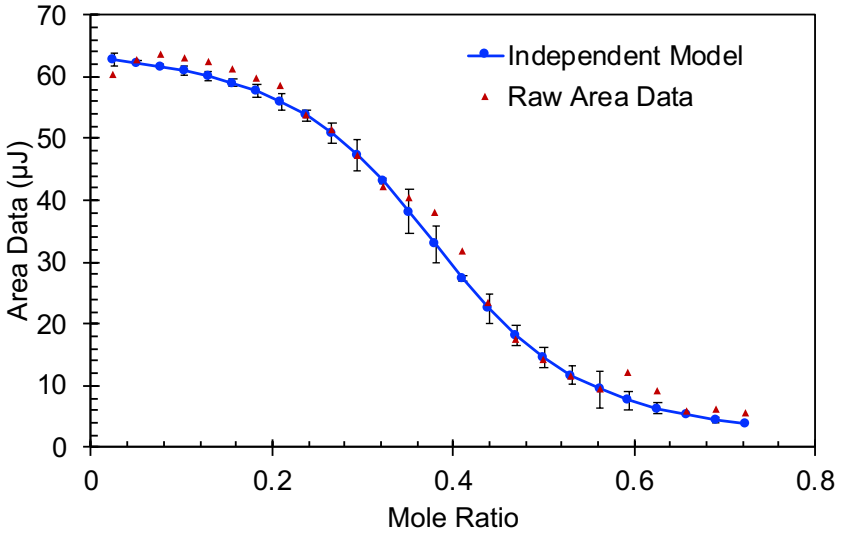


Figure 6.S10: ITC Thermographs of Eu(III) titrations into poly(glycine acrylamide).

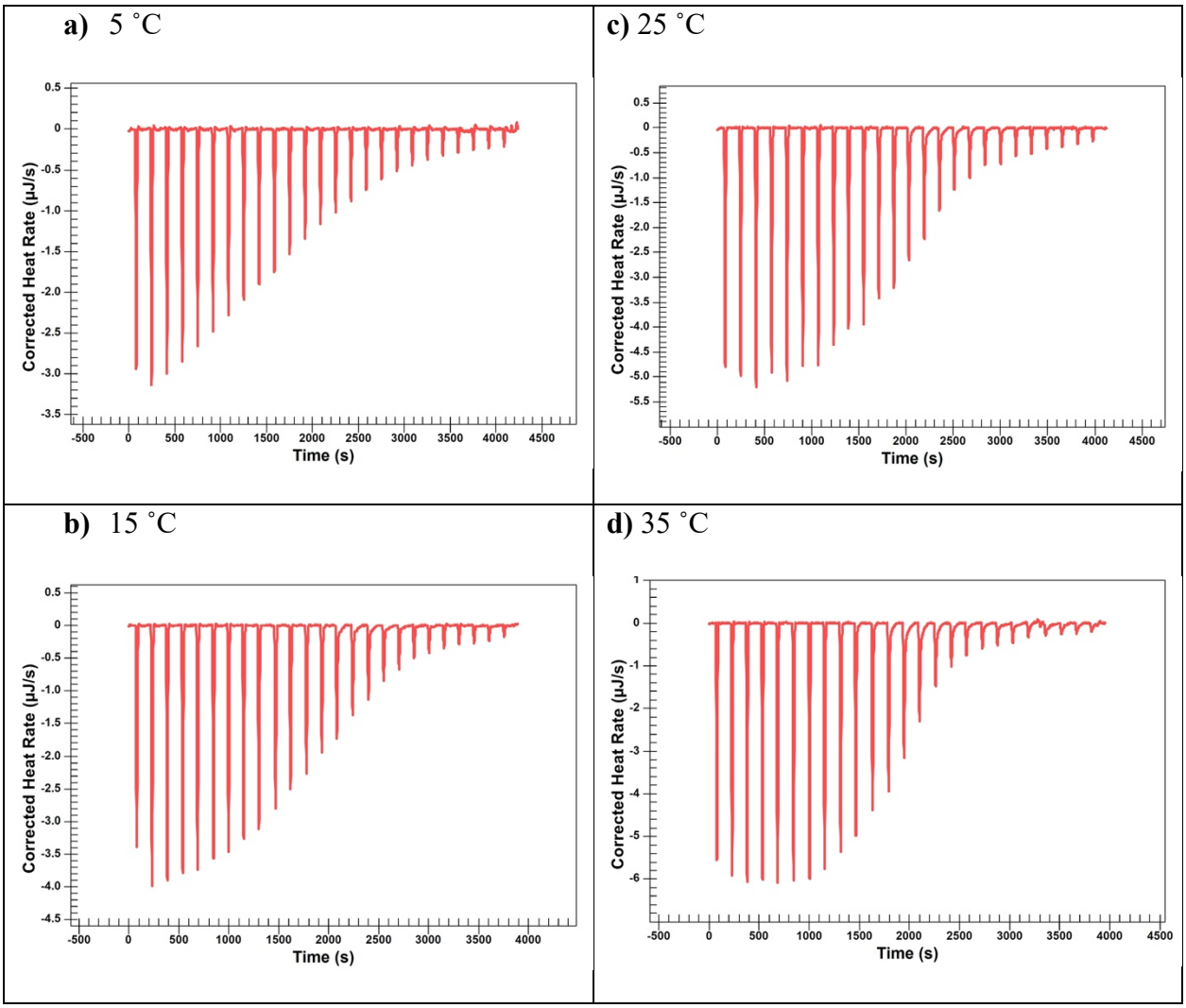


Figure 6.S11: ITC Thermographs of Eu(III) titrations into poly(alanine acrylamide).

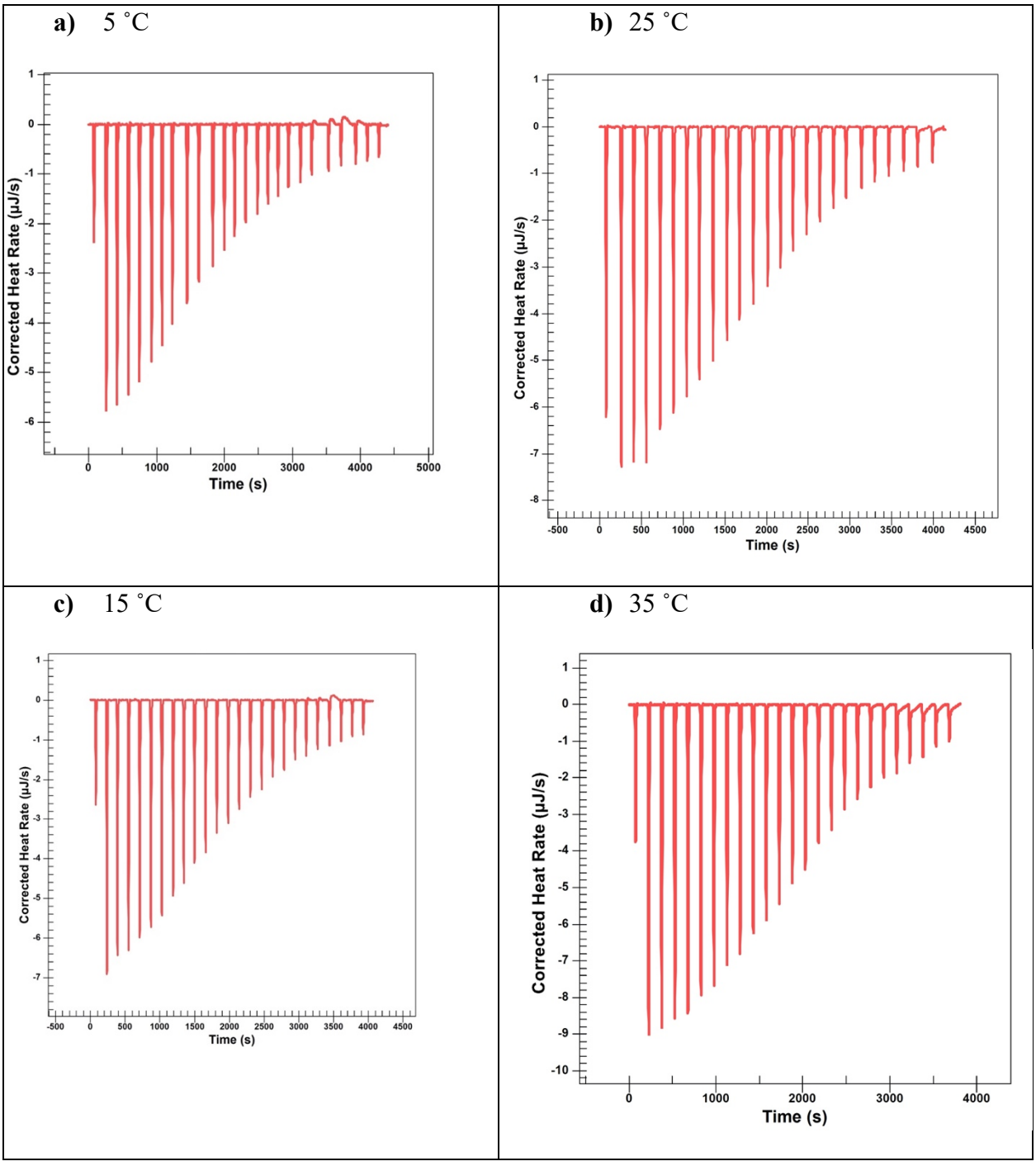


Figure 6.S12: ITC Thermographs of Eu(III) titrations into poly(valine acrylamide).

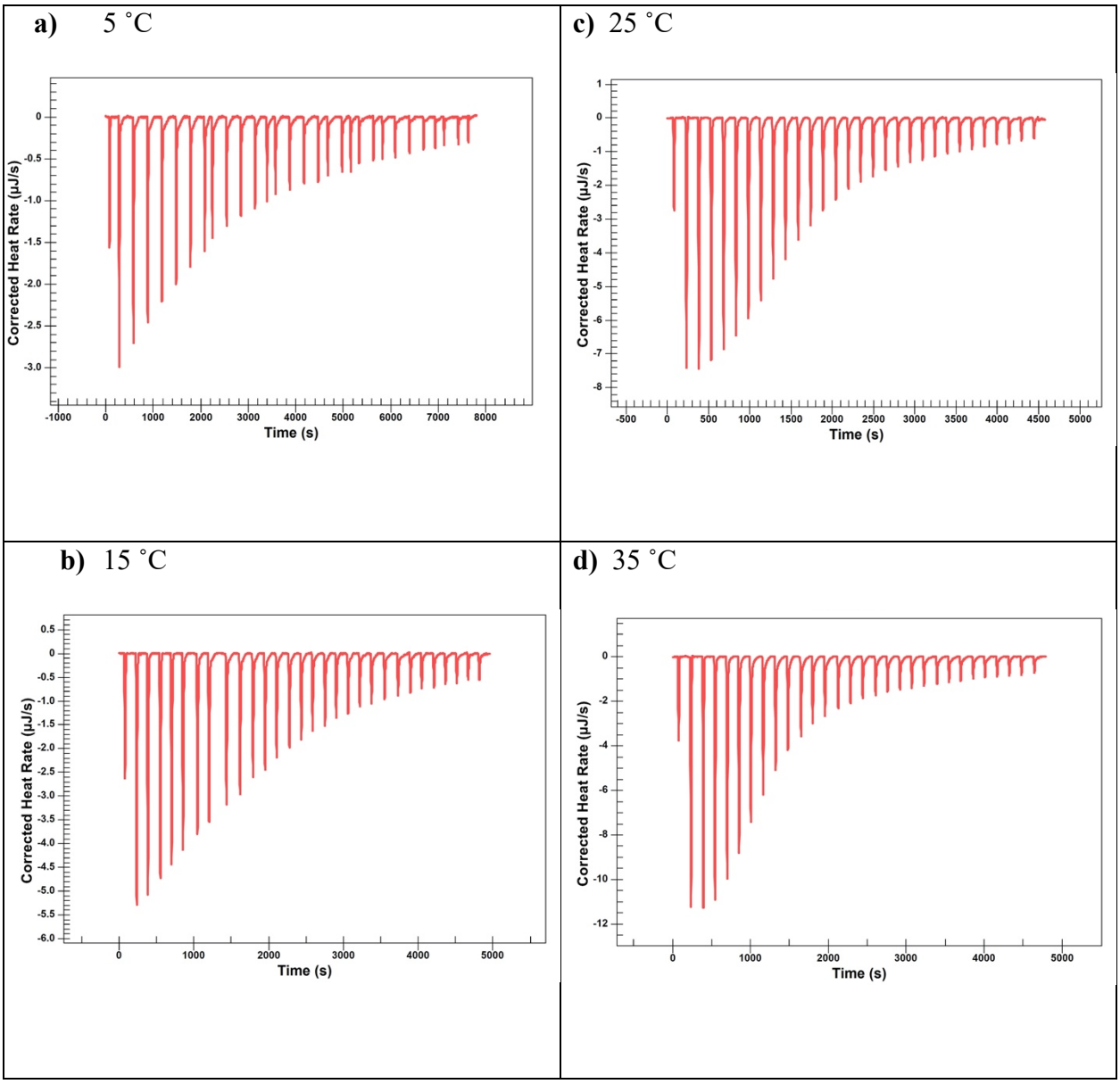
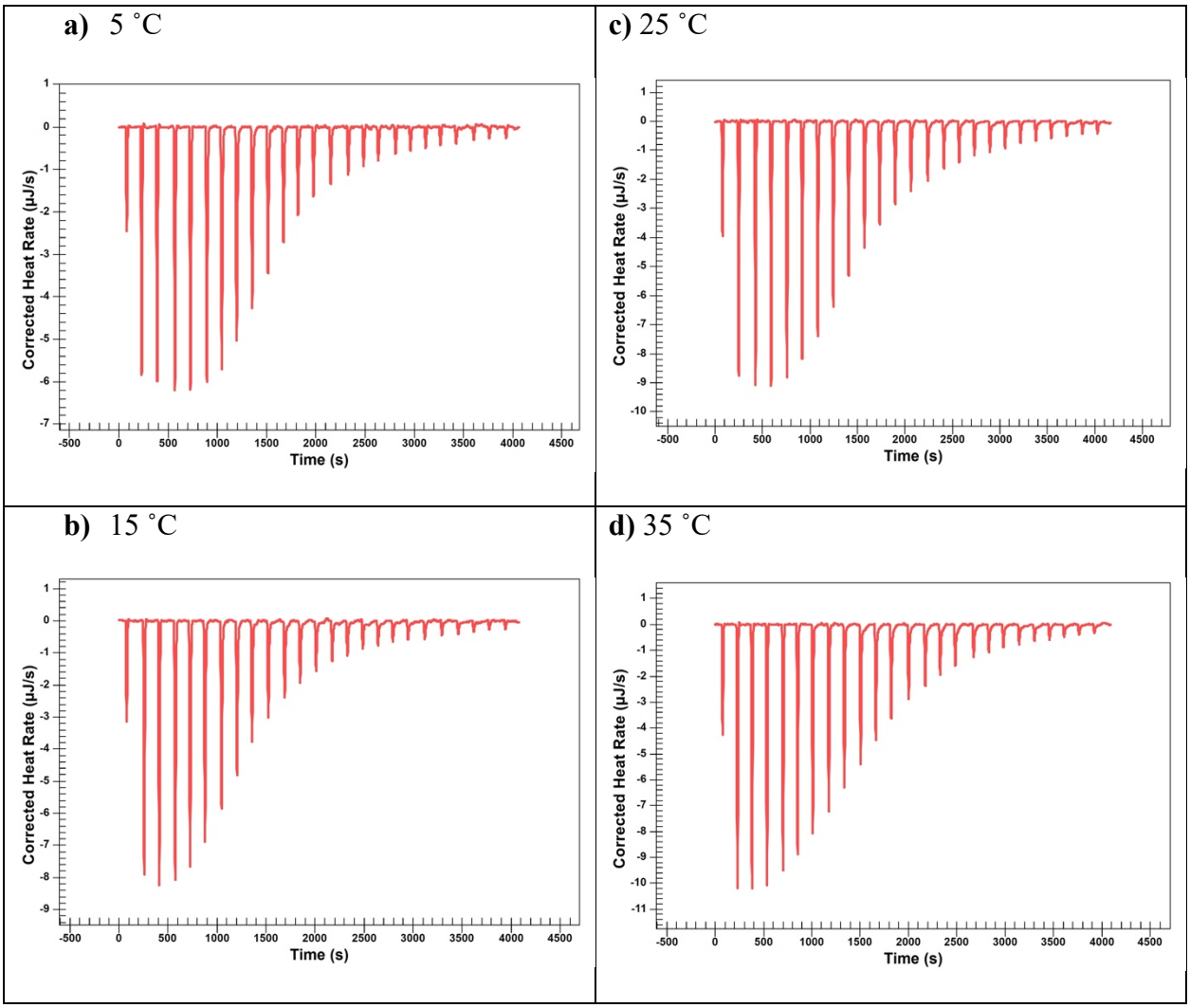


Figure 6.S13: ITC Thermographs of Eu(III) titrations into poly(leucine acrylamide).



Computational Methods:

A 100 % functionalized, 20 unit-long polymer chain was created in Avogadro[4] for poly(DL-leucine acrylamide), poly(DL-alanine acrylamide), poly(DL-valine acrylamide) and poly(glycine acrylamide). Each chain was then explicitly solvated in a 70 × 30 × 50 $Å^3$ H_2O box using Gromacs tools,[5] with Cl^- ions to neutralize the systems. This procedure was repeated adding 20 Eu(III) to each chain. NPT molecular dynamics simulations were then performed with the Tinker software package[6] by using the AMOEBA polarizable force field[43], already developed for amino acids. Parameters for Eu(III) were taken from Ref[7]. 400 ps production trajectories were acquired from a 1 femtosecond timestep and the radial distribution functions calculated from these trajectories with VMD.[7]

Table 6.S3: Polymer structure and calculated solvent accessible surface area from molecular dynamics simulations.

Polymer Side Chain	**Solvent Accessible Surface Area ($Å^2$)**
Glycine	3015.0
DL-Alanine	2930.8
DL-Valine	3470.7
DL-leucine	3777.0

Figure 6.S14: Binding modes observed for poly(amino acid acrylamide)s. Three types of binding modes observed: **a)** Eu(III) binding to the COO^- of a single side chain, **b)** binding to a COO^--COOH pair across two side chains, and **c)** binding to a COO^--COO^- pair across two side chains.

a)

b)

c)

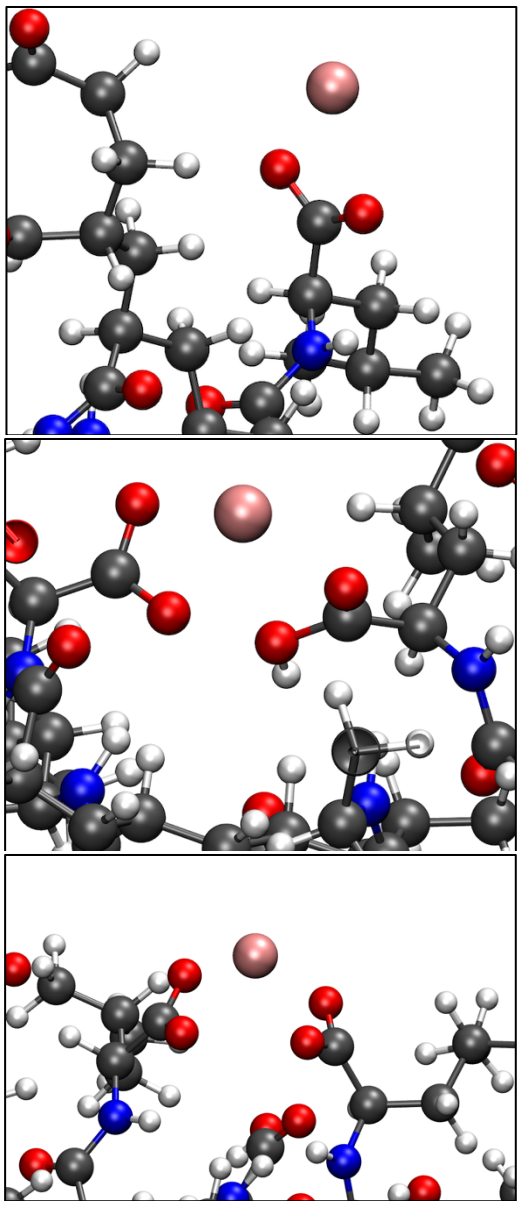
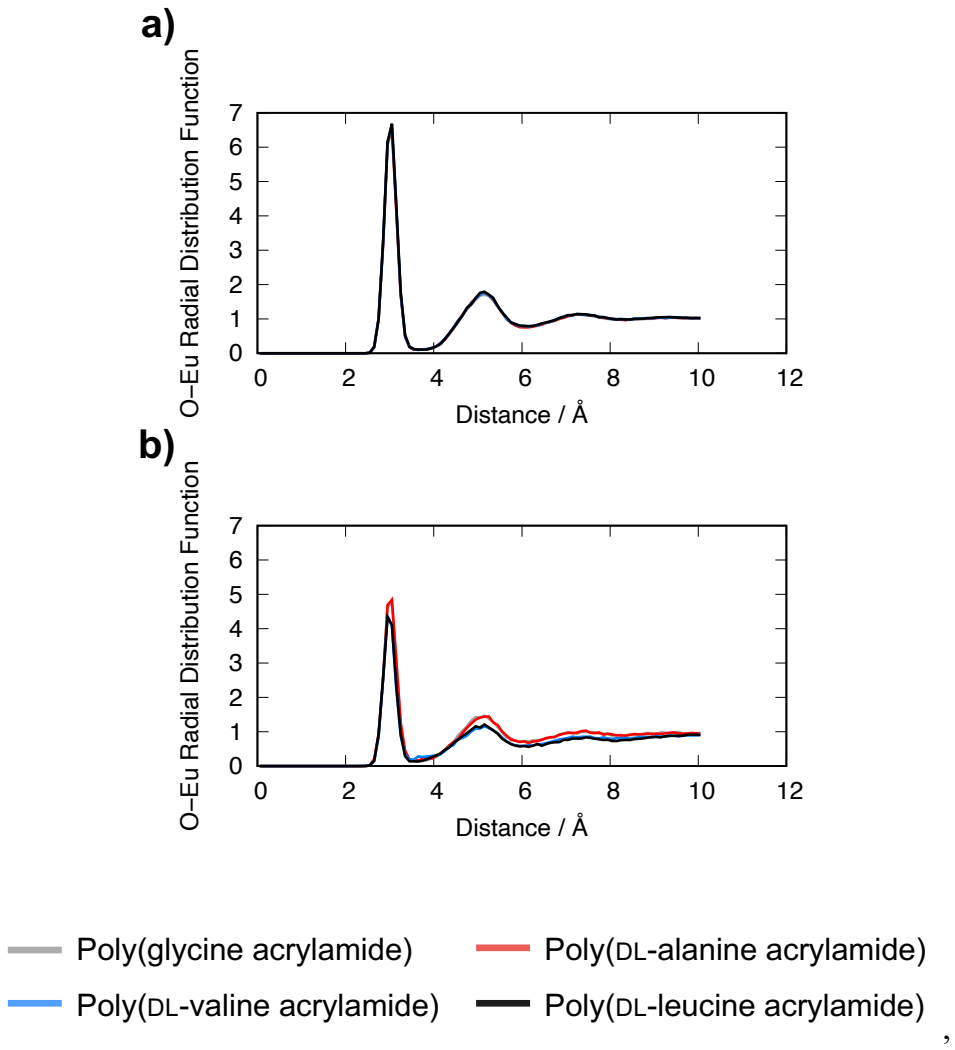
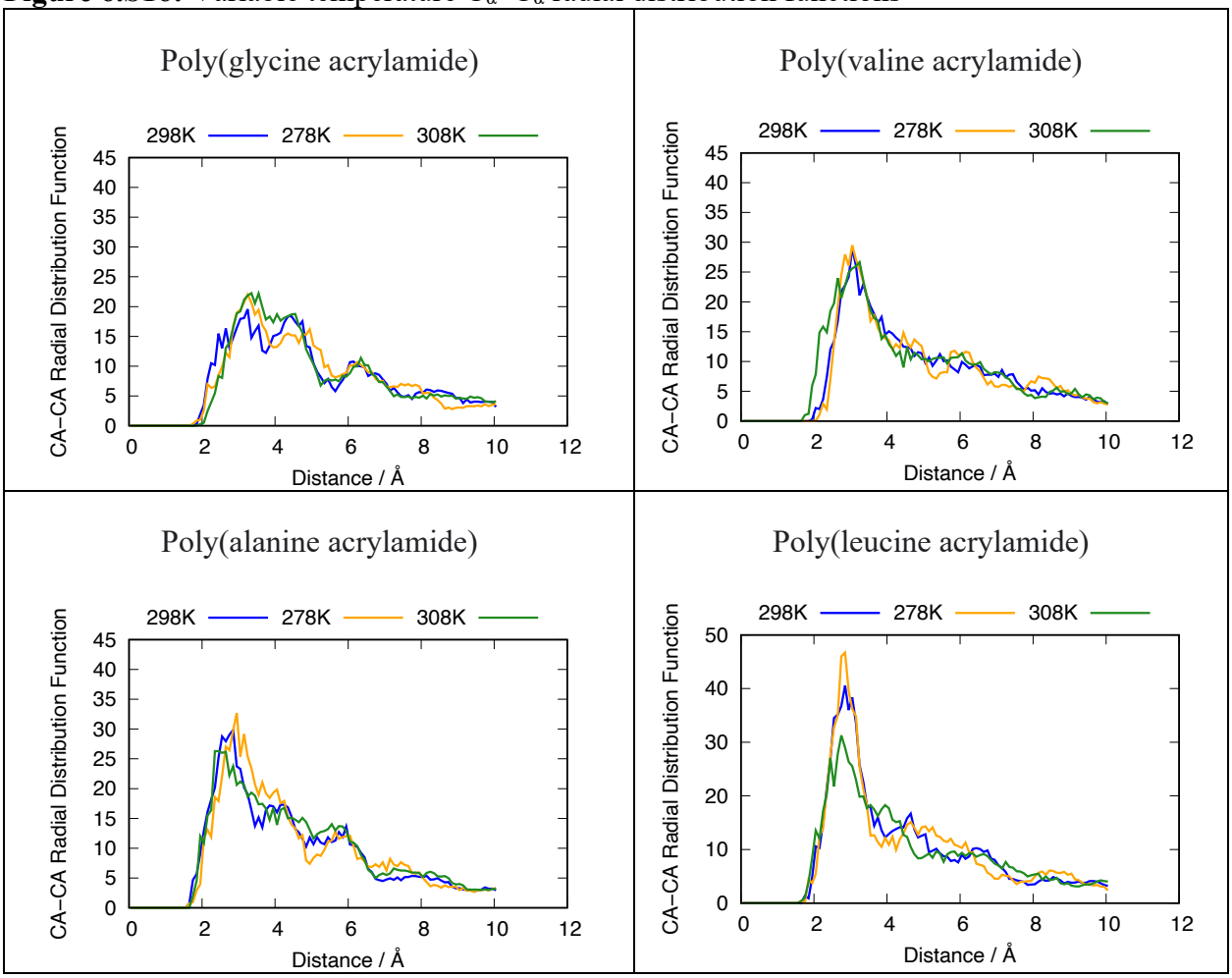


Figure 6.S15: Control radial distribution functions of Eu(III) with respect to water oxygens. Control radial distribution function of Eu(III) with respect to water oxygens. **a)** Eu(III) in solution and **b)** polymer bound Eu(III). Bound Eu(III) has about 2 less coordinated water than Eu(III) in solution, consistent with gaining 2 oxygens from binding to COOH groups. Almost 3 less coordinated water in case of poly(DL-leucine acrylamide), consistent with multiple side chains being involved in the binding of one ion. Note that the binding process also disrupts the ordering of the second solvation shell of the ions: smaller and wider peaks, signature of disorder relative to a more structured network when the ion is in solution.



,

Figure 6.S16: Variable temperature C_α–C_α radial distribution functions



References:

1. Freyer, M. W.; Lewis, E. A., Isothermal Titration Calorimetry: Experimental Design, Data Analysis, and Probing Macromolecule/Ligand Binding and Kinetic Interactions. In *Method. Cell Biol.* , Academic Press: 2008; Vol. 84, pp 79–113.
2. Mizoue, L. S.; Tellinghuisen, J. The role of backlash in the "first injection anomaly" in isothermal titration calorimetry. *Anal. Biochem.* **2004,** 326 (1), 125–127.
3. Willersinn, J.; Bogomolova, A.; Cabré, M. B.; Schmidt, B. V. K. J. Vesicles of double hydrophilic pullulan and poly(acrylamide) block copolymers: a combination of synthetic- and bio-derived blocks. *Polym. Chem.* **2017,** 8 (7), 1244–1254.
4. Hanwell, M. D.; Curtis, D. E.; Lonie, D. C.; Vandermeersch, T.; Zurek, E.; Hutchison, G. R. Avogadro: an advanced semantic chemical editor, visualization, and analysis platform. *J. Cheminformatics* **2012,** 4 (1), 1–17.
5. Pronk, S.; Páll, S.; Schulz, R.; Larsson, P.; Bjelkmar, P.; Apostolov, R.; Shirts, M. R.; Smith, J. C.; Kasson, P. M.; van der Spoel, D.; Hess, B.; Lindahl, E. GROMACS 4.5: a high-throughput and highly parallel open source molecular simulation toolkit. *Bioinformatics* **2013,** 29 (7), 845–854.
6. Rackers, J. A.; Wang, Z.; Lu, C.; Laury, M. L.; Lagardère, L.; Schnieders, M. J.; Piquemal, J.-P.; Ren, P.; Ponder, J. W. Tinker 8: Software Tools for Molecular Design. *J. Chem. Theory Comput.* **2018,** 14 (10), 5273–5289.
7. Humphrey, W.; Dalke, A.; Schulten, K. VMD: Visual molecular dynamics. *J. Mol. Graph.* **1996,** 14 (1), 33–38.

Chapter 7. Polymer Tacticity Effects in Metal–Polymer Chelation Thermodynamics

*William R. Archer[1] and Michael D. Schulz[1]**

1: Department of Chemistry and Macromolecules Innovation Institute

Virginia Tech, Blacksburg, VA USA 24061

7.1 Abstract

Polymer tacticity profoundly affects both bulk and solution properties. Often, tacticity changes play a key role in metal-chelating polymers. We synthesized a series of metal-chelating polymers with systematic variations in the polymer tacticity (99% *m* – 20% *m* diads) and used isothermal titration calorimetry (ITC) to measure the thermodynamics of REE-ion binding for each material. ITC enables the direct determination of the thermodynamic profile (ΔH, ΔG, ΔS, K_a, and stoichiometry) for each polymer–REE biding interaction. We found that binding became more favorable as the percentage of *m* diad decreased, and ΔH and ΔS decreased with decreasing percent *m* diad.

7.2 Introduction

Decades of research have demonstrated a direct link between tacticity—the relative stereochemistry of repeat units—and polymer properties.[1-7] For example, the glass-transition temperature (T_g) of isotactic and syndiotactic poly(methyl methacrylate)[8] differs by almost 81 K, and similar differences are observed for tactic poly(acrylic acid)[9] and poly(styrene).[10] Tacticity effects also appear in solution. For example, atactic poly(methacrylic acid) exhibits an LCST while

isotactic poly(methacrylic acid) exhibits an UCST.[11] Tacticity also plays a critical role in metal-chelating polymers.[12-14]

Metal-chelating polymers are used in several applications, including toxic metal contaminant removal, polymer chelation therapy, and radionuclide delivery for cancer treatments.[15-18] Thus, polymer structure–property relationships are of interest to guide the development of future materials. In particular, rare-earth elements (REEs: Y, Sc, La–Lu)[19] are critical components of many sustainability technologies such as wind turbines (Nd, Dy) and LED light bulbs (Eu, Tb, and Y).[20-22] Thus, as demand for these metals outpaces supply, new and sustainable sources are needed, as well as more efficient methods of extraction and purification.

Polymers often play a central role in new approaches to REE production. For example, polymer-enhanced ultrafiltration (PEUF) uses polymers to selectively coordinate specific metal contaminants by removing polymer–metal complexes using ultrafiltration membranes.[15, 23-25] To date, polymers containing carboxylate,[26] phosphonate,[27] and sulfonate[28] functional groups have proven particularly useful in PEUF applications. Metal-binding thermodynamics are a key consideration in developing new polymers for PEUF and other metal-chelation applications, as well as for elucidating structure–property relationships. However, nearly all the materials currently employed in PEUF applications are atactic.

Polymer conformations are dictated by several factors including charge density, stereochemistry, solvent, and the presence of functional groups.[29-32] Metal-chelating polymers also change their conformations in response to metal binding.[33, 34] We hypothesized that because polymer tacticity influences chain flexibility, increases in tacticity-induced rigidity would increase the ΔH of metal binding. We chose to use poly(methacrylic acid) (PMAA) to explore this hypothesis because of its known metal-binding properties and the synthetic accessibility of tactic

PMAA. Simulations of PMAA have suggested that *isotactic*-PMAA has a larger radius of gyration and exists in an extended chain conformation at high degrees of neutralization.[35] Consequently, we hypothesized that the low chain flexibility of *isotactic*-PMAA would require higher energy to adopt the conformations needed to accommodate metal binding. We synthesized PMAA with varied degrees of tacticity and measured the REE-chelation thermodynamics using isothermal titration calorimetry (ITC). ITC directly measures ΔH, K_a, and the stoichiometry (N) of binding interactions in solution, subsequently enabling the calculation of ΔG, and ΔS of the interaction according to **Equation 7.1**.[36]

$$\Delta G = -RT\ln(K_a) = \Delta H - T\Delta S \qquad \textbf{(7.1)}$$

The thermodynamics measurements presented here enable insight into the relationship between metal-binding thermodynamics, polymer stereostructure, and conformational flexibility, ultimately aiding the design of future metal-chelating materials.

7.3 Results and Discussion

We synthesized poly(methacrylic acid) (PMAA) with varied degrees of stereoregularity by tuning the polymerization conditions. PMAA rich in *rr* triads was synthesized *via* a free-radical polymerization in the presence of catechol. Catechol forms a pseudo-divinyl monomer with methacrylic acid, which promotes racemic addition of the PMAA monomer during polymerization (**Fig. 7.1A**).[37] *isotactic*-PMAA was synthesized by acidic hydrolysis of commercially available *isotactic*-PMMA (**Fig. 7.1B**).[38] Refluxing *isotactic*-PMMA in H_2SO_4(aq) and DI water resulted in hydrolysis of the methyl ester (>93 %). We accessed gradients of PMAA tacticities (40–72 % *m* diad) *via* free radical polymerization of a PMAA–Ca^{2+} dimer in solvents with varied polarities

(**Fig. 7.1C**).[39] For each of the resulting polymers, we integrated the peaks corresponding to the *mm*, *mr*, and *rr* triads of the methyl group in the polymer backbone (**Table 7.1 and Fig. 7.1D**).

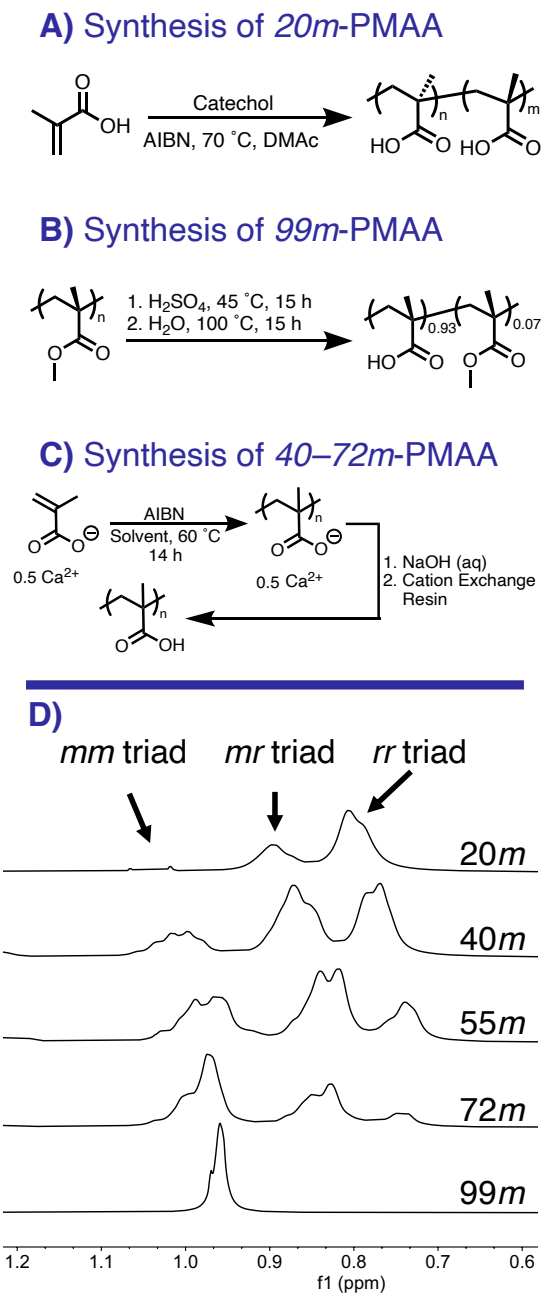


Figure 7.1. Synthesis of **A)** 20*m* PMAA, **B)** 99*m*-PMAA, **C)** 40–72*m*-PMAA, and **D)** overlaid ^{1}H NMR of tactic polymer series.

Table 7.1. Properties of tactic poly(methacrylic acid) series.

Entry	Name	Monomer	Additive	Solvent	Tacticity[e] (*mm*/*mr*/*rr*)
1	20*m*-PMAA[f]	PMAA[a]	Catechol[b]	DMAc[c]	5/30/65
2	40*m*-PMAA[g]	PMAA-Ca[a]	N/A	DMF[d](1)/Water(2)	19/42/39
3	55*m*-PMAA[g]	PMAA-Ca[a]	N/A	DMF[d](2)/Water(1)	32/45/23
4	*72m*-PMAA[g]	PMAA-Ca[a]	N/A	DMF[d]	55/34/11
5	*99m-PMAA*[h]	N/A	N/A	N/A	96/3/1

[a]Polymerization conditions: Monomer = 50 mmol, AIBN = 0.1 mmol, reaction temperature = 60 ˚C, reaction time = 14 h. [b]25 mmol. [c]Dimethylacetamide. [d]Dimethylformamide [e]Determined by the integrated ratio of the backbone methyl signals in the ^{1}H NMR spectrum (MeOD).[f]Free radical polymerization as reported in Ref.[37] [g]Free radical polymerization as reported in Ref.[39] [h]Hydrolysis of commercial isotactic PMMA by H_2SO_4 in water.[38]

We measured REE–polymer binding thermodynamics for a series of REEs (La^{3+}, Nd^{3+}, Eu^{3+}, Gd^{3+}, Dy^{3+}, Ho^{3+}, and Lu^{3+}) and polymer tacticities (99*m*–20*m*). ITC experiments were conducted by titrating each REE ion into the polymer solution in a pH 5 HOAc–NaOAc buffer (**Fig. 7.2**). Control titrations (buffer into polymer, and metal-ion into buffer) enabled the subtraction of enthalpies that were not the direct result of polymer–REE interactions. Each polymer–REE interaction was endothermic. Interestingly, we observed relatively large values for $-T\Delta S$. These entropy-driven interactions are largely the result of the release of complexed water molecules surrounding the polymer and REE ion, consistent with our previous observations of polymer–metal binding thermodynamcis.[40-44] Furthermore, we observed larger $|\Delta H|$ and $|-T\Delta S|$ for the more isotactic PMAAs (**Fig. 7.3**), while only ΔG steadily decreased with increasing *r* diad.

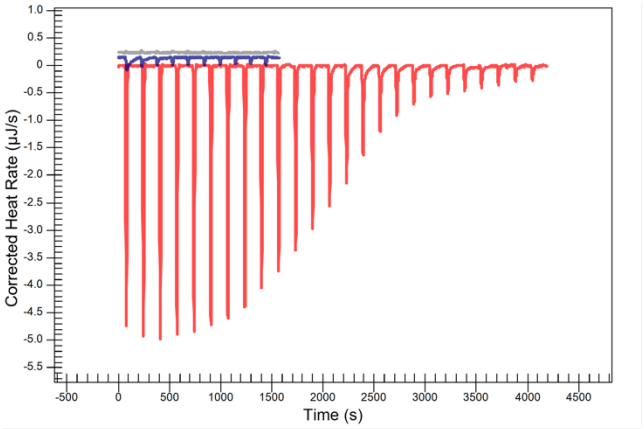


Figure 7.2. Representative ITC thermogram of polymer–REE titration (red) overlaid with control titrations (blue and gray).

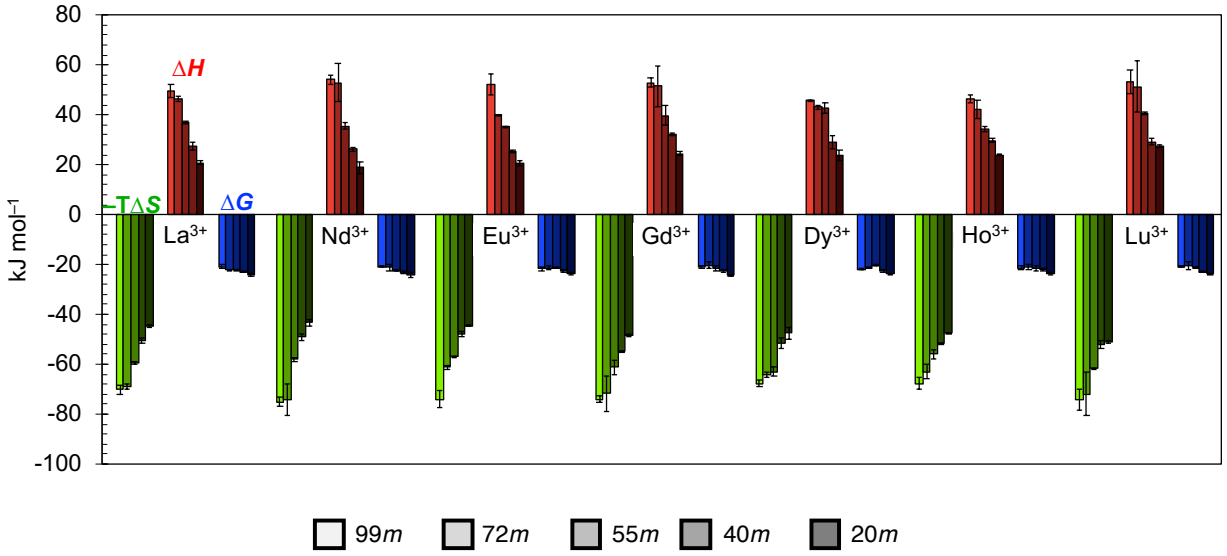


Figure 7.3. Thermodynamic parameters for REE–PMAA binding.

The binding affinity (K_a) reflects the strength of the REE–PMAA complexes in solution, thereby informing the potential utility of these materials in PEUF processes. In some metal-binding applications, K_a must be modulated to balance efficient chelation with the ability to release the metals from the polymer. Interestingly, we observed higher values for K_a with increasing percentage of *r* diads (**Fig. 7.3**). For example, K_a for La^{3+} was $4.4\times10^3 \pm 1.2$ M^{-1} for 99*m*-PMAA and $1.62\times10^4 \pm 0.08$ M^{-1} for 20*m*-PMAA. Higher values for K_a indicate the formation of stronger

polymer–REE complexes, and these alterations in K_a are also reflected in the ΔG value*s* for this polymer series.

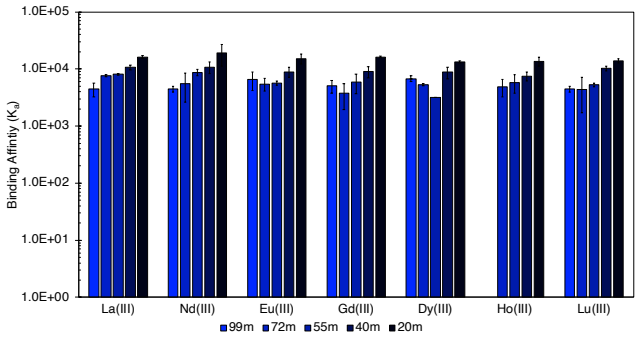


Figure 6.3. ITC binding affinities as a function of percent *m* diad for REE series.

Previous molecular dynamics simulations have reported on the effect of polymer tacticity on PMAA conformations. At high degrees of COOH neutralization, isotactic PMAA exists in an extended-chain conformation.[35] As the degree of carboxylic acid group neutralization increases, the presence of *meso* diads forces those repeat units into the trans configuration, thus causing the polymer chain to further elongate. Furthermore, simulations demonstrated that *syndiotactic*-PMAA exists as a compact coil, even at low degrees of neutralization, with the carboxylates pointing away from the coil, which enables greater access to solvent.[45] Thus, we hypothesize that the more limited flexibility of polymers with more *m* diads limits the polymer conformational degrees of freedom needed to bind a single REE. These conformational limitations manifest as weaker REE binding affinities and less-favorable REE binding thermodynamics.

7.4 Conclusions

In this work, we synthesized a series of PMAA copolymers with targeted degrees of stereoregularity (99*m*–20*m*) to measure the effect of polymer tacticity on REE chelation

thermodynamics using ITC. We found that the binding thermodynamics became more favorable as the percentage of *m* diad decreased (i.e., more syndiotactic polymers). ΔH and ΔS decreased with decreasing percent *m* diad, while the differences in ΔG remained relatively small across this polymer series. These data showcase the importance of polymer tacticity in the design of polymer chelators, ultimately guiding the development of materials for effective REE extractions and separations.

Acknowledgements

The authors wish to acknowledge the Virginia Tech Department of Chemistry Faculty Start-up funds for financial support.

Keywords

Polymer tacticity, Isothermal Titration Calorimetry, Metal Binding, Lanthanides

Conflicts of Interest

The authors declare no conflict of interest.

7.5 References

1. Karasz, F. E.; MacKnight, W. J. The Influence of Stereoregularity on the Glass Transition Temperatures of Vinyl Polymers. *Macromolecules* **1968,** 1 (6), 537–540.
2. Schneider, B.; Štokr, J.; Dirlikov, S.; Mihailov, M. Conformational Structure and Vibrational Spectra of Poly(methyl methacrylate) and of Its Models. *Macromolecules* **1971,** 4 (6), 715–718.
3. Burfield, D. R.; Doi, Y. Differential scanning calorimetry characterization of polypropylene. Dependence of Tg on polymer tacticity and molecular weight. *Macromolecules* **1983,** 16 (4), 702–704.
4. Beaucage, G.; Stein, R. S.; Hashimoto, T.; Hasegawa, H. Tacticity effects on polymer blend miscibility. *Macromolecules* **1991,** 24 (11), 3443–3448.
5. Jones, T. D.; Chaffin, K. A.; Bates, F. S.; Annis, B. K.; Hagaman, E. W.; Kim, M.-H.; Wignall, G. D.; Fan, W.; Waymouth, R. Effect of Tacticity on Coil Dimensions and

Thermodynamic Properties of Polypropylene. *Macromolecules* **2002,** 35 (13), 5061–5068.
6. Huang, C.-L.; Chen, Y.-C.; Hsiao, T.-J.; Tsai, J.-C.; Wang, C. Effect of Tacticity on Viscoelastic Properties of Polystyrene. *Macromolecules* **2011,** 44 (15), 6155–6161.
7. Samal, S.; Thompson, B. C. Influence of Alkyl Chain Spacer Length on the Charge Carrier Mobility of Isotactic Poly(N-carbazolylalkyl acrylates). *ACS Macro Lett.* **2021,** 10 (6), 720–726.
8. Biroš, J.; Larina, T.; Trekoval, J.; Pouchlý, J. Dependence of the glass transition temperature of poly (methyl methacrylates) on their tacticity. *J. Colloid Polym. Sci.* **1982,** 260 (1), 27–30.
9. Maurer, J. J.; Eustace, D. J.; Ratcliffe, C. T. Thermal characterization of poly(acrylic acid). *Macromolecules* **1987,** 20 (1), 196–202.
10. Karasz, F. E.; Bair, H. E.; O'Reilly, J. M. Thermal Properties of Atactic and Isotactic Polystyrene. *J. Phys. Chem.* **1965,** 69 (8), 2657–2667.
11. Hriberšek, P.; Kogej, K. Tacticity and Counterion Modulated Temperature Response of Weak Polyelectrolytes: The Case of Poly(methacrylic acid) Stereoisomers in Aqueous Solutions. *Macromolecules* **2019,** 52 (18), 7028–7041.
12. Kogej, K.; Fonseca, S. M.; Rovisco, J.; Azenha, M. E.; Ramos, M. L.; Seixas de Melo, J. S.; Burrows, H. D. Understanding the Interaction between Trivalent Lanthanide Ions and Stereoregular Polymethacrylates through Luminescence, Binding Isotherms, NMR, and Interaction with Cetylpyridinium Chloride. *Langmuir* **2013,** 29 (47), 14429–14437.
13. Hriberšek, P.; Kogej, K. Effect of Multivalent Cations on Intermolecular Association of Isotactic and Atactic Poly(Methacrylic Acid) Chains in Aqueous Solutions. *Polymers* **2019,** 11 (4), 605.
14. Okamoto, S.; Vyprachticky, D.; Furuya, H.; Abe, A.; Okamoto, Y. Ion Binding Properties of Polycarboxylates Using Terbium(III) as a Fluorescent Probe: Viscosities and Coordinated Water Molecules in Polycarboxylate−Terbium(III) Complexes in Aqueous Solutions. *Macromolecules* **1996,** 29 (10), 3511–3514.
15. Archer, W. R.; Hall, B. A.; Thompson, T. N.; Wadsworth, O. J.; Schulz, M. D. Polymer sequestrants for biological and environmental applications. *Polym. Int.* **2019,** 68 (7), 1220–1237.
16. Popwell, S. J.; Schulz, M. D.; Wagener, K. B.; Batich, C. D.; Miler, R. J.; Lagmay, J.; and Bolch, W. E. Synthesis of Polymeric Phosphonates for Selective Delivery of Radionuclides to Osteosarcoma. *Cancer Biother Radio* **2014,** 29 (7), 273–282.
17. Qian, J.; Sullivan, B.; Peterson, S.; Berkland, C. Nonabsorbable Iron Binding Polymers Prevent Dietary Iron
Absorption for the Treatment of Iron Overload. *ACS Macro. Lett.* **2017,** 6, 350-353.
18. Archer, W. R.; Iftekhar, N.; Fiorito, A.; Winn, S. A.; Schulz, M. D. Synthesis of Phosphonated Polymer Resins for the Extraction of Rare-Earth Elements. *ACS Appl. Polym. Mater.* **2022,** 4 (4), 2506–2512.
19. Mitchell, L. A.; Holliday, B. J. Polymeric Materials for the Separation of f-Elements Utilizing Carbamoylmethylphosphine Oxide Chelating Ligands. *ACS Macro Letters* **2016,** 5 (10), 1100-1103.
20. Bashiri, A.; Nikzad, A.; Maleki, R.; Asadnia, M.; Razmjou, A. Rare Earth Elements Recovery Using Selective Membranes via Extraction and Rejection. *Membranes* **2022,** 12 (1), 80.

21. Jordens, A.; Cheng, Y. P.; Waters, K. E. A review of the beneficiation of rare earth element bearing minerals. *Miner. Eng.* **2013,** 41, 97–114.
22. Massari, S.; Ruberti, M. Rare earth elements as critical raw materials: Focus on international markets and future strategies. *Resour. Policy* **2013,** 38 (1), 36–43.
23. Ma, H.; Burger, C.; Hsiao, B. S.; Chu, B. Highly Permeable Polymer Membranes Containing Directed Channels for Water Purification. *ACS Macro Lett.* **2012,** 1 (6), 723–726.
24. Sujanani, R.; Landsman, M. R.; Jiao, S.; Moon, J. D.; Shell, M. S.; Lawler, D. F.; Katz, L. E.; Freeman, B. D. Designing Solute-Tailored Selectivity in Membranes: Perspectives for Water Reuse and Resource Recovery. *ACS Macro Lett.* **2020,** 9 (11), 1709–1717.
25. Volchek, K.; Krentsel, E.; Zhilin, Y.; Shtereva, G.; Dytnersky, Y. Polymer binding/ultrafiltration as a method for concentration and separation of metals. *J. Membr. Sci.* **1993,** 79 (2), 253–272.
26. Guo, Y.; Zhang, X.; Sun, X.; Kong, D.; Han, M.; Wang, X. Nanoadsorbents Based on NIPAM and Citric Acid: Removal Efficacy of Heavy Metal Ions in Different Media. *ACS Omega* **2019,** 4 (10), 14162-14168.
27. Gomes Rodrigues, D.; Monge, S.; Pellet-Rostaing, S.; Dacheux, N.; Bouyer, D.; Faur, C. A new carbamoylmethylphosphonic acid-based polymer for the selective sorption of rare earth elements. *Chem. Eng. J.* **2019,** 371, 857–867.
28. Kołodyn´ska, D. Diphonix Resin® in sorption of heavy metal ions in the presence of the biodegradable complexing agents of a new generation. *Chem. Eng. J.* **2010,** 159, 27-36.
29. Flory, P. J., *Statistical mechanics of chain molecules*. Repr. ed. with corrections / ed.; Hanser Publishers ; Distributed in the U.S.A. by Oxford University Press: Munich ;New York, 1989.
30. Gupta, A. K. Combined Salt Concentration and Degree-of-Ionization Effect on the Structure of Poly(methacrylic acid) in Aqueous Solutions as Revealed by Molecular Dynamics Simulations. *Ind. Eng. Chem. Res.* **2021,** 60 (13), 4806–4819.
31. Wang, Z.-G. 50th Anniversary Perspective: Polymer Conformation—A Pedagogical Review. *Macromolecules* **2017,** 50 (23), 9073–9114.
32. Xu, Y.; Wang, Z.-G. Coil-to-Globule Transition in Polymeric Solvents. *Macromolecules* **2021,** 54 (23), 10984–10993.
33. Qian, J.; Berkland, C. Conformational Stability Effect of Polymeric Iron Chelators. *iScience* **2019,** 21, 124–134.
34. Fortuna, S.; Fogolari, F.; Scoles, G. Chelating effect in short polymers for the design of bidentate binders of increased affinity and selectivity. *Sci. Rep.* **2015,** 5 (1), 15633.
35. Gupta, A. K.; Natarajan, U. Tacticity effects on conformational structure and hydration of poly-(methacrylic acid) in aqueous solutions-a molecular dynamics simulation study. *Molecular Simulation* **2016,** 42 (9), 725–736.
36. Archer, W. R.; Schulz, M. D. Isothermal titration calorimetry: practical approaches and current applications in soft matter. *Soft Matter* **2020,** 16 (38), 8760–8774.
37. Saito, Y.; Saito, R. Synthesis of syndiotactic poly(methacrylic acid) by free-radical polymerization of the pseudo-divinyl monomer formed with methacrylic acid and catechol. *J. Appl. Polym. Sci.* **2013,** 128 (6), 3528–3533.
38. Semen, J.; Lando, J. B. The Acid Hydrolysis of Isotactic and Syndiotactic Poly(methyl methacrylate). *Macromolecules* **1969,** 2 (6), 570–575.

39. Kaneko, Y.; Iwakiri, N.; Sato, S.; Kadokawa, J.-i. Stereospecific Free-Radical Polymerization of Methacrylic Acid Calcium Salt for Facile Preparation of Isotactic-Rich Polymers. *Macromolecules* **2008,** 41 (2), 489–492.
40. Nishide, H.; Izushi, T.; Arai, H.; Yoshioka, N.; Tsuchida, E. Complexation Constants of Lanthanide Ions with Poly(Methacrylic Acid) and its Copolymers. *JJ. Macromol. Sci. Chem.* **1987,** 24 (3-4), 343–351.
41. Ferrie, L.; Arrambide, C.; Darcos, V.; Prelot, B.; Monge, S. Synthesis and evaluation of functional carboxylic acid based poly(εCL-st-αCOOHεCL)-b-PEG-b-poly(εCL-st-αCOOHεCL) copolymers for neodymium and cerium complexation. *React. Funct. Polym.* **2022,** 171, 105157.
42. Archer, W. R.; Gallagher, C. M. B.; Vaissier Welborn, V.; Schulz, M. D. Exploring the role of polymer hydrophobicity in polymer–metal binding thermodynamics. *Phys. Chem. Chem. Phys.* **2022,** 24 (6), 3579–3585.
43. Archer, W. R.; Fiorito, A.; Heinz-Kunert, S. L.; MacNicol, P. L.; Winn, S. A.; Schulz, M. D. Synthesis and Rare-Earth-Element Chelation Properties of Linear Poly(ethylenimine methylenephosphonate). *Macromolecules* **2020,** 53 (6), 2061–2068.
44. Archer, W. R.; Thompson, T. N.; Schulz, M. D. Effect of Copolymer Structure on Rare-Earth-Element Chelation Thermodynamics. *Macromol. Rapid Commun.* **2021,** 42 (8), 2000614.
45. Jerman, B.; Podlipnik, C.; Kogej, K. Molecular Dynamics Simulation of Poly(methacrylic Acid) Chains in Water. *Acta Chem. Slov.* **2007,** 54, 509–516.

7.5 Supporting Information

Materials:

Trace metals grade REEs, AIBN, 1,4-dioxane, *isotactic* poly(methyl methacrylate) (*iso*-PMMA) (>95 % *m* diad) was purchased from Sigma Aldrich. Methacrylic acid, and *N*,*N*-dimethylacetamide (DMAc) were purchased from Oakwood Chemical. Dialysis bags (pre-treated regenerated cellulose tubing, 1 kDa molecular weight cut-off) were purchased from Spectrum Labs. AIBN was recrystallized from MeOH prior to use. All other chemicals were used as received.

Characterization:

NMR: ^{1}H NMR, and ^{13}C NMR spectra were acquired on an Agilent MR4 400 MHz spectrometer. Chemical shifts in the ^{1}H NMR and ^{13}C NMR spectra were referenced to the residual solvent signal.

Isothermal titration calorimetry experimental procedure:

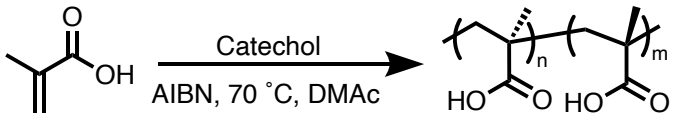
The ITC instrument used was an Affinity-ITC (TA Instruments, New Castle, DE), which operated at constant temperature (278 K). To carry out a binding experiment, a sample solution was prepared by dissolving the polymer and $LnCl_3$ in a pH 5, 100-mM NaOAc–HOAc buffer.

Before the ITC experiment, each solution was degassed for 15 min. The polymer solution (350 μL) was placed in the sample cell and the reference cell was filled with deionized H_2O (300 μL). Both cells were mounted in an adiabatic chamber at a constant temperature during the measurement. A long-needle syringe with a twisted paddle fastened to its end, was filled with the metal-ion solution. The syringe was placed inside the sample cell, and the entire syringe assembly was rotated continuously (185 RPM) to provide proper mixing of the contents of the sample cell within a few seconds after an injection. After reaching thermal equilibrium, the injection of the

metal ion solution was automatically conducted stepwise until the polymer was saturated with metal ion. Due to the possible dilution of the first measurement, the first injection was ignored in the data analysis. The first 1.0-μL injection was followed by a series of 2.0-μL injections. The chosen time interval between two consecutive injections was 300 sec to ensure that the equilibrium was reached before the next injection.

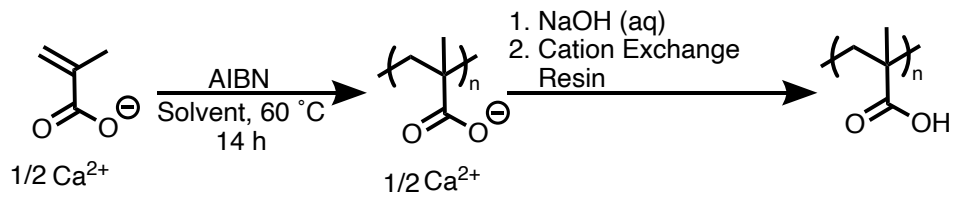
Nonlinear least-squares curve fitting was conducted with TA Instruments Nano Analyze and TA Instruments Independent model. Heats of dilution from control titrations (metal ion into buffer (*no polymer present*), and buffer into polymer (*without metal ion present*)) were subtracted before curve fitting.

Synthesis of 20m-PMAA



20*m*-PMAA was synthesized *via* free-radical polymerization according to a previously reported literature procedure.[1] In general, methacrylic acid (4.6 g, 50.7 mmol, 485 equiv.), catechol (2.8 g, 25.6 mmol, 249 equiv.), and AIBN (16.8 mg, 0.10 mmol, 1.0 equiv.) were combined in a scintillation vial with 7 mL of dry DMAc. The reaction mixture was sparged with N_2 for 20 min and then heated to 60 ˚C for 12 h. The polymer product was collected by precipitation into 1 M HNO_3, and purified by dialysis in 3 M HCl, and DI water for 3 days (2.6 g, 20 % *m* diad).

Synthesis of 40–72m-PMAA



40–72*m*-PMAA was synthesized according to the previously published literature procedure.[2] MAA–Ca dimer was first synthesized by dissolving methacrylic acid (103.2 mmol, 2.0 equiv.) in DI water with $Ca(OH)_2$ (51.8 mmol, 1.0 equiv.). After stirring for 1 h, the aqueous layer was dried to provide a white powder.

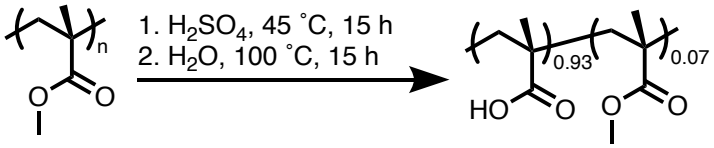
For the polymerization, MAA–Ca dimer monomer (2.28 mmol) was added to a round-bottom flask with the appropriate solvent (DMF, H_2O, or DMF–H_2O). The solution was heated to 60 ˚C, and sparged with N_2. After sparging, AIBN (0.023 mmol) was added to the reaction mixture in one portion, and the reaction continued to stir for 14 h. The polymerization was quenched by exposing to air, and precipitated into acetone. The collected polymer was dissolved in NaOH and stirred with a cation exchange resin for 2 h. The polymer was then removed from the exchange resin, and placed in a dialysis bag, then purified by dialysis against DI water, and 1 M HCl.

1:2 DMF:Water (196 mg polymer after dialysis, 40 % *m* diad.

2:1 DMF:Water (207 mg polymer after dialysis, 55 % *m* diad.

DMF (316 mg polymer after dialysis, 72 % *m* diad.

Synthesis of 99m-PMAA



99*m*-PMAA was obtained from the acidic hydrolysis of *isotactic*-PMMA.[3] In general, *iso*-PMMA (>95 % *m* diad, 200 mg) was dissolved in 50 mL of concentrated H_2SO_4 and bubbled with N_2. After dissolution, the reaction mixture was heated to 45 ˚C for 15 h. The polymer was collected by precipitation into cold acetone, and then refluxed in DI water for 15 h. Percent isolated yield 65–72 % of PMAA.

Figure 7.S1. Representative ^{1}H NMR of poly(methacrylic acid) Polymers at 400 MHz in CD_3OD.

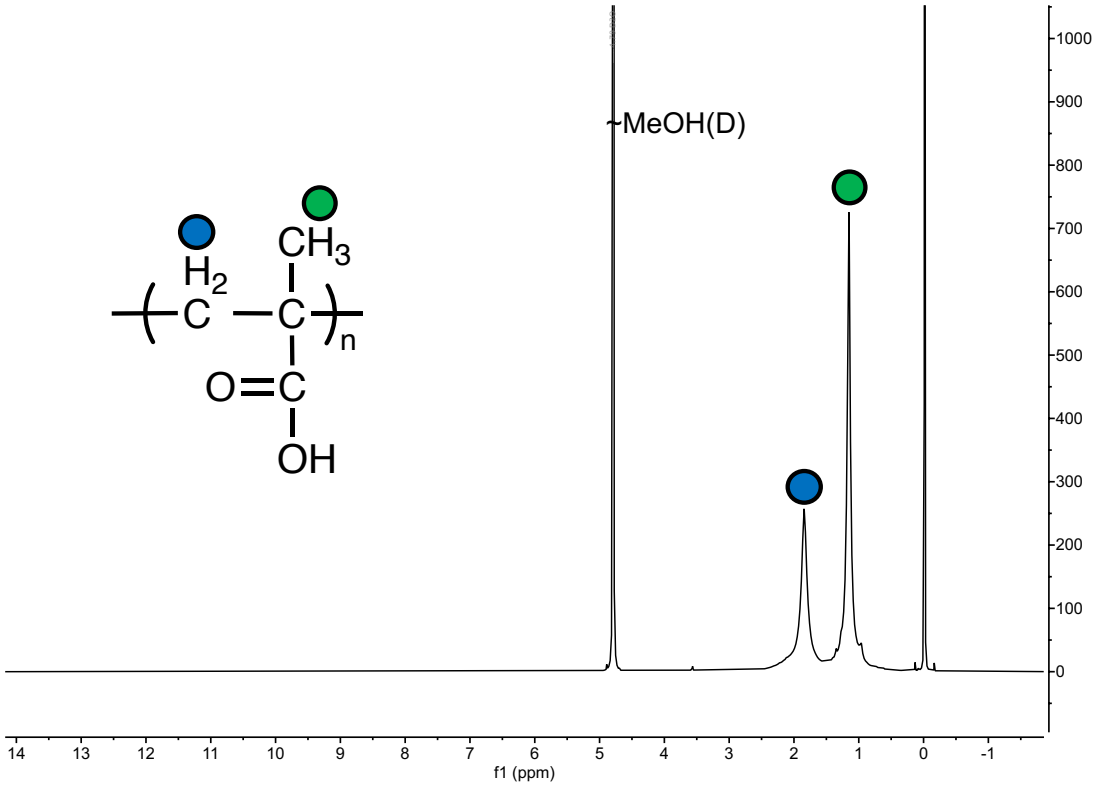


Figure 7.S2. Size exclusion chromatography traces of poly(methacrylic acid) series showing that all samples have approximately the same molar mass.

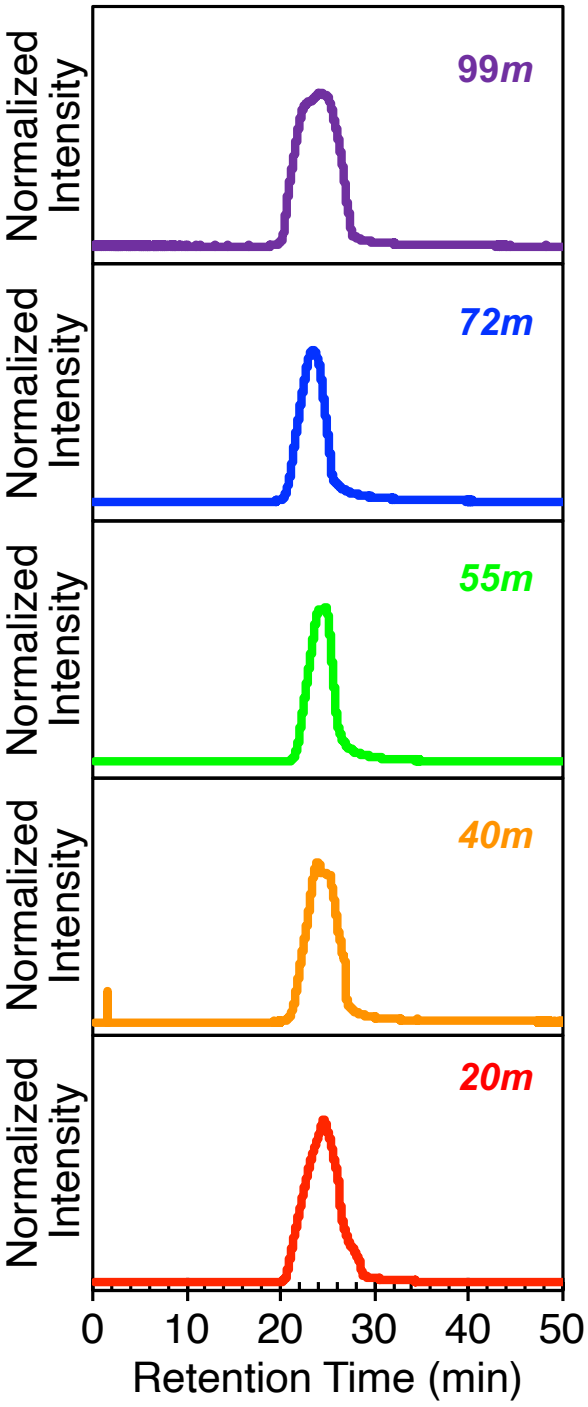


Table 7.S1. Polymer molecular weight of PMAA samples. Size exclusion chromatography (SEC) was performed in water. Data analysis was performed using Astra version 7.2.2.10 software (Wyatt Technologies). Molecular weights are reported relative to the dn/dc of poly(ethylene oxide) standards.

Sample (% *m* diad)	**$M_n^{(SEC)}$ (kg mol^{-1})**	**Đ**
99	489.0	1.2
72	295.1	1.2
55	92.3	1.3
40	179.0	1.1
20	389.5	1.1

Table 7.S2. Metal and Polymer Concentrations used for ITC Experiments

Sample	**Concentration (mM)**							
% *m* diad	**PMAA**	**La^{3+}**	**Nd^{3+}**	**Eu^{3+}**	**Gd^{3+}**	**Dy^{3+}**	**Ho^{3+}**	**Lu^{3+}**
99	27.0	8.0	7.6	7.9	7.4	7.5	7.6	8.0
72	14.5	7.7	7.6	7.7	7.7	7.7	7.7	8.0
55	14.5	8.0	7.7	7.7	7.7	7.7	8.1	8.0
40	14.9	8.0	7.7	7.7	7.7	7.7	8.1	8.0
20	14.9	7.7	7.6	7.7	7.7	7.6	8.0	8.0

Figure 7.S3. ITC binding stoichiometry as a function of percent *m* diad for REE series.

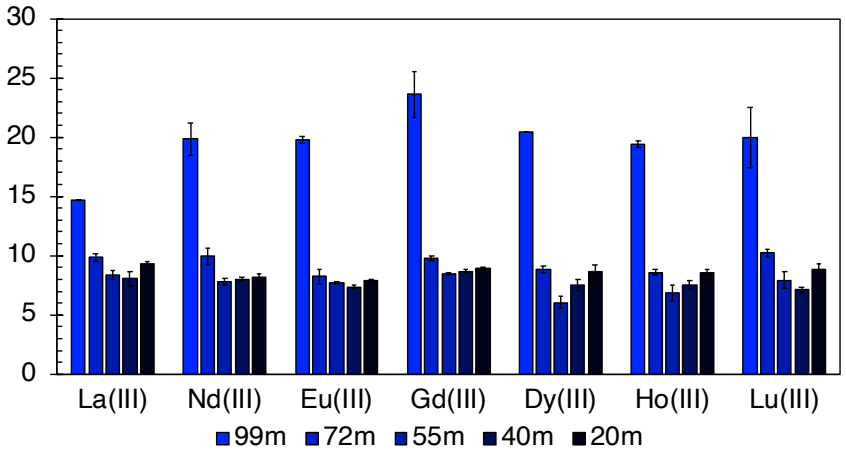


Fig. 7.S4. ITC Thermographs of REE–99m-PMAA Titrations

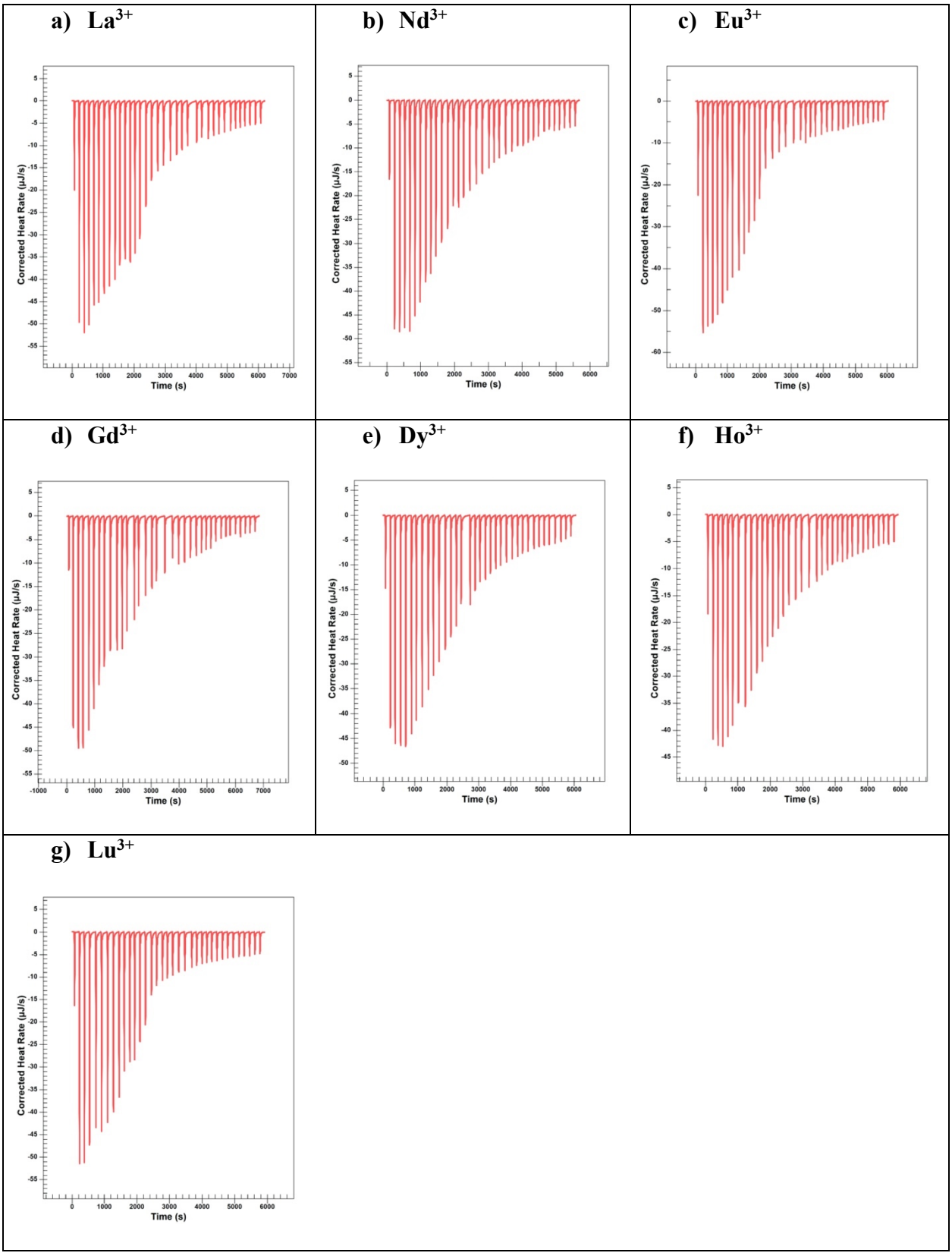


Fig. 7.S5. ITC Thermographs of REE–72m-PMAA Titrations

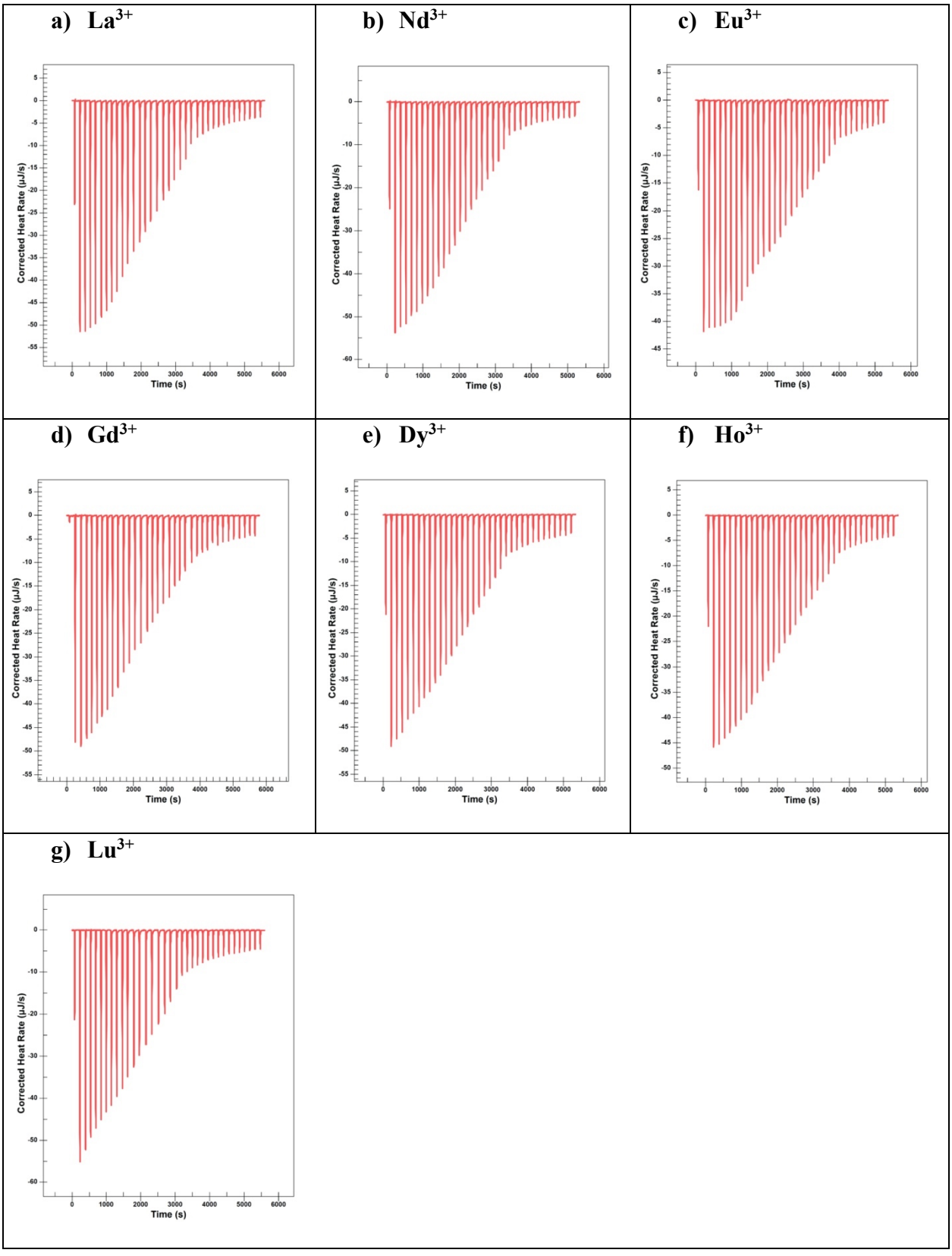


Fig. 7.S6. ITC Thermographs of REE–55m-PMAA Titrations

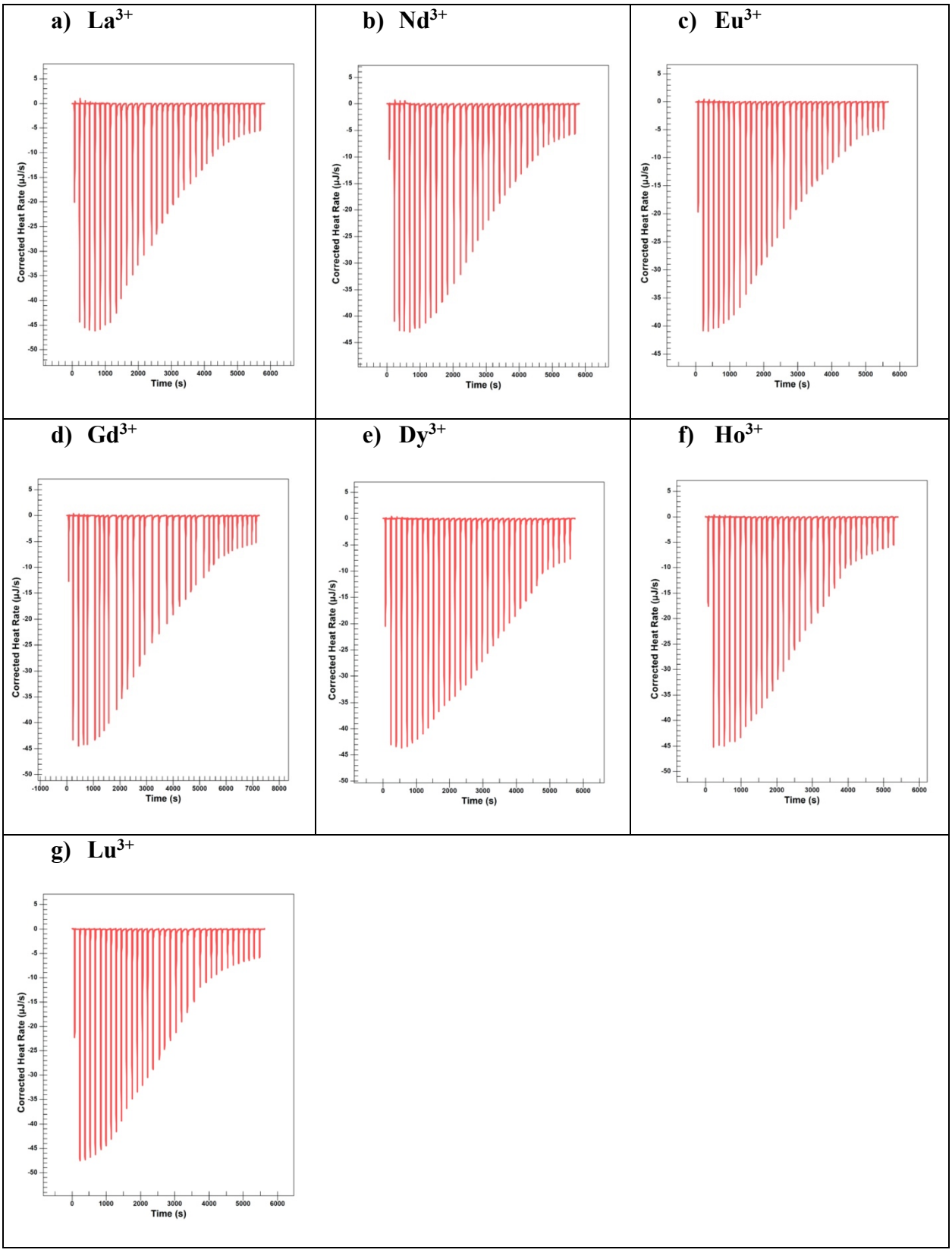


Fig. 7.S7. ITC Thermographs of REE–40m-PMAA Titrations

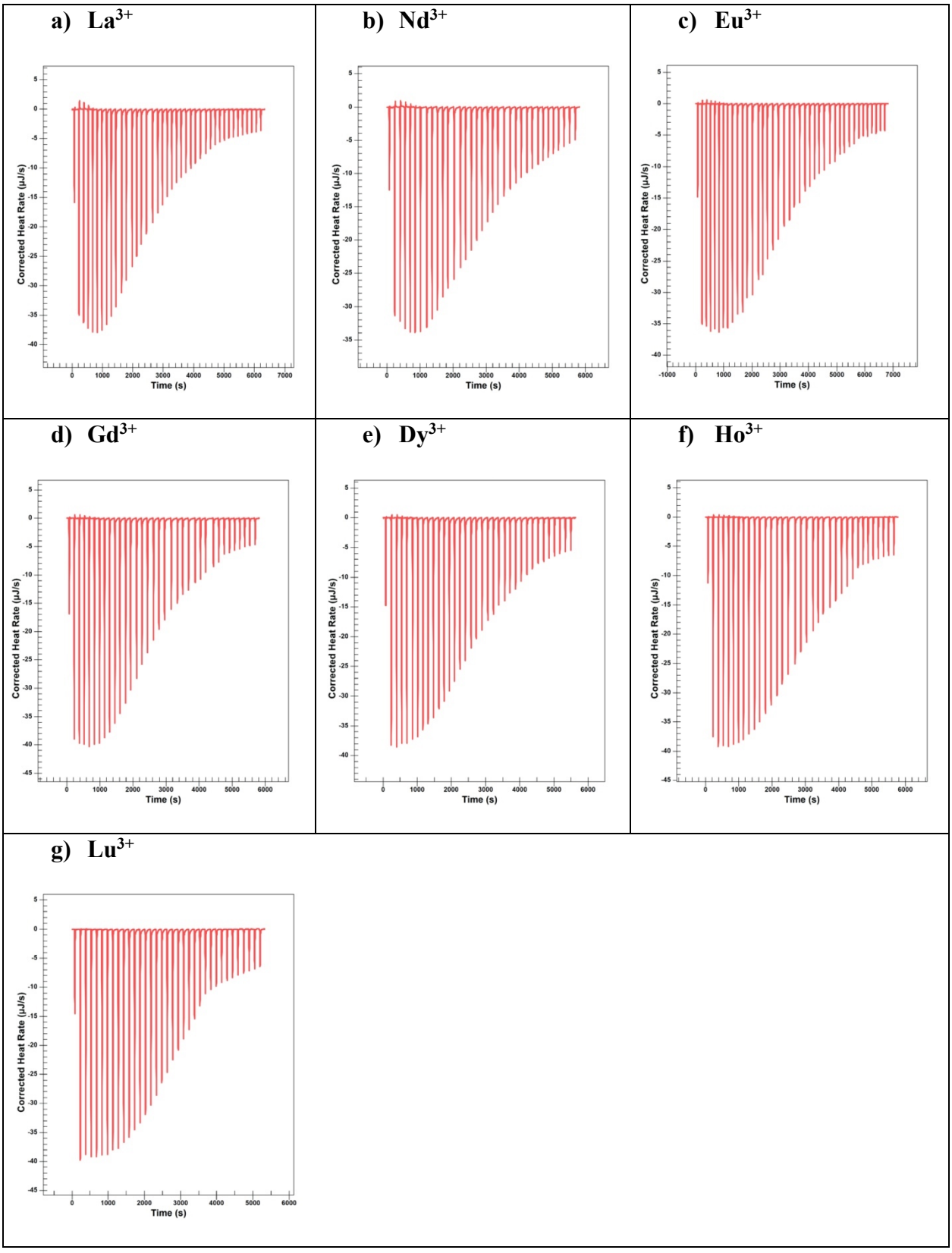
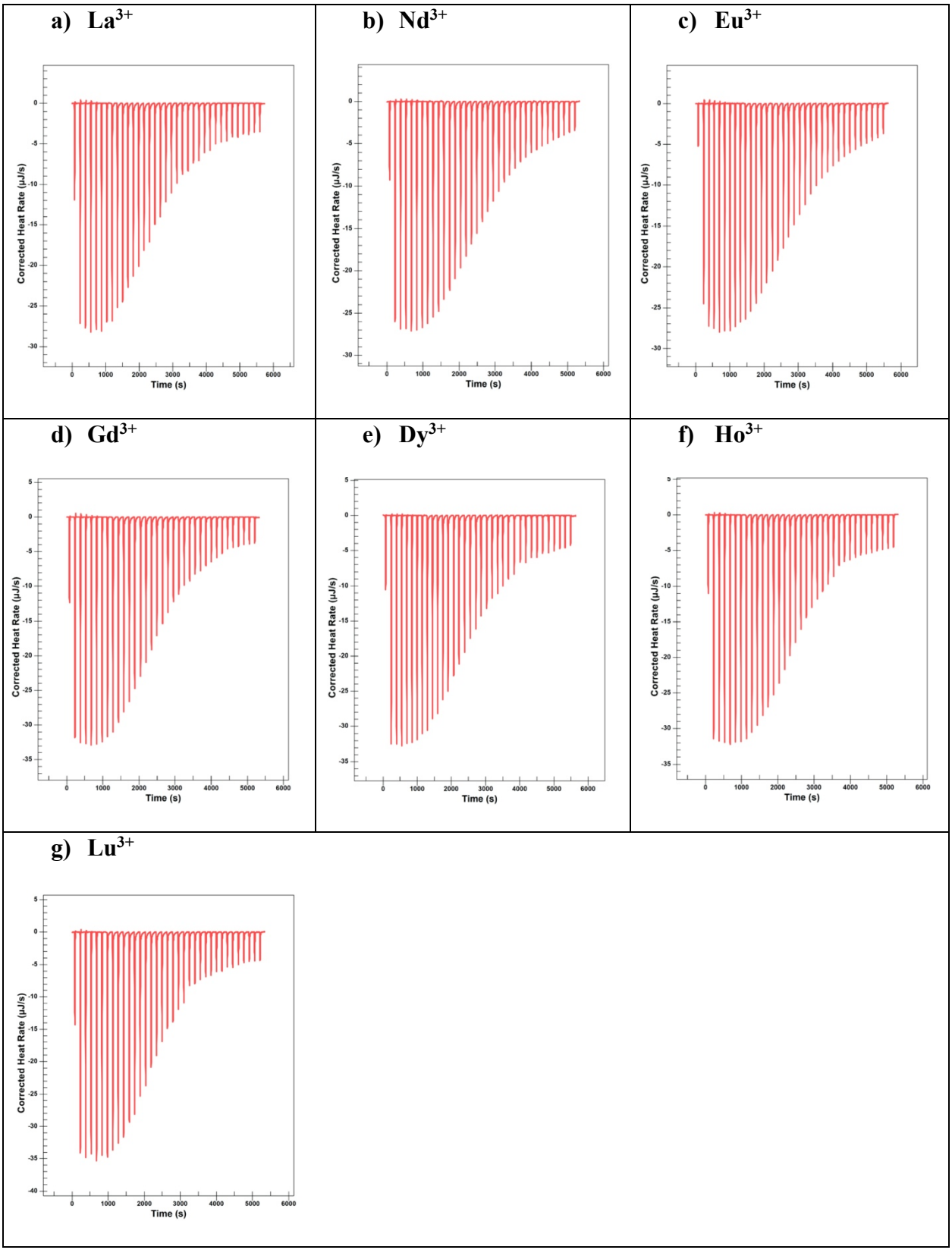


Fig. 7.S8. ITC Thermographs of REE–20m-PMAA Titrations



References:

1. Saito, Y.; Saito, R. Synthesis of syndiotactic poly(methacrylic acid) by free-radical polymerization of the pseudo-divinyl monomer formed with methacrylic acid and catechol. *J. Appl. Polym. Sci.* **2013,** 128 (6), 3528–3533.
2. Kawauchi, T.; Kawauchi, M.; Takeichi, T. Facile Synthesis of Highly Syndiotactic and Isotactic Polymethacrylates via Esterification of Stereoregular Poly(methacrylic acid)s. *Macromolecules* **2011,** 44 (4), 1066–1071.
3. Semen, J.; Lando, J. B. The Acid Hydrolysis of Isotactic and Syndiotactic Poly(methyl methacrylate). *Macromolecules* **1969,** 2 (6), 570–575.

Chapter 8. Summary and Future Outlook

In this dissertation, I set out to measure how perturbations in polymer structure affect the binding of polymers to rare-earth elements (**Fig. 8.1**). Polymers offer many parameters (e.g., molecular weight, architecture, and ligand structure) that can be tuned to potentially enhance metal binding. The field of metal-chelating polymers has long focused on the specific chelating ligand attached to a polymer backbone; however, the research presented in this dissertation indicates that metal chelation is often driven by factors beyond the individual chelating moiety (e.g., (de)solvation or polymer conformation). Throughout this research, I have used isothermal titration calorimetry (ITC) to measure the thermodynamics of polymer–metal binding. Thus, this dissertation represents a new direction in the field of metal-chelating materials. Ultimately, the aim was to produce a depiction of polymer–metal binding that will serve as the foundation for new metal-chelating materials. Such materials will enable the development of efficient metal extraction and separation technologies.

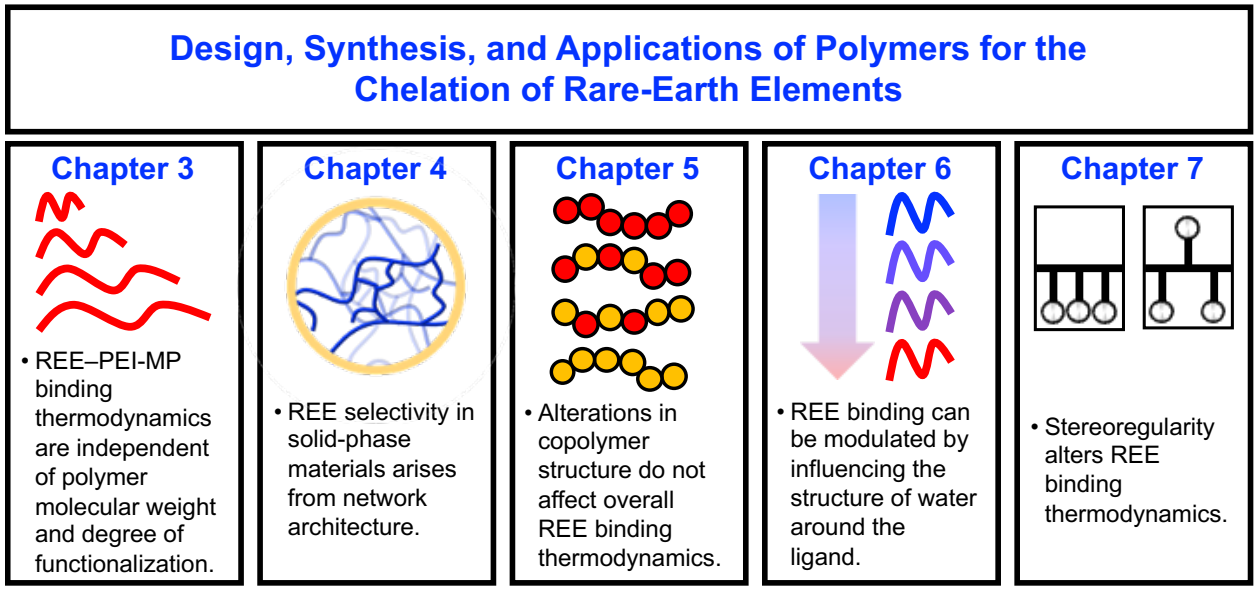


Figure 8.1. Summary of research presented in this dissertation.

Chapter 2 introduced the application of ITC to measure the solution thermodynamics of several soft matter systems. To date, ITC has been used extensively to measure the solution thermodynamics of biological systems (e.g., proteins, enzymes), but with considerably less frequency with soft matter systems. This chapter outlined experimental design parameters for ITC experiments and summarized several literature examples in which ITC was used to measure solution thermodynamics in soft matter systems such as metal-chelating polymers, micellization, and polyelectrolyte interactions. ITC has enabled insight into polymer–metal binding, hydrogel formation, guest–host complexation, (de)micellization, and other soft matter associations. These examples demonstrate the power of ITC to study the thermodynamics of soft matter in solution and serve as a springboard for future experiments in the dissertation research.

I began my work with metal-chelating polymers by exploring the synthesis and rare-earth element (REE) chelation properties of linear poly(ethyleneimine methylenephosphonate) (PEI-MP), a material previously synthesized with only the branched architecture. I synthesized a series of PEI-MP with different molecular weights and used ITC to measure REE solution thermodynamics. I observed consistent binding thermodynamics across a series of six polymer molecular weights and five REEs. On average, the ΔG for the series of PEI-MP molecular weights and REEs was -30 ± 4 kJ mol^{-1}. Dynamic light scattering experiments revealed that *linear* PEI-MP in solution consists of primarily unimolecular polymer chains and a small amount of zwitterionic aggregates. As metal ions are added into the polymer solution, the polymer forms ionic aggregates.

This study with linear PEI-MP demonstrated promising REE-binding properties of phosphonate-containing materials, so we hypothesized that a cross-linked polymer resin functionalized with methylphosphonic acid groups could efficiently capture REE in dilute

solutions. Chapter 4 of this dissertation explored this premise. In this chapter, I cross-linked diethylenetriamine with epichlorohydrin to produce an insoluble polymer resin. I then functionalized the resin with methylenephosphonic acid groups, examined REE capture in flow experiments in which a dilute REE solution was passed over this material, and determined REE capture by inductively coupled plasma-mass spectrometry (ICP-MS). The relatively high capacity of this material demonstrates the advantage of polymer resins incorporating chelating moieties throughout the bulk of the material. Additionally, I used ITC to probe the REE–polymer interaction thermodynamics of a water-soluble polymer analog (PEI-MP), which enabled us to probe the relative contributions of network architecture and ligand identity to the overall binding selectivity.

In addition to phosphonate-containing materials, chapter 5 presented the efficacy of carboxylate containing polymers for REE chelation. Here, we synthesized a series of acrylic acid (AA) and methyl acrylate (MA) statistical copolymers ($\chi_{AA} : \chi_{MA}$ between 1:0 and 0.1:0.9) and examined the effect of copolymer composition on REE binding thermodynamics using ITC. We first examined the binding thermodynamics of poly(AA) to a series of REEs and found that each ion exhibited uniform binding thermodynamics. From this REE series, we chose to closely examine the binding of Eu(III) to poly($AA_{1–0.1}$–*co*–$MA_{0–0.9}$). For our copolymers, we found entropically driven thermodynamics that appear to be independent of copolymer composition (ΔG = –27.1 ± 0.9 kJ mol^{-1}). Interestingly, ITC data for N indicated that incorporating methyl acrylate into the polymer structure slightly reduced the number of repeat units required to bind a REE. This data on the underlying thermodynamics of polymer–REE binding will inform the design of future materials for REE extraction and recovery. This work further suggests the potential application of ITC in evaluating the selectivity of metal ions to predict the behavior of perspective materials for polymer-enhanced ultrafiltration.

Chapter 6 introduced a new parameter in REE chelation: polymer hydrophobicity. Because the REE binding thermodynamics of our previous materials were driven by entropy, presumably resulting from the release of complexed water molecules, we hypothesized that increasing the hydrophobicity of the polymer would increase desolvation during binding. I synthesized poly(tetrafluorophenyl acrylate)—a polymer containing an activated ester that can easily be modified in a modular fashion—and installed chelating carboxylates with varied hydrophilicities. We found that increasing the hydrophobicity of the polymer increased the ΔH dependence on temperature (ΔC_P), which is the result of desolvating the polar carboxylate group and REE ion during metal binding. This work reveals the critical role of polymer structure in REE chelation and highlights the value of combining precise synthesis, thermodynamics measurements, and simulations. Perturbing the structure of water around the chelating sites produced large variations in ΔC_P, which directly affected the temperature dependence of the K_a.

Finally, chapter 7 explored the effect of polymer tacticity on metal chelation. I synthesized a series of poly(methacrylic acid) with targeted degrees of stereoregularity (99*m*–20*m*) to measure the effect of polymer tacticity on REE chelation thermodynamics using ITC. We found that the binding thermodynamics became more favorable as the percentage of *m* diad decreased (i.e., more syndiotactic polymers). These data showcase the importance of polymer tacticity in the design of polymer chelators, ultimately guiding the development of materials for effective REE extractions and separations.

To date, several challenges remain in selective REE chelation. REE selectivity over high concentrations of unwanted metals (e.g., Fe, Al, Cu) in REE feedstocks remains a particular challenge. Additionally, the ability to desorb the chelated metals and regenerate the material is a critical capability that is not yet fully optimized. Typically, desorption and regeneration is

accomplished by adding acid to remove the chelated ions, which often results in the degradation of the material over several uses. While the recyclability of our REE-chelating was not discussed in chapter 4, one could hypothesize that materials that incorporate covalently attached ligands would impart greater chemical stability over multiple cycles of acid regeneration and reuse.

Modern polymerization techniques enable access to polymer architectures that have not yet been explored in these applications. For example, hyperbranched polymers have a high density of terminal functional groups that could be advantageous in selective metal chelation. By tuning the degree of branching of the material, the number of terminal functional groups can subsequently be adjusted. One could hypothesize that the binding thermodynamics could be dominated by the metal–terminal ligand interactions, a trend that could be amplified with higher degrees of branching.

While chapter 3 suggested that alterations in polymer molecular weight do not affect metal binding thermodynamics of linear PEI-MP, we know that multidenticity is critical for efficient metal binding. Consequently, some minimum number of polymer repeat units must be required to bind a metal ion, however the transition between monodentate monomers and multidentate polymer chelators is relatively unexplored. Combining modern polymerization and chromatographic techniques could enable the synthesis of discrete oligomers (e.g., dimer, trimer, tetramer…polymer). Is the binding affinity of a 15-mer more like a 100-mer or a 5-mer of the same repeat unit? Comparing the thermodynamics and stoichiometry parameter of these discrete oligomers would provide insight into the polymer–metal binding process on a *per repeat unit basis* that would aid in the design of future materials.

Alternatively, the chelating ligand attached to the polymer can also be turned. Future work in this area should include exploring the installation of commercially available ligands (e.g.,

diglycolamide and phosphonate ligands) onto the polymer backbone. These ligands may enable greater selectivity *among* the REEs during polymer chelation—an advance not achieved in this work. Many of these commercial ligands are often used in solvent extraction processes, thus incorporating these ligands into polymers could potentially result in oil-soluble polymers that could be incorporated into technologies that are currently employed in REE solvent extraction processes.

The application of polymers for the selective chelation of REEs (and other metals) has a bright future. Beyond REE extraction technologies, polymer chelators find applications in radionuclide delivery, water purification, and chelation therapy for diseases such as aplastic anemia. Thus, an enormous number of unexplored parameters remains in this field depending on the desired application. I look forward to seeing this research evolve with future members of the Schulz group.

Appendix A. Error analysis in the Extrapolation of Thermodynamic Data in Isothermal Titration Calorimetry Experiments

A.1. Introduction: Data quality assessment is paramount for a conscientious interpretation of thermodynamic parameters obtained from isothermal titration calorimetry (ITC) experiments. The precision and accuracy of the measurements dictates the level at which the discussion of data is appropriate and enables insight into the significance of comparison with other data. While buffer selection, data analysis, and application of ITC in soft matter were previously discussed in *Chapter 1: Isothermal Titration Calorimetry: Practical Approaches and Current Applications in Soft Matter*,[1] the aim of this appendix is to provide a basis for performing error analysis when performing ITC experiments.

A.2. Sources of Error: Sources of uncertainty in ITC measurements can originate from both instrumentation and user errors.[2, 3] For example, errors in determining the concentration of the final ligand and receptor solutions would propagate into the fitting of the stoichiometry parameter.[4] Furthermore, the presence of air bubbles, mis-matched buffers, non-homogeneous solutions, or non-optimal stirring speed can each produce noisy thermographs.[5]

Malfunctions in the calorimeter can also produce errors associated with the direct measurement of the heat signal. These can include variations in the injection volumes, improper quantification of the heat released/absorbed in the sample cell, and baseline errors. To mitigate these potential sources of error, several peer-reviewed calibration procedures have been reported that can be performed to ensure that the calorimeter is functioning properly.[6-11]

A.3. Describing Measurement Reproducibility: The experimental reproducibility of the ITC measurements is reported by calculating the mean and standard deviation of multiple measurements.[12] The mean $\bar{x}$ is given as the sum of *N* measurements of the quantity x divided by the number of measurements x_i (Equation A.3.1). The mean is the centroid or average value of the quantity x.

$$\bar{x} \equiv \frac{1}{N}\sum x_i \tag{A.3.1}$$

The mean of the parent population is defined as the limit

$$\mu \equiv \lim_{n\to\infty}\left(\frac{1}{N}\sum x_i\right) \tag{A.3.2}$$

The deviation d_i of any measurement x_i from the mean μ of the parent distribution is defined as the difference between x_i and μ.

$$d_i \equiv x_i - \mu \tag{A.3.3}$$

The dispersion of the measurements is the standard deviation σ. The variance σ^2 is defined as the limit of the average of squares of the deviations from the mean μ:

$$\sigma^2 \equiv \lim_{N\to\infty}\left[\frac{1}{N}\sum (x_i-\mu)^2\right] = \lim_{N\to\infty}\left(\frac{1}{N}\sum x_i^2\right) - \mu^2 \tag{A.3.4}$$

and the standard deviation σ is the square root of the variance.

A.4. Residual Analysis in Non-Linear Regression: ITC parameters are calculated by applying a non-linear regression to a series of data points (i.e., a series of injections). In a nonlinear least

squares analysis, the least squares equation is calculated by minimizing the sum of the weighted squared residuals S (see below, equation A.5.1),

$$S = \sum w_i e^2 \tag{A.5.1}$$

with respect to each of the model parameters β.[12, 13] The minimum value of S is obtained by iteratively altering each parameter, β.[13]

The difference between the measured value, and the predicted value from the non-linear regression is the residual. Residuals are calculated for each data point according to equation A.4.1, where e is the residual, y is the measured value, and $\hat{y}$ is the predicted value from the non-linear regression.

$$\boldsymbol{e = y - \hat{y}} \tag{A.4.1}$$

A residual plot displays the calculated residuals for each measured value. A random pattern of the residual plot (**Fig. A1.A**) indicates a good fit. Non-random (e.g., parabolic) shapes of residual plots indicate poor fits, and a different model should be chosen (**Fig. A1.B–C**).

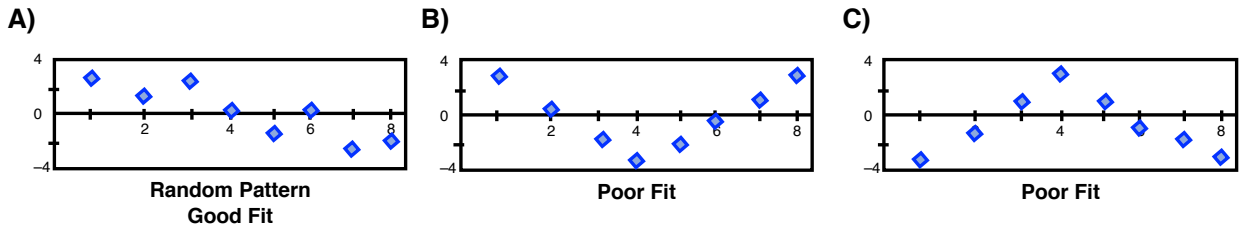


Figure A.1. Example residual plots displaying good and poor fits.

The standard deviation of the fit (residual standard error) can then be computed according to equation A.4.2 where df is the number of degrees of freedom (the total number of measurements–total number of model parameters).

$$Residual\ Standard\ Error = \hat{\sigma} = \sqrt{\frac{\sum_{i=1}^{n}(Y_i - \hat{Y}_i)^2}{df}} \quad (A.4.2)$$

A.5. Calculating residuals from fitting parameters using the ITC NanoAnalyze Software: Monte Carlo sampling methods are often used to determine experimental uncertainties and are estimated from the residuals of the model fit.[2, 14] Several examples of open-source software are available for download that may assist in performing Monte Carlo sampling of ITC data.[15-18] The following subsection presents screen captures outlining the necessary steps to calculate residuals from ITC models within the TA Instruments ITC NanoAnalyze software. These steps will perform a Monte Carlo calculation to help the experimenter understand the statistical significance of the ITC results. In a Monte Carlo calculation, repeat experiments that contain the same parameters of the initial experiment are simulated. First, open the NanoAnalyze the software, and load the desired data set into the program (**Fig. A2**)

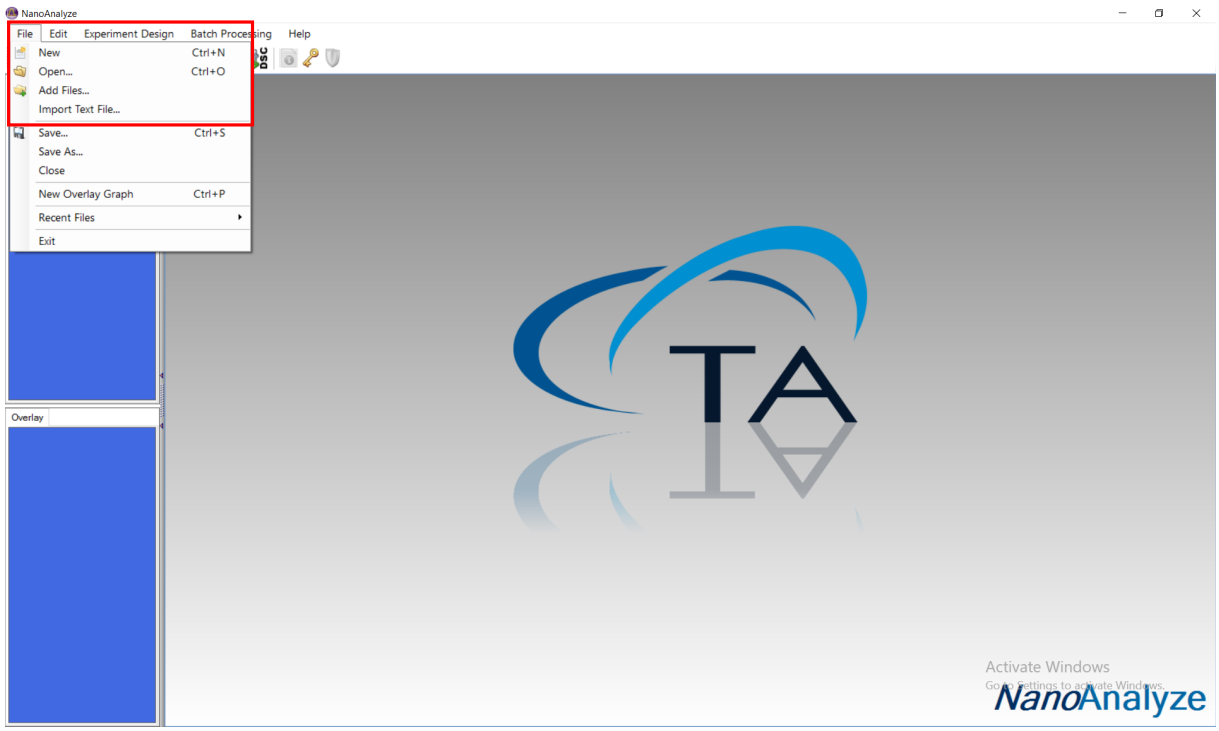


Figure A2. NanoAnalyze software home screen.

Apply the desired model and perform the linear regression to obtain the fit parameters. To view the model residuals, check “Plot Residual” in the graph settings tab. Then, navigate to the “Statistics” tab, located on the top menu bar (**Fig. A3**).

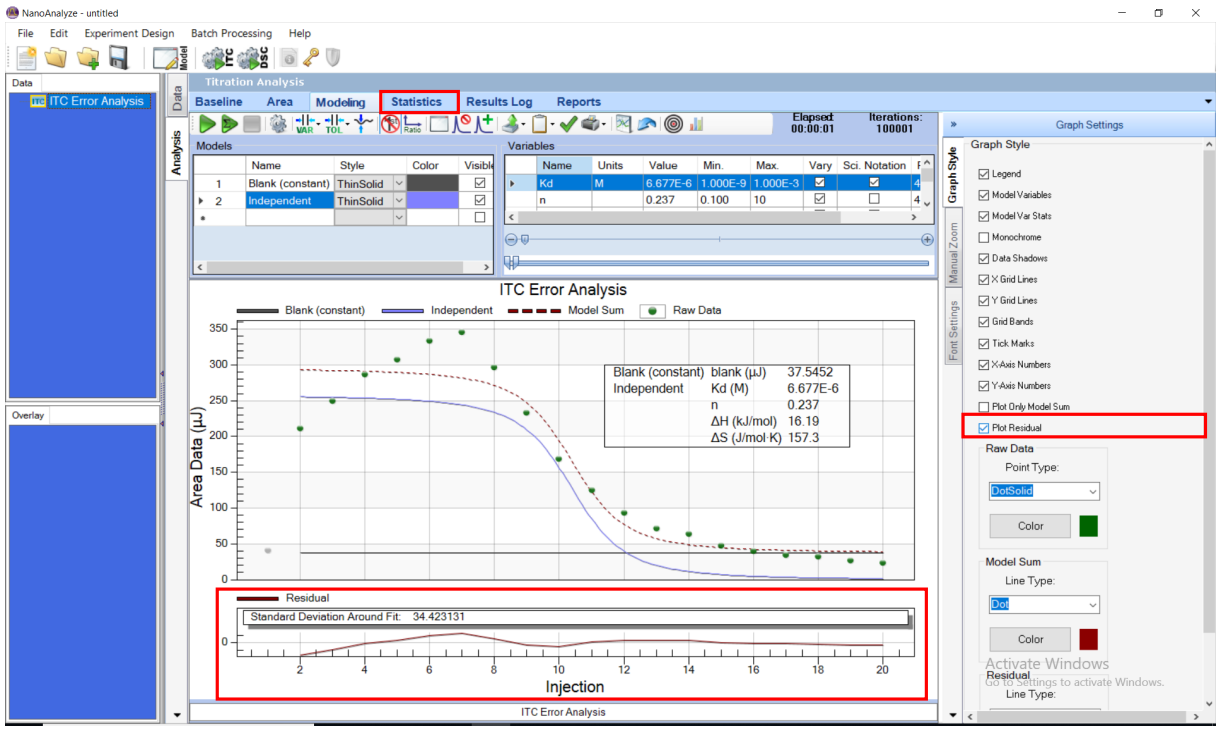


Figure A3. After applying a model, select "Plot Residuals".

In the statistics tab, select the model that you wish to apply the Monte Carlo simulation to. Then, input the desired number of trials, select a confidence interval, and press “Start” (**Fig. A4**).

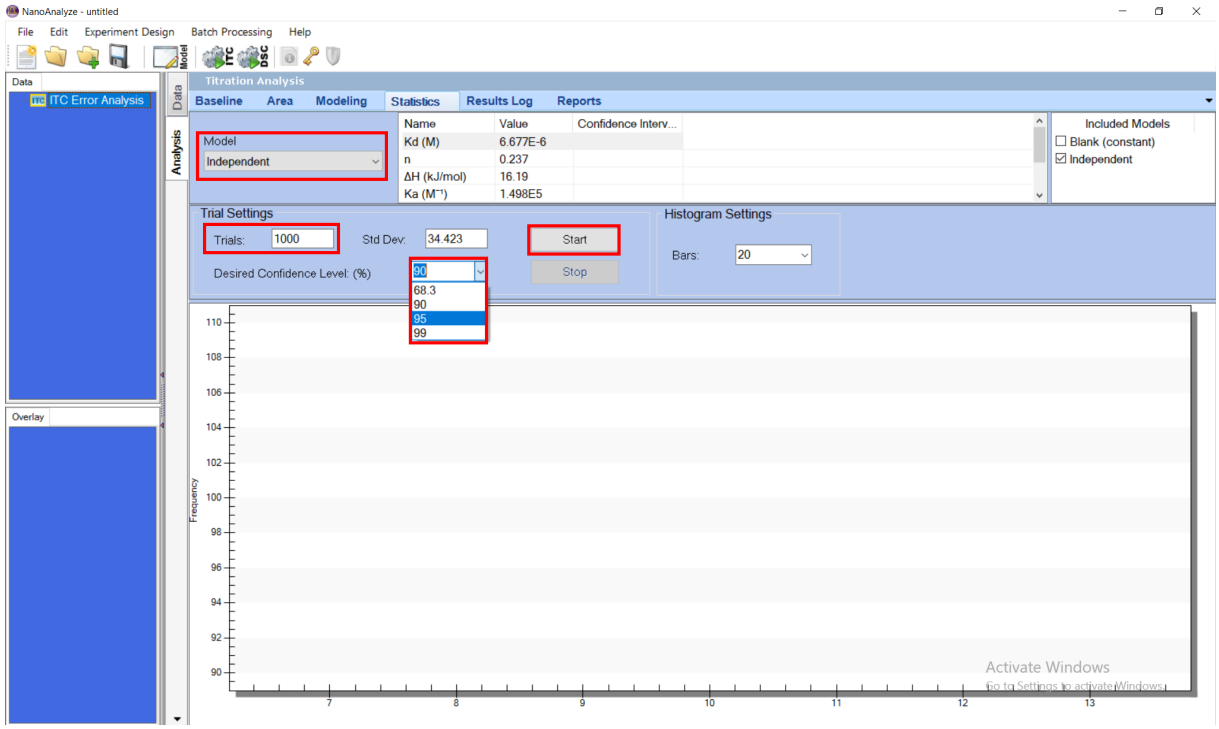


Figure A4. View of the "Statistics" tab in the NanoAnalyze software.

The software now runs a Monte Carlo simulation of 1000 trials and displays a histogram (**Fig. A5**). The histogram graphically represents the calculated distribution of the selected parameter (ΔH, K_d, or N) from the Monte Carlo simulation of the desired number of simulated ITC experiments.

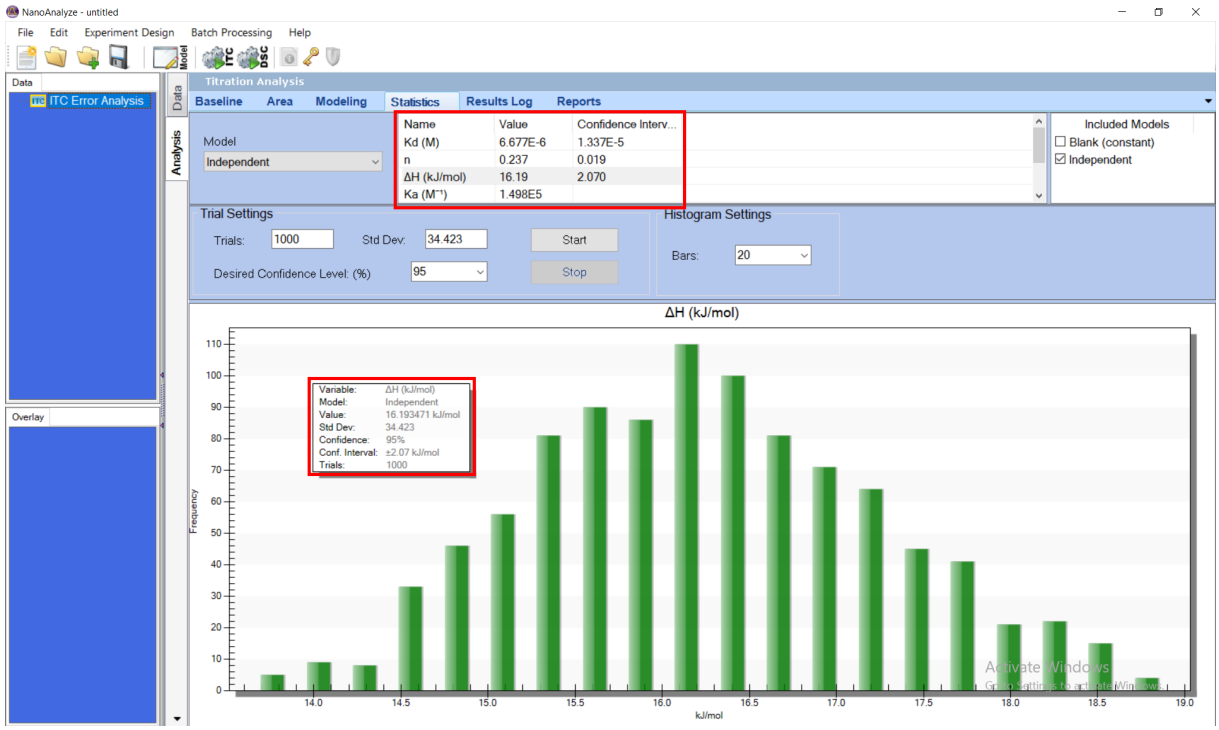


Figure A5. Monte Carlo simulation histogram.

While there is no target minimum value for the residual standard error, the ITC user must remain aware of the uncertainties associated with ITC measurements. As ITC models become more complex (e.g., employing 2 and 3 site models), the number of fitting parameters also increases which further complicates non-linear regression analysis. With careful planning of the experiment, and rigorous attention to model residuals/standard errors, the obtained ITC parameters can be interpreted with confidence.

A.6. References

1. Archer, W. R.; Schulz, M. D. Isothermal titration calorimetry: practical approaches and current applications in soft matter. *Soft Matter* **2020,** 16 (38), 8760–8774.
2. Kantonen, S. A.; Henriksen, N. M.; Gilson, M. K. Evaluation and Minimization of Uncertainty in ITC Binding Measurements: Heat Error, Concentration Error, Saturation, and Stoichiometry. *Biochim. Biophys. Acta Gen. Subj.* **2017,** 1861 (2), 485–498.
3. Baranauskienė, L.; Petrikaitė, V.; Matulienė, J.; Matulis, D. Titration Calorimetry Standards and the Precision of Isothermal Titration Calorimetry Data. *Int. J. Mol. Sci.* **2009,** 10 (6), 2752–2762.

4. Tellinghuisen, J.; Chodera, J. D. Systematic errors in isothermal titration calorimetry: Concentrations and baselines. *Anal. Biochem.* **2011,** 414 (2), 297–299.
5. Mizoue, L. S.; Tellinghuisen, J. The role of backlash in the "first injection anomaly" in isothermal titration calorimetry. *Anal. Biochem.* **2004,** 326 (1), 125–127.
6. Demarse, N. A.; Quinn, C. F.; Eggett, D. L.; Russell, D. J.; Hansen, L. D. Calibration of nanowatt isothermal titration calorimeters with overflow reaction vessels. *Anal. Biochem.* **2011,** 417 (2), 247–255.
7. Tellinghuisen, J. Optimizing Experimental Parameters in Isothermal Titration Calorimetry: Variable Volume Procedures. *J. Phys. Chem. B* **2007,** 111 (39), 11531–11537.
8. Tellinghuisen, J. Calibration in isothermal titration calorimetry: Heat and cell volume from heat of dilution of NaCl(aq). *Anal. Biochem.* **2007,** 360 (1), 47–55.
9. Berg, R. L.; Vanderzee, C. E. Enthalpies of dilution of sodium carbonate and sodium hydrogen carbonate solutions, and the standard enthalpies of ionization of aqueous carbonic acid, at 298.15 K. *J. Chem. Thermo.* **1978,** 10 (11), 1049–1075.
10. Ràfols, C.; Bosch, E.; Barbas, R.; Prohens, R. The Ca2+–EDTA chelation as standard reaction to validate Isothermal Titration Calorimeter measurements (ITC). *Talanta* **2016,** 154, 354–359.
11. O'Brien, L. C.; Root, H. B.; Wei, C.-C.; Jensen, D.; Shabestary, N.; De Meo, C.; Eder, D. J. M2+•EDTA Binding Affinities: A Modern Experiment in Thermodynamics for the Physical Chemistry Laboratory. *J. Chem. Educ.* **2015,** 92 (9), 1547–1551.
12. Bevington, P. R.; Robinson, D. K., *Data Reduction and Error Analysis for the Physical Sciences*. McGraw-Hill Eduction: 2003.
13. Tellinghuisen. A Monte Carlo Study of Precision, Bias, Inconsistency, and Non-Gaussian Distributions in Nonlinear Least Squares. *J. Phys. Chem. A* **2000,** 104 (12), 2834–2844.
14. Freyer, M. W.; Lewis, E. A., Isothermal Titration Calorimetry: Experimental Design, Data Analysis, and Probing Macromolecule/Ligand Binding and Kinetic Interactions. In *Method. Cell Biol.* , Academic Press: 2008; Vol. 84, pp 79–113.
15. Duvvuri, H.; Wheeler, L. C.; Harms, M. J. pytc: Open-Source Python Software for Global Analyses of Isothermal Titration Calorimetry Data. *Biochemistry* **2018,** 57 (18), 2578–2583.
16. Brautigam, C. A.; Zhao, H.; Vargas, C.; Keller, S.; Schuck, P. Integration and global analysis of isothermal titration calorimetry data for studying macromolecular interactions. *Nat. Protoc.* **2016,** 11 (5), 882–894.
17. Zhao, H.; Piszczek, G.; Schuck, P. SEDPHAT – A platform for global ITC analysis and global multi-method analysis of molecular interactions. *Methods* **2015,** 76, 137–148.
18. Keller, S.; Vargas, C.; Zhao, H.; Piszczek, G.; Brautigam, C. A.; Schuck, P. High-Precision Isothermal Titration Calorimetry with Automated Peak-Shape Analysis. *Anal. Chem.* **2012,** 84 (11), 5066–5073.

Appendix B. Journal Copyright Permissions

A portion of Chapter 1 of this dissertation has appeared in *Polymer International*, which belongs to the publisher, Wiley. According to the copyright policies of Wiley, authors retain rights to use their contributions, in full or in part, for inclusion in a theses or dissertation. An acknowledgment to the original published article has been prominently placed at the beginning of chapter 1. Therefore, the permission to include this paper in this dissertation is granted. The published article can be found at:

https://onlinelibrary.wiley.com/doi/10.1002/pi.5774

Chapter 2 of this dissertation has appeared in *Soft Matter*, which belongs to the Royal Society of Chemistry. According to the copyright policies of the Royal Society of Chemistry authors retain rights to use their contributions, in full or in part, for inclusion in a theses or dissertation. An acknowledgment to the original published article has been prominently placed at the beginning of chapter 2. Therefore, the permission to include this paper in this dissertation is granted. The published article can be found at:

https://pubs.rsc.org/en/content/articlelanding/2020/SM/D0SM01345E#!divAbstract .

Chapter 3 of this dissertation has appeared in *Macromolecules*, which belongs to the American Chemical Society. According to the copyright policies of American Chemical society, the authors retain the right to reproduce the article in whole or in part in a thesis or dissertation, provided appropriate citation of the published work is made. An acknowledgment to the original published article has been prominently placed at the beginning of chapter 3. Detailed information on the copyright policy of American Chemical society can be found on

https://pubs.acs.org/page/copyright/permissions_otherpub.html. The published article is available at: https://pubs.acs.org/doi/10.1021/acs.macromol.9b02472 .

Chapter 4 of this dissertation has appeared in *ACS Applied Polymer Materials*, which belongs to the American Chemical Society. According to the copyright policies of American Chemical society, the authors retain the right to reproduce the article in whole or in part in a thesis or dissertation, provided appropriate citation of the published work is made. An acknowledgment to the original published article has been prominently placed at the beginning of chapter 4. Detailed information on the copyright policy of American Chemical society can be found on https://pubs.acs.org/page/copyright/permissions_otherpub.html. The published article is available at: https://pubs.acs.org/doi/10.1021/acsapm.1c01813 .

Chapter 5 of this dissertation has appeared in *Macromolecular Rapid Communications*, which belongs to the publisher, Wiley. According to the copyright policies of Wiley, authors retain rights to use their contributions, in full or in part, for inclusion in a theses or dissertation. An acknowledgment to the original published article has been prominently placed at the beginning of chapter 5. Therefore, the permission to include this paper in this dissertation is granted. The published article can be found at:
https://onlinelibrary.wiley.com/doi/full/10.1002/marc.202000614.

Chapter 6 of this dissertation has appeared in *Physical Chemistry Chemical Physics*, which belongs to the Royal Society of Chemistry. According to the copyright policies of the Royal Society of Chemistry authors retain rights to use their contributions, in full or in part, for inclusion in a theses or dissertation. An acknowledgment to the original published article has been prominently placed

at the beginning of chapter 6. Therefore, the permission to include this paper in this dissertation is granted. The published article can be found at:

https://pubs.rsc.org/en/content/articlelanding/2022/CP/D1CP05263B

Chapters 7 and 8 of this dissertation have not appeared in any journal, and therefore, no permission is required.